

Atg26 is involved in selective autophagy of the major  
coat protein Gag of the *S. cerevisiae* virus L-A

Dissertation

for the award of the degree  
“Doctor rerum naturalium”  
of the Georg-August-University Göttingen

within the doctoral program “Molecular Biology of Cells”  
of the Georg-August-University School of Science (GAUSS)

submitted by  
**Peter Rube**  
from Korbach (Hessen)

Göttingen, 2014

Member of the Thesis Committee (First Reviewer):

Prof. Dr. Michael Thumm  
Center for Biochemistry and Molecular Cell Biology  
Institute of Cellular Biochemistry  
Georg-August-Universität, Göttingen  
Humboldtallee 23  
37073 Göttingen

Member of the Thesis Committee (Second Reviewer):

Prof. Dr. Stefanie Pöggeler  
Department of Eukaryotic Microorganisms  
Georg-August-Universität, Göttingen  
Grisebachstraße 8  
37077 Göttingen

Member of the Thesis Committee:

Dr. Karin Kühnel  
Department of Neurobiology  
Max Planck Institute for Biophysical Chemistry  
Faßberg 11  
37077 Göttingen

Date of oral examination:

Affidavit:

Herewith I declare that I prepared this thesis on my own and with no other sources and aids than quoted.

Peter Rube

*Le silence éternel de ces espaces infinis m'effraie.*

**(Das ewige Schweigen dieser unendlichen Räume macht mich schauern.)**

Blaise Pascal (1623-1662), Pensées

# Content

<b>1 Summary</b>	<b>1</b>
<b>2 Introduction</b>	<b>3</b>
2.1 Prelude	3
2.2 <i>Saccharomyces cerevisiae</i> as model organism	5
2.3 The autophagic core machinery and the membrane sources for autophagosome formation in yeast	6
2.3.1 Induction of unselective macroautophagy	6
2.3.2 The preautophagosomal structure (PAS) and the membrane origins of autophagosomes	7
2.3.3 The Atg1 complex	8
2.3.4 The phosphatidylinositol 3-kinase complex	10
2.3.5 Atg9 vesicles and associated complexes	10
2.3.6 Two ubiquitin-like conjugation systems	12
2.3.7 Autophagosome closure and delivery to the vacuole	15
2.4 Detailed view on Atg8 and its interaction partners	15
2.5 Selective autophagy	19
2.5.1 The Cvt pathway as a role model for selective autophagy	19
2.5.2 Mitophagy	21
2.5.3 Pexophagy and Atg26	22
2.5.3.1 Pexophagy in different yeast species	22
2.5.3.2 Atg26	24
2.5.4 Further selective autophagic pathways in yeast	25
2.6 <i>Saccharomyces cerevisiae</i> virus L-A	27
2.7 Aim of the thesis	30
<b>3 Materials and methods</b>	<b>31</b>
3.1 Materials	31
3.1.1 Yeast strains	31
3.1.2 <i>E. coli</i> strains	33
3.1.3 Plasmids	33
3.1.4 Oligonucleotides	34
3.1.5 Antibodies	37
3.1.6 Commercial available kits	37
3.1.7 Chemicals, supplements, enzymes and protein purification systems	37
3.1.8 Equipment	38
3.1.9 Media	40
3.2 Methods	41
3.2.1 Cultivation of <i>E. coli</i>	41
3.2.2 Cultivation of yeast	41
3.2.3 Molecular biological methods	42
3.2.3.1 Determination of DNA concentration	42
3.2.3.2 Restriction of DNA	42
3.2.3.3 DNA electrophoresis	42
3.2.3.4 Polymerase chain reaction	42
3.2.3.5 Molecular cloning	43
3.2.3.6 Generation of cDNA for molecular cloning	43

3.2.3.7 Preparation of chemically competent <i>E. coli</i> (XL1 blue)	44
3.2.3.8 Preparation of electrocompetent <i>E. coli</i> (BL21/pLysS)	44
3.2.3.9 Transformation of plasmid DNA in chemically competent <i>E. coli</i>	44
3.2.3.10 Transformation of plasmid DNA in electrocompetent <i>E. coli</i>	45
3.2.3.11 Site-directed mutagenesis of plasmids	45
3.2.3.12 Purification of plasmids from <i>E. coli</i>	45
3.2.3.13 Sequencing of DNA	45
3.2.3.14 Plasmid constructs	45
3.2.3.15 Isolation of chromosomal DNA from yeast cells	48
3.2.3.16 Yeast cell transformation	48
3.2.3.17 “Quick and Dirty” variant of yeast cell transformation	49
3.2.3.18 Deletion and chromosomal tagging of genes by homologous recombination	49
3.2.4 Split-ubiquitin assay	49
3.2.5 Microscopy	50
3.2.6 Induction and monitoring of autophagy	50
3.2.7 Biochemical methods	51
3.2.7.1 Cell lyses	51
3.2.7.1.1 Alkaline lysis of yeast cells	51
3.2.7.1.2 Osmotic lysis of spheroplasts	51
3.2.7.2 GST-Atg8 and GST-Atg26 187-569 pull downs	52
3.2.7.2.1 Expression of GST-Atg8 and GST-Atg26 187-569	52
3.2.7.2.2 Purification of GST-Atg8 and GST-Atg26 187-569	52
3.2.7.2.3 GST-Atg8 and Atg26 187-569 pull down assays	53
3.2.7.3 Co-purification of GST-Gag and His-Atg26 187-569	53
3.2.7.3.1 Expression of GST-Gag and His-Atg26 187-569	53
3.2.7.3.2 Co-purification of GST-Gag and His-Atg26 187-569	53
3.2.7.4 GFP- and RFP-TRAP	54
3.2.7.5 SDS-Polyacrylamid-Gel-Electrophoresis (PAGE)	55
3.2.7.6 Immunoblotting	55
3.2.7.7 Coomassie brilliant blue (CBB) staining	56
3.2.7.8 MS analysis	57
<b>4 Results</b>	<b>58</b>
4.1 Optimization of GFP-Atg8-TRAP for quantitative MS analysis	58
4.2 Data mining of the quantitative MS analysis	63
4.3 Validation of the quantitative MS analysis	65
4.4 Atg26 <i>physically</i> interacts with Atg8 via a very C-terminal Atg8 interacting motif (AIM)	72
4.5 Atg26 <i>functionally</i> interacts with Atg8 during autophagy	77
4.6 PAS recruitment of Atg26 depends on Atg8 and Atg1	80
4.7 Identification of the major coat protein of the L-A virus as a new Atg26 interaction partner	83
4.8 Mapping of the Gag binding domains in Atg26	88
4.9 GFP- and mCherry-tagged L-A Gag bind Atg26, but inhibit the endogenous virus	95
4.10 Autophagy of GFP-tagged Gag depends on Atg26	100
4.11 Genetic dissection of GFP-Gag autophagy	103

<b>5 Discussion</b>	<b>109</b>
5.1 Searching for new Atg8 interaction partners	110
5.2 Newly identified Atg8 interaction partners	111
5.3 Atg26 is an AIM-containing protein	114
5.4 Identification of L-A Gag as an Atg26 interaction partner	118
5.5 The PH domain (187-337) and an undefined region (338-569) mediate Gag binding of Atg26	121
5.6 Identification of virus-related Atg26 interaction partners	123
5.7 Atg26 is involved in selective autophagy of L-A Gag	125
5.7.1 GFP-tagged Gag as a tool to measure autophagy of the L-A virus	125
5.7.1.1 Analysis of GFP- and mCherry-tagged Gag in binding studies	125
5.7.1.2 Fluorescence microscopic analysis of GFP and mCherry-tagged Gag	126
5.7.1.3 Detection of autophagic processing of GFP-tagged Gag(Pol)	128
5.7.2 Selective autophagy of L-A Gag	128
5.7.3 Proposed function of Atg26	131
5.8 Conclusion	134
<b>6 Appendix</b>	<b>135</b>
<b>7 Bibliography</b>	<b>136</b>
<b>8 Acknowledgement</b>	<b>160</b>
<b>9 Curriculum vitae</b>	<b>161</b>

# List of Figures

Figure 2.1 Different mechanisms of autophagy	4
Figure 2.2 <i>S. cerevisiae</i> as model organism	5
Figure 2.3 Membrane sources for autophagosome formation	8
Figure 2.4 The Atg17-Atg31-Atg29 complex	9
Figure 2.5 Current model of early stages of phagophore formation	12
Figure 2.6 Two UBL conjugation systems	14
Figure 2.7 AIM-containing Atg8 interactors	17
Figure 2.8 The Cvt pathway	20
Figure 2.9 Pexophagy in <i>Pichia pastoris</i>	23
Figure 2.10 L-A (+) strand, encoded proteins and cis signals with secondary structure	27
Figure 2.11 <i>S. cerevisiae</i> virus L-A	29
Figure 3.1. Arrangement in a semi-dry blotting chamber	56
Figure 4.1 Optimization of immunoprecipitation using GFP-TRAP	61
Figure 4.2 CBB staining of SDS-PAGE as further quality control for the GFP-Atg8-TRAP	62
Figure 4.3 Heatmaps of selected putative Atg8 interactors identified by quantitative mass spectrometry (Dept. of Bioanalytics of Prof. Albert Sickmann)	64
Figure 4.4 Validation of the quantitative MS analysis	66
Figure 4.5 Detailed comparison of immunoblotting and quantitative MS of GFP-Atg8-TRAPs	68
Figure 4.6 Validation of Atg8-Atg26 interaction by the split-ubiquitin assay	70
Figure 4.7 Putative Atg8 interaction motifs in Atg26	73
Figure 4.8 Atg26 has a very C-terminal AIM	75
Figure 4.9 Atg26 is AIM-dependently transported to the vacuole upon autophagy induction	78
Figure 4.10 Atg26 locates AIM-dependently to the PAS	81
Figure 4.11 Identification of L-A Gag as a new Atg26 interaction partner	84
Figure 4.12 Validation of Atg26/L-A interaction at endogenous expression level	86
Figure 4.13 The PH domain (187-337) and an undefined region (338-569) of Atg26 bind L-A Gag	89
Figure 4.14.1 Recombinant expressed GST-Atg26 187-569 binds L-A virus-like particles	90
Figure 4.14.2 MS analysis of the GST-Atg26 187-569 pull down assay	92
Figure 4.15 Investigation of a putative direct Atg26-Gag interaction via pull down and split-ubiquitin assay	94
Figure 4.16 Atg26 binds tagged versions of Gag	96
Figure 4.17 GFP-Gag binds Atg26-HA and mCherry-Gag	99
Figure 4.18 GFP-tagged Gag is transported to the vacuole upon autophagy induction	101/2
Figure 4.19 Genetic dissection of GFP-Gag autophagy	104
Figure 4.20 Known receptors for selective autophagy are not involved in the Atg26-Gag interaction and autophagy of GFP-Atg26	106
Figure 4.21 The C-terminal AIM of Atg26 is necessary for efficient autophagy of GFP-Gag	108
Figure 5.1 Cartoon representation of L-A Gag	119
Figure 5.2 Sequence alignment of Atg26 homologs with regions of known phosphoinositide-binding motifs in PH domains	122
Figure S1 Sequence alignments of L-A Gag (WCG4a) identified in this study with published sequences of L-A, L-A-lus and L-BC.	135



## List of Tables

Table 3.1 Yeast strains	31
Table 3.2 <i>E. coli</i> strains used in this study	33
Table 3.3 Plasmids used in this study	33
Table 3.4.1 Oligonucleotides for cloning and sequencing used in this study	34
Table 3.4.2 Oligonucleotides for for gene deletion and tagging used in this study	36
Table 3.5 Antibodies used in this study	37
Table 3.6 Commercial available kits used in this study	37
Table 3.7 Chemicals, supplements, enzymes and protein purification systems used in this study	37
Table 3.8 Equipment used in this study	38
Table 3.9.1 Yeast media used in this study	40
Table 3.9.2 <i>E. coli</i> media used in this study	40
Table 3.10 Plasmids constructs cloned in this study	46
Table 3.11 Filter sets for live cell imaging	50
Table 3.12 Composition of one SDS Polyacrylamid gel for a Mini-Protean III electrophoresis chamber from Biorad	55
Table 4.1 Tested conditions for optimization of GFP-Atg8-TRAP	59

## Abbreviation

-	without
°C	Degree in Celsius
A	Ampere
aa	Amino acid(s)
ade	Adenine
AIM	Atg8-interacting motif
Arg	Arginine
Ape1	Aminopeptidase 1
APS	Ammonium persulfate
Atg	Autophagy-related protein
CM	Complete minimal medium
Cub	C-terminal part of ubiquitin
Cvt	Cytoplasm-to-Vacuole Targeting
DNA	Desoxyribonucleic acid
DTT	Dithiothreitol
<i>E. coli</i>	<i>Escherichia coli</i>
EDTA	Ethylenediaminetetraacetate-disodium salt
FOA	5-Fluoroorotic Acid
g	gram
g	Gravity
GFP	Green fluorescent protein
Gly	Glycine
GST	Glutathione-S-transferase
h	hour(s)
HA	Human influenza hemagglutinin
His	Histidine
HRPO	Horsereddish peroxidase
IPTG	Isopropyl- $\alpha$ -D-thiogalactopyranoside
KAN	Kanamycin
kDa	kilodalton
l	liter
LB	Lysogeny broth
Leu	Leucine
LIR	LC3-interacting region
Lys	Lysine
M	molar
m	mature
m	meter
m	milli
mCherry	monomeric Cherry
met	Methionine
min	minute
MS	Mass spectrometry
N	Nitrogen
n	nano
NatNT2	Nourseotricine
Nub	N-terminal part of ubiquitin
OD <sub>600</sub>	Optical density (600 nm)
PAS	Pre-autophagosomal structure

PE	Phosphatidylethanolamine
Pgk1	Phosphoglycerate kinase
pH	negative logarithm of H <sup>+</sup> concentration
Phe	Phenylalanine
PI3P	Phosphatidylinositol 3-phosphate
PI(3,5)P <sub>2</sub>	Phosphatidylinositol 3,5-bisphosphate
PMN	Piecemeal Microautophagy of the Nucleus
PMSF	Phenylmethylsulfonylfluoride
<i>Pp/ P. pastoris</i>	<i>Pichia pastoris</i>
pr	Precursor
PROPPIN	β-propeller that binds polyphosphoinositides
RFP	Red fluorescent protein
RNAi	RNA interference
rpm	round per minute
RT	Room temperature
s	second
<i>Sc/ S. cerevisiae</i>	<i>Saccharomyces cerevisiae</i>
SD	Synthetic defined
SDS	Sodium dodecyl sulfate
TAP	Tandem Affinity Purification
TCA	Trichloroacetic acid
TORC1	Target of Rapamycin Complex 1
tRNA	Transfer RNA
Trp	Tryptophan
Ura	Uracile
v/v	volume per volume
V	volt
VLP	Virus-like particle
w/v	weight per volume
wt	Wild type
YPD	Yeast peptone dextrose
μ	micro
β-ME	Beta mercaptoethanol

### 1 Summary

Macroautophagy is a conserved catabolic pathway for the removal and recycling of cytosolic components, damaged or surplus organelles, protein aggregates or intracellular pathogens to maintain cellular homeostasis. It is characterized by the formation of a double-membrane-layered vesicle, called autophagosome, that engulfs intracellular material. In yeast, autophagosome formation is initiated at the pre-autophagosomal structure (PAS). Here, a double-membrane structure, the phagophore, elongates and closes to form the autophagosome. Finally, the outer membrane of the autophagosome fuses with the vacuole releasing the inner membrane together with the cargo in the vacuolar lumen for degradation.

Atg8 is a key component for autophagosome biogenesis and selective cargo recruitment to the phagophore. In this study, a series of GFP-Atg8 variants, including mutants that are unable to bind Atg8-interacting motifs (AIMs), were used as baits for co-immunoprecipitation (CoIPs) and following mass spectrometry analysis to find novel Atg8 interaction partners. This allowed rapid validation of the numerous proteins identified in mass spectrometry.

This approach identified Atg26 as an AIM-dependent interaction partner of Atg8. Atg26 is a sterol glucosyltransferase with a PH and GRAM domain. So far, the function of Atg26 in *S. cerevisiae* was unknown. In this study, using bioinformatics, a C-terminal Atg8-interacting motif (AIM) was predicted in Atg26. Interestingly, this motif was necessary for recruitment of Atg26 to the phagophore and its autophagic degradation, which are common features of known AIM-containing proteins.

To uncover the function of Atg26 in *S. cerevisiae*, CoIPs with GFP-Atg26 as bait were done. Here, the major coat protein Gag of the *S. cerevisiae* virus L-A was identified as an Atg26 interaction partner. L-A is a dsRNA virus of the *Totiviridea* family. It has a single 4.6 kb dsRNA genome with two overlapping ORFs, where ORF1 encodes the major coat protein Gag and ORF2 is a RNA-dependent RNA polymerase (Pol) that is expressed as a 180 kDa Gag-Pol fusion protein. L-A virus-like particles (VLP) are made up of 120 Gag subunits (from which about 2 are Gag-Pol fusion proteins), containing genomic dsRNA inside.

In this study, using truncated versions of Atg26 as baits for CoIPs and pull down assays the Gag binding domain of Atg26 was narrowed down to the PH domain and an undefined following region of Atg26. Atg26 recruitment to the phagophore by its C-

## Summary

terminal AIM and its interaction with L-A Gag suggested an involvement of Atg26 in selective autophagic degradation of the L-A virus. Here, GFP-tagged L-A Gag, showing comparable features as endogenous L-A Gag in binding studies and microscopic analyses, was established as a tool to measure autophagic removal of L-A Gag. During starvation, GFP-tagged Gag was degraded by autophagy, while deletion of *ATG26* caused a 50% reduction of the autophagic rate. Thus, this study showed for the first time that L-A Gag is degraded by autophagy and attributes a direct role in this process to Atg26. Indeed, the selective adapter Atg11 and the PROPPINs Atg21 and Hsv2, which are typical regulators of selective autophagy, are also involved in processing of GFP-Gag. These observations indicate that L-A Gag is degraded by selective autophagy. Taken together, this study suggests that Atg26 might recruit L-A Gag or complete L-A VLPs to the phagophore for degradation by selective autophagy.

## 2 Introduction

### 2.1 Prelude

Autophagy is an evolutionary conserved degradative pathway for maintenance of cellular homeostasis and adaption to environmental changes or other forms of stress.

For large-scale degradation of intracellular material, the cell evolved different transport mechanisms for macromolecules and organelles from the cytosol to the lytic compartment (either the lysosome in higher eukaryotes or the vacuole in fungi and plants) over limiting membranes.

Macroautophagy (hereafter: autophagy) is a highly organized membrane-trafficking pathway for *en masse* degradation of intracellular macromolecules and organelles (Figure 2.1A). Morphologically, this process starts with the formation of the phagophore, a cup-shaped double membrane structure, that expands to engulf cytosolic components. Upon closure, a double-membrane-layered vesicle, the so-called autophagosome, is formed. Finally, the outer membrane of an autophagosome fuses with the lytic compartment (lysosome or vacuole) leading to degradation of the inner autophagosomal membrane together with the cargo (Reggiori and Klionsky, 2013).

Microrautophagy describes an autophagic mechanism, where the lysosomal/vacuole membrane invaginates directly with the engulfed cargo and bud into the lumen for degradation (Figure 2.1B) (Li et al., 2012).

In mammalian cells, a third, non-vesicular way of autophagy exists that mediates direct protein translocation across the lysosome-limiting membrane for degradation (Figure 2.1C). This molecule-by-molecule mechanism is termed chaperone-mediated autophagy (CMA) and recruits KFERQ-motif-containing substrates via the cytosolic chaperone Hsc70. After the substrate protein is unfolded, it is translocated across the lysosomal membrane by the integral protein LAMP2A and the intralysosomal chaperone hsc70 (ly-hsc70) that acts as molecular ratchet (Cuervo and Wong, 2014; Dice, 1990).

Investigation of autophagy provides knowledge for basic subcellular mechanisms such as the rearrangement of membranes. Furthermore, there are many examples that show associations of autophagic malfunctions and diseases. Therefore, autophagy can be used as a diagnostic marker and is in focus as a potential therapeutic target (Schneider et al., 2014).

## Introduction

Historically, autophagy was discovered in the early sixties by the work of Ashford and Porter (1962), which demonstrated that glucagon treatment leads to accumulation of cytosolic components and organelles in the lysosome (Ashford and Porter, 1962). Further studies in mammalian systems revealed that autophagy is a response to nutrient withdrawal (Deter et al., 1967; Mortimore and Pösö, 1987; Seglen et al., 1991). In the nineties of the last century, it was shown that autophagy also exists in *S. cerevisiae* and, in this context, the first autophagy-related genes (*ATGs*) were found by genetic screening (Harding et al., 1995; Klionsky et al., 1992; Matsuura et al., 1997; Takeshige et al., 1992; Thumm et al., 1994; Tsukada and Ohsumi, 1993). Discovery of orthologs in other organisms showed that this process is conserved in eukaryotes. Thus, the knowledge of one model system is transferable to other eukaryotes. In yeast, 38 *ATG* genes had been identified, which are directly associated with autophagy.

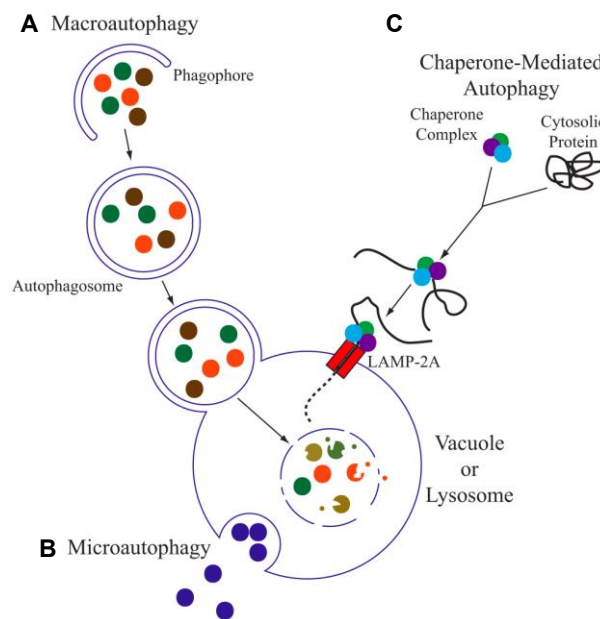


**Figure 2.1 Different mechanisms of autophagy (modified from (Lynch-Day and Klionsky, 2010))**

(A) Macroautophagy starts with the formation of the phagophore, a double-membrane structure that engulfs cytosolic material. The completed autophagosome fuses with the vacuole/lysosome and after lysis of the inner membrane the cargo enters the lumen for degradation.

(B) During microautophagy, the cargo is directly invaginated by the vacuolar/lysosomal membrane. The invaginated membrane together with the engulfed cargo pinches-off into the vacuolar lumen for degradation.

(C) Chaperone-mediated autophagy directly translocates KFERQ-containing proteins across the lysosomal membrane.

## 2.2 *Saccharomyces cerevisiae* as model organism

*Saccharomyces cerevisiae* is a useful tool to study intracellular processes. Elementary biochemical pathways are highly conserved among eukaryotes. The gene homology between yeast and humans is about 60%. Therefore, knowledge derived from studies in yeast is transferable to other eukaryotes and can even be used to investigate human diseases (Gavin et al., 2002; Hartwell, 2004; Mager and Winderickx, 2005; Miller-Fleming et al., 2008).

Yeast was the first eukaryote, whose genome was completely sequenced: The genome of a haploid cell has about 12.000 kb, distributed on 16 chromosomes, with more than 6.000 open reading frames (Goffeau et al., 1996). The parallel development of many tools for precise genetic manipulation based on homologous recombination, the ease of transformation and the available online databases further make yeast a favoured model system (Goffeau et al., 1996; Janke et al., 2004; Knop et al., 1999; Longtine et al., 1998).

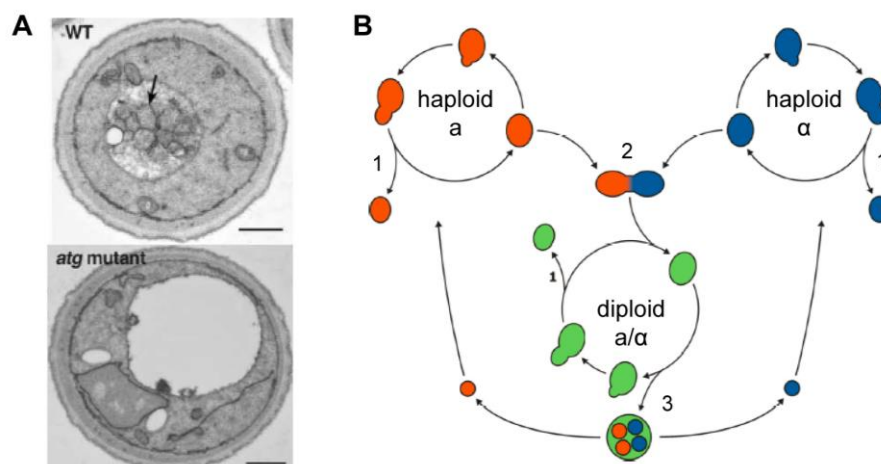


**Figure 2.2 *S. cerevisiae* as model organism**

(A) Morphology of *S. cerevisiae* (EM). Top: During starvation, wt cells accumulate cytosolic material (arrowhead) in the vacuole by autophagy. Bottom: *ATG* mutants are defective in autophagic transport of cytosolic material to the vacuole. Therefore, the vacuole is empty in these strains (modified from (Tallóczy et al., 2002)).

(B) Life cycle of *S. cerevisiae*. (1) The haploid mating types  $Mata$  and  $Mata\alpha$  bud by mitotic division. (2) Haploids generate diploid cells by mating. (3) Sporulation leads to formation of 4-8 (haploid) spores within a single mother cell.

Morphologically, this unicellular eukaryote has a round to oval shape with 5-10  $\mu\text{m}$  in diameter (Figure 2.2A). Budding yeast has a rapid growth rate with a doubling-time of approximately 90 min in nutrient-rich medium. The life cycle consists of three stages (Figure 2.2 B): (1) The haploid mating types,  $Mata$  and  $Mata\alpha$ , bud by mitotic division. (2) Haploids are able to generate diploid cells by mating. (3) Nutritional stress treatment



(such as growth on acetate) of diploids causes sporulation, characterized by meiotic division and formation of 4-8 (haploid) spores within a single mother cell (Neiman, 2005).

### **2.3 The autophagic core machinery and the membrane sources for autophagosome formation in yeast**

Currently, more than 35 *ATG* genes were identified that function in any kind of autophagy. Among them, approximately 18 proteins are elementary for all kinds of autophagy and are therefore classified as the autophagic core machinery. These group of core proteins can be divided in further functional subgroups: i) the Atg1 complex; ii) the phosphatidylinositol 3-kinase complex, iii) Atg9 vesicle associated complexes and iv) the two ubiquitin-like conjugation systems. The following chapters will provide an insight into how autophagy is induced (chapter 2.3.1), where autophagosomes are formed and which membrane origins are used (chapter 2.3.2), how the core machinery proteins are organized (chapter 2.3.3-2.3.6) and, finally, how autophagosomes are delivered to the vacuole for degradation of their cargos (chapter 2.3.7).

#### **2.3.1 Induction of unselective macroautophagy**

In yeast, starvation is the central inducer of autophagy. Different autophagy-inducing mechanisms exist in parallel to sense the kind of nutrient limitation and induce optimal adaptation.

The protein kinase (target of rapamycin) Tor1 and Tor2 together with Kog1, Lst8 and Tco89 form the Tor kinase 1 complex (TORC1) that response to the cellular nitrogen level and negatively regulates autophagy. Under nutrient-rich conditions, TORC1 is activated and hyperphosphorylates Atg1 and Atg13 and thereby inhibits autophagy (Abeliovich et al., 2000; Fujioka et al., 2014; Scott et al., 2000). Rapamycin inhibits Tor and can even be used for pharmacological induction of autophagy (Loewith and Hall, 2011; Noda and Ohsumi, 1998).

The kinase PKA is a further phosphoregulator of Atg1 and Atg13. A high level of glucose leads to production of the second messenger cAMP, which liberates PKA from its regulatory subunit Bcy1. Consequently, PKA is activated and phosphorylates Atg13 and Atg1 (Budovskaya et al., 2004; Yorimitsu et al., 2007). Detailed analyses of Atg13

phosphoregulation showed that PKA phosphorylates Atg13 on different sites than Tor, but also with an autophagy-inhibiting effect (Stephan et al., 2009).

The general control of nutrients (Gcn4) pathway senses the amount of cellular amino acids and regulates autophagy on transcriptional level. A key component of this signalling network is the eIF2 $\alpha$  kinase Gcn2, which is stimulated by unconjugated tRNA (Dever et al., 1992). As a result, the downstream transcription factor Gcn4 is increased translated and activates transcription of *ATG* genes (Ecker et al., 2010; Tallóczy et al., 2002).

### 2.3.2 The preautophagosomal structure (PAS) and the membrane origins of autophagosomes

In fluorescence microscopy, the PAS (preautophagosomal structure or also known as phagophore assembly site) is a punctate structure next to the vacuole. Since the majority of Atg proteins at least transiently locate to the PAS, this compartment is understood as the nucleation site for autophagosome formation (Suzuki et al., 2001; Suzuki et al., 2007). The exact protein and membrane composition of the PAS and thus its definition as subcellular compartment remains enigmatic.

From the PAS as the nucleation site, the phagophore (also called isolation membrane) needs to be elongated by addition of membrane sources to form an autophagosome. Studies on mammalian cells in the early nineties suggested that the ER is involved in autophagosome formation (Dunn, 1990a; Dunn, 1990b). Recent studies in yeast seemed to support this observation by showing that the ER exit sites (ERES), which are subdomains of the ER for COPII vesicle formation, are associated with the PAS. It was published that ERES trigger fusion of COPII vesicles with the phagophore and thus phagophore elongation (Graef et al., 2013; Suzuki et al., 2013). Furthermore, it was recently demonstrated for mammalian cells that the reticulum-Golgi intermediate compartment (ERGIC), an ER site closely related to ERES, is a membrane source for autophagy (Ge et al., 2013). Similar to yeast, ERGIC-generated COPII-vesicles might mediate the membrane transfer from the ER to the expanding phagophore (Ge et al., 2013).

Nonetheless, there exists evidence for further membrane sources: For example Atg9, the only integral membrane protein of the core machinery, is delivered from the trans-Golgi and endosomes to the phagophore (Ohashi and Munro, 2010; Wang et al., 2012;

## Introduction

Yamamoto et al., 2012). The origin of autophagosomal membranes is still discussed, but, all facts considered, membranes from various compartments seems to be involved, including the ER, the Golgi apparatus, endosomes, mitochondria and the plasma membrane (der Vaart et al., 2010; Ge et al., 2014; Hamasaki et al., 2013; Mari et al., 2010; Taylor et al., 2012; Yen et al., 2010; Young et al., 2006).

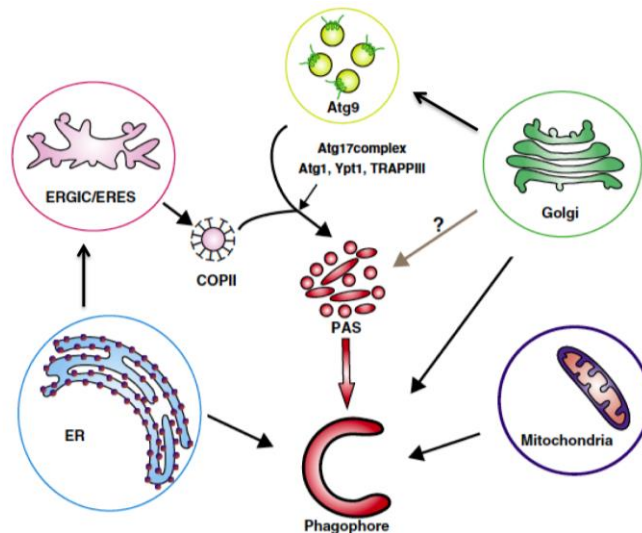


**Figure 2.3 Membrane sources for autophagosome formation (modified from (Ge et al., 2014))**

### 2.3.3 The Atg1 complex

Formation of the Atg1 complex is one of the most upstream events upon autophagy induction. It consists of the serine/threonine kinase Atg1, the regulatory subunit Atg13, and the constitutive ternary complex Atg17-Atg31-Atg29 (Figure 2.4 and 2.5A) (Cheong et al., 2008; Kabeya et al., 2005; Kamada et al., 2000; Matsuura et al., 1997; Straub et al., 1997). Under nutrient-rich condition, TORC1 or other kinases directly phosphorylate Atg1 and Atg13 for inhibition of autophagy induction (chapter 2.3.1) (Abeliovich et al., 2000; Scott et al., 2000; Wang et al., 2001; Wilson and Roach, 2002). Directly after autophagy induction, Atg13 becomes partially dephosphorylated. Previous studies proposed that dephosphorylation of Atg13 leads to interaction with Atg1 and thus nucleation of the Atg1 complex (Fujioka et al., 2014; Kamada et al., 2000). However, Kraft et al (2012) published that Atg1 and Atg13 interact constitutively with each other. This conflicting results would agree with studies in mammalian cells, where ULK1, the mammalian homolog of Atg1, is always assembled with mammalian ATG13 (Hosokawa et al., 2009; Kraft et al., 2012). The early autophagy targeting (EAT) domain of Atg1

## Introduction

mediates interaction with Atg13 (Cheong et al., 2008; Yeh et al., 2011). *In vitro* experiments showed that this domain is also able to selectively bind highly curved vesicles of 20-30 nm in diameter, which is approximately the size of Atg9 vesicles, suggesting an involvement in vesicle tethering in early steps of autophagy (see also chapter 2.3.5) (Figure 2.5D) (Chan et al., 2009; Ragusa et al., 2012).

Besides its complex formation with Atg1, Atg13 also directly interacts with Atg17, a scaffold protein with a crescent-shaped structure (Fujioka et al., 2014; Ragusa et al., 2012). Atg17 is able to dimerise and forms a constitutive ternary complex with Atg31-Atg29 (Kabeya et al., 2009). Thus, taken together, the overall Atg1 complex is thought as a dimer of Atg1-Atg13-Atg17-Atg31-Atg29, forming a S-shaped architecture (Figure 2.4 and 2.5A) (Chew et al., 2013; Ragusa et al., 2012). Upon starvation, the Atg17-Atg31-Atg29 module of the Atg1 complex is required for kinase activity of Atg1 and serves as a scaffold for recruitment of further Atg proteins and membrane sources, such as Atg9 vesicles (chapter 2.3.5) (Figure 2.4B, 2.5D) (Mao et al., 2013a; Stanley et al., 2014).

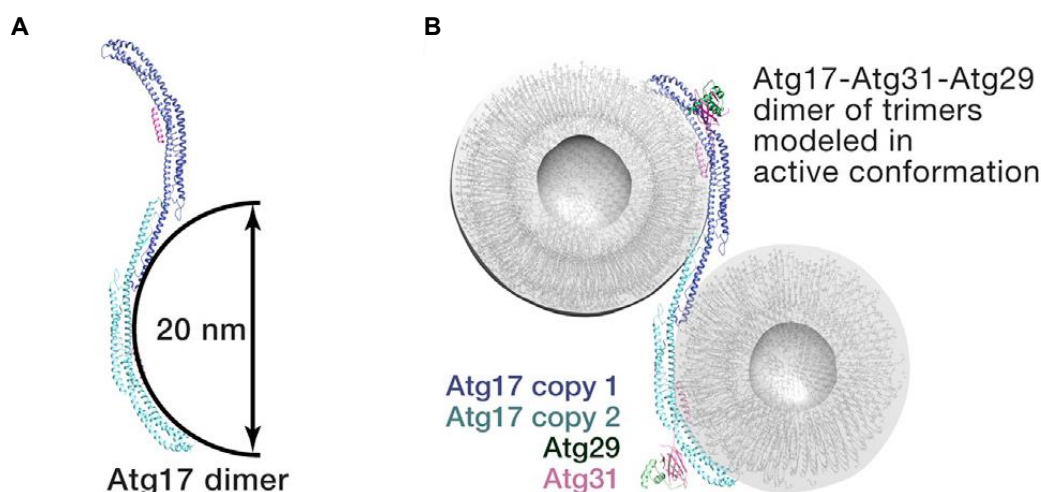


**Figure 2.4 The Atg17-Atg31-Atg29 complex (modified from (Hurley and Schulman, 2014))**

(A) The S-shaped architecture of dimeric Atg17.

(B) Model for the dimeric Atg17-Atg31-Atg29 complex bound to two 20 nm vesicles.

During selective autophagic pathways, Atg17 is functionally replaced by Atg11 that, under these certain conditions, acts as scaffold for assembling the PAS and further has a adaptor function by linking receptor-cargo complexes to the autophagic machinery (Cheong et al., 2008; Okamoto et al., 2009; Suzuki et al., 2007).

Recently, it was shown that Atg9 and Atg2 are putative substrates of Atg1. Detailed analyses of the Atg1-dependent Atg9 phosphorylation suggested that this process is important for initial steps of autophagosome formation (Papinski et al., 2014).

Furthermore, it is proposed that Atg1 phosphorylates the selective receptors Atg19 and Atg32. However, in both cases, the function of Atg1-dependent phosphoregulation remained unclear (Kondo-Okamoto et al., 2012; Pfaffenwimmer et al., 2014).

### 2.3.4 The phosphatidylinositol (PtdIns) 3-kinase complex

Phosphatidylinositol 3-phosphate (PI3P) synthesis is essential for autophagy. In yeast, Vps34 is the only class III PtdIns 3-kinase and forms two complexes, named PtdIns 3-kinase complex I and II (Schu et al., 1993). The former complex is essential for autophagy, whereas the latter plays a role in protein sorting to the vacuole (Kihara et al., 2001). PtdIns 3-kinase complex I is made up of Vps34, Vps15, Vps30/Atg6, Atg14 and Atg38 (Figure 2.5 B) (Araki et al., 2013). In complex II, Atg14 is replaced by Vps38, making this complex non-relevant for autophagy (Kihara et al., 2001). The presence of Atg14 (I) or Vps38 (II) determines the localisation of the complexes and thus where PtdIns3-kinase activity occurs: at the PAS or at endosomes, respectively (Obara et al., 2006). PAS recruitment of the PtdIns3-kinase complex I is mediated by the HORMA domain of Atg13, a component of the Atg1 complex (Figure 2.5 D) (Jao et al., 2013). Production of PI3P at the PAS is necessary to recruit proteins that function in autophagosome formation such as the PI3P-binding protein Atg18 (chapter 2.3.5) (Krick et al., 2006).

### 2.3.5 Atg9 vesicles and associated complexes

Atg9 is the only multi-spanning integral membrane protein of the core machinery necessary for autophagosome biogenesis (Lang et al., 2000; Noda et al., 2000). Atg9-containing vesicles cycle between peripheral sites and the PAS. These Atg9 vesicles are generated at the Golgi-endosomal pathway, which involves the Rab GTPase Sec2, the guanine-nucleotide-exchange factors Sec4 and Sec7, the ADP-ribosylation factors (Arfs) 1/2 and the Golgi-localized PtdIns 4-kinase Pik1 (der Vaart et al., 2010; Geng et al., 2010; Ohashi and Munro, 2010; Wang et al., 2012). Further components, necessary for efficient delivery of Atg9 to the PAS, are the peripheral membrane protein Atg23 and the integral membrane protein Atg27 (Backues et al., 2014; Tucker et al., 2003; Yen et al., 2007). However, the anterograde transport to the PAS is still conflicting: Mari et al (2010) showed that Atg9 locates in cytosolic clusters of vesicles and tubules adjacent to

## Introduction

mitochondria, called Atg9 reservoir. Formation of these tubulovesicular structures might depend on membrane fusion events mediated by the SNARES Sso1/2, Sec9 and Tlg2 (Mari et al., 2010; Nair et al., 2011). In contrast, Yamamoto and co-workers (2012) showed that the majority of Atg9 locates on highly mobile cytoplasmic vesicles, each with about 27 copies of Atg9 (Yamamoto et al., 2012).

It has been proposed that upon induction of autophagy a part of the Atg9 vesicles moves close to the vacuole to initiate nucleation of the phagophore. At the PAS, dimeric Atg17 acts as scaffold for the Atg1 complex and in addition binds directly to Atg9. Atg1 itself might bind the Atg9 vesicles via its EAT domain. Thereby, the Atg1 complex is thought to cluster and tether the Atg9 vesicles for priming membrane fusion events at the PAS (see chapter 2.3.3) (Figure 2.5D) (Ragusa et al., 2012; Sekito et al., 2009; Stanley et al., 2014).

Further findings support that Atg9 vesicles might mediate early steps of phagophore formation: The Rab protein Ypt1 and its multimeric GEF, termed transport protein particle (TRAPP) III complex, are involved in autophagy (Lynch-Day et al., 2010; Meiling-Wesse et al., 2005). It was demonstrated that TRAPP III colocalize with Atg9 vesicles and that Trs85, a TRAPP III component, directly interacts with Atg9 (Figure 2.5 C and D) (Kakuta et al., 2012; Lipatova et al., 2012). Ypt1 is a further factor that recruits Atg1 to the PAS by direct interaction (Wang et al., 2013a). Together, these observations suggest an involvement of the Rab Ypt1 and its GEF TRAPP III in homotypic membrane fusions of Atg9 vesicles or fusion with other membrane sources such as COPII vesicles. These early membrane fusion events might trigger phagophore formation and elongation (Figure 2.5 C and D) (Graef et al., 2013; Tan et al., 2013; Wang et al., 2014).

For the retrograde transport of Atg9 (from the PAS back to the peripheral sites), the Atg1-Atg13 module of the Atg1 complex and the Atg2-Atg18 complex are necessary (Reggiori et al., 2004). Atg18 is an autophagic core protein with a seven-bladed  $\beta$ -propeller structure, classified to the protein family of PROPPINs ( $\beta$ -propellers that bind polyphosphoinositides) (Krick et al., 2012; Michell et al., 2006). Atg21 and Hsv2 are Atg18 homologs and involved in selective kinds of autophagy (Barth et al., 2002; Krick et al., 2008b). PAS localisation of Atg18 and its autophagic function depends on interaction with PI3P and thus the activity of the PtdIns3-kinase complex I. Atg18 and Atg2 interact PI3P-independently with each other. Complex formation is necessary for their PAS localisation and, consequently, their autophagic function (Obara et al., 2008; Rieter et al., 2013).

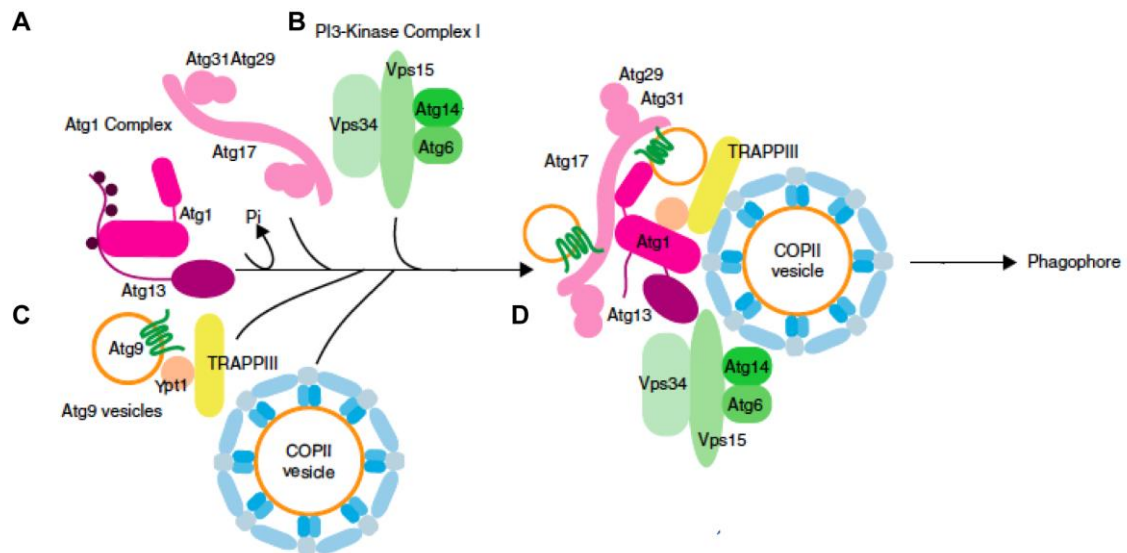


**Figure 2.5 Current model of early stages of phagophore formation (modified from (Ge et al., 2014))**

(A) The Atg1 complex (pink). Upon autophagy, Atg1 and Atg13 become dephosphorylated and bind the S-shaped, dimeric Atg17-Atg29-Atg31 complex.

(B) The PtdIns3-kinase complex I (green) consists of Vps34, Vps15, Vps30/Atg6, Atg14 and Atg38 (not shown). It is recruited to the PAS by the HORMA domain of Atg13.

(C) Atg9 vesicles, Ypt1, TRAPPIII and COPII vesicles are involved in initial events of phagophore formation.

(D) Hypothetic interplay of all components. The Atg1 complex, Ypt1 and the TRAPPIII complex might regulate homotypic fusion of Atg9 vesicles or fusion with COPII vesicles.

### 2.3.6 Two ubiquitin-like conjugation systems

The two ubiquitin-like (UBL) proteins Atg8 and Atg12 are the substrates of two networking ubiquitin-like (UBL) conjugation systems, which are both part of the autophagic core machinery (Ichimura et al., 2000; Mizushima et al., 1998a).

Initially, Atg8 is expressed with an arginine at the very C-terminal position (Atg8FGR), which is removed by the cysteine protease Atg4 before the Atg8 conjugation cascade begins (Figure 2.6A). Consequently, a glycine becomes the very C-terminal residue of Atg8 (Atg8FG) and is a prerequisite for interaction with enzymes of the UBL conjugation system (Kirisako et al., 2000). In contrast to Atg8, Atg12 is not processed before conjugation.

At the beginning of the two networking UBL conjugation systems, the E1-like protein Atg7 activates Atg8 and Atg12 in an ATP-consuming reaction, resulting in an Atg7~UBL intermediate formed by a thioester bond between the catalytic cysteine of Atg7 and the carboxy terminus of Atg8FG or Atg12 (Figure 2.6B) (Mizushima et al., 1998a; Mizushima et al., 1998b; Noda et al., 2011). The C-terminal domain of Atg7 mediates activation of the UBL protein (Atg8 or Atg12) and is necessary for homodimerisation, whereas the N-terminal region recruits the E2-like enzymes Atg3 (for Atg8) or Atg10 (for Atg12). Thus,

## Introduction

the full E1 complex is a dimer of Atg3-Atg7~Atg8 or Atg10-Atg7~Atg12 (Hong et al., 2011; Komatsu et al., 2001). In this configuration, the activated UBL is transferred to its corresponding E2-like enzyme in *trans* (Figure 2.6C) (Klionsky and Schulman, 2014; Noda et al., 2011; Taherbhoy et al., 2011).

Conjugation of Atg12 is a prerequisite for efficient Atg8 lipidation, therefore, this process will be described first: Once transferred to the E2-like Atg10, the activated carboxy terminus of Atg12 forms a thioester bond with the active site cysteine of Atg10 (Figure 2.6C) (Hong et al., 2012; Shintani et al., 1999). Finally, in an E3-independent mechanism, Atg10 interacts directly with Atg5 and initiates formation of a covalent bond between the C-terminus of Atg12 and an internal lysine of Atg5 (Figure 2.6D) (Shintani et al., 1999; Yamaguchi et al., 2012). Notably, Atg5 is a further UBL protein of the autophagic core machinery consisting of two UBL domains linked by a helix-rich domain (Matsushita et al., 2007). In addition to the interaction with Atg12, Atg5 forms a (non-covalent) complex with the autophagic core protein Atg16 (Mizushima et al., 1999). The coiled-coiled domain of Atg16 mediates its homodimerisation that leads to formation of a large dimeric Atg12-Atg5/Atg16 complex (Figure 2.6E) (Fujioka et al., 2010; Kuma et al., 2002). This complex has an E3-like function in the Atg8 conjugation system (Figure 2.6F).

Once activated, Atg8 is transferred from Atg7 (E1) to Atg3 (E2) to form the Atg3~Atg8 intermediate, the membrane associated Atg12-Atg5/Atg16 complex acts as platform to bring activated Atg8 close to its substrate phosphatidylethanolamine (PE) (Figure 2.6F) (Hanada et al., 2007). It was published that direct binding of the Atg12-Atg5 conjugate to Atg3~Atg8 causes a conformational change in the active center of Atg3 and thereby stimulates its conjugase activity (Sakoh-Nakatogawa et al., 2013). Atg8 lipidation is not completely abolished in the absence of this E3-like complex. Therefore, this complex only facilitates the PE-conjugation process (Suzuki et al., 2001).

Initial membrane binding of the Atg5-Atg12/Atg16 complex remains still elusive: There are hints that membrane recruitment of the Atg12-Atg5/Atg16 complex might be mediated by Atg5, containing a putative membrane-binding domain (Romanov et al., 2012). For mammals, it was recently demonstrated that the PROPPIN WIPI2b, an Atg18 ortholog (chapter 2.3.5), directly interacts with ATG16L and thereby PI3P-dependently regulates conjugation of the Atg8 ortholog LC3 (Dooley et al., 2014). In agreement with this model, it was shown in yeast that Atg5 and Atg16 are PI3P-



## Introduction

independently recruited to the PAS (Suzuki et al., 2007).

*In vitro* studies with giant unilamellar vesicles (GUVs) suggested a further function of the Atg12-Atg5/Atg16 complex: After conjugation to PE, lipidated Atg8 in turn forms a complex with Atg12 on the convex outer membrane of the emerging phagophore to stabilize the membrane association of the Atg12-Atg5/Atg16 complex. In this context, Atg16 is thought to act as a crosslinker to organize a continuous meshwork of Atg12-Atg5/Atg8-PE complexes on the emerging autophagosome, resulting in a membrane coat (Kaufmann and Wollert, 2014; Kaufmann et al., 2014). Atg8-PE also locates on the concave inner site of the phagophore, where it acts as a scaffold to recruit autophagic cargos or might fulfill further functions (chapter 2.4).

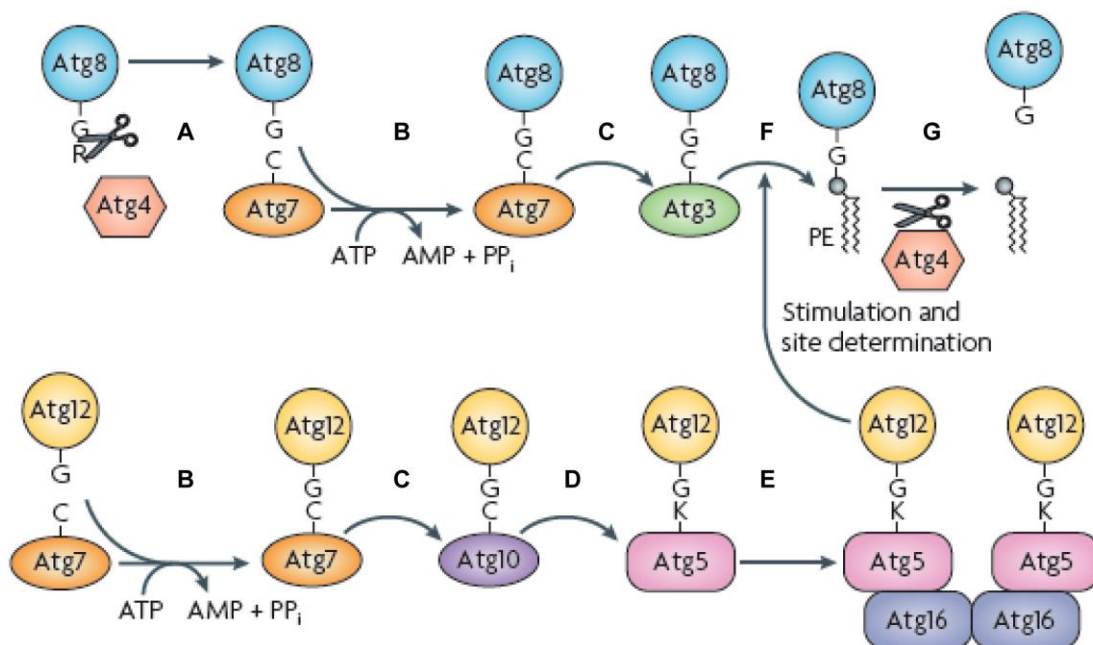


**Figure 2.6 Two UBL conjugation systems (modified from (Nakatogawa et al., 2009))**

(A) The cysteine protease Atg4 cleaves-off the C-terminal arginine of Atg8. (B) Atg8 and Atg12 are activated by Atg7 (E1-like protein). (C) Atg8 is then transferred to the E2-like protein Atg3, whereas Atg12 forms a complex with the E2-like protein Atg10 and (D) becomes covalently linked to Atg5. (E) This conjugate is a component of the large dimeric Atg12-Atg5/Atg16 complex that executes an E3-like function: (F) It stimulates the transfer of Atg8 from Atg3 to PE. (G) Atg4 acts as a deconjugating enzyme to release Atg8 from PE on the outer membrane.

During later stages of autophagy, the cysteine protease Atg4 acts as a deconjugating enzyme to release Atg8 from PE on the outer membrane of the emerging autophagosome for reuse of these Atg8 molecules that had exerted their functions (Figure 2.6G) (Kirisako et al., 2000). Another proposed role of Atg4 is deconjugation of randomly generated, non-functional Atg8-PE on autophagy-independent membranes

(Nair et al., 2012; Nakatogawa et al., 2012a; Yu et al., 2012). Those Atg8-PE conjugates on the inner surface of the emerging autophagosome are not cleaved off and therefore degraded together with the cargos.

### 2.3.7 Autophagosome closure and delivery to the vacuole

Late stages of autophagy include the completion of the phagophore elongation and its closure, resulting in a double membrane vesicle. This completed autophagosome is delivered to the vacuole.

One important factor for these last steps is the PI3P-specific phosphatase Ymr1. Hydrolyses of PI3P by this phosphatase is necessary for disassembly of Atg proteins from the completed autophagosome, allowing its fusion with the vacuole (Cebollero et al., 2012a). Atg4-dependent deconjugation of Atg8 from the mature autophagosome is also critical for efficient autophagy (Nair et al., 2012; Nakatogawa et al., 2012a).

Autophagosome docking and fusion with the vacuole is organized by the vacuolar Rab GTPase Ypt7, its GEF complex Ccz1-Mon1, the SNARE proteins Vam3, Vam7, Vti1 and Ykt6, together with the class C Vps/HOPS complex (Darsow et al., 1997; Ishihara et al., 2001; Meiling-Wesse et al., 2002; Nair et al., 2011; Rieder and Emr, 1997; Wang et al., 2002). The outer membrane of the autophagosome fuses with the vacuolar membrane, whereas the inner membrane vesicle containing the cargo enters the vacuolar lumen. This intraluminal single membrane vesicle is termed autophagic body. Depending on the activity of Atg15, a putative vacuolar lipase, and proteinase A (Pep4), the membranes of autophagic bodies are lysed, allowing vacuolar proteases to degrade the autophagic cargos (Epple et al., 2003; Epple et al., 2001; Huang et al., 2000; Takeshige et al., 1992; Teter et al., 2001). Recycling of resulting metabolites to the cytosol is mediated by the amino acid effluxer Atg22 and further vacuolar permeases (Yang et al., 2006).

## 2.4 Detailed view on Atg8 and its interaction partners

Atg8 has a N-terminal helical region and a C-terminal UBL domain (Figure 2.7C). Yeast cells contain a single gene encoding for Atg8, while mammals have eight homologs of Atg8 that are divided in the two subgroups MAP1LC3 (in short: LC3) and GABARAP based on their sequence homology. It is proposed that the members of the MAP1LC3 group, including LC3A (2 variants), LC3B and LC3C, are involved in early steps of autophagosome formation, whereas GABARAP, GABARAPL1, GABARAPL2 and

## Introduction

GABARAPL3 were shown to have functions in later stages (Weidberg et al., 2010).

Besides its role in autophagosome formation (chapter 2.3.6), lipidated Atg8 also acts as a platform to recruit selective cargos to the phagophore membrane. Especially this function has become focus of interest during the last few years. In yeast, the Cvt pathway (chapter 2.5.1), mitophagy (autophagy of mitochondria, chapter 2.5.2) and pexophagy (autophagy of peroxisomes, chapter 2.5.3) are all receptor-mediated selective pathways. Selective receptors physically link their cargos to lipidated Atg8 and the selective adapter Atg11 on the concave inner membrane of the phagophore. Selective receptors contain one or more Atg8-interacting motifs (AIMs), also called WXXL-motifs or LC3-interacting regions (LIRs), that bind the UBL domain of Atg8. Mapping and structural analyses of AIMs was first done for the mammalian sequestosome-1-like receptor p62 and the yeast Cvt pathway receptor Atg19 (Ichimura et al., 2008; Noda et al., 2008; Pankiv et al., 2007). Soon after, many further AIM/LIR-containing proteins were identified (Figure 2.7A). The consensus sequence of canonical AIMs is  $W_0/F_0/Y_0-X_{+1}-X_{+2}-L_{+3}/I_{+3}/V_{+3}$ , indicating that an aromatic amino acid at position 0 and a hydrophobic amino acid at position +3 are strictly required (Birgisdottir et al., 2013). Acidic residues and phosphorylation sites often accumulate closely to AIMs, because negatively charged residues increase the affinity to Atg8 (Figure 2.7B) (Alemu et al., 2012; Birgisdottir et al., 2013; Farré et al., 2013; Noda et al., 2008; Noda et al., 2010). Nonetheless, there also exist cryptic AIM variants. Recently, the Cvt receptor Atg19 was shown to have functional cryptic AIMs in addition to the conventional very C-terminal AIM (see chapter 2.5.1) (Noda et al., 2008; Sawa-Makarska et al., 2014).

In yeast, four selective receptors are known, including the Cvt pathway receptors Atg19 and Atg34, the mitophagy receptor Atg32 and the pexophagy receptor Atg36 (in *Pichia pastoris* pPATg30) (Farré et al., 2013; Farré et al., 2008; Kanki et al., 2009; Okamoto et al., 2009; Shintani et al., 2002; Watanabe et al., 2010).

In mammals, typical examples for AIM-containing selective receptors are the sequestosome-1-like receptors (SLRs) p62, NBR1, optineurin and NDP52/CALCO2. p62 and NBR1 are involved in aggrephagy and pexophagy (Deosaran et al., 2013; Kirkin et al., 2009a). Xenophagy (autophagy of intracellular microbes) is also mediated by p62, but in this case together with NDP52 and optineurin (Thurston et al., 2009; Wild et al., 2011).

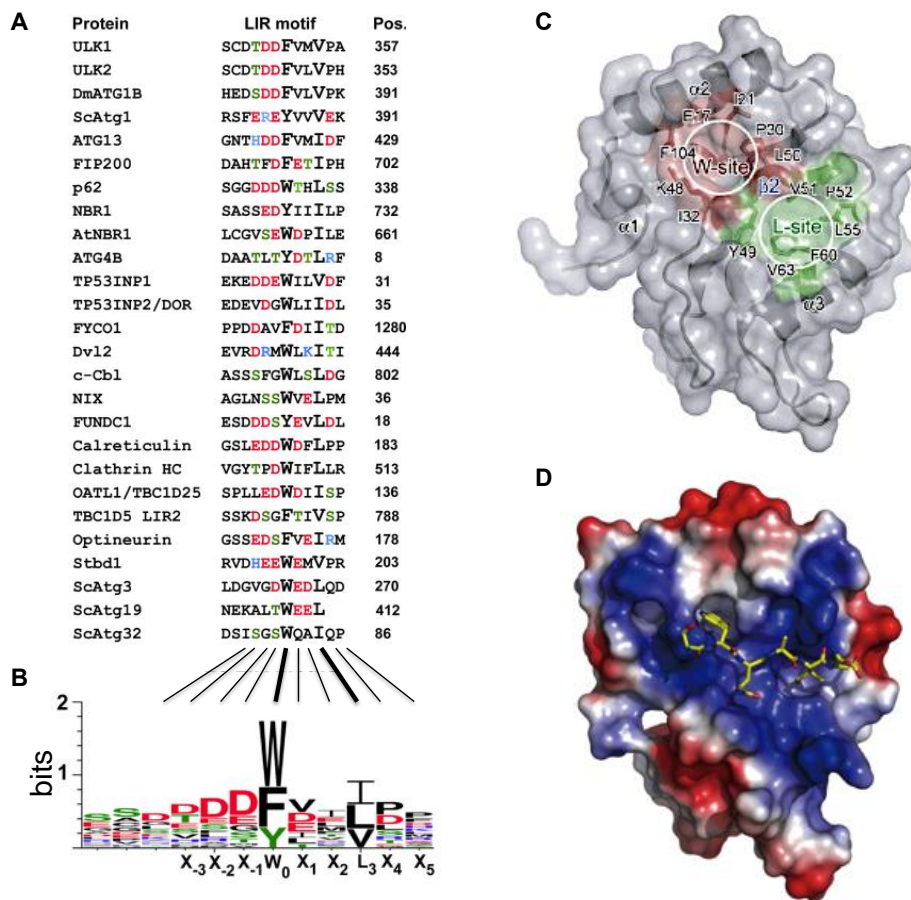


**Figure 2.7 AIM-containing Atg8 interactors**

(A) Sequence alignment of 26 published AIMs (black=hydrophobic; red=acidic; blue=basic; green=hydroxyl group)(modified from (Alemu et al., 2012)).

(B) Sequence logo of the sequences in (A). The total height of the stack shows the sequence conservation at the respective position. The height of the letter within the stack indicates the relative frequency of the amino acid (modified from (Alemu et al., 2012))

(C) Structure of Atg8. The W-site/HP1 (red) binds the aromatic residue on position 0, whereas the L-site/HP2 mediates interaction with the hydrophobic residue on position +3 of AIMs (Noda et al., 2010).

(D) Atg8 (surface model) in complex with the AIM of Atg32 (S<sub>-1</sub>W<sub>0</sub>Q<sub>+1</sub>A<sub>+2</sub>L<sub>+3</sub>; stick model). The colours of the surface indicate the electrostatic potential (blue=positive; red=negative) (Kondo-Okamoto et al., 2012).

However, many AIMs were identified in autophagic core proteins that have no receptor function. It was shown for the E2-like protein Atg3 to interact with Atg8 via an AIM. This interaction might liberate Atg8 from its complex with Atg19, leading to PE-conjugation during the Cvt pathway (Yamaguchi et al., 2010). The AIM in mammalian ATG4B has a regulatory function that promotes its Atg8-deconjugation activity (Satoo et al., 2009). Furthermore, it was published in two independent studies that the serine/threonine kinase Atg1 AIM-dependently interacts with Atg8. This interaction seems to be relevant for the Cvt pathway (chapter 2.5.1) and late stages of autophagosome biogenesis, but the exact function remains elusive (Kraft et al., 2012;

## Introduction

Nakatogawa et al., 2012b). In mammals, the AIM in ULK1/2, the ortholog of yeast Atg1, has a preference for the mammalian Atg8-subfamily GABARAP that might stabilize the ULK complex on the phagophore (Alemu et al., 2012). Recently, Kaufmann et al (2014) showed a direct interaction between Atg8 and Atg12 based on a non-canonical, non-contiguous AIM, where Phe185 and Ile111 of Atg12 three-dimensionally form the critical distance analogous to the aromatic residue on position 0 and the hydrophobic residue on position +3 of canonical AIMs. It is thought that the Atg8-Atg12 interaction might stabilize the proposed Atg12-Atg5/Atg16 membrane coat (chapter 2.3.6) (Kaufmann et al., 2014).

Regarding the structure, Atg8 and its orthologs have a N-terminal helical arm (1-24) and a C-terminal UBL domain (25-117). The UBL domain forms two hydrophobic pockets for AIM binding. One hydrophobic pocket, named W-site or HP1, is located at the interface between the second  $\beta$ -sheet ( $\beta$ 2) and the second alpha-helix ( $\alpha$ 2). The other hydrophobic pocket, called L-site or HP2, is formed between the second  $\beta$ -sheet ( $\beta$ 2) and the third alpha helix ( $\alpha$ 3) of Atg8. The W-site binds the aromatic residue on position 0, whereas the L-site mediates interaction with the hydrophobic residue on position +3 of AIMs (Figure 2.7C and D) (Klionsky and Schulman, 2014; Noda et al., 2010). Besides these hydrophobic interactions, there also exist many examples for electrostatic attractions to increase the affinity: It was published that the acidic residues on the relative positions +1 and +2 of the very C-terminal AIM of Atg19 (A<sub>-3</sub>L<sub>-2</sub>T<sub>-1</sub>W<sub>0</sub>E<sub>+1</sub>E<sub>+2</sub>L<sub>+3</sub>) interact with the basic residues R67 and R28 of the UBL domain of Atg8 (Noda et al., 2008). But it was also shown that neutral, polar residues, such as the glutamine on relative position +1 of the Atg32 AIM (S<sub>-3</sub>G<sub>-2</sub>S<sub>-1</sub>W<sub>0</sub>Q<sub>+1</sub>A<sub>+2</sub>L<sub>+3</sub>), are involved in electrostatic interaction (Figure 2.7D) (Kondo-Okamoto et al., 2012). In mammals, the basic residues R10 and R11 of the N-terminal arm of LC3B bind the acidic residues on the relative position -2 and -1 of the p62 AIM (D<sub>-3</sub>D<sub>-2</sub>D<sub>-1</sub>W<sub>0</sub>T<sub>+1</sub>H<sub>+2</sub>L<sub>+3</sub>), or the phosphorylated serine on the relative position -1 of the optineurin AIM (E<sub>-3</sub>D<sub>-2</sub>Sp<sub>-1</sub>F<sub>0</sub>V<sub>+1</sub>E<sub>+2</sub>I<sub>+3</sub>) (Ichimura et al., 2008; Noda et al., 2010; Wild et al., 2011). Yeast Atg8 has no basic residues on these positions. Thus, K46 and K48 or (positively charged) amino acids on other sites might fulfill this function (Noda et al., 2010).

The non-UBL N-terminal region is necessary for efficient autophagy (Nakatogawa et al., 2007). A conformational polymorphism of this region was detected by NMR spectroscopy analysis. It has been proposed that this feature might be important for

Atg8 oligomerisation (Schwarten et al., 2010). Furthermore, interaction studies revealed that the FK motif (F5K6), a highly conserved sequence in this region, mediates complex formation with the Cdc48 adaptor Shp1 (Krick et al., 2010). This interaction plays a role during autophagosome biogenesis (Krick et al., 2011).

## 2.5 Selective autophagy

Originally, autophagy was defined as a non-selective, bulk degradation pathway initiated by starvation. However, especially in the last decade, genetic screens investigating yeast mutants that only affect specific degradation of organelles, but not non-selective, bulk autophagy, increased the evidence of selective autophagic pathways.

### 2.5.1 The Cvt pathway as a role model for selective autophagy

The cytoplasm to vacuole targeting (Cvt) pathway was the first discovered selective autophagic mechanism and is thus also the best-characterized (Baba et al., 1997; Harding et al., 1995). However, the Cvt pathway is a constitutive and biosynthetic process that selectively targets resident hydrolases to the vacuole. It is categorized as selective autophagy, because it requires the autophagic core machinery and is mechanistically equivalent to the other receptor-mediated selective pathways such as mitophagy (chapter 2.5.2) or pexophagy (chapter 2.5.3).

Cvt vesicles are formed in the cytosol to delivery their cargos, including the resident enzymes aminopeptidase 1 (Ape1),  $\alpha$ -mannosidase (Ams1) and aspartyl aminopeptidase (Ape4), to the vacuole, where they fulfill their functions (Hutchins and Klionsky, 2001; Klionsky et al., 1992; Yuga et al., 2011). Morphologically, a Cvt vesicle is about 150 nm in diameter and, therefore, much smaller than an autophagosome with a size range of about 300-900 nm (Baba et al., 1997).

The precursor of aminopeptidase 1 (prApe1) is a key component for the assembly of the Cvt complex. First, prApe1 self-assembles to dodecameric complexes (Figure 2.8A). Then, this dodecamers generate the complete Ape1 complex (Figure 2.8B). Moreover, oligomers of Ape4 and Ams1 dock on the prApe1 complex by interaction with the Cvt receptor Atg19 to complete the cargo composition of the Cvt complex (Figure 2.8C). It was shown that Atg19 first interacts with the cargos, subsequently, with Atg11 and finally with Atg8 for Cvt complex recruitment to the phagophore (Figure 2.8D and E)

## Introduction

(Scott et al., 2001; Shintani et al., 2002; Uetz et al., 2000; Yorimitsu and Klionsky, 2005). Atg34, a secondary Cvt receptor and homolog of Atg19, has similar properties as Atg19 regarding its interaction with Ams1, Atg11 and Atg8, but only substitutes Atg19 as an Ams1 receptor during starvation (Suzuki et al., 2010).

Detailed interaction studies showed that the coiled-coiled domain of Atg19 (amino acid 153-191) binds the propeptide of prApe1 and thereby associates with the Cvt complex (Shintani et al., 2002). More C-terminally in Atg19, a region mediates interaction with Ams1. Complex formation with Atg11 and Atg8 depends on sequences of the C-terminal region of Atg19 (Shintani et al., 2002). Recent studies showed that the essential kinase Hrr25 phosphorylates Atg19 in the Atg11-binding site and that this post-translational modification promotes interaction with Atg11, suggesting a phosphoregulation of the Cvt pathway (Pfaffenwimmer et al., 2014; Tanaka et al., 2014; Yorimitsu and Klionsky, 2005). Interaction with Atg8 is mediated by the very C-terminal canonical AIM and recently discovered cryptic AIMs (Sawa-Makarska et al., 2014; Shintani et al., 2002). Sawa-Makarska et al. (2014) demonstrated that these multiple Atg8 interaction sites in Atg19 are activated due to the interaction with the propeptide of Ape1. Further experiments in this study using giant unilamellar vesicles (GUVs) as *in vitro* model system suggested that the multiple AIMs in Atg19 help to tightly wrap the Atg8-positive isolation membrane around the cargo for exclusion of non-specific material (Sawa-Makarska et al., 2014).

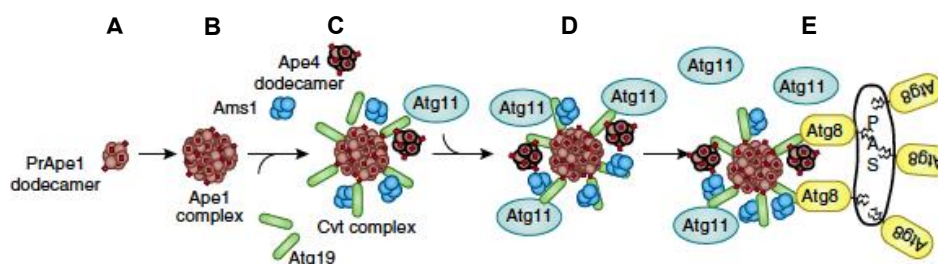


**Figure 2.8 The Cvt pathway (modified from (Klionsky and Schulman, 2014))**

(A) prApe1 self-assembles to dodecameric complexes. (B) Subsequently, dodecameric complexes aggregate to the Ape1 complex. (C) Oligomers of Ape4 and Ams1 interact with the Cvt receptor Atg19 and, thereby, dock on the prApe1 complex to complete the cargo composition of the Cvt complex. (D and E) Atg19 links the cargos to Atg11 and Atg8 for Cvt complex recruitment to the phagophore.

Another important component of the Cvt pathway is Atg21, which is a homolog of Atg18 and, consequently, belongs to the PROPPIN family (chapter 2.3.5) (Dove et al., 2009; Krick et al., 2006; Nair et al., 2010; Stromhaug et al., 2004). Atg21 is essential for the Cvt pathway and necessary for efficient starvation-induced autophagy (Meiling-Wesse et al.,

2004). It was shown that Atg21 recruits Atg5 and Atg8 to the PAS and that lipidation of Atg8 is reduced in the absence of Atg21 (Meiling-Wesse et al., 2004; Stromhaug et al., 2004).

Cvt vesicles are formed and targeted to the vacuole by the same mechanisms as described for unselective, bulk autophagy (chapter 2.3.7) (Lynch-Day and Klionsky, 2010). In the vacuole, the N-terminal propeptide of Ape1 is cleaved off to activate its hydrolytic activity (Klionsky et al., 1992).

### 2.5.2 Mitophagy

The autophagic transport of surplus or dysfunctional mitochondria to the vacuole is named mitophagy. During respiration, mitochondria produce reactive oxygen species (ROS) as byproducts. Excess of ROS is hazardous for mitochondria since they cause damage in these organelles. Mitophagy might act as a cellular reaction to oxidative stress for elimination of dysfunctional mitochondria to maintain the cellular homeostasis (Liu et al., 2014; Okamoto, 2014).

The mitogen-activated protein (MAP) kinases Slt2 and Hog1 as components of two distinct MAPK cascades are mitophagy-inducing regulators, but it remained unclear whether they have direct substrates in the mitophagy-organising machinery (Mao et al., 2011).

Regarding the membrane origin of mitophagosomes, recent studies indicate that the ER-mitochondria encounter structure (ERMES), a site that connects ER and mitochondria, is necessary for mitophagy, but not for unselective macroautophagy (Bockler and Westermann, 2014). For mammalian cells, Hamasaki et al. (2013) recently published that ERMES might be the origin of autophagosome biogenesis in general (Hamasaki et al., 2013).

Upon oxidative stress, expression of the mitophagy receptor Atg32 is highly induced (Okamoto et al., 2009). As for the Cvt receptor Atg19, the molecular function of Atg32 can be best described by focusing on the domain structure and its interaction partners: The N-terminal domain is cytosolic, whereas the C-terminal end is exposed to the intermembrane space (IMS) of mitochondria; an outer-membrane(OM)-spanning helical domain connects both domains and thus anchors Atg32 to mitochondria (Okamoto et al., 2009). The cytosolic domain contains a module for recruiting Atg8 and Atg11 via an AIM or an Atg11-binding consensus sequence, respectively (Farré et al., 2013; Kondo-



## Introduction

Okamoto et al., 2012). Similar to Atg19, Atg32 becomes phosphorylated in the Atg11 binding site to increase the affinity for Atg11. The housekeeping kinase casein kinase (CK) 2 seems to be responsible for this phosphorylation and is essential for mitophagy (Aoki et al., 2011; Kanki et al., 2013).

Complex formation of Atg32 and Atg11 links mitochondria to the autophagic machinery. Additionally, Atg11 recruits the dynamin-related GTPase Dnm1 and further components of the mitochondrial fission machinery. In this context, it was hypothesized that the fission machinery generates small mitochondria fragments for its degradation by mitophagy (Mao et al., 2013b).

It was published for the C-terminal IMS domain of Atg32 that this region is proteolytic processed by the mitochondrial i-AAA protease Yme1. Interaction studies suggested that this post-translational modification acts as a further enhancer for Atg11 binding and thus positively regulates mitophagy (Wang et al., 2013b). However, the function of Yme1 is still under debate: in another study, a slightly increased level of mitophagy was demonstrated by deletion of *YME1* (Welter et al., 2013).

### 2.5.3 Pexophagy and Atg26

#### 2.5.3.1 Pexophagy in different yeast species

The main metabolic functions of peroxisomes are (catalytic)  $\beta$ -oxidation of long-chain fatty acids and  $H_2O_2$  detoxification by conversion into oxygen and water. Peroxisomes are highly dynamic organelles. Their abundance can be rapidly altered in response to environmental changes. One mechanism to drastically reduce surplus peroxisomes is pexophagy. For *S. cerevisiae*, it was shown that growth on medium containing oleic acid as the sole carbon source causes proliferation of peroxisomes. When shifted to nitrogen starvation medium with glucose as carbon source, such a high number of peroxisomes is no longer economical and thus pexophagy is induced (Hutchins et al., 1999).

In this selective autophagy pathway, Atg36 functions as selective receptor analogous to Atg19 or Atg32 (Motley et al., 2012). Atg36 becomes anchored to peroxisomes by Pex3, a peroxisomal membrane protein (PMP) necessary for peroxisome biogenesis (Ma et al., 2011). As other receptors, Atg36 interacts with Atg8 and Atg11 for cargo linkage to the phagophore and to the autophagic machinery (Farré et al., 2013; Motley et al., 2012).

Most of the knowledge concerning pexophagy derives from investigation in the methylotrophic yeasts *Pichia pastoris*, *Yarrowia lipolytica* and *Hansenula polymorpha*. In

## Introduction

these organisms, methanolic media induce high enzymatic activity of the peroxisomal alcohol oxidase that utilize methanol as carbon source. Thus, shift to other carbon sources needs broad alteration in metabolism. The regulation of pexophagy in these fungi is more complex, depending on the carbon source, the ATP level and the specific organism (Ano et al., 2005). For example, if *P. pastoris* is transferred from methanol to glucose, micropexophagy is initiated to degrade large peroxisomes, whereas growth on ethanol induces degradation of peroxisomes by macropexophagy (Figure 2.8) (Tuttle and Dunn, 1995). Interestingly, micropexophagy seems to combine mechanisms of micro- and macroautophagy (Figure 2.8B): Analogous to microautophagy, clusters of peroxisomes were engulfed by a vacuolar protrusion, named vacuolar sequestering membrane (VSM), that often septates during this process. In parallel, the micropexophagic apparatus (MIPA) is initiated at the PAS and forms a cup-shaped double-membrane along the removed peroxisomes equivalent to the macroautophagic isolation membrane. Thereby, MIPA links the tips of the VSM (Farré et al., 2009; Mukaiyama et al., 2004; Oku et al., 2003).

In *P. pastoris*, the functional homolog to *ScAtg36* is *Ppatg30*, which correspondingly interacts Pex3 and additionally with Pex14, a further peroxisomal membrane protein. As receptor, Atg30 binds *Ppatg8* and *Ppatg11*. Furthermore, an interaction with the scaffold *Ppatg17* was published (Farré et al., 2008; Farré et al., 2013).

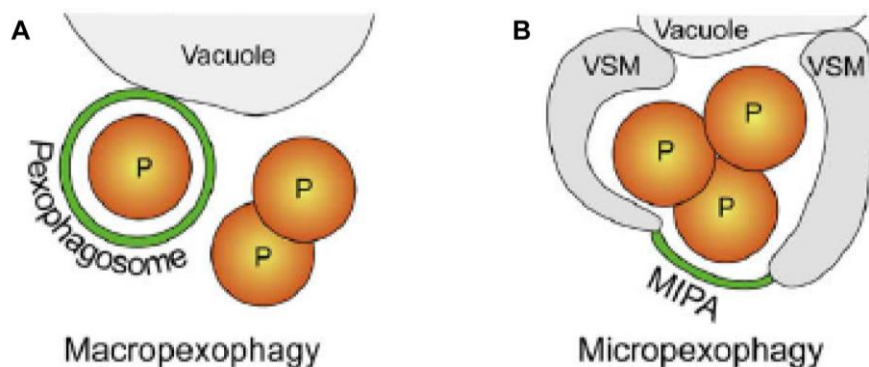


**Figure 2.9 Pexophagy in *Pichia pastoris* (modified from (Manjithaya et al., 2010))**

(A) Macropexophagy. Pexophagosomes are formed around peroxisomes.

(B) Micropexophagy. Clusters of peroxisomes are engulfed by the vacuolar sequestering membrane (VSM). MIPA links the tips of the VSM by forming a cup-shaped double-membrane along the removed peroxisomes.

### 2.5.3.2 Atg26

Atg26 (Ugt51/PAZ4/PDG3) is described as an autophagy-related protein, because of its involvement in pexophagy in the methylotrophic yeast *Pichia pastoris* (*Pp*) (Mukaiyama et al., 2002; Oku et al., 2003). In this model organism, *PpAtg26* is essential for degradation of large methanol-induced peroxisomes by micropexophagy. It is only partially involved in macropexophagic removal of medium-sized, oleate-induced peroxisomes and dispensable for pexophagy of small peroxisomes (Nazarko et al., 2009).

Atg26 is a large, 136 kDa protein containing a C-terminal sterol glucoside (SG) transferase (UDP-glucose:sterol  $\beta$ -D-glucosyltransferase, short: UGT) domain. UGT domains catalyse the transfer of activated sugar molecules to sterols. Glycosylation increases the water solubility of otherwise lipophilic membrane sterols. Investigation of the enzymatic activity in different species revealed that the substrate specificity is relatively constricted concerning UDP-activated sugar, which is predominantly UDP-glucose, whereas the acceptor sterols are divers (Chaturvedi et al., 2011; Warnecke et al., 1999). In general, the direct effectors of SG are unknown and the physiological function of SGs or UGTs, respectively, are divers. In many cases, production of SG is a stress response (Chaturvedi et al., 2011).

However, in the case of Atg26 from *P. pastoris*, it was published that, during micropexophagy, production of SG by *PpAtg26* facilitates elongation of the large double membrane structures of the MIPA (see chapter 2.5.3). In this context, it has been proposed that glucose residues of SGs protrudes into the soluble phase of the membrane and act as scaffolds for further elongation reaction (Mukaiyama et al., 2004; Nazarko et al., 2007a; Yamashita et al., 2006).

*PpAtg26* locates PI4P-dependently to the MIPA during micropexophagy (Figure 2.9B), but also to the isolation membrane of pexophagosomes during macropexophagy of medium-sized peroxisomes (Figure 2.9A). The lipid PI4P is generated at the PAS by the PI4P kinase Pik4 (Yamashita et al., 2006; Yamashita et al., 2007). The GRAM (glucosyltransferase, Rab-like GTPase activators, and myo-tubularins) domain of *PpAtg26* mediates direct interaction with PI4P and, thereby, MIPA/PAS recruitment of Atg26 (Oku et al., 2003; Yamashita et al., 2006). Sequence analyses also predicted a PH domain in the N-terminal region of Atg26. PH domains were shown to recognize PIPs (Lemmon, 2008). However, the putative affinity to specific lipids, the target membrane

and the concrete physiological function of the PH domain in (*Pp*)Atg26 have to be elucidated (Nazarko et al., 2007b; Oku et al., 2003; Stasyk et al., 2003; Yu et al., 2004).

A further species that implicates Atg26 in pexophagy is the plant pathogenic fungus *Colletotrichum orbiculare*. Remarkable, degradation of peroxisomes in the fungal infection structure is necessary for host invasion. It was further shown that *CoAtg26* enhances pexophagy in this structure and, consequently, acts as an important factor for the pathogenicity of this fungus (Asakura et al., 2009).

In addition to the function in pexophagy and pexophagy-dependent host invasion, Atg26 was shown to be necessary for efficient Ape1 maturation in *P. pastoris* (Farré et al., 2007; Nazarko et al., 2007a).

In *S. cerevisiae*, no function of Atg26 in autophagy or in other cellular processes has been shown. But, its involvement in unselective macroautophagy, the Cvt pathway, pexophagy, mitophagy and PMN has been excluded in previous studies (Cao and Klionsky, 2007; Krick et al., 2008b; Okamoto et al., 2009).

### 2.5.4 Further selective pathways in yeast

Nucleophagy, ribophagy, ER-phagy, lipophagy and autophagy of retrotransposon virus-like particles are further selective autophagic pathways in *S. cerevisiae*.

During **nucleophagy**, small parts of the nucleus are invaginated by the vacuolar membrane. This process is also called piecemeal microautophagy of the nucleus (PMN) and involves the autophagic core machinery (Krick et al., 2008b; Roberts et al., 2003). Morphological studies showed that PMN occurs on nucleus-vacuole junctions (NVJs), where non-essential parts of the nucleus pinch-off into the vacuole lumen. NVJ formation needs the interaction between the outer nuclear membrane protein Nvj1 and the Armadillo-repeat protein Vac8, a multifunctional scaffold myristylated to the vacuolar membrane (Pan and Goldfarb, 1998; Pan et al., 2000).

**Ribophagy** is a selective autophagic mechanism to eliminate excess of ribosomes during nutrient depletion. The selectivity of this pathway was demonstrated by the involvement of ubiquitin ligase Rsp5 and the ubiquitin protease Ubp3/Bre5, which are both not required for unselective, bulk macroautophagy (Kraft et al., 2008). Whether ubiquitylation of ribosomes is necessary for this process or whether selective receptors are involved in cargo recognition remains unclear.

The early secretory pathway starts with the passage through the endoplasmic reticulum

## Introduction

(ER) where integral or secretory proteins are folded and modified. Excess of unfolded proteins leads to ER stress that stimulates the unfolded protein response (UPS) for thorough remodelling of the ER (Bernales et al., 2006b). For supporting UPS, damaged ER becomes enclosed by an autophagosome-like structure, a process termed **ER-phagy/reticulophagy** (Bernales et al., 2006a; Yorimitsu et al., 2006). Notably, autophagic proteins are essential for survival under ER stress condition, but not vacuolar proteases. Thus, only sequestration of damaged ER seems to be the central function of this selective pathway (Bernales et al., 2006a). Upon nitrogen starvation, ER is also transported to the vacuole by macroautophagy with a higher abundance than cytosolic material, indicating a selective mechanism for enhanced ER uptake (Hamasaki et al., 2005). To further support selectivity, it was shown for ER-stress- and starvation-induced ER-phagy that Atg11, Atg19, Atg20 and the actin cytoskeleton are involved. These factors are all indicators for selective autophagy (Bernales et al., 2006a; Hamasaki et al., 2005; Lipatova et al., 2013; Mazon et al., 2007).

**Lipophagy** describes an autophagic pathway that selectively transports lipid storage organelles, called lipid droplets, to the vacuole for their degradation. Fatty acids are stored as triacylglycerols (TAGs). Under nutrient-rich conditions or excess of fatty acids, TAGs together with sterol esters and further components are bundled in lipid droplets (LDs) (Walther and Farese, 2012). Recently, van Zutphen et al. (2014) discovered in yeast that lipid droplet can be degraded by selective microautophagy during nitrogen starvation (van Zutphen et al., 2014). This process involves the autophagic core machinery and especially the putative vacuolar lipase Atg15 that might be necessary for degradation of invaginated LDs. Equivalent to further microautophagic pathways, Vac8 was shown to be essential for lipophagy (Oku et al., 2006; Roberts et al., 2003; van Zutphen et al., 2014).

A further selective pathway described in yeast is **autophagy of virus-like particles (VLP)** of the retrotransposon Ty1. Retrotransposons are transposable DNA elements that are transcribed as RNA intermediates. Ty1 is the most abundant retrotransposon in yeast. Its RNA encodes the coat proteins p49Gag and the fusion protein p199Gag-Pol, including the coat protein Gag and a reverse-transcriptase as C-terminal part. The Ty1 virus-like particle functions as a protecting cage for reverse transcription of Ty1 mRNA back to cDNA. Finally, the Ty1 cDNA can insert at a further site of the host DNA and thereby generates mutations (Beauregard et al., 2008). Recently, Suzuki et al. (2011)

## Introduction

showed that Ty1 VLPs are degraded during starvation by selective autophagy in an Atg19-dependent mechanism (Suzuki et al., 2011). In addition, Atg11 and Ape1 are required for this kind of selective autophagy. It was further demonstrated via IEM and fluorescence microscopy that in wild type cells Ty1 VLPs surround the Ape1 complex, whereas absence of Atg19 causes clustering of VLPs beyond the Ape1 complex. These observations altogether suggest a model, where Atg19 facilitates recruitment of Ty1 VLP clusters to the Cvt complex for their autophagic degradation and, thus, down-regulates Ty1 transposition (Suzuki et al., 2011).

### 2.6 *Saccharomyces cerevisiae* virus L-A

The *S. cerevisiae* virus L-A is a dsRNA virus of the *Totiviridea* family. It has a single 4.6 kb genomic segment with two overlapping ORFs. ORF1 encodes the 76 kDa major capsid protein Gag that is necessary for encapsidation. ORF2 is a RNA-dependent RNA polymerase (Pol) that is expressed as a 180 kDa Gag-Pol fusion protein caused by a -1 ribosomal frameshift (Figure 2.10) (Dinman et al., 1991). The 39-nm icosahedral architecture of the L-A virus-like particle (VLP) is made up of about 120 Gag subunits (from which about 2 are Gag-Pol fusion proteins) and functions as a specialized, protecting compartment for replication and transcription of the dsRNA located inside the VLP (Naitow et al., 2002; Wickner et al., 2013). As shown for other dsRNA viruses, the L-A VLP has a T=1 structure, which is a lattice of 60 asymmetric dimers of Gag as one unit (Figure 2.11A) (Castón et al., 1997; Luque et al., 2010; Naitow et al., 2002).

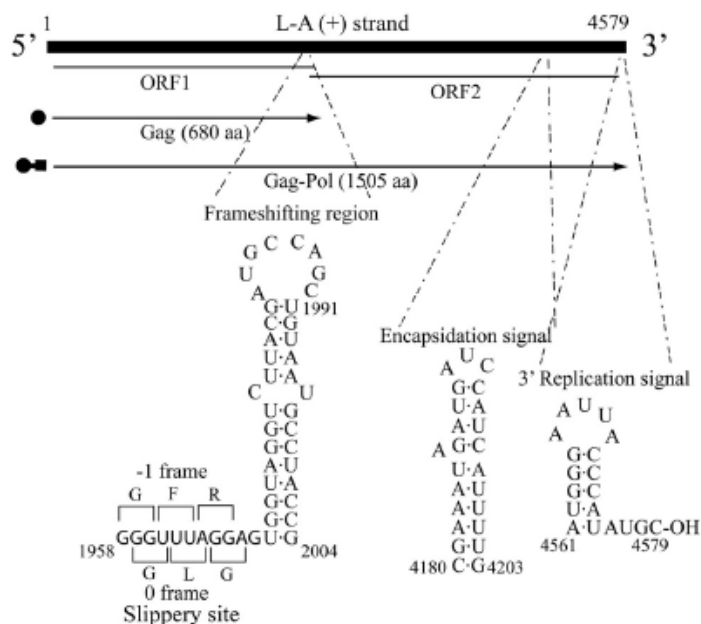


**Figure 2.10 L-A (+) strand, encoded proteins and cis signals with secondary structures (from (Rodríguez-Cousiño et al., 2013))**

The (+) transcript encodes two overlapping ORFs. ORF1 encodes the major coat protein Gag. ORF2 encodes Pol that is expressed as a Gag-Pol fusion protein caused by a -1 ribosomal frameshift (frameshifting region). Gag-Pol binds the encapsidation signal to incorporate (+) transcripts in L-A VLPs. Replication is initiated by the 3' replication signal.

## Introduction

Single-stranded (+) transcripts are synthesized inside the coat, using the dsRNA genome as template, and then extruded from the virus particle for translation and/or formation of new VLPs (Figure 2.11C). For efficient translation and the stability of single stranded (+) RNA, the virus uses a cap-snatching mechanism, where the m<sup>7</sup>Gp moiety of the host mRNA is transferred to the diphosphorylated 5' end of the viral transcript by the enzymatic activity of Gag. This mechanism occurs outside the particle, where Gag exposes a trench-like structure as active site. In this trench, the m<sup>7</sup>Gp moiety of the host mRNA becomes covalently attached to His154, forming a m<sup>7</sup>Gp-Gag intermediate, and is then transferred to the virus (+) RNA (Figure 2.11B and C) (Blanc et al., 1992; Fujimura and Esteban, 2013; Fujimura and Esteban, 2011).

During this post-transcriptional phase, the 5' exonuclease activity of Xrn1/SKI1/KEM1, specific for uncapped RNA, acts as defence against L-A transcripts (Figure 2.11C). Increased L-A proliferation was shown when *XRN1* is deleted. Vice versa, overexpression of Xrn1 can be used to eliminate L-A (Esteban et al., 2008; Masison et al., 1995). These virus-specific phenotypes obviously indicated that the cap-snatching mechanism is not 100% efficient. Further proteins with anti-viral activity are Ski2, 3, 6, 7 and 8 that inhibit translation of non-polyA mRNA such as the L-A (+) transcripts (Benard et al., 1998; Benard et al., 1999; Masison et al., 1995). Also in the context of translation, some 60S ribosomal subunit associated proteins were shown to promote the virus copy number (Edskes et al., 1998; Ohtake et al., 1995).

After translation of the virus transcripts, the products Gag and Gag-Pol act as building blocks for L-A VLPs. At this step of the replication cycle, again some of the host genes are involved: *MAK3*, *MAK10* and *MAK31* encode a N-acetyltransferase complex that acetylates the first methionine of Gag and thereby promotes Gag stability and virus assembly (Tercero and Wickner, 1992; Tercero et al., 1993).

For formation of new virus-like particles, the Gag-Pol fusion protein recognizes an encapsidation signal of the viral (+) transcript, located 400 nt from the 3' end forming a stem-loop (Figure 2.10). Addition of Gag as building blocks results in formation of the viral coat, containing a single (+) transcript (Fujimura et al., 1992a; Ribas et al., 1994). However, Gag is also sufficient for coat formation without Gag-Pol (Fujimura et al., 1992b; Powilleit et al., 2007). Gag-Pol synthesizes a new (-) transcript to generate a novel dsRNA genome inside the emerging virus particle, completing the replication cycle (Figure 2.11C).

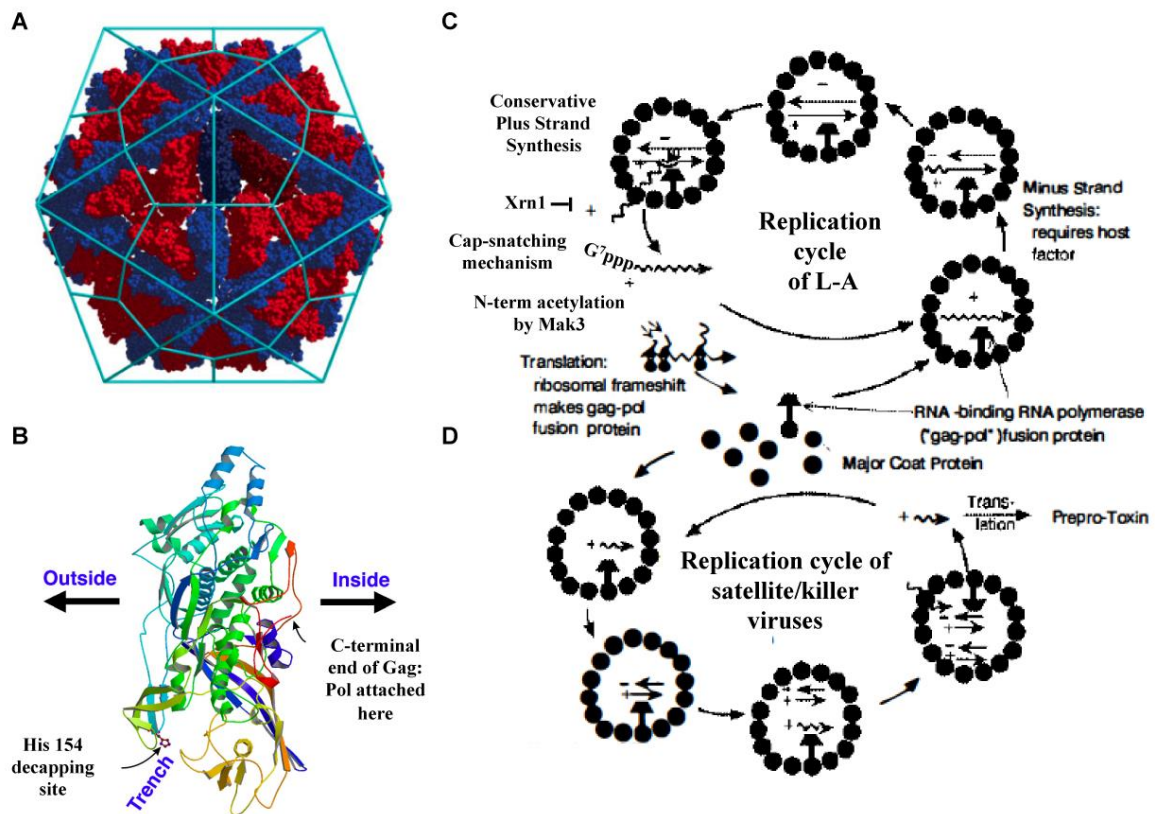


**Figure 2.11** *S. cerevisiae* virus L-A

(A) Structure of the whole L-A capsid (VLP). Lines indicate the icosahedral architecture, formed by 120 Gag subunits, where about two are Gag-Pol fusion proteins. Molecules marked in blue or red indicate two different structural forms of Gag that build a T=1 lattice of 60 asymmetric dimers of Gag (from (Tang et al., 2005)).

(B) Structure of the major coat protein Gag. The enzymatic trench is outside the VLP, whereas the N-terminus and C-terminus (extended as Gag-Pol) are exposed inside the VLP (modified from (Naitow et al., 2002)).

(C and D) Replication cycle of the L-A virus and satellite/killer viruses (modified from (Wickner, 1992)).

Like other fungal viruses, the L-A virus has no extracellular mechanism of infection. Therefore, vertical cytoplasmic transmission from mother to daughter cells and horizontal transmission during mating are the ways of infection. It is important to mention that L-A can act as a helper virus for satellite viruses that encode the propeptides of killer toxins (prepro-toxin) (Figure 2.11D). The processed peptide is secreted by infected host strains and kills non-infected strains. The satellite viruses use the multifunctional building blocks Gag and Gag-Pol of L-A for their own replication (Figure 2.11D). Therefore, yeast strains carrying a killer virus and L-A, as necessary helper virus, have a selective advantage over non-infected strains (Schmitt and Breinig, 2006; Wickner et al., 2013).



### 2.7 Aim of the thesis

Atg8 is a key component of the autophagic machinery, necessary for autophagosome biogenesis. Furthermore, Atg8 mediates cargo recognition during selective autophagy (Klionsky and Schulman, 2014). Therefore, Atg8 is an ideal bait for proteomic approaches to find new proteins that are involved in autophagy or related processes. A central goal of this study was to establish a CoIP protocol with Atg8 as bait to capture new Atg8 binding partners for their identification in following MS analysis.

By MS analysis of this study, Atg26 was identified as an Atg8 interaction partner, indicating that Atg26 might be involved in autophagic processes in *S. cerevisiae*. It was shown that Atg26 is involved in mirco- and macropexophagy in *P. pastoris* (Oku et al., 2003; Yamashita et al., 2006), whereas its function in *S. cerevisiae* was unknown so far (Cao and Klionsky, 2007; Krick et al., 2008b; Okamoto et al., 2009). Therefore, a further aim of this study was the analysis of the autophagic function of Atg26 in *S. cerevisiae*.

## 3 Materials and Methods

### 3.1 Materials

#### 3.1.1 Yeast strains

**Table 3.1** Yeast strains

<i>S. cerevisiae</i> strains	Genotype	Reference
WCG4	WCG4a MAT $\alpha$ <i>his 2-11,15 leu 2-3,112 ura 3</i>	AG Thumm (University Göttingen)
<i>ape1</i> $\Delta$	WCG4a MAT $\alpha$ <i>his 2-11,15 leu 2-3,112 ura 3</i> <i>ape1</i> $\Delta$ :: <i>kan</i>	AG Thumm (University Göttingen)
<i>atg1</i> $\Delta$	WCG4a MAT $\alpha$ <i>his 2-11,15 leu 2-3,112 ura 3</i> <i>atg1</i> $\Delta$ :: <i>KAN</i>	AG Thumm (University Göttingen)
<i>atg1</i> $\Delta$ <i>pep4</i>	WCG4a MAT $\alpha$ <i>his 2-11,15 leu 2-3,112 ura 3</i> <i>atg1</i> $\Delta$ :: <i>KAN pep4</i> $\Delta$ :: <i>HIS3</i>	AG Thumm (University Göttingen)
<i>atg8</i> $\Delta$	WCG4a MAT $\alpha$ <i>his 2-11,15 leu 2-3,112 ura 3</i> <i>atg8</i> $\Delta$ :: <i>KAN</i>	AG Thumm (University Göttingen)
<i>atg11</i> $\Delta$	WCG4a MAT $\alpha$ <i>his 2-11,15 leu 2-3,112 ura 3</i> <i>atg11</i> $\Delta$ :: <i>HISMX6</i>	AG Thumm (University Göttingen)
<i>atg18</i> $\Delta$	WCG4a MAT $\alpha$ <i>his 2-11,15 leu 2-3,112 ura 3</i> <i>Atg18</i> $\Delta$ :: <i>KAN</i>	AG Thumm (University Göttingen)
<i>atg19</i> $\Delta$	WCG4a MAT $\alpha$ <i>his 2-11,15 leu 2-3,112 ura 3</i> <i>atg19</i> $\Delta$ :: <i>KAN</i>	AG Thumm (University Göttingen)
<i>atg19</i> $\Delta$ <i>atg34</i> $\Delta$	WCG4a MAT $\alpha$ <i>his 2-11,15 leu 2-3,112 ura 3</i> <i>atg19</i> $\Delta$ :: <i>KAN</i>	This study
<i>atg21</i> $\Delta$	WCG4a MAT $\alpha$ <i>his 2-11,15 leu 2-3,112 ura 3</i> <i>atg21</i> $\Delta$ :: <i>KAN</i>	AG Thumm (University Göttingen)
<i>atg26</i> $\Delta$	WCG4a MAT $\alpha$ <i>his 2-11,15 leu 2-3,112 ura 3</i> <i>atg26</i> $\Delta$ :: <i>NatNT2</i>	AG Thumm (University Göttingen)
<i>atg32</i> $\Delta$	WCG4a MAT $\alpha$ <i>his 2-11,15 leu 2-3,112 ura 3</i> <i>atg32</i> $\Delta$ :: <i>NatNT3</i>	AG Thumm (University Göttingen)
<i>atg34</i> $\Delta$	WCG4a MAT $\alpha$ <i>his 2-11,15 leu 2-3,112 ura 3</i> <i>atg34</i> $\Delta$ :: <i>NatNT4</i>	This study
<i>atg36</i> $\Delta$	WCG4a MAT $\alpha$ <i>his 2-11,15 leu 2-3,112 ura 3</i> <i>atg36</i> $\Delta$ :: <i>NatNT5</i>	This study
<i>hsv2</i> $\Delta$	WCG4a MAT $\alpha$ <i>his 2-11,15 leu 2-3,112 ura 3</i> <i>ygr223c</i> $\Delta$ :: <i>kanMX6</i>	AG Thumm (University Göttingen)
<i>hsv2</i> $\Delta$ <i>atg26</i> $\Delta$	WCG4a MAT $\alpha$ <i>his 2-11,15 leu 2-3,112 ura 3</i> <i>ygr223c</i> $\Delta$ :: <i>kanMX6 atg26</i> $\Delta$ :: <i>NatNT7</i>	AG Thumm (University Göttingen)

## Materials and Methods

<i>pep4Δ</i>	WCG4a MAT α <i>his 2-11,15 leu 2-3,112 ura 3</i> <i>pep4Δ::His</i>	AG Thumm (University Göttingen)
<i>xrn1Δ</i>	WCG4a MAT α <i>his 2-11,15 leu 2-3,112 ura 3</i> <i>xrn1Δ::NatNT7</i>	This study
<i>Sey 6210</i>	Sey 6210 MAT a <i>ura 3-52 leu 2-3,112 his 3-Δ200</i> <i>lys 2-801 trp1-Δ901 suc 2-Δ9 mel GAL</i>	G. F. von Mollard (University Bielefeld)
<i>BY4741</i>	ATTC201388 Mat a <i>ura 3 leu 2 his 3</i>	Euroscarf
<i>Atg26-GFP</i>	ATTC201388 Mat a <i>ura 3 leu 2 his 3</i> <i>ATG26-GFP::HIS3MX6</i>	Invitrogen
<i>Atg26-GFP xrn1Δ</i>	ATTC201388 Mat a <i>ura 3 leu 2 his 3</i> <i>ATG26-GFP::HIS3MX6 xrn1Δ::NatNT2</i>	Invitrogen/ This study
<i>Cop1-GFP</i>	ATTC201388 Mat a <i>ura 3 leu 2 his 3</i> <i>COP1-GFP::HIS3MX6</i>	Invitrogen
<i>Ede1-GFP</i>	ATTC201388 Mat a <i>ura 3 leu 2 his 3</i> <i>EDE1-GFP::HIS3MX6</i>	Invitrogen
<i>Enp1-GFP</i>	ATTC201388 Mat a <i>ura 3 leu 2 his 3</i> <i>ENP1-GFP::HIS3MX6</i>	Invitrogen
<i>Gyp1-GFP</i>	ATTC201388 Mat a <i>ura 3 leu 2 his 3</i> <i>GYP1-GFP::HIS3MX6</i>	Invitrogen
<i>Hsp42-GFP</i>	ATTC201388 Mat a <i>ura 3 leu 2 his 3</i> <i>HSP42-GFP::HIS3MX6</i>	Invitrogen
<i>Rio2-GFP</i>	ATTC201388 Mat a <i>ura 3 leu 2 his 3</i> <i>RIO2-GFP::HIS3MX6</i>	Invitrogen
<i>Rrp12-GFP</i>	ATTC201388 Mat a <i>ura 3 leu 2 his 3</i> <i>RRP12-GFP::HIS3MX6</i>	Invitrogen
<i>Rsp7-GFP</i>	ATTC201388 Mat a <i>ura 3 leu 2 his 3</i> <i>RSP7-GFP::HIS3MX6</i>	Invitrogen
<i>Sap185-GFP</i>	ATTC201388 Mat a <i>ura 3 leu 2 his 3</i> <i>SAP185-GFP::HIS3MX6</i>	Invitrogen
<i>Sfb3-GFP</i>	ATTC201388 Mat a <i>ura 3 leu 2 his 3</i> <i>SFB3-GFP::HIS3MX6</i>	Invitrogen
<i>Sec21-GFP</i>	ATTC201388 Mat a <i>ura 3 leu 2 his 3</i> <i>SEC21-GFP::HIS3MX6</i>	Invitrogen
<i>Sec23-GFP</i>	ATTC201388 Mat a <i>ura 3 leu 2 his 3</i> <i>SEC23-GFP::HIS3MX6</i>	Invitrogen
<i>Sec26-GFP</i>	ATTC201388 Mat a <i>ura 3 leu 2 his 3</i> <i>SEC26-GFP::HIS3MX6</i>	Invitrogen
<i>Sec27-GFP</i>	ATTC201388 Mat a <i>ura 3 leu 2 his 3</i> <i>SEC27-GFP::HIS3MX6</i>	Invitrogen

## 3.1.2 *E. coli* strains

**Table 3.2 *E. coli* strains used in this study**

<i>E. coli</i> strain	Genotype	Reference
DH5 $\alpha$	F'( $\Phi$ 80 ( $\Delta$ lacZ) M15) $\Delta$ (lacZYA-argF) U169 recA1 endA1 hsdR17 rK-mK + supE44 thi-1 gyrA relA	(Hanahan, 1983)
BL21 (DE3) pLysS	F <sup>+</sup> <i>dcm ompT hsdSB (rB-, mB-) gal</i> $\lambda$ (DE3); pLysS ( <i>CamR</i> )	Stratagene

## 3.1.3 Plasmids

**Table 3.3 Plasmids used in this study**

Name/Insert	Genotype	Reference
Atg21-TAP	pRS425 2 $\mu$ LEU2 Atg21-TAP	AG Thumm
Atg26 1-1194-Cub	pRS313 CEN6 HIS3 MET25 Atg26 1-1194-Cub-RURA3	this study
Atg26 1-186-Cub	pRS313 CEN6 HIS3 MET25 Atg26 1-186-Cub-RURA3	this study
Atg26 1-337-Cub	pRS313 CEN6 HIS3 MET25 Atg26 1-337-Cub-RURA3	this study
Atg26 1-569-Cub	pRS313 CEN6 HIS3 MET25 Atg26 1-569-Cub-RURA3	this study
Atg26 187-337-Cub	pRS313 CEN6 HIS3 MET25 Atg26 187-337-Cub-RURA3	this study
Atg26 338-1198-Cub	pRS313 CEN6 HIS3 MET25 Atg26 338-1198-Cub-RURA3	this study
Atg26-Cub	pRS313 CEN6 HIS3 MET25 Atg26 -Cub-RURA3	AG Thumm
GFP	pYES2 2 $\mu$ URA3 GFP	this study
GFP-Atg26	pUG34 CEN6 HIS3 GFP-Atg26	this study
GFP-Atg26	pUG36 CEN6 URA3 GFP-Atg26	this study
GFP-Atg26 1-1194	pUG34 CEN6 HIS3 GFP-Atg26 1-1194	this study
GFP-Atg26 1-186	pUG34 CEN6 HIS3 GFP-Atg26 1-186	this study
GFP-Atg26 1-337	pUG34 CEN6 HIS3 GFP-Atg26 1-337	this study
GFP-Atg26 1-569	pUG34 CEN6 HIS3 GFP-Atg26 1-569	this study
GFP-Atg26 1-636	pUG34 CEN6 HIS3 GFP-Atg26 1-636	this study
GFP-Atg26 1-744	pUG34 CEN6 HIS3 GFP-Atg26 1-744	this study
GFP-Atg26 187-337	pUG34 CEN6 HIS3 GFP-Atg26 187-337	this study
GFP-Atg26 187-374	pUG34 CEN6 HIS3 GFP-Atg26 187-374	this study
GFP-Atg26 187-1198	pUG34 CEN6 HIS3 GFP-Atg26 187-1198	this study
GFP-Atg26 187-569	pUG34 CEN6 HIS3 GFP-Atg26 187-569	this study
GFP-Atg26 338-1198	pUG34 CEN6 HIS3 GFP-Atg26 338-1198	this study
GFP-Atg26 338-744	pUG34 CEN6 HIS3 GFP-Atg26 338-744	this study
GFP-Atg26 570-1198	pUG34 CEN6 HIS3 GFP-Atg26 570-1198	this study
GFP-Atg26 I1198A	pUG34 CEN6 HIS3 GFP-Atg26 I1198A	this study
GFP-Atg8	pYES2 2 $\mu$ URA3 GFP-Atg8	AG Thumm
GFP-Atg8 S3AT4A	pYES2 2 $\mu$ URA3 GFP-Atg8 S3AT4A	this study
GFP-Atg8 F5GK6G	pYES2 2 $\mu$ URA3 GFP-Atg8 F5GK6G	this study

## Materials and Methods

GFP-Atg8 L50A	pYES2 2 $\mu$ URA3 GFP-Atg8 L50A	AG Thumm
GFP-Atg8 Y49A	pYES2 2 $\mu$ URA3 GFP-Atg8 Y49A	AG Thumm
GFP-LA Gag (WCG4)	pUG34 CEN6 HIS3 GFP-LA Gag	this study
GFP-LA Gag (WCG4)	pUG36 CEN6 URA3 GFP-LA Gag	this study
GFP-LA GagPol (WCG4)	pUG36 CEN6 URA3 GFP-LA GagPol	this study
GST-Atg26	pGEX 4T3 GST-Atg26	this study
GST-Atg26 187-569	pGEX 4T3 GST Atg26 187-569	this study
His-LA Gag	pPROEX htb - His-LA Gag	this study
LA Gag-Cub	pRS313 CEN6 HIS3 MET25 LA Gag-Cub-RURA3	this study
Nub-LA Gag	pRS314 CEN6 TRP1 CUP1 Nub-LA Gag	this study
LA Gag-GFP	pUG35 CEN6 URA3 LA Gag-GFP	this study
mCherry	pUG34 CEN6 HIS3 mCherry	this study
mCherry-Atg11	pUG36 CEN6 URA3 mCherry Atg11	this study
mCherry-Atg19	pUG34 CEN6 HIS3 mCherry-Atg19	this study
mCherry-Atg26	pUG34 CEN6 HIS3 mCherry-Atg26	this study
mCherry-Atg26 1-1194	pUG34 CEN6 HIS3 mCherry-Atg26 1-1194	this study
mCherry-Atg26 I1198A	pUG34 CEN6 HIS3 mCherry-Atg26 I1198A	this study
mCherry-Atg8	pUG36 CEN6 URA3 mCherry-Atg8	this study
mCherry-LA Gag	pUG36 CEN6 URA3 mCherry LA Gag	this study
Pgk1-GFP	pRS316 CEN6 URA3 Pgk1-GFP	AG Thumm

### 3.1.4 Oligonucleotides

**Table 3.4.1 Oligonucleotides for cloning and sequencing used in this study**

Name	Sequence
Atg11forBamHI	tcaggatccATGGCAGACGCTGATGAATATAG
Atg11revXhoI	TAGctcgagTCAAACCTCCCTGGTATGAAACC
Atg11Seq1	GTAGACAATGGTATGACTTCAAATGG
Atg11Seq2	CTGATTTCAAACGTCTAAACGAATATCAC
Atg11Seq3	GGTTAACTAATGAAGAACAATCGCATAG
Atg11Seq4	GGGGAATATCACTCAATTATATGACAATAAG
Atg26 Seq2 Fwd	CAACTTCGGCTGTGCCTTC
Atg26 Seq2 Rev	GAAGGCACAGCCGAAGTTG
Atg26_Cub_Sall_rev	ATTCCTACTTgtcgacCCAATCATCGTCCACCCTTCATC
Atg26_Cub_StuI_fwd	AGTAGCAATtagcctATGCCCATCACTCAAATCATATC
Atg26_L2_Cub_StuI_for	AGTAGCAATtagcctATGGCTCAGAATTCTGAAAACAATTCGATAAG
Atg26_Seq1_fwd	CAATGTGGCTAAGTTGAGAC
Atg26_Seq3_fwd	GAGGTACCGTTAATGATTG
Atg26_Seq3_rev	CAATCATTAACGGTACCTC

## Materials and Methods

Atg26_Seq4_fwd	GTTTCGATTGTAGTCTCTAATG
Atg26_Seq4_rev	CATTAGAGACTACAATCGAAC
Atg26delAIM_Cub_SalI_rev	ATTCTACTTgtcgacCCCCCTTCATCCGTTGTTTC
Atg26forBamHI	tcaggatccATGCCATCACTCAAATCATATCAGCG
Atg26L2.1forBam	tcaggatccATGGCTCAGAAATCTGAAAACAATTCGATAAG
Atg26MAP1_Cub_SalI_rev	ATTCTACTTgtcgacCCCACATTGTCTTTTGACAGTTTTTCCC
Atg26MAP2_Cub_SalI_rev	ATTCTACTTgtcgacCCTGCGAACTGCTCCTTTTTCAAAG
Atg26MAP3_Cub_SalI_rev	ATTCTACTTgtcgacCCGTTAGCAGAAACCTCTTCTGTTTC
Atg26PH_Cub_StuI_for	AGTAGCAATaggcctATGGCTAAGTTGAGACAGCGG
Atg26PHforBam	tcaggatccATGGCTAAGTTGAGACAGCGG
Atg26revXho	TAGctcgagTTAAATCATCGTCCACCCTTCATCC
Atg26woWTMlrevXhoI	TAGctcgagttaCCCTTCATCCGTTGTTTCAGC
Atg26WTMarevXhoI	TAGctcgagTTAagcCATCGTCCACCCTTCATCC
Atg8 seq 0f	GGAGGCCGGTTATTTTCGG
Atg8 seq 1f	GAAGGCCGAGTCGGAGAG
Atg8 seq 1r	CTCTCCGACTCCGCCTTC
Atg8 seq 2f	GGACGGGTTTTTGTATGTCAC
Atg8 seq 2r	GTGACATACAAAAACCCGTCC
Cherry seq for	Gg'gcctacaacgtcaacatc
<i>Cntrlxrn1</i> rev	Ctattaaagtaacctcgaataacttcg
gag_revXho	TAGctcgagTTACTCTACTAAAACATTTGTCCGC
GagCubforStuI	tcaaggcctATGCTAAGATTTGTTACTAAAACTCTCAAG
GagCubrevSal1	taggtcgacCCCTCTACTAAAACATTTGTCCGC
gagpol_forBam	tcaggatccATGCTAAGATTTGTTACTAAAACTCTC
gagpol_revXho	TAGctcgagTTACAGTATGACCTGTAATGCC
GagrevSalnonstop	TAGgtcgacCTCTACTAAAACATTTGTCCGC
GFP rev	GGTAAAAGGACAGGGCCATC
GFP seq for	Ggttctgttcaattagctgac
GFPAtg8for	tcaaagcttATGAAGTCTACATTTAAGTCTG
GFPAtg8rev	TAGCTCGAGCTACCTGCCAAATGTATTTTCTCC
Map1Atg26revXh	TAGctcgagttaCACATTGTCTTTTGACAGTTTTTCCCTAG
Map2.2Atg26revXh	TAGctcgagttaAGCTCTTAATCTCAATGTTAAAGCTTTGTTG
Map2Atg26revXh	TAGctcgagttaTGCGAACTGCTCCTTTTTCAAAG
Map3Atg26revXh	TAGctcgagttaGTTAGCAGAAACCTCTTCTGTTTC
Map4Atg26revXh	TAGctcgagttaTTCTTTATAGCATGTCTCCACATCAAC
Map5Atg26revXh	TAGctcgagttaTAATCCAAACTTATAACTCTTGTGTTGGTTTTATG
Met 25 seq for	Gcgtctgttagaaaggaag
MET25-Cherry for	Tgtgtagttctagaatggtgagcaagggcgaggag
MET25-Cherry rev	TgtgtagttctagaCTTGACAGCTCGTCCATGCC

## Materials and Methods

Nui_Gag_for_BamH	tcaGGATCCCTGGGTCTGGGCTAAGATTTGTTACTAAAACTC
Nui-Atg26_BamHI_fwd	AGTAGCAATggatccctgggtctgggCCCATCACTCAAATCATATCAG
Nui-Atg26_Sall_rev	ATTCCTACTTgtcgacGCTCCTTGTACGCCTTTATAC
Nui-Gag_cyterm_rev_Sall	tagGTCGACACTCACTATAGGGCGAATTGGGTAC
pGEX-4T3_fwd	GATCATGTAACCCATCC
pGEX-4T3_rev	GCCACCTGACGTCTAAG
<i>preCntrlxrn1for</i>	<i>AGGACGATTCTGTACTATAAGG</i>
Seqgag1	CCAACTAGCTGATAAGTTCCG
Seqgag2	GCTGCTAACAAGTATCTCCG
Seqgagpol1	CGTCTTCGTTTGCATACAAATCG
Seqgagpol2	GGCTATATTCGTGTGTGCGC
Seqgagpol3	TGCGCGAGCACAGCCG
SeqrevAtg26WTMI	TGCAGCGTACGaatcatcgtcca

**Table 3.4.2 Oligonucleotides for gene deletion and chromosomal tagging used in this study**

Name	Sequence
ATG26 KO S1	CAGAAGTTCAGTTGCACTTTATGCTTTGGTGAAAATCCGTATAACTTAAAAGAATG <i>CGTACGCTGCAGGTCGAC</i>
ATG26 KO S2	ctattaatgattagatgttacgctttttataaaagtgagagtgatactcggTTAATCGATGAATTCGAGCTCG
Atg26 S3	gcaaccaaactgacacctgctgaaacaacggatgaagggtggacgatgattCGTACGCTGCAGGTCGAC
Atg26delwtmi S3	gaaaatgtagatgcaaccaaactgacacctgctgaaacaacggatgaagggCGTACGCTGCAGGTCGAC
Atg36 Ko S1	TGTATTCAGGGCTTAAAATACTAAAATTTGGTGGTCAGTACAGCTCATTAAATGCGT <i>ACGCTGCAGGTCGAC</i>
Atg36 S2	AACTGATGGTGTTCGACAACGTTTTTGAATGAGGGTATCTAACTTTCTTCTAATCG <i>ATGAATTCGAGCTCG</i>
S1 Atg34	GAAACTAGTTCCTATAGGTTGAGTGTCTATCAAAAATTTACGGAGACGCGATGCGT <i>ACGCTGCAGGTCGAC</i>
S1kan_xrn1d	AAAAATCAACACTTGTAAACAACAGCAGCAACAAATATATATCAGTACGGTATGCAG <i>CTGAAGCTTCGTACGC</i>
S1nat_xrn1d	AAAAATCAACACTTGTAAACAACAGCAGCAACAAATATATATCAGTACGGTATGCGT <i>ACGCTGCAGGTCGAC</i>
S2 Atg34	AGTTAAATAAGTACTATAGCCAAAGAACTGGAAGAATATAAAAAAGCATTTAATC <i>GATGAATTCGAGCTCG</i>
S2kan_xrn1d	GATATACTATTAAGTAACCTCGAATATACTTCGTTTTTAGTCGTATGTTCTAGCAT <i>AGGCCACTAGTGGATCTG</i>
S2nat_xrn1d	GATATACTATTAAGTAACCTCGAATATACTTCGTTTTTAGTCGTATGTTCTAATCG <i>ATGAATTCGAGCTCG</i>

## 3.1.5 Antibodies

**Table 3.5 Antibodies used in this study**

<b>Antibody</b>	<b>Dilution</b> (in TBST containing 1% skim milk powder (w/v))	<b>Source</b>
anti-mouse-HRPO-conjugate	1 : 10.000	Dianova, Hamburg
anti-rabbit-HRPO-conjugate	1 : 5.000	Medac, Hamburg
anti-rat-HRPO-conjugate	1 : 10.000	Jackson ImmunoResearch, UK
rabbit-anti-ApEl	1 : 1.000	Eurogentech, Belgium
mouse-anti-GFP	1 : 1.000	Roche, Mannheim
rabbit-anti-FAS	1 : 1.000	E. Schweitzer
mouse-anti-PGK	1 : 10.000	Molecular Probes, Leiden, NL
rat-anti-Red	1 : 1.000	Chromotek, München
mouse-anti-HA	1 : 10.000	Santa Cruz Bio-technology, Heidelberg
rabbit-anti-COP1	1 : 5.000	Gift from Hans Dieter Schmitt
rabbit-anti-LA Gag	1 : 10.000	AG Thumm
rabbit-anti-GST	1 : 10.000	AG Thumm

## 3.1.6 Commercial available kits

**Table 3.6: Commercial available Kits used in this study**

<b>Name of the Kit</b>	<b>Source</b>
First Strand cDNA Synthesis Kit	Thermo Scientific
ECL Western Blotting Detection Reagents	Amersham Biosciences
QIAquick Gel Extraction Kit	Qiagen, Hilden
QIAquick PCR Purification Kit	Qiagen, Hilden
Wizard Plus SV Miniprep Kit	Promega, Mannheim

## 3.1.7 Chemicals, supplements, enzymes and protein purification systems

**Table 3.7: Chemicals, supplements, enzymes and protein purification systems used in this study**

<b>Name</b>	<b>Source</b>
Bacto Agar	Becton Dickinson, Heidelberg
Bacto Peptone	Becton Dickinson, Heidelberg
Bacto Tryptone	Becton Dickinson, Heidelberg
Bacto Yeast Extract	Becton Dickonson, Heidelberg
Benzonase	Sigma, Deisenhofen
clon NAT (nourseotricine)	Werner BioAgents, Jena
Complete <sup>TM</sup> protease inhibitor (EDTA-free)	Roche, Mannheim



## Materials and Methods

Deoxyadenosin-triphosphate (dATP)	NEB, Frankfurt
Deoxycytidin-triphosphate (dCTP)	NEB, Frankfurt
Deoxyguanosin-triphosphate (dGTP)	NEB, Frankfurt
Deoxythymidin-triphosphate (dTTP)	NEB, Frankfurt
Difco Yeast nitrogen base w/o amino acids and ammonium	Becton Dickinson, Heidelberg
Difco Yeast nitrogen base w/o amino acids	Becton Dickinson, Heidelberg
DNA polymerase (FideliTaq)	USB, Santa Clara, USA
DNA polymerase (Klenow)	NEB, Frankfurt
DNA polymerase (KOD)	Novagen, Darmstadt
DNA polymerase (Taq)	NEB, Frankfurt
DNA polymerase (Vent)	NEB, Frankfurt
DNA-marker (1kb DNA-ladder)	NEB, Frankfurt
GFP-TRAP	Chromotek, München
Glass beads	Schütt, Göttingen
Glutathione Sepharose 4B	GE Healthcare, München
Herring-sperm-DNA	Promega, Madison, USA
Precision Plus Protein All Blue Standards	Biorad, Munich
Protease inhibitor cocktail (bacteria)	Sigma, Deisenhofen
Restriction enzymes	NEB, Frankfurt
RFP-TRAP	Chromotek, München
RNase A	Applichem, Darmstadt
Skim milk powder	Granovita, Lüneburg
Supplements for yeast media	Becton Dickinson, Heidelberg
T4-Ligase	NEB, Frankfurt
Zymolyase T100	Seikagaku, Japan

### 3.1.8 Equipment

**Table 3.8 Equipment used in this study**

<b>Name</b>	<b>Source</b>
Agarose gel equipment	Bio-Rad Laboratories GmbH, München
Autoclave	Adolf Wolf, SANoclav, Bad Überkingen-Hausen
Autoclave DX200	Systec, Wetztenberg
Bench	BDK Luft- und Reinraumtechnik GmbH, Sonnenbühl
Blot Shaker GFL 3019	GFL, Burgwedel
Centrifuge 5404R	Eppendorf, Hamburg
Centrifuge 5415D	Eppendorf, Hamburg
Centrifuge 5415R	Eppendorf, Hamburg
Centrifuge 5804	Eppendorf, Hamburg
Chemical balance	Sartorius, Göttingen
Cuvettes for electroporation; 2mm	peqlab, Erlangen
Cuvettes no. 67.742	Sarstedt, Nümbrecht

## Materials and Methods

Electroporator 2510	Eppendorf; Hamburg
Freezer (-20°C)	Liebherr, Bulle, CH
Freezer (-80°C)	Heareus, Hanau
Glassbeads	Schütt, Göttingen
Hood	BDK Luft- und Reinraumtechnik GmbH, Sonnenbrühl
Incubator (37°C)	Heraeus, Hanau
Incubator 4200	Innova, USA
Incubator Thermomixer comfort	Eppendorf, Hamburg
Labshaker for diverse culture sizes	A. Kühner, Birsfelden, Schweiz
LAS 3000 Intelligent Dark Box	Fuji/Raytest, Benelux
Magnetic stirrer MR 3001	Heidolph, Kelheim
Microscope cover slips	Menzel-Gläser, Braunschweig
Microscope DeltaVision, Olympus IX71	Applied Precision, USA
Microscope slides (76x26mm)	Menzel-Gläser, Braunschweig
Microwave R-939	Sharp, Hamburg
Multivortex IKA vibray VXR basic	IKA, Staufen
OmniTrays Nunc	SIGMA-ALDRICH, St. Louis, USA
Over head shaker Roto-Shake Genie	Scientific Industries Inc, USA
PCR Mastercycler gradient	Eppendorf, Hamburg
pH meter pH537	WTW, Weilheim
Photometer	Eppendorf, Hamburg
Pipette tips, petri dishes, ...	Sarstedt, Nümbrecht / Eppendorf, Hamburg
Pipettes	Eppendorf, Hamburg
PowerPac Basic Power Supply	Bio-Rad Laboratories GmbH, München
PowerPac HC Power Supply	Bio-Rad Laboratories GmbH, München
PVDF membrane Hybond-P	Amersham; GE healthcare, Freiburg
Refrigerator (4°C)	Bosch, Stuttgart / Liebherr, Bulle, CH
Rotor JA 10	Beckmann, Krefeld
Rotor JA 20	Beckmann, Krefeld
Rotor TLA-100.3	Beckmann, Krefeld
SDS-PAGE equipment BioRAD Mini Protean cell	Bio-Rad Laboratories GmbH, München
Sterile filter	Whatman, GE healthcare, München
Superose™ 6 10/300 GL column	Amersham Pharmacia Biotech, Schweden
Thermomixer Comfort	Eppendorf, Hamburg
Transilluminator TI 1	Whatman Biometra, Göttingen
Ultracentrifuge	Beckman, Krefeld
vacuum pump	Vacuubrand, Wertheim
Water bath SWB25	Thermo Electron, Karlsruhe
Western Blot equipment Trans Blot Cell	Bio-Rad Laboratories GmbH, München

## Materials and Methods

### 3.1.9 Media

The media used in this study were prepared with deionized water (ddH<sub>2</sub>O). The respective pH was adjusted using NaOH or HCl. All media were autoclaved at 121°C for 20 min for sterilization. Percent values of this chapter indicate weight per volume (w/v). Preparation of solid media to generate plates was done by adding 2% of preheated, sterile agar to the respective medium.

**Table 3.9.1 Yeast media used in this study**

Name	Supplements
YPD medium, pH 5.5	1% Bacto Yeast Extract, 2% Bacto Pepton, 2% D-glucose
CM medium, pH 5.6*	0.67% Yeast Nitrogen Base w/o amino acids, 2% D-glucose and dropout-mix: 0.0117% of each of L-alanine, L-methionine, L-arginine, L-phenylalanine, L-asparagine, L-proline, L-aspartic acid, L-serine, L-cysteine, L-threonine, L-glutamine, L-tyrosine, L-glutamic acid, L-valine, L-glycine, myo-inositol, L-isoleucine and p-aminobenzoic acid
CM medium w/o methionine, pH 5.6*	see CM-medium, pH 5.6: Dropout-mix w/o methionine
SD(-N) medium	0.67% Yeast Nitrogen Base w/o amino acids and w/o ammonium sulfate, 2% D-glucose
MV medium*	0.67% Yeast Nitrogen Base w/o amino acids, 2% D-glucose

\*Following supplements were added depending on selection of genetic markers: 0.4 mM L-tryptophan, 0.3 mM adenine, 1 mM L-lysine, 0.2 mM uracil, 0.3 mM L-histidine and/or 1.7 mM L-leucine

**Table 3.9.2 *E. coli* media used in this study**

Name	Supplements
LB-medium, pH 7.5	1% Bacto Trypton, 0.5% Bacto Yeast extract, 0.5% sodium chloride For plasmid selection: 75 µg/ml ampicillin, 50 µg/ml kanamycin, and/or 25 µg/ml chloramphenicol
SOC-medium, pH 7.5	2% Bacto Trypton, 0.5% Bacto Yeast extract, 0.4% D-glucose 10 mM sodium chloride, 10 mM magnesium sulfate 10 mM magnesium chloride, 2.5 mM potassium chloride

### 3.2 Methods

#### 3.2.1 Cultivation of *E. coli*

For molecular biological methods, the *E. coli* strains XL1 blue and DH5 $\alpha$  were used. Recombinant expression of proteins was performed in BL21 (DE3) pLysS *E. coli* cells. LB medium is the standard growth medium of liquid *E. coli* culture. For plasmid selection, the relevant antibiotics were supplemented. In most cases (plasmid isolation, preparation of competent cells, transformation), cells were shaken at 37°C and 220 rpm. Quantification of liquid cultures was performed by measuring the cell density at OD<sub>600</sub>. *E. coli* can be stored in LB medium or on LB agar plates at 4°C for 3–5 weeks. For long-time storage, cryo-stocks were prepared with 700  $\mu$ l of an over night liquid culture supplemented with 700  $\mu$ l of 60% glycerol. Cryo-stocks were stored at -80°C. *E. coli*s were grown on LB agar plates supplemented with the appropriate antibiotics for selection of positive clones after transformation (see chapter 3.2.3).

#### 3.2.2 Cultivation of yeast

YPD medium supplemented with 2% glucose was used as nutrient rich-medium. For selection of genetic markers, liquid yeast cultures were inoculated in the synthetic selection medium CM supplemented with the relevant components and lacking the supplements for selection of positive clones. Liquid yeast cultures were typically grown at 30°C with 220 rpm if not indicated otherwise. The cell density was measured at OD<sub>600</sub>. In most cases, a preculture was inoculated to achieve the desired cell density of the main culture for the experiment. For this, the preculture was diluted depending on the growth rate of the respective strain. Yeast can be stored in medium or on agar plates at 4°C for 6 weeks. For long-time storage, cryo-stocks were prepared with 700  $\mu$ l of an over night liquid culture supplemented with 700  $\mu$ l of 30% glycerol.

### 3.2.3 Molecular biological methods

#### 3.2.3.1 Determination of DNA concentration

DNA concentrations were measured using the UV spectrophotometer (GE Healthcare).

#### 3.2.3.2 Restriction of DNA

Restriction enzymes are standard tools to analyse DNA and to generate defined DNA fragments for cloning (chapter 3.2.3.5). Standard protocols were used according to the manufacturer's instructions (NEB). For an analytic digestion, 0.5–1.0 µg DNA was used. The reaction was incubated for 1–2 h at the optimal enzyme temperature and analysed by DNA electrophoresis (chapter 3.2.3.3).

#### 3.2.3.3 DNA electrophoresis

DNA electrophoresis is a typical molecular biological technic to analyse and determine the size of DNA fragments. Before electrophoresis, DNA sample buffer (1 M Tris/HCl pH 8.0, 50% (v/v) glycerol, 0.1% (w/v) bromphenolblue) was mixed with the DNA. The DNA sample was separated in a 1% agarose gel (w/v) in TAE (40 mM Tris/acetate pH 8.1, 2 mM EDTA, 0.114% acetic acid) supplemented with 1 µg/ml ethidiumbromide for visualization under UV light. The *Standard Tri Dye 1 kb* (NEB) was used as DNA ladder to predict the size of the separated fragments.

#### 3.2.3.4 Polymerase chain reaction

Polymerase chain reaction is used to amplify DNA fragments determined by (two) flanking oligonucleotides (primers). For cloning, DNA fragments were amplified by PCR using *KOD Hot Start DNA Polymerase* (Novagen). For genetic analysis of chromosomally tagged or knockout strains, PCR was performed with Taq DNA polymerase (NEB). Yeast chromosomal DNA or plasmid DNA was used as template in a 50 µl scale PCR. Standard PCRs were done according to the recommendations of the manufacturer. The respective program of the thermocycler was adapted to the size of the product (elongation time) and the annealing temperature of the primers.

## Materials and Methods

### 3.2.3.5 Molecular cloning

DNA fragments (inserts) with flanking restriction sites were generated by performing PCR with primers containing respective restriction sites. The PCR product was checked by DNA electrophoresis (chapter 3.2.3.3) and purified by using the Gel Extraction Kit from Qiagen. Then, the PCR product and the target plasmid (5–10 µg) were digested with the corresponding restriction enzymes in a 50 µl reaction following the manufacturers advice from NEB. At the optimal enzyme temperature, the reaction was incubated for 2-4 hours. To avoid religation in the following ligation reaction, 1 µl of CIP was added to the reaction of the vector. Next, the products were again purified with the Gel Extraction Kit from Qiagen (using the protocol for purification of PCR products). The concentrations of the eluted fragments were determined (chapter 3.2.3.1) to calculate the optimal molar ratio of insert and vector (5:1) for the ligation reaction:

$$mass_{insert} = 5 \times mass_{vector} \times \frac{length_{insert}}{length_{vector}}$$

Ligation was done in a 20 µl scale with 50-100 ng of vector DNA and the respective amount of insert DNA. The reaction was performed by using T4-DNA-ligase according to the recommendations of the manufacturer (NEB). For selection and amplification of the vectors with the insert of interest, chemically competent *E. coli* (XL1 blue) (chapter 3.2.3.7) were transformed with the complete volume of the ligation reaction.

### 3.2.3.6 Generation of cDNA for molecular cloning

For cloning of the cDNA of the L-A virus RNA in vectors, the 4.6 kb dsRNA genomic segment was separated by DNA electrophoresis, purified and used as a template for generation of cDNA. The cDNA was then used for standard PCR.

In detail: 20 µl of the 50 µl bound fraction of the GFP-Atg26-Trap (chapter 3.2.7.4) was removed, and mixed with 10 µl ddH<sub>2</sub>O and 5 µl DNA sample buffer (1 M Tris/HCl pH 8.0, 50% (v/v) glycerol, 0.1% (w/v) bromphenolblue). Co-precipitated dsRNA was separated from mRNA and rRNA by DNA electrophoresis (chapter 3.2.3.3) and purified by using the Gel Extraction Kit from Qiagen. For elution, 30 µl of ddH<sub>2</sub>O was used.

cDNA was generated by using the *First Strand cDNA Synthesis Kit* (Thermo Scientific) following the manufacturer advice. 10 µl of the RNA sample was mixed with 2.5 µM of

## Materials and Methods

each primer (*gagpol\_forBam* and *gag\_revXho*, table 3.4.1). The reaction was filled up to 11  $\mu$ l with ddH<sub>2</sub>O. The sample was incubated at 65°C for 5 min. On ice, 4  $\mu$ l 5 x reaction buffer, 1  $\mu$ l RiboLock RNase Inhibitor, 2  $\mu$ l dNTP Mix (10 mM each) and 2  $\mu$ l M-MuLV Reverse Transcriptase was supplemented. Then, the sample was incubated at 37°C for 1 hour. Finally, the reaction was terminated at 70°C for 5 min. The cDNA sample was used for molecular cloning as described in chapter 3.2.3.5.

### 3.2.3.7 Preparation of chemically competent *E. coli* (XL1 blue)

XL1 blue cells were used to generate chemically competent *E. coli*. For this, a 400 ml culture of OD<sub>600</sub>~0.6 (growing in LB medium) was harvested by centrifugation (3000 g, 10 min, 4°C). The pellet was resuspended in 150 ml buffer I (30 mM potassium acetate pH 5.8, 100 mM rubidium chloride, 10 mM calcium chloride, 50 mM manganese(II) chloride, 15% glycerol) and incubated for 15 min on ice. After a centrifugation step (3000 g, 10 min, 4°C), the cell sediment was resuspended in 15 ml buffer II (10 mM MOPS pH 6.8, 10 mM rubidiumchloride, 75 mM calcium chloride, 15% glycerin). Aliquots of 100  $\mu$ l were stored at -80°C.

### 3.2.3.8 Preparation of electrocompetent *E. coli* (BL21/pLysS)

For preparation of electrocompetent BL21/pLysS cells, a 1 l culture of OD<sub>600</sub>~0.5 (growth medium: LB with 25  $\mu$ g/ml chloramphenicol) was cooled on ice for 10 min and sedimented by centrifugation (3000 g, 10 min, 4°C). The cells were washed twice with ice-cold ddH<sub>2</sub>O and once with ice-cold 10% (v/v) glycerine. After the last centrifugation, the cell sediment was resuspended in 2 ml ice-cold 10% (v/v) glycerin. Aliquots of 50  $\mu$ l were stored at -80°C.

### 3.2.3.9 Transformation of plasmid DNA in chemically competent *E. coli*

For *E. coli* transformation with ligated vectors, 30-50  $\mu$ l of chemically competent XL1 blue cells were thawed on ice and the complete ligation reaction (chapter 3.2.3.5) was added. After 30 min of incubation on ice, the cells were heat-shocked at 42°C for 90 sec. Then, the sample was cooled-down on ice for 2 min. For recovery, the cells were resuspended in 1 ml SOC medium and shaken for 40 min at 37°C. Finally, the cells were sedimented and plated on LB agar containing the respective antibiotics for plasmid selection. The plates were incubated over night at 37°C. On the next day, clones were

## Materials and Methods

picked and prepared for plasmid isolation (chapter 3.2.3.12), tested for correct insertion by analytic restriction enzym digestion and sequencing (chapter 3.2.3.2 and 3.2.3.13)

### 3.2.3.10 Transformation of plasmid DNA in electrocompetent *E. coli*

Electrocompetent cells (BL21/pLYS) were thawed on ice. Then, 50–100 ng of plasmid DNA was added to the cells and transferred to a pre-chilled electroporation tube. The electroporation was performed at 2500 Volt using Electroporator 2510 (Eppendorf). Then, the cells were transferred to 1 ml SOC medium and incubated at 37°C for 40 min under shaking. The cells were harvested and plated on LB agar with the appropriate antibiotics.

### 3.2.3.11 Site-directed mutagenesis of plasmids

Site-directed mutagenesis of plasmids was made by using the *QuickChange site-directed mutagenesis kit* (Agilent). To introduce desired point mutations in a sequence, two complementary primers with the exchanged nucleotides were designed and applied for the protocol according to the manufacturer's instructions. Introduced point mutations were confirmed by sequencing (chapter 3.2.3.13).

### 3.2.3.12 Purification of plasmids from *E. coli*

For small-scale plasmid purification, the *Wizard Plus SV Minipreps DNA Purification System* (Promega) was used according to the recommendations of the manufacturer.

### 3.2.3.13 Sequencing of DNA

All cloned constructs containing inserts generated by PCR were verified by sequencing. Sequencing was done by GATC Biotech (Konstanz). For the sequencing reactions, the samples (plasmid DNA and the relevant primers) were prepared according to the manufacturer's instructions.

### 3.2.3.14 Plasmid constructs

Table 3.10 lists all plasmids that were generated in this study. Furthermore, it contains all necessary information about the construction of the plasmids.

Examples: For construction of pYES2 GFP-Atg8 F5GK6G, *Atg8 F5GK6G* (insert) was



## Materials and Methods

amplified with GFPAtg8for and GFPAtg8rev (primer: table 3.4.1) using pRS316-GFP-Atg8 F5GK6G as PCR template. The DNA fragment was digested with HindIII and XhoI (restriction enzymes) and cloned in pYES2 (vector backbone).

For construction of pUG34-Atg26, pUG34-mCherry-Atg26 was digested with BamHI and XhoI to generate the insert *Atg26*. Then, *Atg26* was cloned in pUG34 (vector backbone).

For construction of *Atg26\_1-186-Cub*, *Atg26 1-186* was amplified with *Atg26\_Cub\_StuI\_fwd* and *Atg26MAP1\_Cub\_SalI\_rev* (primer), where pUG34-Atg26 was used as PCR template. The PCR product was digested with StuI (blunt cutter) and SalI. The targeted vector pRS313-Met25-Ste14-Cub-RURA was digested with ClaI and treated with the DNA-polymerase Klenow to generate a blunt site. Subsequently, it was digested with SalI. Then, the DNA fragment *Atg26 1-186* was cloned in pRS313-Met25-Ste14-Cub-RURA by ligation of two blunt sites (StuI/Cla(blunt)) and SalI sites.

**Table 3.10 Plasmids constructs cloned in this study**

Title of the plasmid	Vector backbone	Insert	PCR template or insert origin	Oligonucleotides (Primer)	Restriction enzymes
pYES2 GFP-Atg8 F5GK6G	pYES2	GFP-Atg8 F5GK6G	PCR: pRS316-GFP-Atg8 F5GK6G	GFPAtg8for/GFP-Atg8rev	HindIII/XhoI
pYES2 GFP-Atg8 S3AT4A	pYES2	GFP-Atg8 S3AT4A	PCR: pRS316-GFP-Atg8 S3AT4A	GFPAtg8for/GFP-Atg8rev	HindIII/XhoI
pYES2-GFP	pYES2	GFP		GFPAtg8for/GFP rev	HindIII/XhoI
pUG34 mCherry	pUG34	Met25-mCherry	cloned from pUG36-mCherry	-	SacI/Spel
pUG34 mCherry-Atg19	pUG34 mCherry	Atg19	cloned from pUG36-CVT19	-	BamHI/XhoI
pUG36 mCherry-Atg8	pUG36 mCherry	Atg8	pRS 316-GFP-Atg8	Atg8 wt BamHI/GFP-Atg8rev	BamHI/XhoI
pUG34 mCherry-Atg26	pUG34 mCherry	Atg26	PCR template: genomic DNA	Atg26forBamHI/Atg26 revXho	BamHI/XhoI
pUG34 mCherry-Atg26 1-1194	pUG34 mCherry	Atg26 1-1194	PCR template: pUG34 mCherry-Atg26	Atg26forBamHI/Atg26 woWTMirevXhoI	BamHI/XhoI
pUG34 mCherry-Atg26 I1198A	pUG34 mCherry	Atg26 I1198A	PCR template: pUG34 mCherry-Atg26	Atg26forBamHI/Atg26 WTMarevXhoI	BamHI/XhoI
pUG34 Atg26	pUG34	Atg26	cloned from pUG34 mCherry-Atg26	-	BamHI/XhoI
pUG34 Atg26 1-1194	pUG34	Atg26 1-1194	cloned from pUG34 mCherry-Atg26 1-1194	-	BamHI/XhoI
pUG34 Atg26 I1198A	pUG34	Atg26 I1198A	cloned from pUG34 mCherry-Atg26 I1198A	-	BamHI/XhoI
pUG34 Atg26 1-186	pUG34	Atg26 1-189	PCR: pUG34 -Atg26	Atg26forBamHI/Map1 Atg26revXh	BamHI/XhoI
pUG34 Atg26 1-337	pUG34	Atg26 1-337	PCR: pUG34 -Atg26	Atg26forBamHI/Map2	BamHI/

## Materials and Methods

				Atg26revXh	XhoI
pUG34 Atg26 1-569	pUG34	Atg26 1-569	PCR: pUG34 -Atg26	Atg26forBamHI/Map3 Atg26revXh	BamHI/ XhoI
pUG34 Atg26 1-635	pUG34	Atg26 1-635	PCR: pUG34 -Atg26	Atg26forBamHI/Map4 Atg26revXh	BamHI/ XhoI
pUG34 Atg26 1-744	pUG34	Atg26 1-744	PCR: pUG34 -Atg26	Atg26forBamHI/Map5 Atg26revXh	BamHI/ XhoI
pUG34 Atg26 187-337	pUG34	Atg26 187 - 337	PCR: pUG34 -Atg26	Atg26PHforBam/Map2 Atg26revXh	BamHI/ XhoI
pUG34 Atg26 187-374	pUG34	Atg26 187- 374	PCR: pUG34 -Atg26	Atg26PHforBam/Map2. 2Atg26revXh	BamHI/ XhoI
pUG34 Atg26 338-744	pUG34	Atg26 338- 744	PCR: pUG34 -Atg26	Atg26L2.1forBam/Map 5Atg26revXh	BamHI/ XhoI
pUG34 Atg26 338- 1198	pUG34	Atg26 338- 1198	PCR: pUG34 -Atg26	Atg26L2.1forBam/Atg2 6revXho	BamHI/ XhoI
pUG34 Atg26 187- 1198	pUG34	Atg26 187- 1198	PCR: pUG34 -Atg26	Atg26forBamHI/Atg26 revXho	BamHI/ XhoI
pUG34 Atg26 187-569	pUG34	Atg26 187- 569	PCR: pUG34 -Atg26	Atg26forBamHI/Map3 Atg26revXh	BamHI/ XhoI
pUG34 Atg26 570- 1198	pUG34	Atg26 570- 1198	PCR: pUG34 -Atg26	Atg26forBamHI/Atg26 revXho	BamHI/ XhoI
pUG36 mCherry LA Gag	pUG36 mCherry	LA Gag (WCG4)	PCR template: LA cDNA	gagpol_forBam/gag_rev Xho	BamHI/ XhoI
pUG34 LA Gag	pUG34	LA Gag (WCG4)	PCR template: LA cDNA	gagpol_forBam/gag_rev Xho	BamHI/ XhoI
pUG36 LA Gag	pUG36	LA Gag (WCG4)	PCR template: LA cDNA	gagpol_forBam/gag_rev Xho	BamHI/ XhoI
pUG36 LA GagPol	pUG36	LA GagPol (WCG4)	PCR template: LA cDNA	gagpol_forBam/gagpol_ revXho	BamHI/ XhoI
pUG35 LA Gag	pUG35	LA Gag (WCG4)	PCR template: pUG36 mCherry LA Gag	-	BamHI/ Sall
pUG36 Atg26	pUG36 mCherry	Atg26	cloned from pUG34- Atg26	-	BamHI/ XhoI
pUG36 mCherry Atg11	pUG36 mCherry	Atg11	PCR template: genomic DNA	Atg11forBamHI/Atg11 revXhoI	BamHI/ XhoI
Atg26_1-186 - Cub	pRS313-Met25- Ste14-Cub-RURA	Atg26 1-186	PCR: pUG34 -Atg26	Atg26_Cub_StuI_fwd/At g26MAP1_Cub_Sall_rev	Stu/Clai(Blu nt)/Sall
Atg26_1-337 - Cub	pRS313-Met25- Ste14-Cub-RURA	Atg26 1-337	PCR: pUG34 -Atg26	Atg26_Cub_StuI_fwd/At g26MAP2_Cub_Sall_rev	Stu/Clai(Blu nt)/Sall
Atg26_1-569 - Cub	pRS313-Met25- Ste14-Cub-RURA	Atg26 1-569	PCR: pUG34 -Atg26	Atg26_Cub_StuI_fwd/At g26MAP3_Cub_Sall_rev	Stu/Clai(Blu nt)/Sall
Atg26_338-1198 - Cub	pRS313-Met25- Ste14-Cub-RURA	Atg26 338- 1189	PCR: pUG34 -Atg26	Atg26_L2_Cub_StuI _for/Atg26_Cub_Sall_rev	Stu/Clai(Blu nt)/Sall
Atg26_1-1194 - Cub	pRS313-Met25- Ste14-Cub-RURA	Atg26 1- 1194	PCR: pUG34 -Atg26	Atg26_Cub_StuI_fwd/At g26delAIM_Cub_Sall_rev	Stu/Clai(Blu nt)/Sall
Atg26_187-337 -Cub	pRS313-Met25- Ste14-Cub-RURA	Atg26 187 - 337	PCR: pUG34 -Atg26	Atg26PH_Cub_StuI_fw/ Atg26MAP1_Cub_Sall_rev	Stu/Clai(Blu nt)/Sall
Gag-Cub	pRS313-Met25- Ste14-Cub-RURA	LA Gag (WCG4)	PCR: pUG36 LA Gag	GagCubforStuI/GagCub revSal1	Stu/Clai(Blu nt)/Sall

## Materials and Methods

Nui-Gag	pRS313-CUP1	LA Gag (WCG4)	PCR: pUG36 LA Gag	Nui_Gag_for_BamH/Nui-Gag_cyterm_rev_Sall	BamHI/Sall
pGEX 4T3 Atg26	pGEX 4T3	Atg26	cloned from pUG34-Atg26	-	BamHI/XhoI
pGEX 4T3 Atg26	pGEX 4T4	Atg26 187-569	cloned from pUG34-Atg26 187-569	-	BamHI/XhoI
pPROEX htb - LA Gag	pPROEX htb	LA Gag (WCG4)	cloned from pUG36 LA Gag	-	BamHI/XhoI

### 3.2.3.15 Isolation of chromosomal DNA from yeast cells

In order to isolate genomic DNA from yeast, 2 ml of an over night culture was sedimented by centrifugation and washed with ddH<sub>2</sub>O (13.000 rpm, 1 min). The cell pellet was resuspended in 200 µl breaking buffer (10 mM Tris/HCl pH 8.0, 100 mM NaCl, 1 mM EDTA, 1% SDS, 2% Triton X-100) and supplemented with 200 µl phenol:chloroform:isomyl (25:24:1) and ~200 µl glass beads. The cells were vortexed for 1 min and then cooled-down on ice for 1 min. These two steps were repeated four times. After supplying 200 µl ddH<sub>2</sub>O, the sample was sedimented by centrifugation (13.000 g, 10 min, 4°C) to generate an upper phase containing the chromosomal DNA. The upper phase was transferred to a new reaction tube and 1 ml of ice-cold ethanol (stored at -20°C) was added. The sample was mixed and precipitated by incubation at -20°C for 10 min. Then, the sample was again centrifuged (13.000 g, 10 min, 4°C) and the resulting supernatant removed. The pellet was resuspended in 400 µl ddH<sub>2</sub>O and supplemented with 3 µl RNase A (10 mg/ml). After 5 min of incubation at 37°C for RNA digestion, 1 ml ice-cold ethanol with 10 µl 5 M ammonium acetate was added and incubated for 15 min at -20°C. Then, the DNA was again sedimented by centrifugation (13.000 g, 10 min, 4°C). The supernatant was removed and the dried pellet resuspended in 30 µl ddH<sub>2</sub>O.

### 3.2.3.16 Yeast cell transformation

A 50 ml liquid culture of OD<sub>600</sub>~0.5 was harvested by centrifugation (2000 rpm, 5 min, RT). The cells were washed two times with ddH<sub>2</sub>O and once with LiOAc-Sorb (100 mM lithium acetate, 10 mM Tris/acetate pH 8.0, 1 mM EDTA, 1 M sorbitol). After the last washing step, the supernatant was removed and the sedimented cells were resuspended in 100-500 µl LiOAc-Sorb and incubated at 30°C for 15 min. Then, 50-100 µl of the cells was added to a cocktail of 5 µl herring sperm DNA (10 mg/ml), 3-10 µl of DNA and 300 µl PEG in Li-TE (100 mM lithium acetate, 10 mM Tris/acetate pH 8.0, 1 mM EDTA, 40%

## Materials and Methods

(v/v) PEG 3350). Subsequently, the sample was incubated at 30°C for 30 min and then heat-shocked at 42°C for 15 min. Afterwards, the cells were sedimented (2000 rpm, 5 min, RT) and resuspended in 2 ml YPD for recovery. Finally, the cells were sedimented again and plated on YPD agar containing the respective antibiotics for selection of genetic markers. After 2-3 days of incubation at 30°C, colonies were picked and used for further studies.

### 3.2.3.17 “Quick and Dirty” variant of yeast cell transformation

For transformation with plasmid DNA, a short variant of yeast cell transformation was used: Yeast cells were directly picked from agar plates and resuspended in 5 µl herring sperm DNA (10 mg/ml), 3-10 µl of plasmid DNA and 300 µl PEG in Li-TE (100 mM lithium acetate, 10 mM Tris/acetate pH 8.0, 1 mM EDTA, 40% (v/v) PEG 3350). After 30 min of incubation at 30°C and a heat shock at 42°C for 15 min, the cells were harvested by centrifugation (2000 rpm, 5 min, RT), resuspended in 200 µl ddH<sub>2</sub>O and plated on CM agar. The plates were incubated for 2-3 days at 30°C.

### 3.2.3.18 Deletion and chromosomal tagging of genes by homologous recombination

In this study, the methods of deletion and chromosomal tagging of genes were based on the protocol of Janke et al. (2004). PCR-amplified cassettes were transformed in yeast (chapter 3.2.3.16) and integrated by homologous recombination at the chromosomal locus of interest resulting in deletion or tagging of the desired gene (Janke et al., 2004).

## 3.2.4 Split-ubiquitin assay

Yeast cells were transformed with the Cub and Nub vectors. Each vector contained the gene of interest that was expressed as a fusion protein with either the N-terminal or the C-terminal half (plus R-Ura3) of ubiquitin. A yeast preculture was set to OD<sub>600</sub>~1.0. This cell density was used for a series of 10-fold dilutions up to 10000. From these dilutions, 4 µl was dropped on three different solid plates: The first plate was used to test the general growth of the cells independent of the expression or interaction of the two tested proteins (CM w/o Trp and His). The second plate contained the selective medium CM (w/o Trp and His), 250 µM methionine and 100 µM CuSO<sub>4</sub> to induce expression. Furthermore, 1 mg/ml FOA was added for positive selection of interaction partners. The

## Materials and Methods

third plate consists of the selection medium MV lacking uracil (MV w/o Trp, His and Ura) for negative selection of interaction.

### 3.2.5 Microscopy

Intracellular expressed fluorescent proteins are detectable by (*in vivo*) fluorescence microscopy. The expression of a fusion protein, containing a protein of interest and a fluorescent protein as tag, is used to visualize the intracellular localization. In this study, two fluorescent proteins GFP and mCherry were used. For *in vivo* fluorescence microscopy, 5  $\mu$ l of a yeast culture was transferred to a glass slide and fixed with a cover slip. Fluorescence microscopy was performed with a DeltaVision Deconvolution microscope (Olympus IX71, Applied Precision) by using the 100 x objective and the filter sets for live cell imaging (table 3.11). A stack of at least 18 pictures with focal planes 0.20  $\mu$ m apart was captured by the equipped CoolSNAP HQ camera and deconvoluted using the software SoftWoRx (Applied Precision). Analysis and processing of the pictures were performed by using Fiji or SoftWoRx.

**Table 3.11 Filter sets for live cell imaging**

Filter set	Excitation wavelength (nm)	Emission wavelength (nm)
GFP	475/28	525/50
mCherry	575/25	632/60
Pol	-50/28	-50/0

### 3.2.6 Induction and monitoring of autophagy

Nitrogen-free medium (SD-N) was used to induce autophagy in yeast cells. As the GFP moiety of GFP-tagged proteins is stable in the vacuole, accumulation of free GFP in this compartment shows the autophagic processing of such proteins. In this study, detection of free GFP was done by immunoblotting (chapter 3.2.7.5/6) or by fluorescence microscopy (chapter 3.2.5). 5 ml yeast culture of  $OD_{600} \sim 3$  was sedimented by centrifugation (2000 rpm, 5 min, RT). The cells were washed once with SD-N and set to  $OD_{600} \sim 10$  in SD-N. Then, samples (1-4  $OD_{600}$ ) were taken at different time points (t= 0, 2, 4, 6 h) for alkaline lysis (chapter 3.2.7.1.1) and immunoblot analysis (chapter 3.2.7.5/6). The detected signals were quantified using AIDA software. For fluorescence microscopy of starved cells, samples were analysed as described in chapter 3.2.5.

### 3.2.7 Biochemical methods

#### 3.2.7.1 Cell lyses

##### 3.2.7.1.1 Alkaline lysis of yeast cells

Cells (1-4 OD<sub>600</sub>) were harvested by centrifugation (7.000 rpm, 5 min, RT). The supernatant was removed and the pellet resuspended in ice-cold ddH<sub>2</sub>O. Subsequently, 150 µl lysis solution (1.85 M NaOH, 7.5% β-mercaptoethanol) was added and mixed. After 10 min of incubation on ice, 150 µl of 50% (w/v) TCA was supplemented. The probe was mixed and incubated on ice for at least 10 min. After centrifugation (13.000 g, 10 min, 4°C), the supernatant was removed. The pellet was washed twice with ice-cold acetone (stored at -20°C). After the last centrifugation step, the supernatant was removed and the pellet was air dried at 37°C. Finally, the pellet was dissolved in 100 µl 2 x laemmli buffer (116 mM Tris/HCl pH 6.8, 12% (w/v) glycerol, 3.42% (w/v) SDS, 0.004% bromphenolblue, 2% β-mercaptoethanol).

##### 3.2.7.1.2 Osmotic lysis of spheroplasts

250 OD<sub>600</sub> of cells were harvested (2000 rpm, 5min, 4°C) and washed with 13 ml ice-cold 10 mM NaN<sub>3</sub>. After removing the supernatant, the cell sediment was resuspended in 2.5 ml SP buffer (50 mM potassium phosphate buffer pH 7.5, 10 mM NaN<sub>3</sub>, 1.4 M sorbitol, 40 mM βMe). 100 µl of zymolase 100T (0.75 mg solved in 100 µl SP buffer and 15 min preincubated at 30°C) was added and the reaction was incubated in a water bath at 30°C (40 rpm) for 30 min. The spheroplasts were sedimented (1000 g, 10 min, 4°C) and washed with a glass stick in 2.5 ml SP buffer. For this, ice-cold SP buffer was added in 0.5 ml steps (5 x 0.5 = 2.5ml) to avoid re-aggregation of the spheroplasts. After centrifugation (2000 g, 10 min, 4°C), the spheroplasts were lysed hypotonically with a small potter homogenizer (size: 2 ml) in lysis buffer (1 x PBS pH 7.4, 5 mM MgCl<sub>2</sub>, 0.2 M sorbitol, protease inhibitors, 1 x Complete (w/o EDTA) (Roche), 1 mM PMSF). For this, the spheroplast pellet was carefully resuspended in 250 µl of ice-cold lysis buffer and transferred to a cold potter homogenizer. Then, the spheroplasts were treated with 2 x 15 “beats” of the potter (the potter homogenizer with the cell lysate was cooled down on ice for 1 min after the first 15 beats). 250 µl ice-cold lysis buffer was added to the cell lysate (in the potter) and transferred to an eppendorf cup (on ice). After this step, the volume of cell lysate was about 750 µl. 1% Triton (37.5 µl of 20% Triton stock in 750 µl

## Materials and Methods

cell lysate) was added and the sample was inverted 10 times. After sedimentation of the cell debris (2700 g, 5 min, 4°C), the supernatant (~500 µl) was used for further studies.

### 3.2.7.2 GST-Atg8 and GST-Atg26 187-569 pull downs

#### 3.2.7.2.1 Expression of GST-Atg8 and GST-Atg26 187-569

For expression of GST-Atg8 or GST-Atg26 187-569, Bl21/pLys *E. coli* were transformed with the respective plasmids (pGEX 4T3-GST-Atg8 or pGEX 4T3-GST-Atg26 187-569) (chapter 3.2.3.17). Liquid pre-culture were inoculated and incubated over night at 37°C under shaking. On the next day, the culture was diluted to OD<sub>600</sub>~0.2 and shaken (220 rpm) for 90 min at 37°C. To induce expression, 0.2 mM IPTG was added. Furthermore, 1mM PMSF was supplied to avoid degradation. Protein expression was performed for 4-5 hours at 30°C under shaking (220 rpm). Then, the cells were sedimented by centrifugation (5000 rpm, 5 min, RT), washed with 1 x PBS and frozen with liquid nitrogen. The pellets were stored at -80°C.

#### 3.2.7.2.2 Purification of GST-Atg8 and GST-Atg26 187-569

The cell pellet was resuspended in 5 ml ice-cold lysis buffer (1 x PBS pH 7.4, 2 mM MgCl<sub>2</sub>, protease inhibitors (Sigma)) supplemented with 1 µl benzonase. Next, 1 % Triton X-100 was added and the sample was carefully inverted 5 times. After this, the sample was centrifuged (10.000 rpm (JA20 rotor), 10 min, 4°C). For analysis of the input fraction by SDS-PAGE, 15 µl of the resulting supernatant was removed and diluted with 15 µl 4 x laemmli buffer (232 mM Tris/HCl pH 6.8, 24% (w/v) glycerol, 6.84% (w/v) SDS, 0.008% bromphenolblue, 4% β-mercaptoethanol). The supernatant was incubated with 100 µl 50% slurry of 1 x PBS-equilibrated Glutathione Sepharose™ 4B (GE healthcare) for 40 min at 4°C under shaking. After sedimentation of the GST-Atg8/GST-Atg26 187-569 coupled glutathione sepharose beads (500 g, 5min, 4°C), the supernatant was removed. The pellet was washed 3 times with 500 µl ice-cold 1 x PBS. After this, the supernatant was removed and the GST-Atg8 or GST-Atg26 187-569 coupled glutathione sepharose was used for pull down assays.

## Materials and Methods

### 3.2.7.2.3 GST-Atg8 and Atg26 187-569 pull down assays

40-100 OD<sub>600</sub> of yeast cells were centrifuged (2000 rpm, 5 min, 4°C). The pellet was washed with 5 ml ice cold 1 x PBS (2000 rpm, 5min, 4°C). Next, the cells were resuspended in 1 ml ice-cold lyses puffer (1 x PBS pH 7.4, 5 mM MgCl<sub>2</sub>, 0.2 M sorbitol, 0.5 % Triton, protease inhibitors, 1 x Complete (w/o EDTA) (Roche), 1 mM PMSF) and transferred to an eppendorf cup. 200 µl of glass beads were added. For cell lysis, the sample was harshly mixed for 20 min at 4°C. After sedimentation of the glass beads (5000 rpm, 5 min at 4°C), the supernatant was used for GST-Atg8 or GST-Atg26 187-569 pull down assays. For analysis of the input fraction by immunoblotting, 25 µl of supernatant was removed and diluted with 25 µl 4 x laemmli. GST-Atg8-or GST-Atg26 187-569-coupled glutathione sepharose beads were incubated with the supernatant of crude yeast cell extract for 2–4 hours under constant inverting (Roto-shake Genie, mixing action: roll). Incubation with GST-coupled beads was used as negative control. After incubation, the glutathione sepharose was washed 3 times with 1 ml ice-cold lyses buffer (500 g, 5min, 4°C). For elution of the bound fraction, the sepharose beads were resuspended in 50 µl 2 x laemmli buffer and boiled 10 minutes at 95°C. The beads were sedimented (500 g, 5 min, 4°C) and the supernatant was used for SDS-PAGE and immunoblot analysis.

### 3.2.7.3 Co-purification of GST-Gag and His-Atg26 187-569

#### 3.2.7.3.1 Expression of GST-Gag and His-Atg26 187-569

GST-Gag and His-Atg26 187-569 were expressed as described for GST-Atg8 and GST-Atg26 187-569 in chapter 3.2.7.2.1 with the modification that protein expression was performed over night at 16°C.

#### 3.2.7.3.2 Co-purification of GST-Gag and His-Atg26 187-569

The pellet of His-Atg26 187-569 expressing cells was resuspended in 10 ml ice-cold lysis buffer (1 x PBS pH 7.4, 2 mM MgCl<sub>2</sub>, protease inhibitors (Sigma)) supplemented with 1 µl benzonase. 5 ml of the resulting cell lysate was then used for resuspension and lysis of pellets from GST-Gag or GST (negative control) expressing cell. Next, 1% Triton X-100 was added and the samples were carefully inverted 5 times. After this, the samples were centrifuged at 2700 rpm for 10 min at 4°C. For analysis of the input fraction by SDS-PAGE (chapter 3.2.7.5), 15 µl of the resulting supernatant was removed and diluted with



## Materials and Methods

15 µl 4 x laemmli buffer (232 mM Tris/HCl pH 6.8, 24% (w/v) glycerol, 6.84% (w/v) SDS, 0.008% bromphenolblue, 4% β-mercaptoethanol). The supernatants were incubated with 70 µl 50% slurry of 1 x PBS-equilibrated glutathione sepharose™ 4B (GE healthcare) for 1 h at 4°C under shaking. After sedimentation of the GST-Gag or GST coupled glutathione sepharose beads (500 g, 5min, 4°C), the supernatant was removed. The pellet was washed 3 times with 1000 µl ice-cold lysis buffer. For elution of the bound fraction, the sepharose beads were resuspended in 50 µl 2 x laemmli buffer and boiled for 10 minutes at 95°C. The beads were sedimented (500 g, 5min, 4°C) and the supernatant was used for immunoblot analysis.

### 3.2.7.4 GFP- and RFP-TRAP

The GFP(/RFP)-TRAP protocol of this study was used for purification of GFP(/mCherry)-tagged proteins together with associated protein complexes from cell extracts. Before incubation of cell lysates with the GFP(/RFP)-TRAP\_A beads, the beads were equilibrated. For this 10-12 µl of the bead slurry was resuspended in 500 µl wash buffer (1 x PBS pH 7.4, 5 mM MgCl<sub>2</sub>, 0.2 M sorbitol, 0.5% Triton, protease inhibitors, 1 x Complete (w/o EDTA) (Roche), 1 mM PMSF), inverted ten times and sedimented (2000 g, 2 min, 4°C). The supernatant was removed. 250 OD of cells expressing the GFP(/RFP) tagged proteins of interest were osmotic lysed as described in chapter 3.2.7.1.2. For analysis of the input fraction by SDS-PAGE and immunoblotting (chapter 3.2.7.5/6), 25 µl of the resulting cell lysate (~500 µl) was removed and diluted with 25 µl 4 x laemmli. The cell lysate was added to the equilibrated GFP(/RFP)-TRAP®\_A beads and incubated for 2-3 h at 4°C under constant inverting (Roto-shake Genie, mixing action: roll). After incubation, the sample was centrifuged (2000 g, 2 min, 4°C). For immunoblot analysis of the non-bound fraction, 25 µl of the supernatant was diluted with 25 µl 4 x laemmli buffer. The beads were washed three times with 1 ml ice-cold wash buffer (2000 g, 2 min, 4°C). For elution of the bound fraction, the beads were resuspended in 50 µl 2 x laemmli buffer and boiled 10 minutes at 95°C. Beads were collected by centrifugation at 2000 g for 2 min at 4°C. The supernatant (bound fraction) and the input fraction were analysed by SDS-PAGE and immunoblotting (chapter 3.2.7.5/6).

## Materials and Methods

### 3.2.7.5 SDS-Polyacrylamid-Gel-Electrophoresis (PAGE)

Discontinuous SDS-PAGE is a biochemical method to separate proteins according to their electrophoretic mobility, which negatively correlates with the molecular weight (Lämmli, 1970). SDS-PAGE was performed in a Mini-Protean III electrophoresis chamber from Biorad according to the recommendations of the manufacturer. The SDS-polyacrylamid-gels were produced as described in table 3.12.

**Table 3.12 Composition of one SDS Polyacrylamid gel for a Mini-Protean III electrophoresis chamber from Biorad**

Components	10 % Separating Gel	5 % Collecting Gel
ddH <sub>2</sub> O	1.9 ml	3.0 ml
1.5 M Tris, pH 8.8	1.25 ml	-
0.5 M Tris PH 6.8	-	1.25 ml
Protogel	1.8 ml	1.8 ml
10% (w/v) SDS	50 µl	50 µl
10% (w/v) APS	50 µl	50 µl
TEMED	2.5 µl	5 µl

A gel chamber was filled with SDS running buffer (200 mM glycerol, 25 mM Tris, 0.1% SDS). The protein marker *Precision Plus Protein All Blue Standard* (Bio-Rad) was used to estimate the molecular weight of the separated proteins. For SDS-PAGE, samples were dissolved in laemmli. Typically, 10–15 µl of a protein sample was loaded per lane. The electrophoresis was performed at 80-150 V. When bromphenolblue of the laemmli buffer reached the end of the gel, the run was stopped. The gel was used for immunoblotting (chapter 3.2.7.6) or Coomassie staining (chapter 3.2.7.7).

### 3.2.7.6 Immunoblotting

Immunoblotting is used to detect proteins separated by SDS-PAGE and in following steps transferred onto a PVDF membrane. For transferring the proteins separated by SDS-PAGE onto a membrane, the PA gel and 6 Whatman papers (6 x 9 cm) were soaked in blotting buffer (192 mM glycin, 25 mM Tris, 20% methanol) and the PVDF membrane (6 x 9 cm) in 20% methanol. The components were arranged in a semi-dry blotting chamber as shown in Figure 3.1.

## Materials and Methods

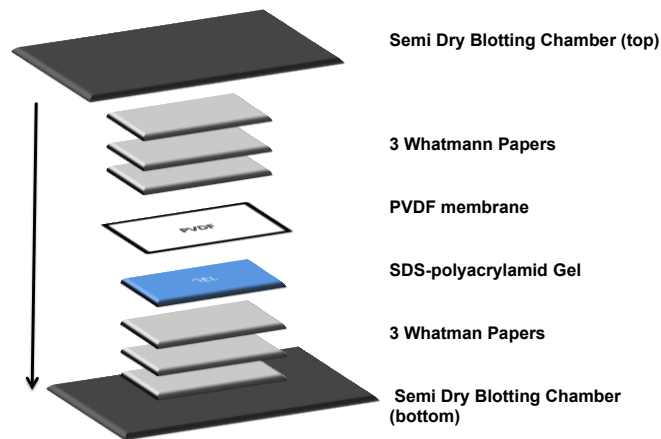


**Figure 3.1. Arrangement in a semi-dry blotting chamber**

Blotting was performed at 75 mA (per gel) for 90 min. After protein transfer, the membrane was incubated in TBST blocking buffer (20 mM Tris/HCl pH 7.6, 137 mM NaCl, 0.1% (w/v) Tween20, 10% (w/v) skim milk powder) for at least 30 min at room temperature or over night at 4°C. After blocking, the membrane was washed with TBST (20 mM Tris/HCl pH 7.6, 137 mM NaCl, 0.1% (w/v) Tween20) for 5 min. This step was repeated 3 times. Next, the membrane was incubated with the first antibody, diluted in TBST with 1% skim milk powder (dilution of the used antibodies in table 3.5) over night at 4°C. After this, the membrane was washed 3 times with TBST (3 x 5 min). The membrane was incubated with HRP-coupled secondary antibodies for 1 hour at room temperature. After incubation, the membrane was washed 3 times with TBST (3 x 5 min). For immunodetection, the ECL™ system (USB) and LAS-3000 (Fujifilm) was used following the manufacturer advice. The detected signals were quantified by using AIDA software.

### 3.2.7.7 Coomassie brilliant blue (CBB) staining

CBB staining is a biochemical standard method to visualize proteins separated by SDS-PAGE. The CBB staining method described here is based on a protocol of Wang et al. (Pink et al., 2010; Wang et al., 2007, personal communication). After SDS-PAGE (chapter 3.2.7.5), the gel was fixed with fixation buffer 1 (10% (v/v) phosphoric acid, 10% (v/v) methanol, 40% ethanol) for 1 h. Then, the gel was incubated in fixation buffer 2 (1% (v/v) phosphoric acid, 10% (v/v) ammonium sulphate) for 2 hours. After fixation, the gel was treated with staining buffer (10% phosphoric acid, 45% ethanol, 0.125% CBB G-250) over night. On the next day, the gel was incubated in destaining buffer (5% (v/v)

## Materials and Methods

phosphoric acid, 40% ethanol) for 1 h and finally in water for 24 h.

### 3.2.7.8 MS analysis

CBB-stained protein bands of SDS-polyacrylamid gels were removed and in-gel digest was done using trypsin. The gel sections were washed with 25mM  $\text{NH}_4\text{HCO}_3$ /water, 25 mM  $\text{NH}_4\text{HCO}_3$ /50% acetonitrile and 100% acetonitrile. Then, disulfides were reduced with 10 mM dithiothreitol, 25 mM  $\text{NH}_4\text{HCO}_3$ /water for 1 h at 56°C. After washing of the gel piece as described above and performing carbamidomethylation using 25 mM iodoacetoamide in 25 mM  $\text{NH}_4\text{HCO}_3$ /water, the in-gel digest was carried out using 120 ng trypsin at 37°C over night. Peptide extraction was done with 0.1% trifluoroacetic acid (TFA). Next, peptides were separated by reverse-phase chromatography (EASY-nLC; Bruker Daltonics) using a C18 column (PepMap 100 C18 nano-column; Dionex) and a 9.5%–90% acetonitrile gradient (in 0.1% TFA) for 80 min. The matrix used for MALDI was  $\alpha$ -cyano-4 hydroxycinnamic acid (HCCA) (4.5% saturated HCCA in 90% acetonitrile, 0.1% TFA and 1mM  $\text{NH}_4\text{H}_2\text{PO}_4$ ). It was mixed with the eluate of the reverse-phase chromatography and spotted automatically on a target (ProteinSpotter II; Bruker Daltonics). MALDI-TOF/TOF analysis was carried out using an ultraflextreme setup (Bruker Daltonics), which recorded MS as well as post-source decay MS/MS. Different software packages were used for data analysis and interpretation (WARP-LC, AutoXecute, Flex-Analysis and Biotoools; Bruker Daltonics). The data were searched against NCBI peptide database (<http://ncbi.nlm.nih.gov/BLAST/>) using an in-house Mascot server. Sample preparation and analysis with MALDI-TOF/TOF were performed by Olaf Bernhard and Dr. Bernhard Schmidt (Institute of Cellular Biochemistry, University of Göttingen).

## 4 Results

### 4.1 Optimization of GFP-Atg8-TRAP for quantitative MS analysis

A fundamental goal of this study was the establishment of a CoIP protocol with Atg8 as bait to identify new Atg8 interaction partners in following MS analysis. For optimization of the CoIPs, different factors were tested (Table 4.1): the tag of Atg8 and thus the CoIP system, different deletion strains to stabilize complexes of interest, marker proteins to evaluate the quality of the CoIPs, and cellular growth conditions. Furthermore, cell lyses and buffer conditions were optimized.

Plasmid encoded GFP-tagged Atg8 was fully functional and therefore GFP-TRAP was used as CoIP system (Amar et al., 2006; Schmidhals et al., 2010) ([www.chromotek.com](http://www.chromotek.com)). Co-purification of known direct interaction partners of Atg8, like the Cvt pathway receptor Atg19 (Shintani et al., 2002) and the PROPPIN Atg21 (Juris et al, unpublished), were tested as quality controls using plasmid expressed mCherry-Atg19 and Atg21-TAP (Table 4.1). Furthermore, isolation of the whole Cvt cargo complex (Ape1) was tested to verify the stability of GFP-Atg8 complexes during CoIP (Ho et al., 2009). Co-expression of mCherry-Atg19 should also force the accumulation of Cvt pathway associated proteins. The non-Cvt pathway proteins Fas1 and Fas2 were used as further marker proteins. The binding properties and the biological context of the interaction between Atg8 and Fas1/2 are still unclear.

The experiments for GFP-TRAP optimization showed that osmotic lyses of spheroplasts with PBS-based buffer (1 x PBS pH 7.4, 5 mM MgCl<sub>2</sub>, 0.2 M sorbitol, protease inhibitors, 1 x Complete (w/o EDTA) (Roche), 1 mM PMSF) gave the best results (Table 4.1). This buffer condition was applied in all following GFP-TRAP experiments of this thesis (chapter 3.2.7.1.2). To accumulate early Atg8 complexes at the PAS, an *atg1Δ/pep4Δ* strain was used. Deletion of *ATG1* disrupts autophagic transport of GFP-Atg8 and thereby its vacuolar degradation (Straub et al., 1997). The additional lack of vacuolar proteinase A (Pep4) further minimizes protein degradation during CoIP (Takeshige et al., 1992). To saturate the GFP-TRAP beads, the expression level of GFP-Atg8 was increased by using an inducible *GAL* promoter (pYES2-GFP-Atg8). Overexpression should also force the oligomerisation and, thus, the active conformation of bead-bound GFP-Atg8 (Nakatogawa et al., 2007; Schwarten et al., 2010)(see Table 4.1).

**Table 4.1 Tested conditions for optimization of GFP-Atg8-TRAP**

Deletion strains	Plasmid Expression ( <i>promoter/tag</i> )			Cellular condition	Lyses		Incubation	
	Atg8	Atg21	Atg19		method	buffer	time	detergent
<i>atg1/4Δ</i>	ATG8/GFP	ATG21/TAP	-	starvation	glassbeads	TRIS	1h	0.5% NP40
<i>atg4/8Δ</i>	ATG8/GFP	ATG21/TAP	-	starvation	glassbeads/ NP40	TRIS	1h	0.5% NP40
<i>atg4/8Δ</i>	ATG8/GFP	ATG21/TAP	-	starvation	glasseads	TRIS	1h	0.5% NP40
<i>atg4/8Δ</i>	ATG8/GFP	ATG21/TAP	-	starvation	spheroplast Douncer	MOPS	1h	-
<i>atg4/8Δ</i>	ATG8/GFP	ATG21/TAP	-	starvation	spheroplast Douncer	MOPS	1h	1% Triton
<i>atg4/8Δ</i>	ATG8/GFP	ATG21/TAP	-	starvation	spheroplast Douncer	PBS	1h	1% Triton
<i>atg8Δ</i>	GAL/GFP	ATG21/TAP	-	growth	spheroplast Douncer	PBS	1h	1% Triton
<i>atg1Δ</i>	GAL/GFP	ATG21/TAP	-	growth	spheroplast Douncer	PBS	1h	1% Triton
<i>atg1Δ</i>	GAL/GFP	ATG21/TAP	-	growth	spheroplast Douncer	PBS	1h	1% Triton
<i>atg1Δ/ pep4Δ</i>	GAL/GFP	ATG21/TAP	-	growth	spheroplast Douncer	PBS	1h	1% Triton
<i>atg1Δ/ pep4Δ</i>	GAL/GFP	ATG21/TAP	<i>MET25/ mCherry</i>	growth	spheroplast homogenizer	PBS	2h	1% Triton

For interpretation of the planned MS analysis (chapter 4.2), it was important to exclude false-positive interaction partners. Thus, different (GFP-)Atg8 mutants were used for the GFP-TRAP to validate specific interactions and to determine the Atg8 binding surfaces. Atg8 wild type (wt) and two Atg8 mutants of the UBL domain, including a W-site mutation (GFP-Atg8 L50A) and a L-site mutation (GFP-Atg8 Y49A), were integrated in the GFP-Atg8-TRAP optimization. These two sites mediate interaction with Atg8-interacting motifs (AIM) (Noda et al., 2008; Noda et al., 2010) and thus might give hints for AIM-dependent interactions. Furthermore, two Atg8 mutants of the N-terminal arm were tested: Mutations of the non-conserved S3T4 sequence (GFP-Atg8 S3AT4A) and mutations of the highly conserved FK-motif (GFP-Atg8 F5GK6G). It was shown for the FK motif that it mediates complex formation with the Cdc48 adaptor Shp1 (Krick et al., 2010). GFP-Atg8 S3AT4A was used as further positive control (Figure 4.1A).

In the optimized GFP-TRAP analyses, growing *atg1Δ/pep4Δ* cells (OD<sub>600</sub>~3) expressing mCherry-Atg19 and Atg21-TAP together with the variants of GFP-Atg8 were used. To induce high expression of GFP-Atg8 (*GAL* promoter) and mCherry-Atg19 (*MET25* promoter), cells were grown over night in CM medium with 2 % galactose as carbon source and without methionine. Spheroplasts were osmotically lysed (chapter 3.2.7.1.2)

## Results

and cell lysates (input) incubated with GFP-TRAP beads to couple GFP-Atg8 together with associated complexes. After washing, GFP-Atg8 and putative interaction partners were eluted by 2 x l mmli (bound fraction)(chapter 3.2.7.4). The input fraction and the bound fraction (GFP-Atg8-TRAP) were analysed by immunoblotting (Figure 4.1B). The optimized GFP-TRAP was repeated in 8 independent experiments. The respective immunoblots were quantified and normalized to the amount of bound GFP-Atg8. Furthermore, interactions with GFP-Atg8 wt were set to 100% (Figure 4.1C).

Consistently with previous results of my lab (Juris et al, unpublished), the GFP-Atg8-TRAP showed that Atg8 interacts with Atg21. Highly reduced interactions were detectable when the W-site (L50A: 29%) or the FK-motif (F5GK6G: 45%) was mutated (Figure 4.1B and C). As expected, the mutations of the non-conserved ST sequence (S3AT4A) had no influence on the interaction between Atg21 and Atg8 (Figure 4.1B and C). The AIM-containing receptor protein Atg19 needed both AIM-binding sites for interaction as already published (Noda et al., 2008). Consistently, the Cvt pathway cargo prApeI that is linked to Atg8 by Atg19 had a comparable interaction pattern: a more than 85% reduced level of interaction with Atg8 L50A or Atg8 Y49A. Modifications in the N-terminal domain of Atg8 had fewer effects on the interaction with Atg19/pApe1 (Figure 4.1B and C). In contrast to the other tested marker proteins, complex formation between Fas1/Fas2 and Atg8 did not depend on the W-site (L50), but on the L-site (Y49) and the FK-motif (Figure 4.1B and C).

Under the same growth conditions as described above, subcellular localisation of mCherry-Atg19 and the different GFP-Atg8 variants were monitored by fluorescence microscopy (Figure 4.1D, left). In agreement with previous reports (Shintani et al., 2002), an early block of the Cvt pathway (*atg1Δpep4Δ*) led to strong accumulation of (mCherry-)Atg19 and (GFP-)Atg8 at the PAS. It was also confirmed by this analysis that GFP-Atg8 Y49A and L50A showed extremely smaller PAS dot-like structure or even no PAS localisation (Amar et al., 2006; Nakatogawa et al., 2007). To quantify colocalisation of mCherry-Atg19 and the different GFP-Atg8 variants, Pearson's correlation coefficients ( $R^2$ ) between the GFP and the mCherry signals were calculated using SoftwoRx software (Applied Precision) (Figure 4.1D, right). Consistently with the GFP-Atg8-TRAP, quantifications indicated that mutations of the AIM-binding sites (L50A or Y49A) had drastic negative effects on the colocalisation of Atg8 and Atg19 (Figure 4.1D).

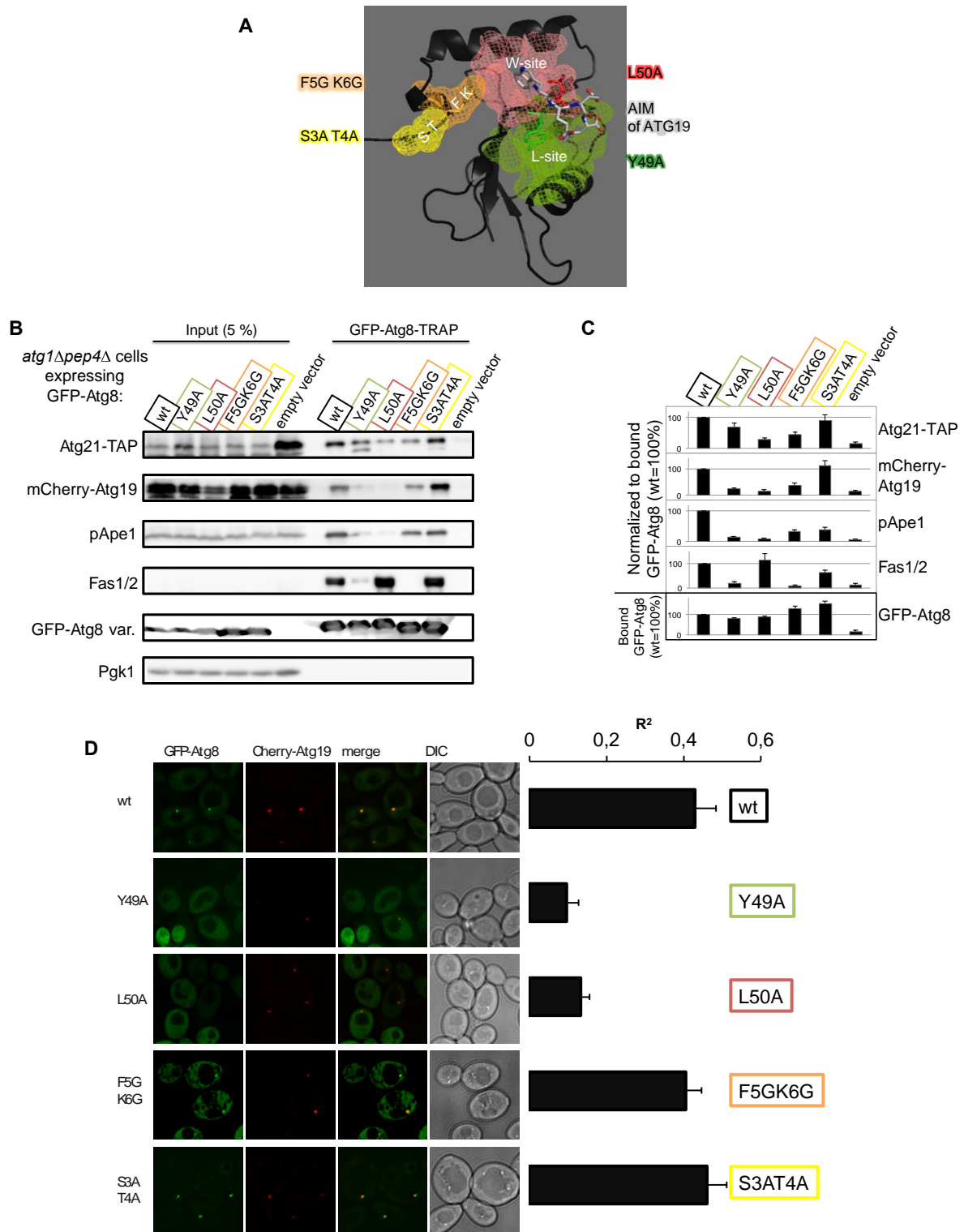


**Figure 4.1 Optimization of immunoprecipitation using GFP-TRAP**

(A) Cartoon representation of Atg8 with the indicated residues that were mutated for the GFP-TRAP: GFP-Atg8 L50A (red), Y49A (green), F5G/K6G (orange) and S3A/T4A (yellow).

(B, C) GFP-Atg8 TRAP. *atg1Δ/pep4Δ* cells expressing GFP-Atg8 variants together with mCherry-Atg19 and Atg21-TAP were grown to  $OD_{600} \sim 3$ , osmotically lysed and subjected to GFP-TRAP. Input and bound fractions (GFP-Atg8-TRAP) were analysed by immunoblots and quantified (C). Data of 8 independent experiments were quantified and normalised to the bait. Interactions with GFP-Atg8 wt were set to 100%.

(D) *atg1Δ/pep4Δ* cells expressing GFP-Atg8 variants together with mCherry-Atg19 and Atg21-TAP were grown to  $OD_{600} \sim 3$  and analysed by fluorescence microscopy. Colocalisation was quantified by calculating the Pearson's correlation coefficients ( $R^2$ ) of GFP- and mCherry signals. Error bars indicate  $\pm$ SEM (C and D).



## Results

In further studies, the bound fractions of the established GFP-Atg8-TRAP were analysed by colloidal Coomassie (CBB) staining of SDS-PAGE to estimate the overall amount and the diversity of the co-purified interaction partners (Figure 4.2A): As expected, the negative control (empty vector) had the minimum of stained bands. The other samples showed the expected GFP-Atg8 bands at about 37 kDa and various additional bands with individual band patterns in each lane, supporting the extensive immunoblot analysis of the different marker proteins (Figure 4.1B and C). Taken together, the robustness of the optimized GFP-Atg8-TRAP seemed promising for quantitative MS analysis to find new Atg8 interaction partner.

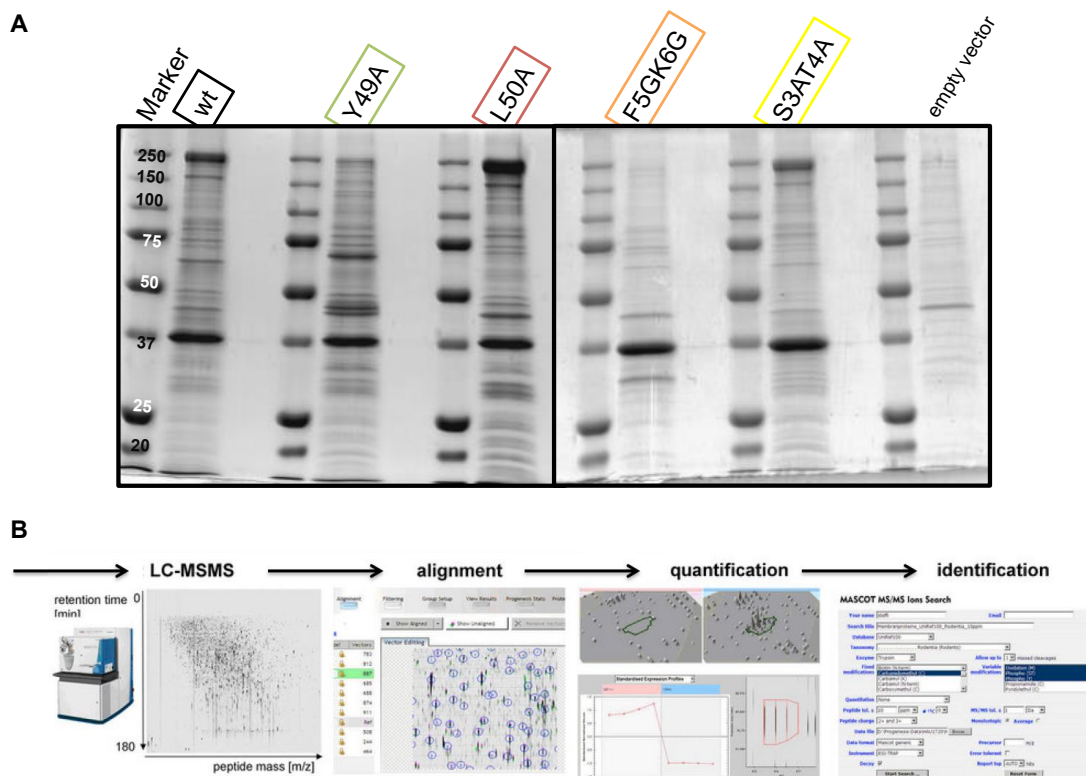


**Figure 4.2 CBB staining of SDS-PAGE as further quality control for the GFP-Atg8-TRAP**

(A) Protein extracts of *atg1Δ/pep4Δ* cells expressing GFP-Atg8 variants together with mCherry-Atg19 and Atg21-TAP were incubated with GFP-TRAP beads. Co-purified proteins were subjected to SDS-PAGE followed by CBB staining.

(B) For identification of putative, novel Atg8 interaction partners, the GFP-Atg8 samples were analysed by quantitative, label-free mass spectrometry in collaboration with the Department of Bioanalytics of Prof. Albert Sickmann (Leibniz-Institut für Analytische Wissenschaften, ISAS eV, D-44227 Dortmund, Germany). The samples were analysed by LC-MS/MS. Quantification was performed using the software Progenesis QI, Nonlinear Dynamics.

In collaboration with the Department of Bioanalytics of Prof. Albert Sickmann, the GFP-TRAP samples were analysed in a quantitative, label-free MS protocol done by Yvonne Pasing (Leibniz-Institut für Analytische Wissenschaften, ISAS eV, D-44227 Dortmund, Germany). The label-free workflow included liquid chromatography with tandem mass

spectrometry (LC-MS/MS), peptide/protein quantification (Progenesis Q1, Nonlinear Dynamics) and protein identification (summarized in Figure 4.2B). Data mining and validation of the newly identified, putative Atg8 interaction partners were an aspect of this thesis and is described in chapter 4.2 and 4.3.

### 4.2 Data mining of the quantitative MS analysis

On the basis of the label-free quantitative MS analysis of the different Atg8 mutants, newly identified proteins were sorted by their individual interaction patterns. The relative protein abundances of the different samples were illustrated in a colour code (heat map) from white (0-fold) to orange (1-fold=wt level) to red (2-fold and more) (see legend on the bottom of Figure 4.3E).

A total of about 430 proteins were identified (Figure 4.3D). Around 340 candidates non-specifically bind Atg8 under the chosen buffer conditions, indicated by interactions with almost all Atg8 mutants (examples in Figure 4.3E). Further categorization of approximately 90 putative specific Atg8 binders was done with a detailed view on the AIM-binding sites: if there was a more than 10% (0.9-fold) reduced level compared to wt (1) or wt (2), the mutated site (L50A, Y49A) was classified as a putative interaction surface. Since mutations of the N-terminal region (F5GK6G; S3AT4A) showed an abnormally increased level of interaction in most cases, they were not considered in this first round of sorting.

About 50 interactors needed both AIM-binding sites of Atg8 for interaction (Figure 4.3A and D). This group of putative AIM-containing/-dependent Atg8 binders was supported by the unbiased selection of already known AIM-containing/-dependent proteins: Atg3 and especially the Cvt pathway proteins Atg19, Atg34 and Ape1 (Ichimura et al., 2000; Shintani et al., 2002; Suzuki et al., 2010; Yamaguchi et al., 2010). But there were also some unclear candidates that were sorted in alternative groups (marked with an asterisk in Figure 4.3B and C): For example, the COPI complex proteins Cop1, Sec21, Sec27, Sec26 and Sec28 showed a hardly decreased interaction when the L-site was mutated (Y49A). An obviously lower interaction was detectable in GFP-Atg8 L50A samples. Consequently, the COPI vesicle proteins were also grouped in "L50A" (Figure 4.3.C). Together with these proteins, the L50A-group contained 20 candidates.

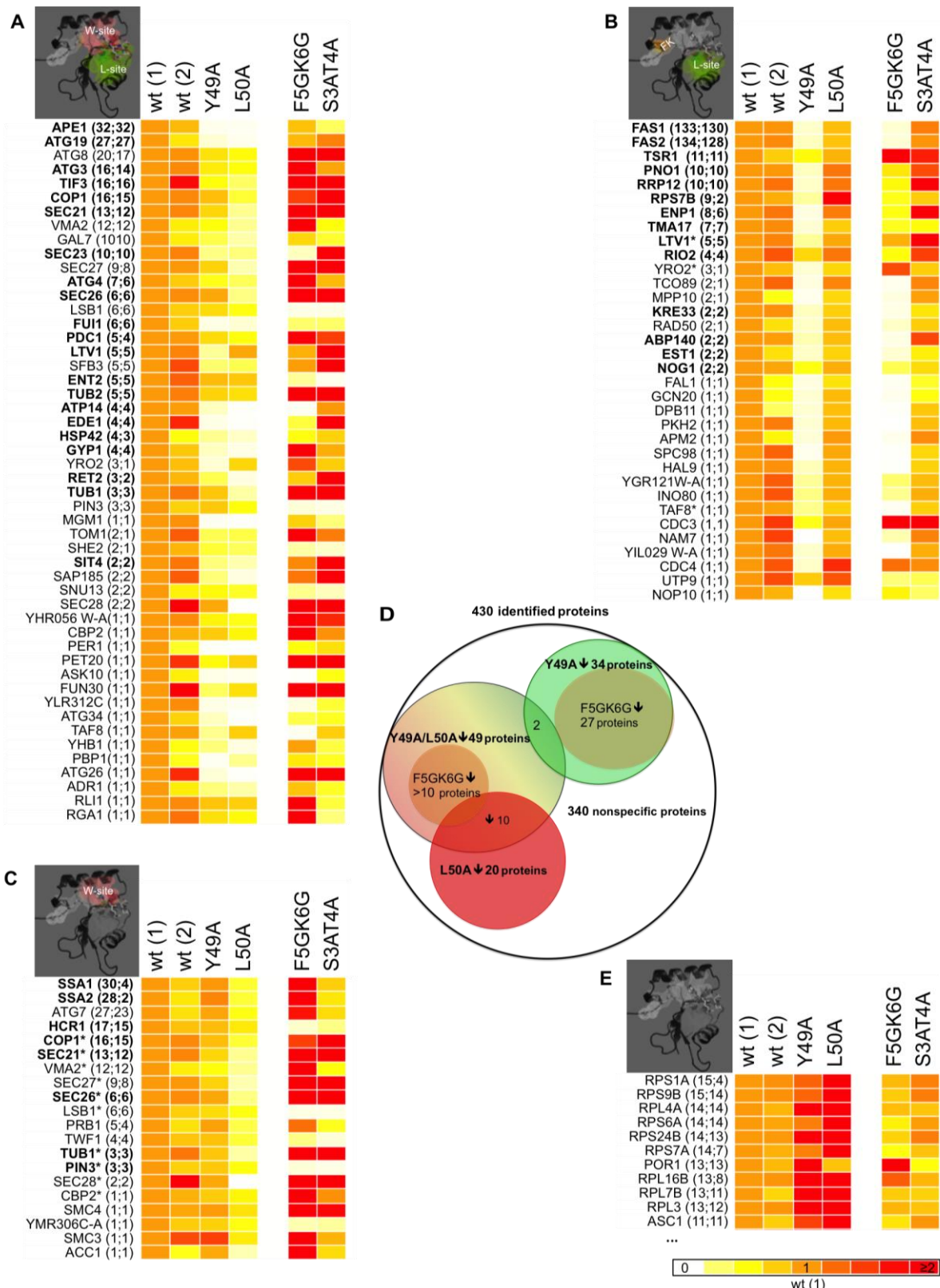


**Figure 4.3 Heatmaps of selected putative Atg8 interactors identified by quantitative mass spectrometry (Dept. of Bioanalytics of Prof. Albert Sickmann)**

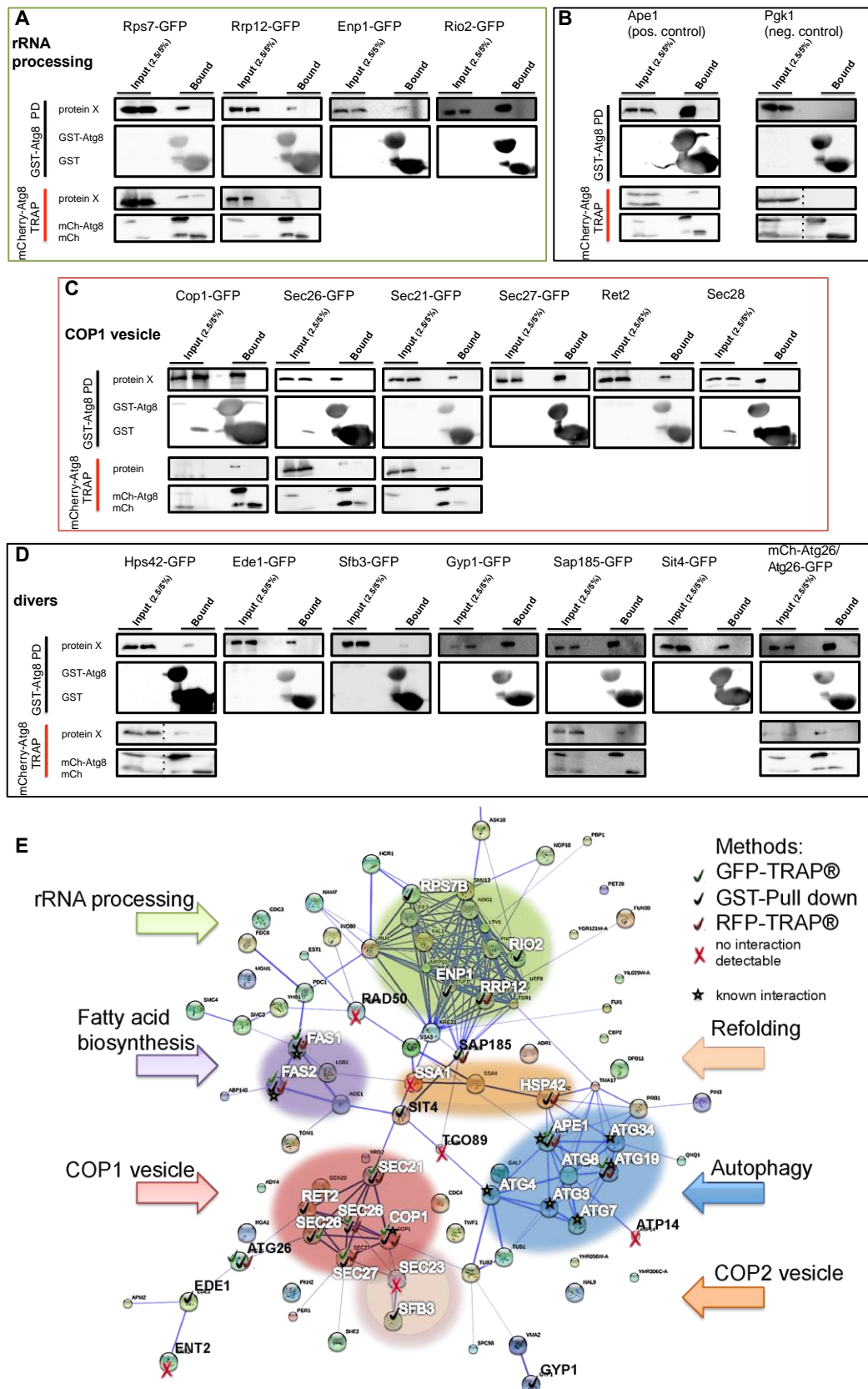
The normalized protein abundances of sample wt (1) were set to 1(-fold). The colour code (heat map) shows a spectrum from white (0-fold) to orange (1-fold = wt (1) level) to red (2-fold and more). Interaction surfaces of Atg8 were grouped as follows: (A) both AIM-binding sites, (B) the L-site (and the FK motif), (C) the W-site or (E) examples for unspecific interactors. Numbers in brackets indicate the peptide count and the peptides used for quantification. Asterisks mark putative binding partners that are sorted in two groups. Proteins written in bold were not identified in the negative control (empty vector, not quantified). (D) Summary of the protein sorting.

Figure 4.3B shows 34 candidates that needed only the L-site (Y49) of the AIM binding site for interaction. Interestingly, a highly decreased interaction was also detected for many of these Atg8 binders if the FK-motif was mutated (F5GK6G). Fas1 and 2 were typical exemplars of this category (Figure 4.3B).

In summary, from 430 identified proteins, 90 were sorted as putative, specific Atg8 interactors. As a supporting fact, this selection also included already known, published Atg8 binders.

### 4.3 Validation of the quantitative MS analysis

Validation of the quantitative MS analysis was performed by GST-Atg8 pull downs (PD) (modified from (Krick et al., 2010), chapter 3.2.7.2). Lysates from cells that chromosomally express GFP-tagged potential Atg8 interactors (Invitrogen) (Huh et al., 2003) were used as inputs (Figure 4.4A-D, immunoblots on the top). With this modus operandi, putative interaction partners of GST-Atg8 were easily detectable by using a GFP antibody for immunoblotting. Another option was labelling of the PD fractions with protein specific antibodies (against Ape1, Pgc1, Ret2 and Sec28) or the detection of tagged proteins expressed on plasmid (mCherry-Atg26). For the GST-Atg8 PDs, recombinant expressed GST-Atg8 was coupled to glutathione sepharose beads. Then, the GST-Atg8 beads were incubated with crude cell extract (input 2.5%), washed and eluted with 2 x laemmli (bound). Glutathione beads coupled with recombinantly expressed GST alone were used as negative control. The quality of the PDs was checked with antibodies against the positive control Ape1 and the negative control Pgc1 that should bind neither GST-Atg8 nor GST alone (Figure 4.4B). All in all, 17 of 25 tested putative novel Atg8 interaction partners were confirmed by this method (Figure 4.4A, C and D).



**Figure 4.4 Validation of the quantitative MS analysis**

Interesting candidates of the quantitative MS were analysed by GST-Atg8 PDs (top) or mCherry-Atg8-TRAP (bottom) (A, B, C and D). For the GST-Atg8 PD, crude cell extracts from cells chromosomally expressing the protein of interest were incubated with GST-Atg8- or GST-coupled beads. For the mCherry-Atg8-TRAP, cells expressing mCherry-Atg8 or mCherry alone together with chromosomally GFP-tagged proteins of interest were grown to  $OD_{600} \sim 3$ , osmotically lysed and subjected to RFP-TRAP beads. Input

## Results

and bound fractions were analysed by immunoblotting.

(D) Functional grouping of newly identified Atg8 interaction partners and validation by GST-Atg8 PD assay (white mark), GFP-Atg8-TRAP (green mark) and mCherry-Atg8-TRAP (red mark). Functional protein association network of all specific interaction partners was created by [www.string-db.org](http://www.string-db.org).

---

An alternative method was the mCherry-Atg8-TRAP (Figure 4.4A-D, immunoblots on the bottom)(chapter 3.2.7.1.2 and 3.2.7.4). Therefore, growing cells ( $OD_{600} \sim 3$ ) chromosomally expressing the GFP-tagged proteins of interest together with mCherry-Atg8 or mCherry alone were osmotically lysed. Then, the lysate (input) was incubated with RFP (mCherry) antibody-coupled beads (RFP-TRAP, Chromotek). After extended washing, the co-purified proteins were eluted with 2 x laemmli (bound). One immense drawback of this method was the tendency of many tested proteins to unspecifically bind the control beads (mCherry alone) in a relative high level such as Rps7b-GFP (Figure 4.4A). Besides, mCherry-Atg8 showed a higher stability than mCherry alone that further increased the difficulties of interpretation.

To visualize a functional protein association network of the selected 90 proteins (chapter 4.2.), the biological database STRING ([string-db.org](http://string-db.org)) was used (Figure 4.4E). The output of STRING reflects the confidence score of published experimental data for interactions, co-expression, co-reference in paper abstracts (pubmed), the similar genetic context in different species and so on (Szklarczyk et al., 2010). In this overview based on STRING, novel putative Atg8 interactors were grouped concerning their cellular function as follows: autophagic proteins (Atg3, Atg4, Atg7, Atg19, Ape1, Atg34), COPI vesicle proteins (Cop1, Sec21, Sec27,...), COPII proteins (Sec23, Sfb3), (nucleolar/nuclear) rRNA processing proteins (Rrp12, Pno1, Rio2, ...), chaperones (Hsp42, Ssa1,...) and proteins that are involved in fatty acid biosynthesis (Fas1, Fas2,..) (Figure 4.4E). However, many identified proteins could not be grouped, because there was no functional link or the function was still unclear.

# Results

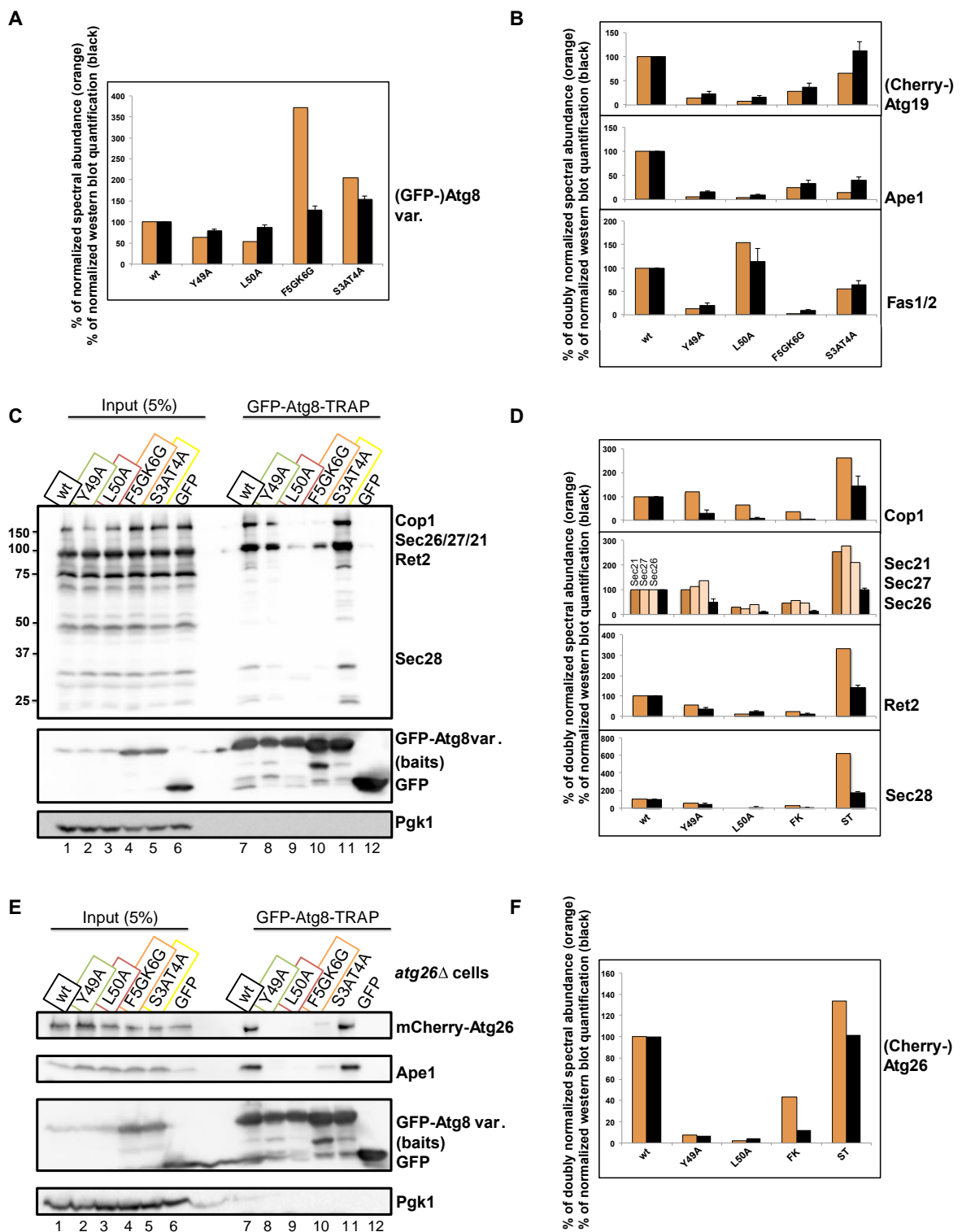


**Figure 4.5 Detailed comparison of immunoblotting and quantitative MS of GFP-Atg8-TRAPs**

GFP-Atg8-TRAP bound fractions were quantified and normalized to respective GFP-Atg8 variants (baits) for comparing immunoblots (black bars) and the protein abundance measured by qMS (orange bars) (Dept. of Bioanalytics of Prof. Albert Sickmann).

(A) Comparison of the GFP-Atg8 variants (baits). These data were used for normalization by calculating the ratio of putative interactors and respective GFP-Atg8 variants ( $signal_{interactor}/signal_{GFP-Atg8\ var}$ ) (B, D, F). Interactions with GFP-Atg8 wt (mean of wt (1) and (2)) were set to 100%.

Crude cells extracts from (B) *atg1/pep4* $\Delta$  cells expressing GFP-Atg8 variants together with mCherry-Atg19 and Atg21-TAP, (C and D) cells expressing GFP-Atg8 variants, or (E and F) *atg26* $\Delta$  cells expressing GFP-Atg8 variants together with mCherry-Atg26 were incubated with GFP-TRAP beads and analysed in n=8 (B), n=3 (D) or n=2 (F) independent experiments. Samples were immunoblotted and quantified. Error

bars indicate  $\pm$ SEM.

---

More detailed experimental validation was performed by comparing quantitative MS data and the immunoblot quantifications (Figure 4.5). As mentioned above, the GFP-Atg8 F5GK6G and GFP-Atg8 S3AT4A samples seemed to have a higher abundance for the identified proteins. This result was modified by the observation that also the bait levels were increased in these samples (Figure 4.5A). Therefore, the abundances of the identified proteins were normalized to the respective abundance of Atg8. Then, the normalized abundances of the wt samples (mean of wt (1) and wt (2)) were set at 100% and the other samples adapted. The immunoblots were quantified as described in chapter 4.1 (Figure 4.1C).

Comparison of both protein detection methods clearly suggests that the quantitative MS data of the marker proteins (Atg19, Ape1, Fas1 and Fas2) were in good agreement with the immunoblot analysis (Figure 4.5B). Therefore, this quantitative MS analysis seemed promising for further predictions of newly identified Atg8 binding partners and the surfaces that mediate these interactions.

To proof these results, some newly identified Atg8 binders already validated by GST-Atg8 PD or mCherry-Atg8-TRAP (Figure 4.4) were tested using the standard GFP-Atg8-TRAP protocol and quantified as described above (Figure 4.5C and D). In this context, the COPI vesicle coatomer proteins Cop1, Sec21, Sec27, Sec26, Ret2 and Sec28 were analysed (Figure 4.5C and D). Lysates from growing wild type cells ( $OD_{600} \sim 3$ ) expressing GFP-Atg8 variants or GFP alone were used. In immunoblot analyses, COPI vesicle proteins were detected with a polyclonal antibody against the whole complex. Since Sec21, Sec27 and Sec26 have nearly the same molecular weight, it was not possible to discriminate between these proteins. However, MS data and immunoblot analysis both showed consistently that complex formation between Atg8 and COPI proteins strongly depends on the W-site and the FK-motif of Atg8 (Figure 4.5C lanes 9 and 10).

Another interesting candidate was Atg26, since its function in *S. cerevisiae* was still unknown (Cao and Klionsky, 2007)(Figure 4.5D and E). Methodically, the standard GFP-Atg8-TRAP protocol was performed with *atg26* $\Delta$  cells expressing the different variants of GFP-Atg8 or GFP alone together with mCherry-Atg26. Again, immunoblot analysis and normalised quantitative MS data had a high similarity: Both methods indicated that the AIM-binding sites of Atg8 (Figure 4.5E lane 8 and 9) mediate interaction with (Cherry-)



## Results

Atg26, suggesting that Atg26 is an AIM-containing protein or somehow indirectly binds Atg8 in an AIM-dependent manner.

For further validation of the Atg8-Atg26 interaction, the split-ubiquitin assay was performed (Figure 4.6A). The split-ubiquitin assay detects protein interactions in living yeast cells (chapter 3.2.4) (Müller and Johnsson, 2008). For these *in vivo* studies, SEY6210 cells were transformed with the plasmids CUP1-Nub-Atg8 (bait) or pRS314 (negative control) in combination with Cub-Atg26 (prey). Nub constructs contain the N-terminal half of ubiquitin, followed by the protein of interest (in this case Atg8), whereas the Cub plasmids start with the protein of interest (here Atg26), followed by the C-terminal part of ubiquitin and the reporter protein R-Ura3. Protein interaction reassembles ubiquitin and in further steps causes degradation of R-Ura3. Due to this, R-Ura3 cannot convert supplemented 5-fluoroorotic acid (5-FOA) into the toxic compound 5-fluorouracil. This means, a high growth rate on 5-FOA plates indicates interaction between the bait and prey. Since R-Ura3 is able to synthesize uracil, slowed growth on medium without uracil also indicates protein interaction. As positive control, the known binding partners Ste14 and Ubc6 were used. Absence of the prey (-), which means transformation with the empty vector pRS314, was used as negative control. Expression of the fusion constructs was induced by 100  $\mu\text{M}$   $\text{CuSO}_4$  (Nub constructs) and 250  $\mu\text{M}$  methionine (Cub constructs). Cells were diluted in 10-fold steps and spotted on CM (-Trp/-His)(growth control), CM +FOA (-Trp/-His) (growth implies protein interaction) and MV -Ura (-Trp/-His) (decreased growth implies protein interaction). The result of the FOA plate confirmed the Atg8-Atg26 interaction, indicated by the high growth rate of cells expressing Nub-Atg8 and Cub-Atg26. The growth test on the -Ura plate also implied interaction for these constructs, but the negative control showed nearly the same extremely slowed growth rate.

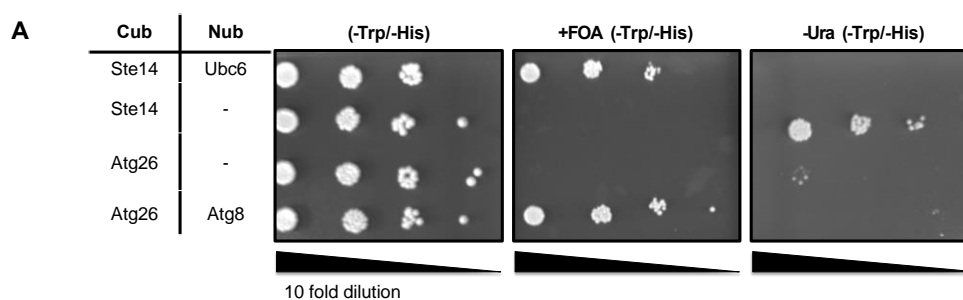


**Figure 4.6 Validation of Atg8-Atg26 interaction by the split-ubiquitin assay**

Split-ubiquitin assay. The N-terminal part of ubiquitin (Nub) is fused to the bait and its C-terminal part (Cub) to the prey. Protein interaction restores ubiquitin and leads to degradation of destabilised R-Ura3 variant. Bait/prey interaction is recorded by increased growth on 5-FOA-containing medium or by decreased growth rate on medium lacking uracil.

## Results

In the following analyses, a direct AIM-dependent interaction between Atg8 and Atg26 was confirmed and the AIM of Atg26 was exactly mapped (chapter 4.4 and 4.5). These observations strongly supported these initial GFP-Atg8-TRAP experiments and the followed quantitative MS analysis described here in the first three chapters (chapter 4.1, 4.2 and 4.3).

#### 4.4 Atg26 *physically* interacts with Atg8 via a very C-terminal Atg8 interacting motif (AIM)

Atg26 is a sterol glucosyltransferase (UDPGT domain) with two putative phosphoinositide-binding domains (PH and GRAM domain) (Yamashita et al., 2006). In *P. pastoris*, Atg26 is essential for degradation of very large methanol-induced peroxisomes, whereas the function of Atg26 was still enigmatic in *S. cerevisiae*, as no involvement of Atg26 in any type of autophagy was detected so far (Cao and Klionsky, 2007; Nazarko et al., 2007a; Nazarko et al., 2009).

The results from chapter 4.3 (Figure 4.5.E, D) showed that Atg26 had similar interaction pattern as already known AIM-dependent Atg8 binding partners, suggesting that Atg26 itself may contain an AIM. To test this hypothesis, the protein sequence of Atg26 was carefully analysed *in silico* for potential AIMs (Figure 4.7). For this, AIM criteria were established based on published AIMs or sequence analysis (Figure 4.7A) (Alemu et al., 2012). The AIM consensus sequence is  $W_0/F_0/Y_0-X_{+1}-X_{+2}-L_{+3}/I_{+3}/V_{+3}$  meaning that aromatic residues on position 0 and hydrophobic residues on position +3 are required for binding Atg8 (Figure 4.6A, grey background). All in all, fifteen sequences in Atg26 were found that fulfill these essential criteria (Figure 4.6B). Further important sequence properties were avoidance of basic residues (Figure 4.7A; blue letters, -1 unit on position  $X_{-4}$ ,  $X_{-3}$ ,  $X_4$ , and  $X_5$ ; -2 units on position  $X_{-2}$ ,  $X_{-1}$ ,  $X_1$ ,  $X_2$ ) and the accumulation of acidic residues (Figure 4.6A; red letters, +1 unit on position  $X_{-4}$ ,  $X_{-3}$ ,  $X_4$ , and  $X_5$ ; +2 units on position  $X_{-2}$ ,  $X_{-1}$ ) in this region. Only four putative AIMs showed all these characteristics (Figure 4.7B, STELYFPVLT, AIDDFMFVFM, EADVYCILNK and TDEGW $\underline{TMI}$ ). These four hypothetical AIMs were further analysed by fungi sequence alignment and illustrated by sequence logos (WebLogo 3.3) (Figure 4.7C). The resulting sequence logos indicated that only the very C-terminal putative AIM (*ScAtg26* 1191-1198) had a conserved sequence, especially at the essential positions 0 ( $W_0$ ) and +3 ( $L_3$ ) (Figure 4.7 C and D).

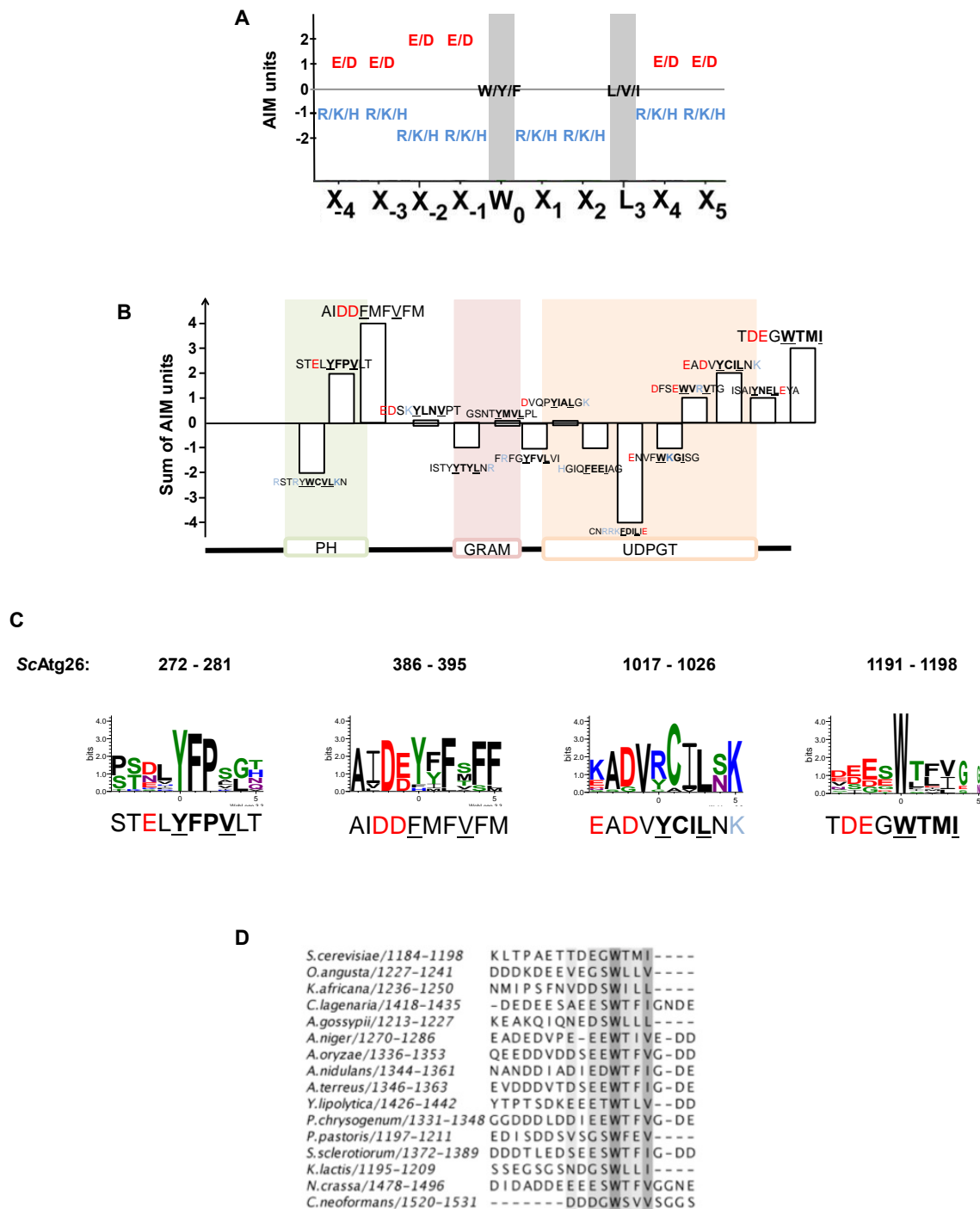


**Figure 4.7 Putative Atg8 interaction motifs (AIMs) in Atg26**

(A) Sequence criteria for putative AIMs based on published AIMs and sequence analyses. The canonical W/Y/F and L/I/V residues on position 0 and +3 are requirements for AIMs (grey). Blue letters indicate basic residues that are avoided in these regions (-1 unit for R/K/H on position X<sub>-4</sub>, X<sub>-3</sub>, X<sub>4</sub>, and X<sub>5</sub>; -2 units for R/K/H on position X<sub>-2</sub>, X<sub>-1</sub>, X<sub>1</sub>, X<sub>2</sub>). Red letters illustrate acidic residues that accumulate in AIMs (+1 unit for E/D on position X<sub>-4</sub>, X<sub>-3</sub>, X<sub>4</sub>, and X<sub>5</sub>; +2 units on position X<sub>-2</sub>, X<sub>-1</sub>).

(B) Searching for putative AIMs in Atg26. The x-axis schematically shows the positions of the putative AIMs and the respective predicted domain (PFAM database). The sum of AIM units from respective putative AIMs selected by the sequence criteria of (A) is indicated by the y-axis.

(C) Atg26 sequence logos of most prominent putative AIMs based on 16 fungal species were created by WebLogo 3.3. The total height of the stack shows the sequence conservation at the respective position. The height of the letter within the stack indicates the relative frequency of the amino acid.

(D) Sequence alignment of the very C-terminal AIM of Atg26 was created with Jalview 2.8 using the MAFFT algorithm.

## Results

To analyse if this very C-terminal sequence mediates complex formation with Atg8 or if other regions are involved, various truncated or mutated versions of Atg26 were cloned in mCherry and GFP vectors and tested by different methods (Figure 4.8). Atg26 fragments were created based on the predicted and published domain structure (Pfam, (Yamashita et al., 2006)). For detailed investigation of the C-terminal putative AIM, the versions Atg26 I1198A and Atg26 1-1194 ( $\Delta$ WTMI) were cloned (Figure 4.8A).

Atg8 binding sites within Atg26 were mapped by GFP-TRAP with the different GFP-tagged Atg26 variants as baits (chapter 3.2.7.4). Stationary *atg26* $\Delta$  cells expressing the different GFP-Atg26 fragments together with mCherry-Atg8 were analysed (Figure 4.8B). Although some truncated versions of GFP-Atg26 (Fig4.8B lane 3-5 and 11-13) were less stable and therefore barely comparable to wild type (GFP-Atg26 wt), co-purification of mCherry-Atg8 in the bound fraction of GFP-Atg26 wt and its absence in GFP-Atg26 1-1194 ( $\Delta$ WTMI) (Figure 4.8B, compare lane 15 and 16) clearly indicated that the predicted C-terminal AIM is necessary for Atg26-Atg8 interaction.

These findings were confirmed by a (standard) GST-Atg8 pull down assay (chapter 3.2.7.2). For this method, lysates from *atg26* $\Delta$  cells expressing mCherry-Atg26 or mCherry-Atg26 1-1194 ( $\Delta$ WTMI) were used as inputs for incubation with GST-Atg8- or GST-coupled sepharose beads. GST-Atg8 showed a clear interaction with mCherry-Atg26 wt (as already shown in Figure 4.4) and almost no complex formation with mCherry-Atg26 1-1194 ( $\Delta$ WTMI) (Figure 4.8C).

A GFP-Atg8-TRAP with lysate from *atg26* $\Delta$  cells expressing GFP-Atg8 or GFP in combination with mCherry-Atg26 wt, I1198A or 1-1194 ( $\Delta$ WTMI) could further validate this AIM (Figure 4.8D). The fusion protein mCherry-Atg26 I1198A containing an isoleucine to alanine mutation of position +3 in the tested AIM was an additional control. In agreement with the GFP-Atg26-TRAP and GST-Atg8 PD, it was possible to monitor a step-by-step decreased Atg26-Atg8 interaction, depending on the degree of modifications in the AIM (Figure 4.8D lane 7 to 9).

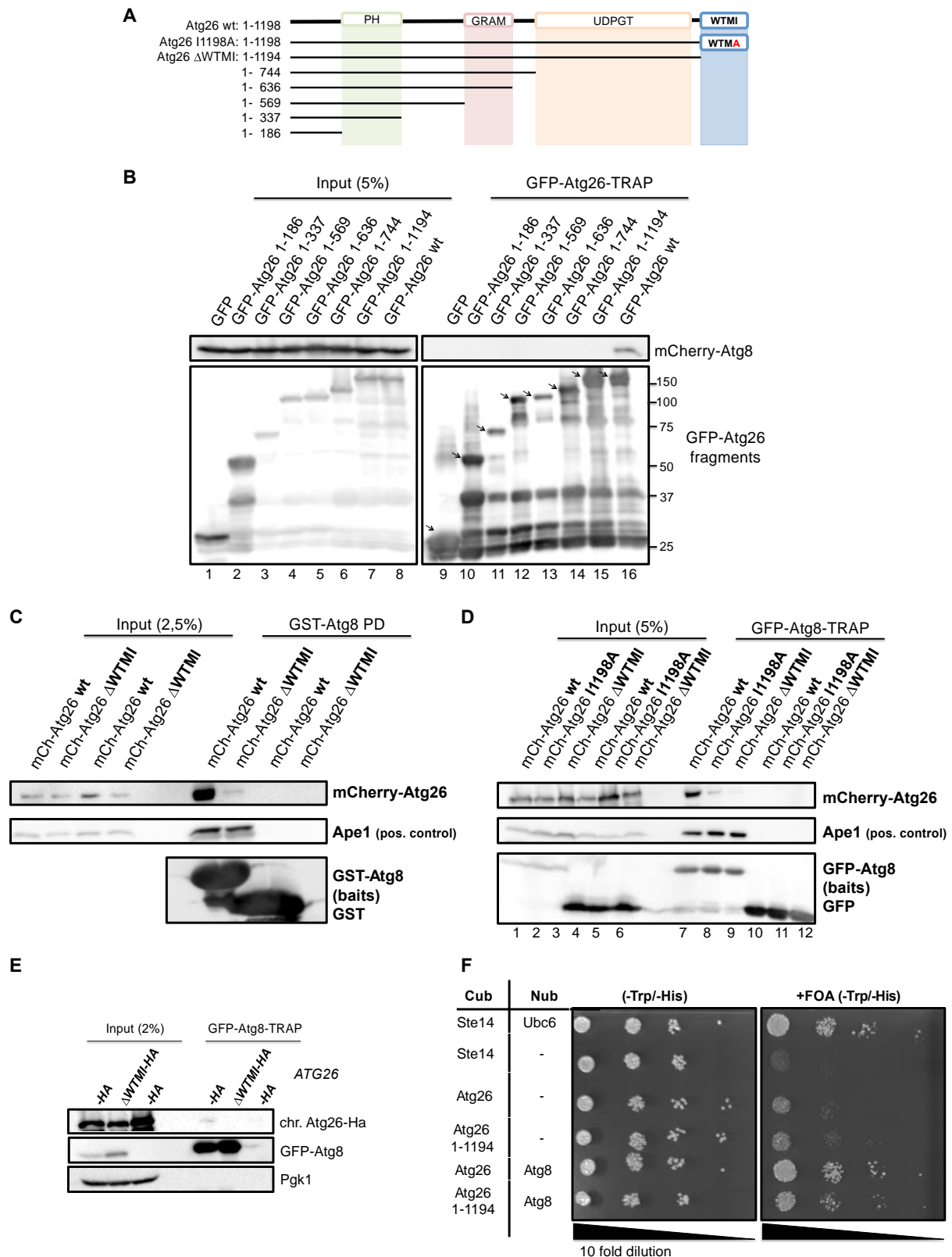


**Figure 4.8 Atg26 has a very C-terminal AIM**

(A) Scheme of the Atg26 domain composition and respective truncated versions.

(B) GFP-TRAP with truncated versions of GFP-Atg26. Protein extracts from *atg26Δ* cells expressing variants of GFP-Atg26 or GFP together with mCherry-Atg8 were subjected to GFP-TRAP and analysed by immunoblotting. Arrowheads indicate GFP-Atg26 fragments with the expected molecular weight.

(C) GST-Atg8 PD. Crude cell extracts from cells expressing mCherry-Atg26 wt or  $\Delta$ WTMI were incubated with GST-Atg8- or GST-coupled beads. Input and bound fractions were analysed by immunoblotting.

(D) GFP-Atg8-TRAP. Crude cells extracts from *atg26Δ* cells expressing GFP-Atg8 or GFP alone together

## Results

with mCherry-Atg26 wt, I1198A or  $\Delta$ WTMI were incubated with GFP-TRAP beads. Input and bound fractions were analysed by immunoblotting.

(E) GFP-Atg8-TRAP. *ATG26  $\Delta$ WTMI-HA* or *ATG26  $\Delta$ WTMI-HA* cells expressing GFP-Atg8 from its endogenous promoter or the empty vector were starved for 4 h in SD-N containing 1 mM PMSF, then, osmotically lysed and used for GFP-TRAP. Input and bound fractions (GFP-Atg8-TRAP) were analysed by immunoblotting.

(F) Split-ubiquitin assay. The N-terminal part of ubiquitin (Nub) is fused to the bait and its C-terminal part (Cub) to the prey. Protein interaction restores ubiquitin and leads to degradation of a destabilised R-Ura3 variant. Bait/prey interaction is detected by the growth on 5-FOA-containing medium.

---

A further GFP-Atg8-TRAP was performed with *ATG26*- and *ATG26  $\Delta$ WTMI-HA* cells ectopically expressing GFP-Atg8 under endogenous promoter. This experiment was done to find out whether GFP-Atg8 from endogenous promoter is able to co-isolate endogenous Atg26-HA. Before lyses and incubation with GFP-TRAP beads, cells were starved for 4 h in SD-N containing 1 mM PMSF to inhibit the vacuolar protease (Prb1). Detection of a GFP-Atg8/Atg26-HA interaction was difficult, because of the weak signal. Nonetheless, this interaction was specific, since Atg26  $\Delta$ WTMI-HA was not co-isolated (Figure 4.8E).

A further method to investigate protein-protein interaction was the split-ubiquitin assay (Figure 4.8F)(chapter 3.2.4). This method reports bait-prey interaction by increased cell growth rate on 5-FOA-containing medium (Müller and Johnsson, 2008). For these interaction studies, SEY6210 cells were transformed with CUP1-Nub-Atg8 or pRS314 (negative control) in combination with Cub-Atg26 or Cub-Atg26 1-1194 ( $\Delta$ WTMI). Expression of the fusion constructs was induced by 100  $\mu$ M CuSO<sub>4</sub> (Nub constructs) and 250  $\mu$ M methionine (Cub constructs). Cells were diluted in 10-fold steps and spotted on CM (-Trp/-His)(growth control) and CM +FOA (-Trp/-His) (growth implies protein interaction). Co-expression of Nub-Atg8 and Atg26-Cub resulted in growth on FOA plates, comparable to the positive control Ste14-Cub/Nub-Ubc6, whereas, in agreement with the results above, co-expression of Nub-Atg8 and Atg26 1-1194-Cub caused a decreased growth rate, again confirming that the very C-terminal AIM of Atg26 mediates complex formation with Atg8 (Figure 4.8F).

In conclusion, the hypothetical C-terminal AIM of Atg26 was validated in 5 different interaction studies that consistently showed the requirement of this sequence for complex formation of Atg8 and Atg26.

### 4.5 Atg26 functionally interacts with Atg8 during autophagy

During autophagy, intracellular material is transported to the vacuole for degradation to maintain the cellular homeostasis (Figure 4.9A). By treating cells with vacuolar protease (PrB1) inhibitor PMSF during starvation, autophagic bodies accumulate in the vacuole (Takeshige et al., 1992). After 4 h of nutrient depletion, GFP-Atg26 also accumulates in autophagic bodies of PMSF-treated *atg26Δ* cells ectopically expressing GFP-Atg26 and mCherry-Atg8 (positive control), as shown by fluorescence microscopy (Figure 4.9B).

The GFP moiety of GFP-tagged proteins is proteolysis-resistant in the vacuole. Therefore, it is possible to measure the autophagic transport of such fusion proteins by detecting accumulation of free GFP in the vacuole (Figure 4.9A) (Klionsky et al., 2007). This method is called vacuolar degradation assay and was used to quantify the autophagic rate of Atg26 and the influence of its C-terminal AIM. Growing *atg26Δ* cells ( $OD_{600} \sim 2$ ) ectopically expressing GFP-Atg26 variants were shifted to starvation medium (SD-N) to a final concentration of  $OD_{600} \sim 10$ . At the indicated time points ( $t = 0, 2$  and  $4$  h), samples were taken for alkaline lysis (chapter 3.2.7.1.1). Samples were analysed by immunoblots (Figure 4.9C). Quantification was done by calculating the ratio of free GFP and cytosolic GFP-Atg26. The time point of 4 h of GFP-Atg26 wt was set to 100% (Figure 4.9E). During starvation, *atg26Δ* cells clearly accumulate free GFP, resulting from degradation of GFP-Atg26 wt. In contrast, deletion of the autophagy-essential gene *ATG1* blocked this accumulation, suggesting that GFP-Atg26 wt is transported to the vacuole by autophagy. Moreover, it was possible to demonstrate that the C-terminal AIM of Atg26 significantly influences its delivery to the vacuole: GFP-Atg26 I1198A and  $\Delta$ WTMI showed a more than 60% reduced autophagic rate compared to GFP-Atg26 wt (Figure 4.9E). This observation gave a hint that Atg26 is a selective cargo/target of autophagy.



# Results

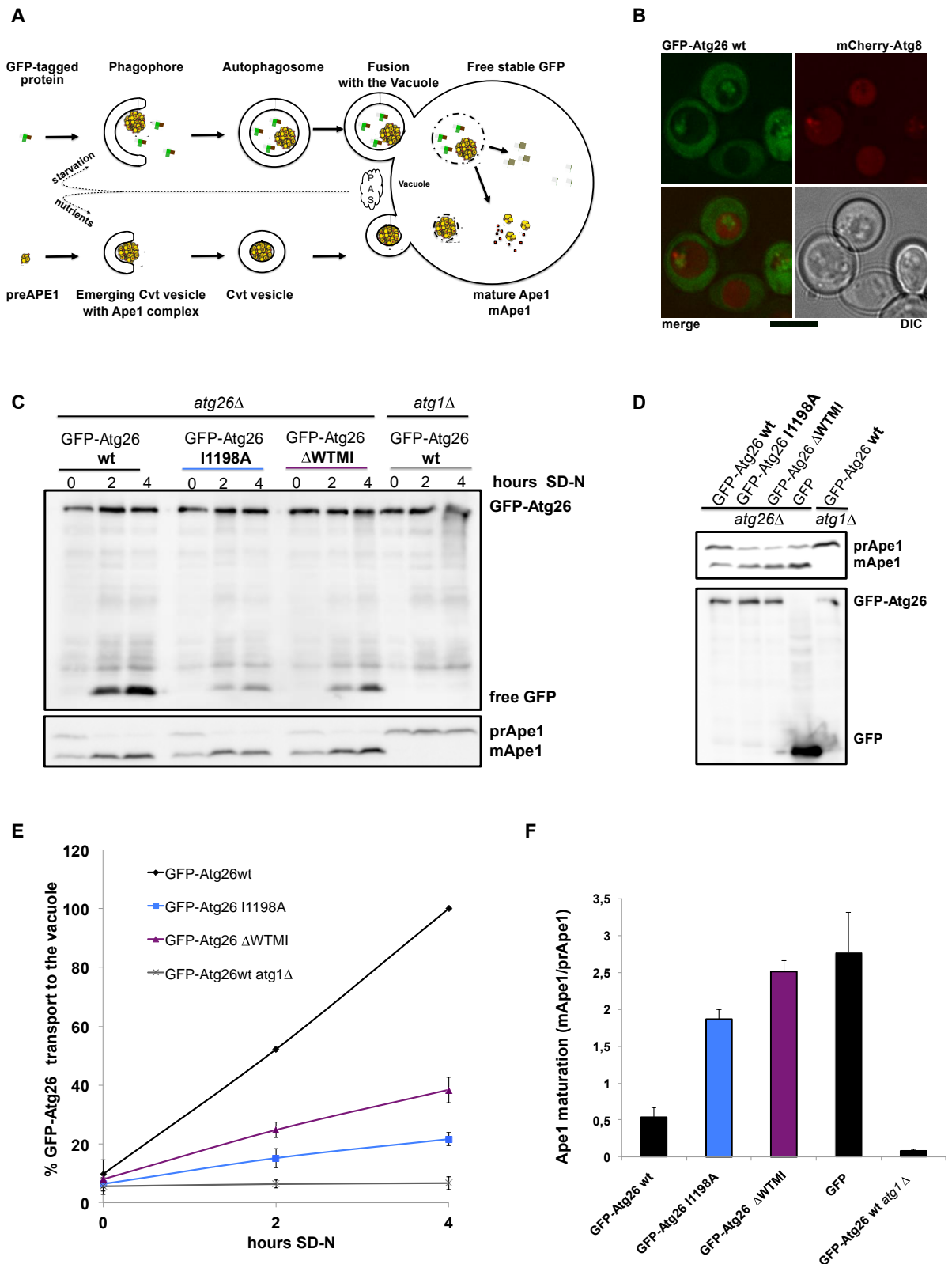


**Figure 4.9 Atg26 is AIM-dependently transported to the vacuole upon autophagy induction**  
 (A) Scheme of the vacuolar degradation assay (autophagy of GFP-tagged proteins) and the Cvt pathway.  
 (B) PMSF treatment during starvation. Growing *atg26Δ* cells expressing GFP-Atg26 and mCherry-Atg8 were shifted to starvation medium (SD-N) containing 1 mM PMSF for 3 h. The localization of GFP and mCherry were visualized by fluorescence microscopy. Scale bar: 5  $\mu$ m.  
 (C and E) Vacuolar degradation assay. Growing *atg26Δ* or *atg1Δ* cells expressing GFP-Atg26 wt, I1198A or  $\Delta$ WTMI were shifted to SD-N. Samples were taken at the indicated time points. Samples were analysed by immunoblots and quantified by calculating the ratio of free GFP and cytosolic GFP-Atg26.  
 (D and F) Ape1 maturation at late-log phase in *atg26Δ* or *atg1Δ* cells overexpressing GFP-Atg26 variants.

## Results

Ape1 delivery to the vacuole and maturation was estimated by calculating the ratio of mApe1 and prApe1 (n=3). Error bars indicate  $\pm$ SEM.

---

The vacuolar enzyme Ape1 is selectively delivered to the vacuole by the Cvt pathway. In the vacuole, precursor of Ape1 (prApe1) is processed to mature Ape1 (mApe1) detectable by a molecular weight shift in immunoblot analysis (Figure 4.9A) (Klionsky et al., 2007). In this context, the physiological relevance of the C-terminal AIM was further supported by showing that overexpression of GFP-Atg26 wt reduced Ape1 maturation (Figure 4.9D). To induce high expression of GFP-Atg26 (*MET25* promoter), cells were grown over night in CM medium lacking methionine. Samples were taken at a density of  $OD_{600} \sim 5$  for alkaline lysis and immunoblot analysis. Overexpression of GFP-Atg26 wt caused a clear inhibition of the Cvt pathway, indicated by a higher amount of prApe1 compared to mApe1, while overexpression of GFP alone showed more mApe1, as expected at late-log phase. Notably, this effect of GFP-Atg26 was strongly reduced when the C-terminal AIM was mutated (I1198A) or deleted (1-1194) (Figure 4.9D and F).

Taken together, the experiments of this chapter further validate the AIM-based physical interaction between Atg8 and Atg26 (chapter 4.4). Additionally, these data demonstrated that the AIM is required for autophagic degradation of GFP-Atg26. Besides, it was shown that overexpression of GFP-Atg26 inhibits the Cvt pathway.

### 4.6 PAS recruitment of Atg26 depends on Atg8 and Atg1

The preautophagosomal structure (PAS) is located close to the vacuole and initiates autophagosome formation. Most of the Atg proteins are at least transiently located there. Thus, the PAS is understood as the initiation site for autophagosome and Cvt vesicle formation (Suzuki et al., 2007). To further investigate whether Atg26 has an autophagic function in *S. cerevisiae*, the subcellular localisation of GFP-Atg26 was monitored by fluorescence microscopy. Therefore, *atg26Δ*, *atg1Δ* and wt cells expressing a low level of GFP-Atg26 (*MET25* promoter) together with mCherry-Atg8 (*MET25* promoter) as PAS marker were grown in standard CM medium (0.8 mM methionine) over night and then shifted to starvation medium (SD-N) to a final cell density of  $OD_{600} \sim 10$ . After 2 to 3 hours of starvation, cells were analysed by fluorescence microscopy. Images were deconvoluted by SoftWoRx (Applied precision). For quantitative analysis, the percentage of GFP-Atg26 dots that were colocalized with mCherry-Atg8 dots was calculated (Figure 4.10B). As further quantitative method, the Pearson's correlation coefficients ( $R^2$ ) between the GFP and the mCherry signals from cells with mCherry-Atg8 dots were calculated (Figure 4.10C)

GFP-Atg26 wt showed a diffuse cytosolic distribution with an additional accumulation at the PAS, visualized by colocalisation with the PAS marker mCherry-Atg8 (Figure 4.10A). In contrast, GFP-Atg26 1-1194 and I1198A had faint and rarely PAS signals. GFP-Atg26 wt showed a relative high colocalisation with mCherry-Atg8 at about 70%. The relatively rare colocalisation rate of GFP-Atg26 I1198A or 1-1194 with mCherry-Atg8 (>30%) indicated that interaction with Atg8 is required for PAS localisation of Atg26. As a supporting fact, the measured Pearson's correlation coefficient for GFP-Atg26 wt and mCherry-Atg8 dots was about 0.2, whereas the AIM mutants were under 0.05 (Figure 4.10C).

The serine/threonine kinase Atg1 was another factor that influenced PAS recruitment of Atg26. Microscopy of *atg1Δ* cells showed a diffuse cytosolic distribution of GFP-Atg26 that hardly concentrated at the PAS (Figure 4.10A). These observations were supported by both quantification methods (Figure 4.10B and C). To exclude an influence of the endogenous Atg26 on GFP-Atg26 localisation in *atg1Δ* cells, wt cells expressing GFP-Atg26 wt were examined. As expected, these cells showed no obvious differences to *atg26Δ* cells.

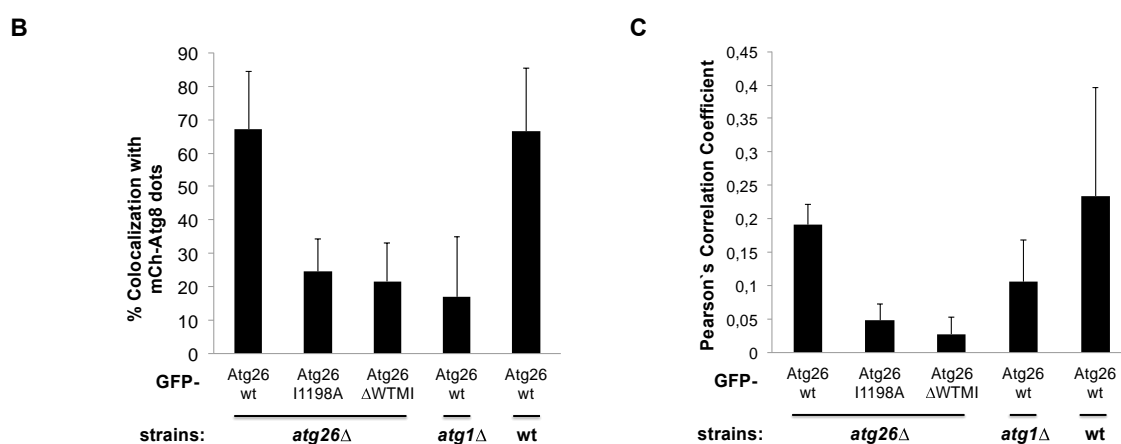
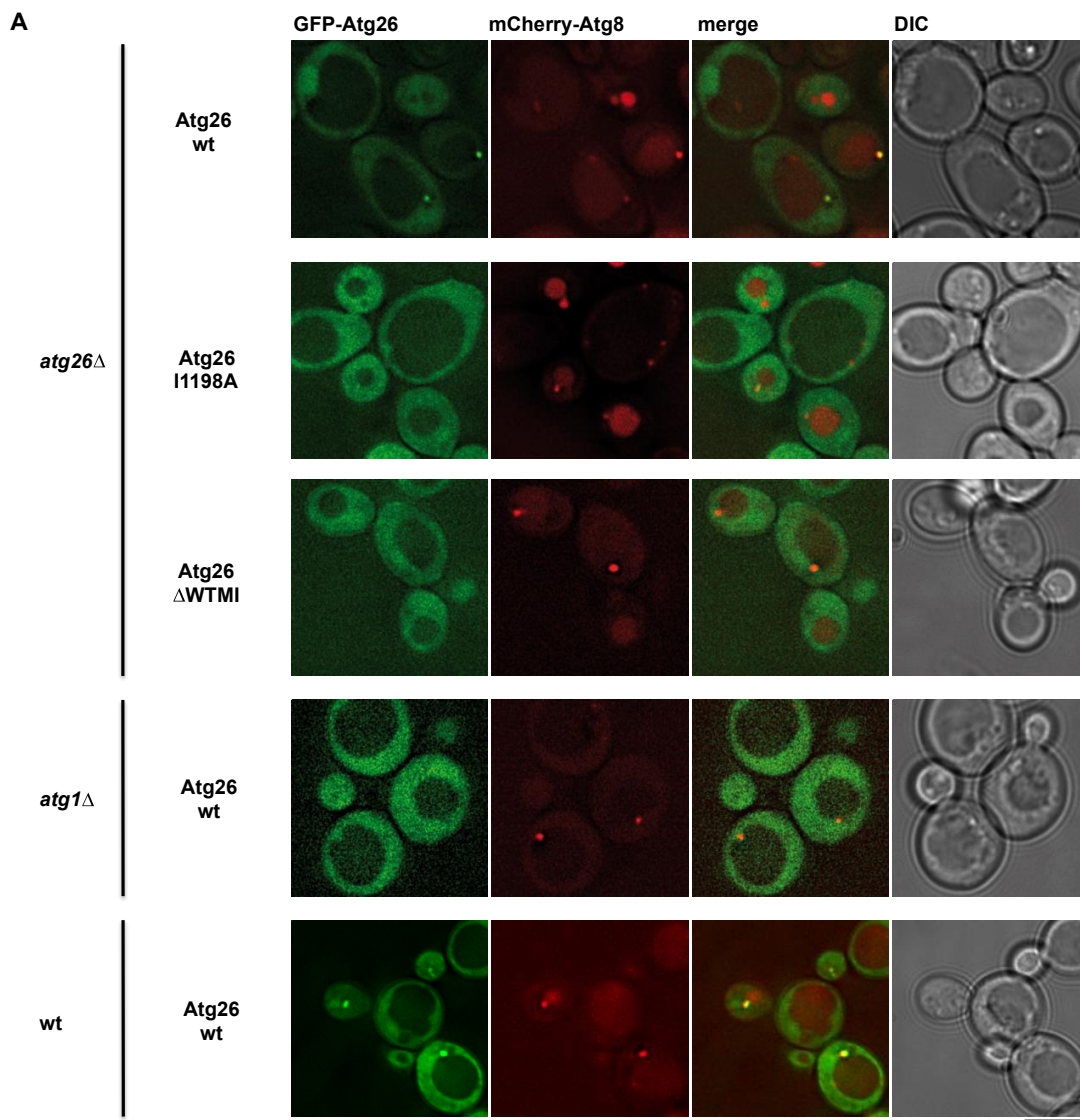


**Figure 4.10 Atg26 locates AIM-dependently to the PAS**

(A) wt, *atg26Δ* or *atg1Δ* strains ectopically expressing GFP-Atg26 wt, I1198A or ΔWTMI together with mCherry-Atg8 were grown to mid-log phase, then shifted to starvation medium for 2–4 hours and analysed by fluorescence microscopy. Scale bar: 5 μm.

(B) Graphs show the percentage of GFP-Atg26 dots that were colocalized with mCherry-Atg8 dots.

(C) Quantification of microscopic data by calculating the Pearson's correlation coefficient (GFP and mCherry signals) in cells with a mCherry-Atg8 PAS dot. Diffuse cytosolic or vacuolar signals were

## Results

determined as thresholds. Error bars indicate  $\pm$ SEM.

---

These microscopic data further support the hypothesis that Atg26 is an autophagy-related protein that acts in cooperation with Atg8 and, possibly, Atg1 during autophagy.

## 4.7 Identification of the major coat protein of the L-A virus as a new Atg26 interaction partner

*Saccharomyces cerevisiae* virus L-A is a dsRNA virus of the *Totiviridae* family. It has a single 4.6 kb genomic segment with two overlapping ORFs. ORF1 encodes the 76 kDa major capsid protein Gag that is necessary for encapsidation. ORF2 is a RNA-dependent RNA polymerase (Pol) that is expressed as a 180 kDa Gag-Pol fusion protein formed by a -1 ribosomal frameshift (Fujimura and Wickner, 1988). The icosahedral virus architecture is made up of 120 Gag subunits with 2 Gag-Pol fusion proteins and genomic dsRNA in the inside (Naitow et al., 2002; Tang et al., 2005; Wickner et al., 2013).

This chapter describes the co-isolation of L-A Gag via GFP-Atg26-TRAP and its identification as a new Atg26 interaction partner by mass spectrometry analysis. These findings need a short introduction: Most experiments of this thesis were done with our laboratory yeast strain WCG4a (Mata *ura3 his3-11,15 leu2-3,112*) that is infected by the L-A virus. L-A infection of WCG4a was first shown by the experiments of this chapter. All WCG4a deletion strains of our lab derived from this strain and thus should contain L-A virus particles, because the way of infection is from mother to daughter cells (or during mating). However, some deletion strains spontaneously lost the virus such as *Δl-a/atg1Δ* ("*Δl-a*" indicates absence of L-A virus). Of course, absence of the L-A virus in *Δl-a/atg1Δ* strain was also first discovered by the GFP-Atg26-TRAP and the respective MS analysis in this chapter. Parallel analysis of an infected strain (*atg26Δ*) and a strain lacking L-A (*Δl-a/atg1Δ*) enormously helped to identify L-A Gag as an Atg26 interaction partner. The following part describes the methodology and the results in detail.

For a standard GFP-Atg26-TRAP protocol, *atg26Δ* cells expressing GFP-Atg26 wt, I1198A,  $\Delta$ WTMI or GFP alone together with mCherry-Atg8 (*MET25* promoter) were grown to late-log phase ( $OD_{600} \sim 5$ ) and osmotically lysed. Then, cell extracts were incubated with GFP-TRAP beads. In parallel, crude cell extracts from *Δl-a/atg1Δ* cells expressing GFP-Atg26 wt or GFP alone together with mCherry-Atg8 were analysed by GFP-TRAP. This *Δl-a/atg1Δ* strain was initially used to check whether disruption of autophagy by deletion of *ATG1* influences interaction with mCherry-Atg8 and whether it displays differences in CBB staining of SDS-PAGE.

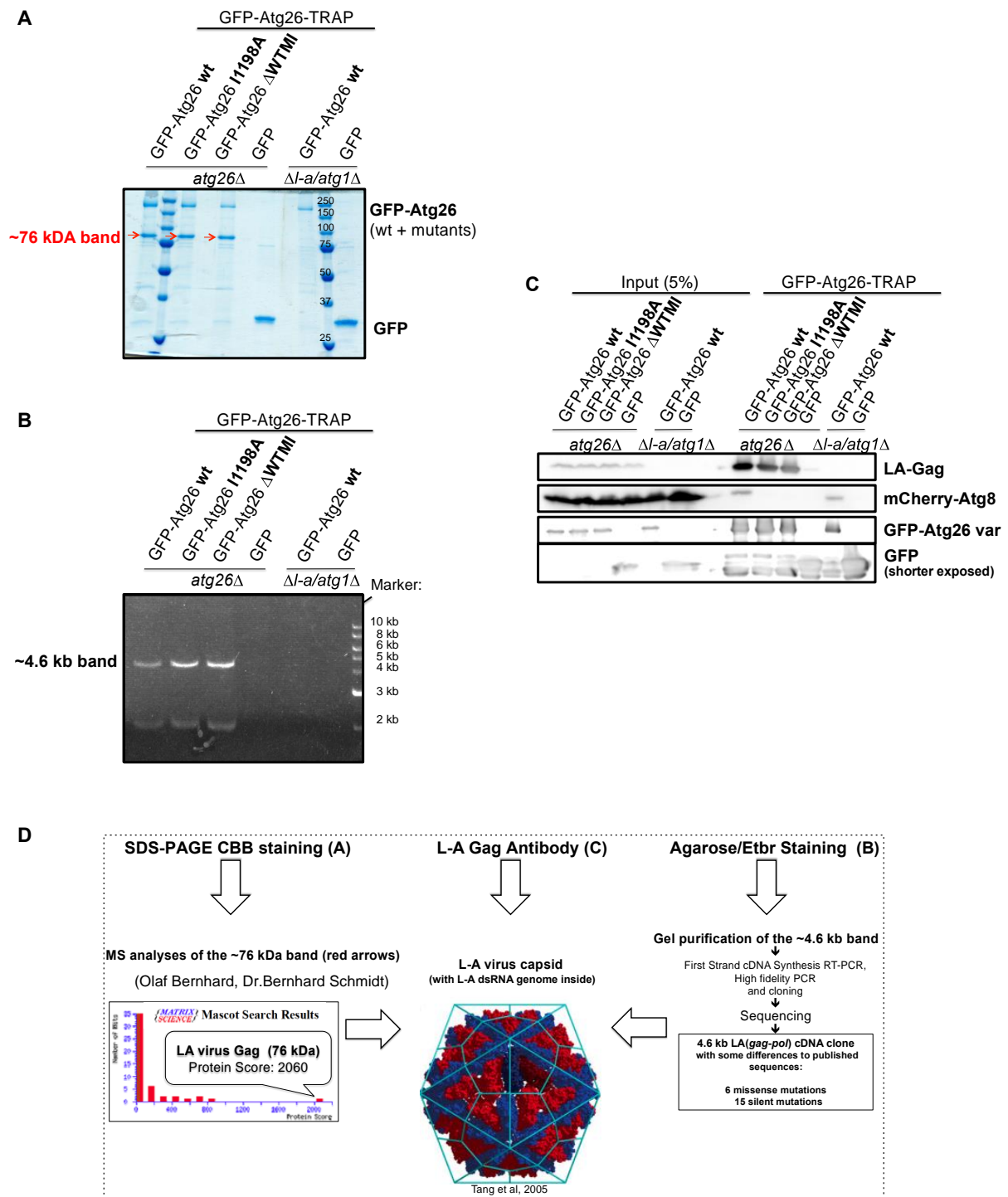


**Figure 4.11 Identification of L-A Gag as a new Atg26 interaction partner**

Crude cell extracts from *atg26* $\Delta$  or  $\Delta$ -*a/atg1* $\Delta$  strains (WCG4a) expressing GFP-Atg26 variants or GFP alone together with mCherry-Atg8 were subjected to GFP-TRAP. Input and bound fractions were analysed as follows:

(A) CBB staining of SDS-PAGE of the GFP-TRAP bound fractions. By MS analysis (Olaf Bernhard, Bernhard Schmidt), the 76 kDa band was identified as the major coat protein of the *S. cerevisiae* virus L-A.

(B) Agarose gel electrophoresis and EtBr staining of the GFP-TRAP bound fractions. The 4.6 kb band was reverse-transcribed to cDNA by RT-PCR, cloned and identified as the genomic segment of the L-A virus.

(C) Immunoblotting of the GFP-TRAP input and bound fractions. GFP-Atg26/Gag interaction was monitored and validated by immunoblotting with anti-Gag antibody.

(D) Summary of all three methods that confirm the Atg26/Gag interaction.

## Results

Analyses of the bound fractions by CBB staining of SDS-PAGE showed a distinct band between 75 and 100 kDa in *atg26Δ* cells but not in *Δl-a/atg1Δ* cells (Figure 4.11A, red arrows). At that time point, it was absolutely unclear that the strain-dependent differences were based on virus infection (*atg26Δ*) or virus loss (*Δl-a/atg1Δ*), respectively. The absence of this distinct band in *Δl-a/atg1Δ* cells excluded the possibility that it was a degradation product of the over 150 kDa GFP-Atg26 variants. Therefore, these observations gave clear hints that this band might derive from a specific interactor. Another interesting point was the relative high amount of this band comparable to the baits GFP-Atg26 wt, I1198A or 1-1194 ( $\Delta$ WTMI), suggesting strong affinity or complex formation with a high molecular weight complex of homo-multimers. Furthermore, interaction with all GFP-Atg26 variants indicated an Atg8-independent interaction.

In collaboration with the lab of Bernhard Schmidt, this distinct ~76 kDa band was analysed by mass spectrometry (chapter 3.2.7.8). With a protein score of 2060, this band was identified as the major coat protein Gag of the *S. cerevisiae* virus L-A (Figure 4.11D). Remarkably, co-purification of a ~4.6 kb RNA fragment by GFP-Atg26-TRAP was detectable using electrophoresis of 1% agarose and ethidiumbromid (EtBr) staining (Figure 4.11B). In further experiments, this putative L-A dsRNA segment was gel-purified, reverse-transcribed in cDNA by RT-PCR and cloned in the vectors pGEX-4T3, pUG34, pUG35, pUG36 and pUG36-mCherry (Figure 4.11D; chapter 3.2.3.6). By sequencing of three independent cDNA clones, the ~4.6 kb segments were identified as the coding sequences for ORF1 (*GAG*) and ORF2 (*POL*) of the L-A virus. The viral dsRNA sequence of our laboratory strain WCG4a showed a few differences to published L-A sequences: there were 15 silent and 6 missense “mutations” (Gag: Ile328Val, Lys383Arg, Gly542Ser and Asn633Ser; Pol: Lys720Arg, Val754Ala). This methodology on RNA level additionally confirmed L-A infection of our laboratory strain WCG4a and, of course, that Atg26 interacts with Gag or even with completely formed virus-like particles (VLPs). An additional ~2 kb fragment was co-isolated by the GFP-Atg26-TRAP (Figure 4.11B), but not further analysed. It was proposed that this fragment corresponds to genomic dsRNA of killer viruses that use L-A virus particles for their own replication (Schmitt and Breinig, 2006). Otherwise, it might be single-stranded L-A RNA ((+) transcript).

An antibody against L-A Gag was further used to validate complex formation between Atg26 and L-A Gag (multimers) (Figure 4.11C). Immunoblot analysis were in agreement



## Results

with CBB staining and EtBr staining (Figure 4.11A and B). The input fraction showed that the tested  $\Delta l-a/atg1\Delta$  strain was not infected by the L-A virus. This observation raised the question whether deletion of *ATG1* inhibits virus infection or formation in *S. cerevisiae*. Later experiments showed that further *atg1\Delta* strains created independently from  $\Delta l-a/atg1\Delta$  were infected by L-A, suggesting spontaneous loss of the virus in  $\Delta l-a/atg1\Delta$ . Thus, deletion of *ATG1* has no obvious virus-specific phenotype. Besides, it was discovered that further deletions strains of our laboratory yeast collection were not infected, supporting the hypothesis of spontaneous loss during the knock out procedure. Immunoblotting also demonstrated an interaction between GFP-Atg26 wt and mCherry-Atg8 independently from L-A or Atg1, respectively, shown by the bound fraction of mCherry-Atg8 in  $\Delta l-a/atg1\Delta$  cells (Figure 4.11C). In this context, it should be mentioned that the virus is no prerequisite for the PAS localisation (not shown) and autophagic degradation of GFP-Atg26 (Figure 4.20D), as both were unchanged without virus.

To find out whether endogenous Atg26 is able to co-isolate detectable quantities of endogenous Gag and how this interaction might be influenced in further strains, wt and *xrn1\Delta* cells of a BY4741 background (MATa his3 $\Delta$ 1 leu2 $\Delta$ 0 met15 $\Delta$ 0 ura3 $\Delta$ 0) chromosomally expressing GFP-tagged or untagged Atg26 were grown to late stationary phase, lysed and subjected to GFP-TRAP. Deletion of *XRN1*, encoding a exoribonuclease with anti-viral activity, leads to an excess of L-A virus particles (Esteban et al., 2008). Therefore, *xrn1\Delta* cells were used to check how expression of Atg26 and its interaction with Gag is influenced. These GFP-TRAP experiments were analysed by immunoblotting and EtBr staining of agarose gels (Figure 4.12A and B).

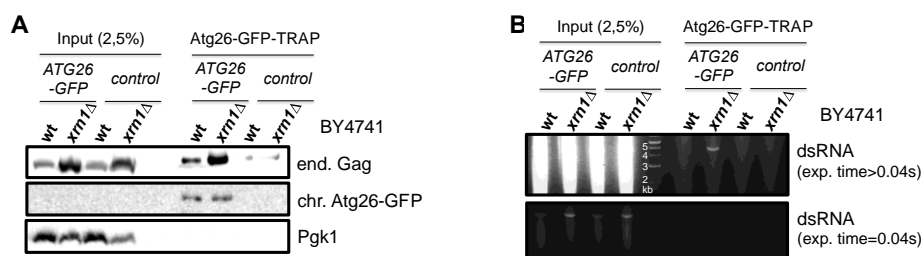


**Figure 4.12 Validation of Atg26/L-A interaction at endogenous expression level**

Crude cell extracts from *ATG26-GFP*, *ATG26-GFP/xrn1\Delta*, wild type or *xrn1\Delta* cells of the BY4741 background were subjected to GFP-TRAP. Input and bound fractions were analysed as follows:

- (A) Immunoblot analysis and
- (B) EtBr staining of agarose gels.

## Results

Although Atg26-GFP as bait was hardly detectable in the input fractions, its co-immunoprecipitation and co-purification of Gag were demonstrated by immunoblotting of the bound fractions (Figure 4.12A). As expected, *xrn1* $\Delta$  cells had a higher amount of L-A virus particles and thus more Gag was co-isolated (Figure 4.12A). Moreover, these data indicated that Atg26 seemed not to be up-regulated if L-A is increased. EtBr staining of agarose gels indicated that co-purification of detectable amounts of dsRNA was only possible by using the *xrn1* $\Delta$  strain expressing Atg26-GFP

In conclusion, L-A Gag was identified as a new Atg26 interaction partner by MS analysis. These findings were validated by immunoblot analysis using an anti-Gag antibody and cDNA sequencing of co-purified L-A dsRNA.

### 4.8 Mapping of the Gag binding domains in Atg26

In the previous chapter (4.7), the major coat protein of the L-A virus was identified as an Atg26 binder. To map the region in Atg26 necessary for Gag binding, various truncated versions of Atg26 were analysed via GFP-TRAP (Figure 4.13). Based on domain prediction ([www.sanger.ac.uk/Software/Pfam](http://www.sanger.ac.uk/Software/Pfam)) and previous reports (Asakura et al., 2009; Yamashita et al., 2006), Atg26 fragments were cloned in a GFP vector containing a *MET25* promoter for inducible expression (pUG34) (Figure 4.13D). Different variants of GFP-Atg26 or GFP alone were expressed in *atg26Δ* cells (WCG4a), immunoprecipitated and analysed by immunoblotting (Figure 4.13A and further examples in C) and CBB staining of SDS-PAGE (Figure 4.13B). Cells expressing GFP-Atg26 1-636 lost spontaneously the virus during transformation procedure (indicated by “*Δl-a*”) and thus were used as negative control (Figure 4.13A, lane 5 and 15, B). Immunoblots using anti-GFP or anti-Gag antibodies were quantified without including their degradation products (Figure 4.13E and F).

Almost all truncated version of GFP-Atg26, except Atg26 1-1194, were less stable than the full-length version (summarized in Figure 4.13E). Especially the fragments 187-337 (PH domain) and 187-374 (extended PH domain, not shown) were hardly detectable (Figure 4.13C lane 11, E). Nonetheless, the expression levels of the other fragments were adequate to map Gag binding.

The interaction studies clearly demonstrated that region 187-569 of Atg26 is most important for Atg26-Gag complex formation (summarized in Figures 4.13D-F). This region contains a PH domain (187-337) and an undefined region (338-569). Each region was able to bind Gag on its own, as shown by the fragments GFP-Atg26 1-337 and 338-1198 (Figure 4.13 A lanes 13 and 18). However, only in combination, a high level of interaction was detectable, indicated by the constructs GFP-Atg26 1-569 and 187-569 (Figure 4.13A lanes 17 and 16; C, lanes 3, 12 and 18). The undefined N-terminal region (1-186) and the C-terminal half (570-1198), including the GRAM domain, the glucosyltransferase domain (UDPGT) and the AIM, seemed to be only slightly involved in Gag binding (Figure 4.13A, lanes 12 and 19; C lanes 2, 9 and 20).

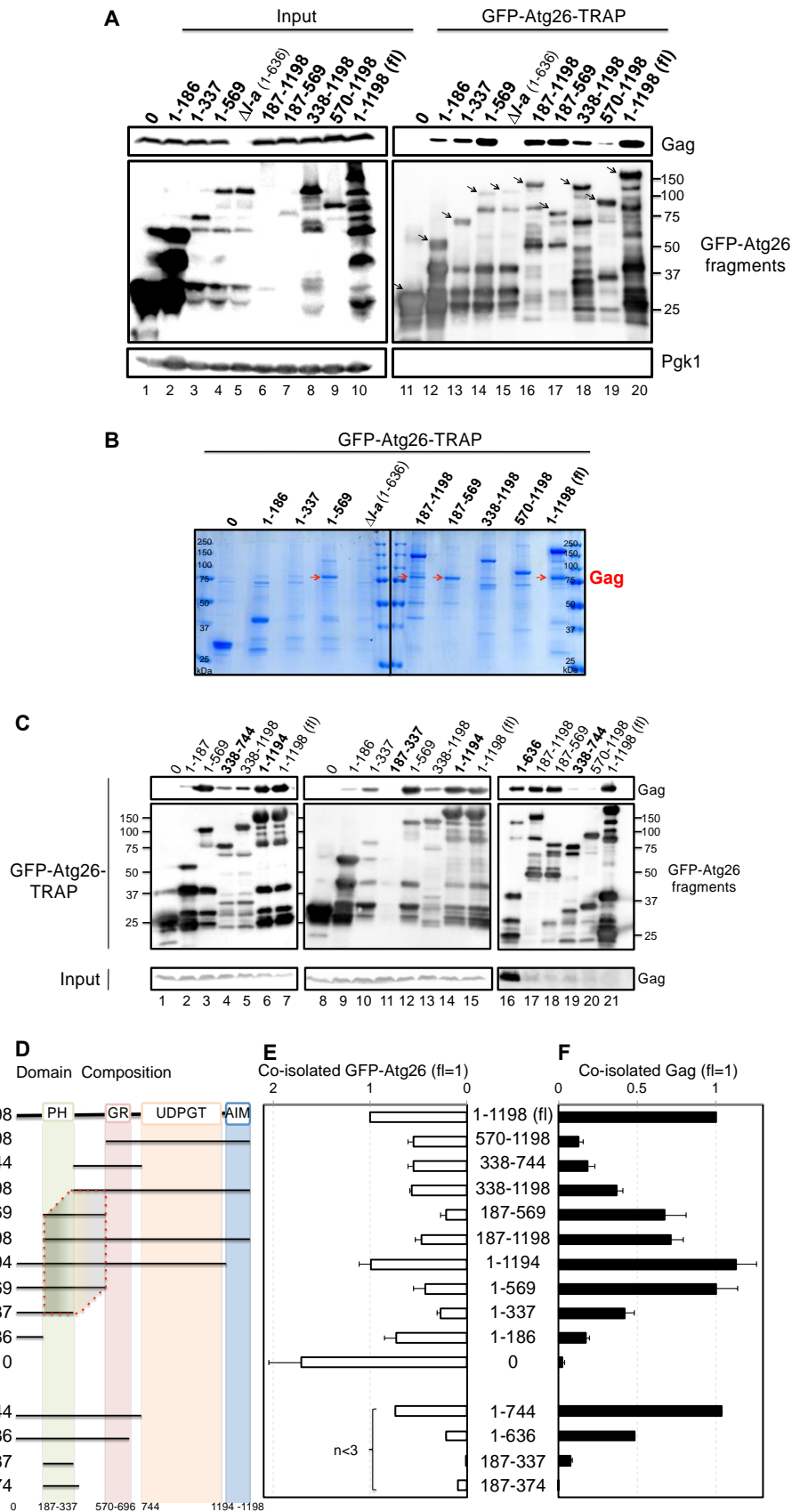


**Figure 4.13 The PH domain (187-337) and an undefined region (338-569) of Atg26 bind L-A Gag**  
 GFP-TRAP with truncated versions of GFP-Atg26. Protein extracts from *atg26Δ* cells expressing variants of GFP-Atg26 or GFP were subjected to GFP-TRAP and analysed by:  
 (A and C) immunoblotting (arrowheads indicate GFP-Atg26 fragments used for quantification)  
 (B) CBB staining of SDS-PAGE  
 (D-F) Summary: Schematic of the Atg26 domains and respective quantifications of the immunoblots.

## Results

For further interaction studies, pull down assays using purified recombinant (*E. coli*-) expressed Atg26 have been established. Bl21 cells were transformed with pGEX-4T3-GST-Atg26 (not shown), pGEX-4T3-GST-Atg26 187-569 or pGEX-4T3 GST (control). The about 150 kDa, full-length GST-Atg26 construct was not expressible in *E. coli* (not shown). Using pGEX-4T3-GST-Atg26 187-569, it was possible to express and purify suitable amounts of recombinant protein (Figure 4.14.1A, Bound) for pull down assays (Figure 4.14.1A, Pull down). Protein extracts from *atg26Δ* cells (WCG4a) were used for incubation with GST-Atg26 187-569 or GST-coupled beads. The samples were analysed by CBB staining of SDS-PAGE (Figure 4.14.1A), immunoblotting (Figure 4.14.1B) and EtBr staining of agarose gels (Figure 4.14.1C). Detection of Gag or viral dsRNA via immunoblotting or EtBr staining of agarose gels again confirmed that the region 187-569 mediates interaction with L-A virus-like particles (VLPs). In addition, this GST-tagged Atg26 fragment seemed to fold properly in the used prokaryotic expression system.

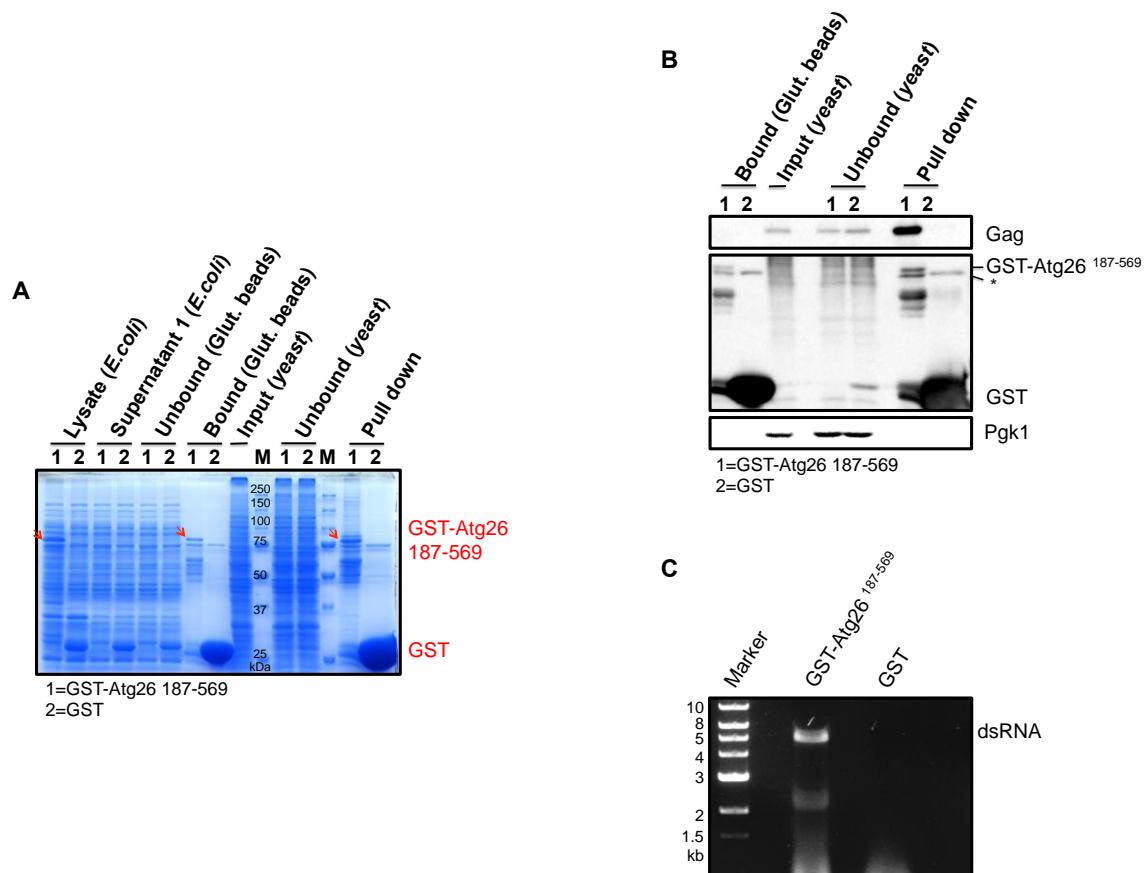


**Figure 4.14.1 Recombinant expressed GST-Atg26 187-569 binds L-A virus-like particles**

Cell extracts from *E. coli* (Bl21, pLys) expressing GST-Atg26 187-569 (1) or GST alone (2) were incubated with glutathione sepharose beads (Glut. beads). After GST coupling, cell lysate from *atg26Δ* cells were incubated with respective beads. GST purifications and pull down assays were analysed by: (A) CBB staining of SDS-PAGE, (B) immunoblotting and (C) EtBr staining of agarose gels.

## Results

Additionally, the bound fraction of GST-Atg26 187-569 was analysed by MS in collaboration with Olaf Bernhard und Dr. Bernhard Schmidt. Samples (CBB-stained bands of interest) for MS analysis were chosen after detailed comparison between the CBB-stained SDS-PAGE bound fractions. Here, the GST-Atg26 187-569 sample clearly showed additional bands compared to the GST sample (Figure 4.14.2A). Together with the detected co-isolation of L-A Gag via immunblotting (Figure 4.14.2B), these results showed the success of the pull down assay. To avoid MS analysis of degradation products, only distinct bands with higher molecular weight than GST-Atg26 187-569 (>75 kDa) were considered. Thus, a virus-related Atg26 (187-569) proteome with putative interactors over 75 kDa was the expected outcome of the MS analysis (chapter 3.2.7.8). Identified peptides were evaluated regarding their score: proteins with a score over 50 were listed in a table (Figure 4.14.2B). The only exception and in parallel a negative example was Msp1 identified in band 1 (>250 kDa): With a score of 39, this mitochondrial protein had the highest score in this band. Together with the molecular weight of only 40.3 kDa, Msp1 was an unlikely interaction partner of Atg26 187-569. For the same reasons, Kin3 could be classified as an unsure candidate, indicated by a score of 58 and molecular weight of 51.2 kDa (band 2, >150 kDa). In most cases, the scores of the other listed candidates were at least about 100 and the calculated molecular weights were in correlation with those estimated via SDS-PAGE analysis (Figure 4.14.2B).

To get an impression of the cellular function and the interrelationships of the identified proteins, the STRING database was used to create functional protein association networks based on available experimental evidence (Figure 4.14.2C). Since STRING had no available data for the L-A virus proteins Gag and RdRP (Gag-Pol), these proteins were not considered.

Obviously, many rRNA processing proteins were co-isolated especially the Mak21-Noc2-Rrp5 complex and Kre33. Remarkably, the 5'-3' exonuclease Xrn1, a down-regulator of L-A, was identified by MS. Xrn1 and Mak21 were the only candidates with a published L-A virus phenotype (Edskes et al., 1998; Esteban et al., 2008; Masison et al., 1995). STRING sorted Gcn2 in a group of proteins that are involved in translation. However, it should also be mentioned that this kinase is a key regulator of amino acid starvation-induced autophagy (Ecker et al., 2010; Tallóczy et al., 2002). Another identified kinase involved in autophagy-inducing cascades is Ksp1, which acts in the TORC1 pathway (Huber et al., 2009; Umekawa and Klionsky, 2012).

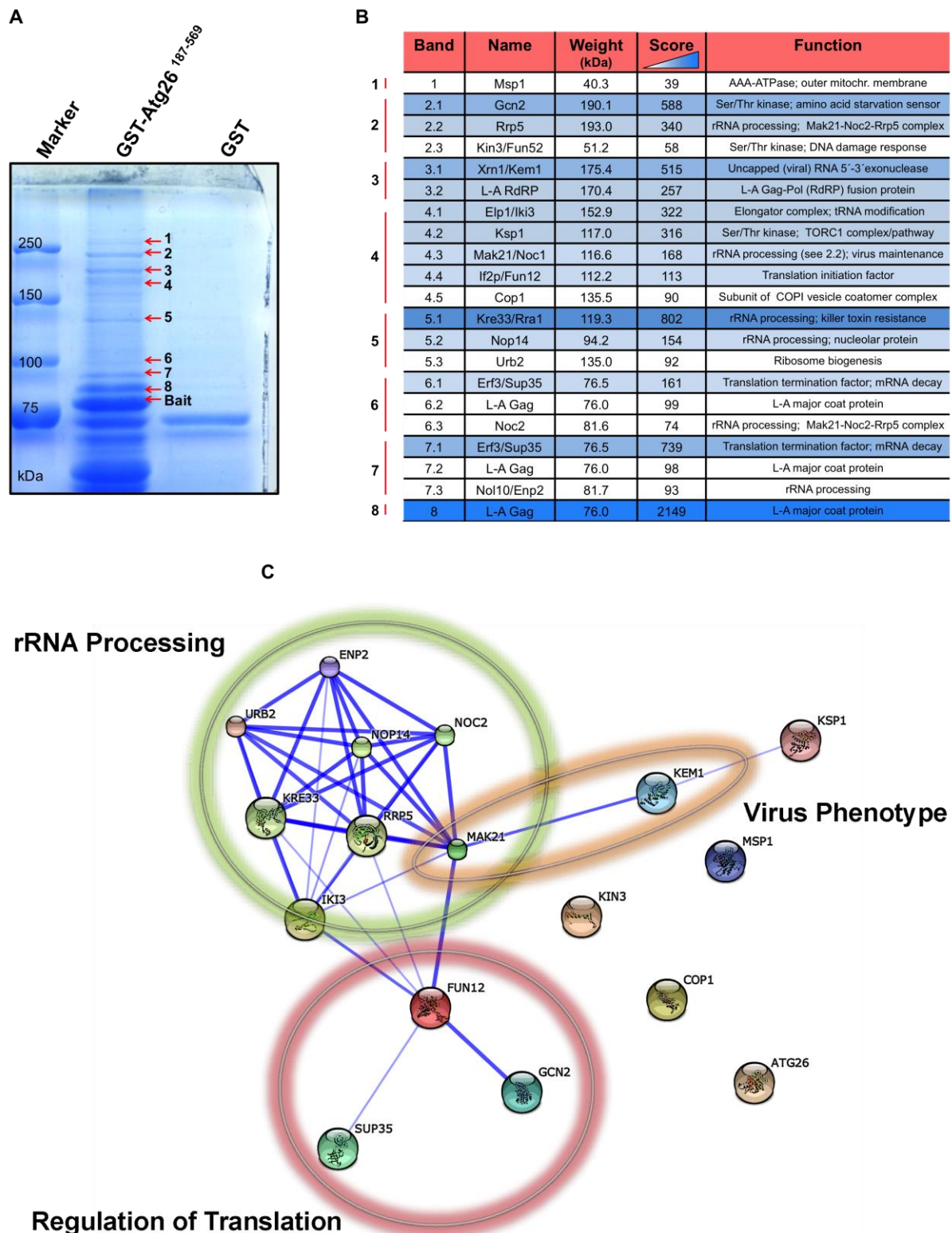


**Figure 4.14.2 MS analysis of the GST-Atg26 187-569 pull down assay**

(A) CBB-stained SDS-PAGE, labelled bands were analysed by MS

(B) Identified proteins. The colour code illustrates the confidence score from white (<100), to dark blue (<1000) to magenta (>1000). Information about the proteins were from STRING ([www.string-db.org](http://www.string-db.org)) and SGD ([www.yeastgenome.org](http://www.yeastgenome.org)).

(C) Functional grouping of MS-identified Atg26 (187-569) interaction partners by STRING ([www.string-db.org](http://www.string-db.org)). L-A Gag and L-A RdRP (Gag-Pol) were not considered, since they are no host proteins.

## Results

The experiments shown above clearly demonstrated an interaction between Atg26 (187-569) and L-A VLPs. However, it is still an open question whether Atg26 directly interacts with Gag or whether further factors are involved in complex formation. A simplified, direct pull down assay with *E. coli*-expressed pGEX-4T3-GST-Gag and pROEX His-Atg26 187-569 was used to answer this question (Figure 4.15A and B). Therefore, both constructs were separately expressed in BL21 cells. The samples were mixed during cell lysis (Lysate). As control, pGEX-4T3-GST- and pROEX-His-Atg26-187-569-expressing *E. coli* were mixed during lysis to experimentally exclude unspecific interaction with GST-coupled beads. After sedimentation of the cell debris (2700 g pellet), the supernatant was incubated with glutathione beads. Then, the beads were washed and the bound proteins eluted with 2 x Laemmli.

Comparison of the supernatant and pellet fractions of GST-Gag revealed that the majority of GST-Gag was sedimented, suggesting an accumulation in inclusion bodies during expression in *E. coli* (Figure 4.15A and B, Supernatant, Pellet). Nonetheless, using the supernatant, it was possible to couple detectable amounts of GST-Gag on glutathione beads (Figure 4.15A and B, Co-purification). As shown by immunoblotting, small amounts of His-Atg26 187-569 were co-purified by GST-Gag, but not by GST alone, giving a first hint for a direct interaction (Figure 4.15B).

The split-ubiquitin assay was a further method to prove a direct interaction (Figure 4.15C). This *in vivo* method is based on the ability of the N- and the C-terminal halves of ubiquitin (Nub and Cub) to reassemble when they are brought into close proximity by bait-prey interaction (chapter 3.2.4) (Müller and Johnsson, 2008). As a readout, the stability and thereby the activity of the split-ubiquitin reporter protein R-Ura3 is analysed. Bait-prey interaction reduces cell growth on uracil-free medium (-Ura) and increases growth on medium containing 5-fluoroorotic acid (+FOA). SEY6210 cells were transformed with CUP1-Nub-Gag or pRS314 (negative control), in combination with Cub-Atg26 (fl), Cub-Atg26 1-569 or Cub-Atg26 570-1198. Expression of the fusion constructs was induced by 100  $\mu\text{M}$   $\text{CuSO}_4$  (Nub constructs) and 250  $\mu\text{M}$  methionine (Cub constructs). Cells were diluted in 10-fold steps and spotted on agar plates containing CM (-Trp/-His)(growth control), CM +FOA (-Trp/-His) (growth implies protein interaction) or MV -Ura (-Trp/-His) (no growth implies protein interaction).



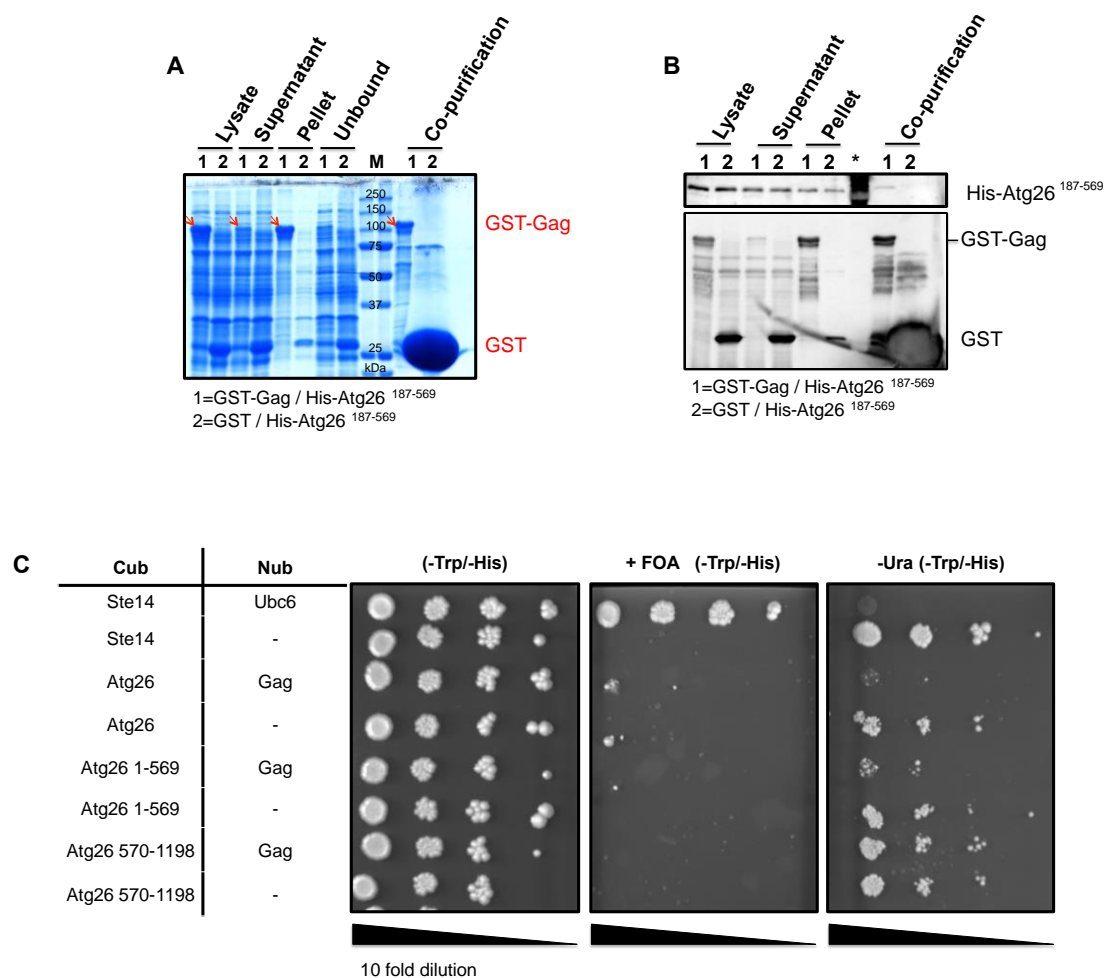


**Figure 4.15 Investigation of a putative direct Atg26-Gag interaction via pull down and split-ubiquitin assay**

(A and B) Cell extracts from *E. coli* (Bl21, pLysS) expressing GST-Gag (1) or GST (2) were mixed with lysate from cells expressing His-Atg26<sup>187-569</sup> and incubated with glutathione sepharose beads (Glut. beads). Co-purification was monitored by (A) CBB-staining of SDS-PAGE and (B) immunoblotting. The asterisk indicates unspecific signals of the marker lane.

(C) Split-ubiquitin assay. The N-terminal part of ubiquitin (Nub) is fused to the bait and its C-terminal part (Cub) to the prey. Protein interaction restores ubiquitin and leads to degradation of a destabilised R-Ura3 variant. Bait/prey interaction is detected by increased growth on 5-FOA-containing medium or by decreased growth rate on medium lacking uracil.

On the CM +FOA plate, cells expressing Nub-Gag in combination with the Atg26 constructs had no higher growth rate than the negative controls (-), suggesting no interaction. Inconsistently with these results, expression of Nub-Gag together with Cub-Atg26 or Cub-Atg26 1-569 led to decreased growth on -Ura plates, which would indicate an interaction between Atg26 and Gag. Furthermore, these results would be inline with all mapping studies above where especially the region 187-569 of Atg26 was shown to mediate Gag binding but not Atg26 570-1198. However, the split-ubiquitin assay did not coherently validate an (direct) interaction between Atg26 and Gag (Figure 4.15C).

## 4.9 GFP- and mCherry-tagged L-A Gag bind Atg26, but inhibit the endogenous virus

To validate the interaction between Atg26 and L-A Gag in more detail and to investigate the function of this interaction, cDNA clones of *GAG* and *GAGPOL* RNA were cloned in GFP and mCherry vectors with inducible *MET25* promoters (pUG34, pUG35, pUG36 and pUG36-mCherry). A mCherry-tagged L-A Gag construct was tested using the established GFP-Atg26-TRAP protocol and analysed by immunoblotting (Figure 4.16A), CBB staining of SDS-PAGE and EtBr staining of agarose gels (Figure 4.16B). For this, *atg26Δ* cells expressing GFP-Atg26 wt, I1198A, 1-1194 ( $\Delta$ WTMI) or GFP alone together with mCherry-Gag were grown to late-log phase, osmotically lysed and used for the GFP-TRAP (Figure 4.16A lanes 8-11). As further control, GFP-Atg26 wt was overexpressed without the mCherry-Gag construct (Figure 4.16A, lane 5 and 12). To check whether interaction with mCherry-Gag is influenced by the absence of endogenous L-A Gag, GFP-Atg26 wt or GFP alone in combination with mCherry-Gag were expressed in  $\Delta l-a/atg1\Delta$  cells (" $\Delta l-a$ " indicates loss of L-A virus) for its analysis via GFP-TRAP (Figure 4.16A, lanes 13 and 14).

On the one hand, immunoblot analysis clearly showed an interaction of GFP-Atg26 and mCherry-Gag, suggesting that the mCherry tag had no effect on Atg26 binding (Figure 4.16A lane 8-10 and 13). On the other hand, the results demonstrated that expression of mCherry-Gag or the presence of *mCHERRY-GAG* RNA interfere with the endogenous L-A virus of our laboratory strain (WCG4a). Co-isolation of detectable amounts of endogenous Gag was only possible in the absence of the mCherry-Gag construct (Figure 4.16A lane 12). Comparison of the  $\Delta l-a/atg1\Delta$  and *atg26Δ* strains showed no differences in complex formation between GFP-Atg26 and mCherry-Gag, implying that interaction of GFP-Atg26 and mCherry-Gag occurs independent of endogenous Gag. CBB staining of SDS-PAGE and EtBr staining of agarose gels supported the observation that expression of mCherry-Gag inhibited endogenous L-A (Figure 4.16B).

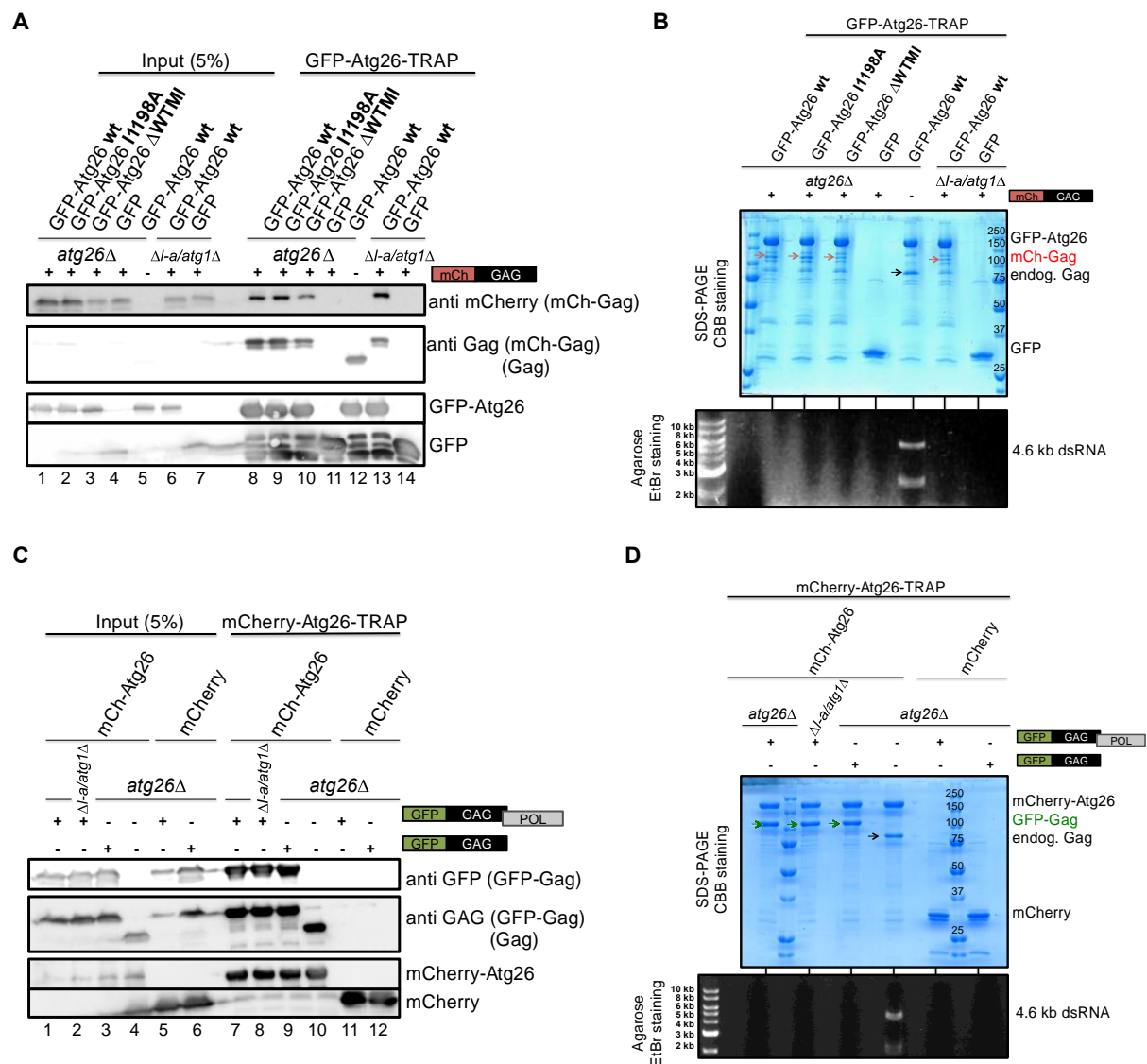


**Figure 4.16 Atg26 binds tagged versions of Gag**

(A, B) GFP-Atg26-TRAP. Extracts from *atg26Δ* or *Δl-a/atg1Δ* cells expressing GFP-Atg26 variants or GFP together with mCherry-Gag or mCherry alone were incubated with GFP-TRAP beads. Input and bound fractions were analysed by (A) immunoblotting, (B: top) CBB staining of SDS-PAGE and (B: bottom) EtBr staining of agarose gels. “*Δl-a*” indicates loss of L-A virus.

(C, D) mCherry-Atg26-TRAP. Extracts from *atg26Δ* or *Δl-a/atg1Δ* cells expressing mCherry-Atg26 or mCherry alone together with GFP-Gag, GFP-GagPol or GFP alone were incubated with RFP-TRAP beads. Input and bound fractions were analysed by (C) immunoblotting, (D: top) CBB staining of SDS-PAGE and (D: bottom) EtBr staining of agarose gels. “*Δl-a*” indicates loss of L-A virus.

N-terminally GFP-tagged versions of Gag and GagPol were analysed by mCherry-Atg26-TRAP (Figure 4.16C and D). The construct GFP-GagPol included the second overlapping ORF (*POL*), encoding a RNA-dependent RNA polymerase. In previous studies, it was shown for the endogenous virus that a random -1 ribosomal frameshift in *GAGPOL* causes a 1:60 ratio of Gag-Pol to Gag expression (chapter 2.6) (Dinman et al., 1991; Valle et al., 1993). However, a band of the triple fusion protein GFP-Gag-Pol with a putative

## Results

molecular weight over 200 kDa was generally not detectable by immunoblotting or CBB staining of SDS-PAGE. It can be speculated that the expected 60-fold lower expression of GFP-Gag-Pol compared to GFP-Gag was too weak for detection.

Furthermore, it was tested in this mCherry-Atg26-TRAP whether the absence of the endogenous L-A influences the interaction between mCherry-Atg26 and GFP-Gag by using the virus-lacking strain *Δl-a/atg1Δ* (Figure 4.16C lane 2 and 8). mCherry-Atg26 was also expressed without GFP-tagged Gag constructs to detect the interaction between mCherry-Atg26 and endogenous Gag (Figure 4.16C lanes 4 and 10; D). Cells co-expressing mCherry alone together with GFP-GagPol or GFP-Gag were used as negative controls (Figure 4.16C, lanes 5, 6 and 11, 12). All constructs were overexpressed by full induction of the *MET25* promoter (growth without methionine).

Remarkably, GFP-Gag from both constructs, GFP-Gag or GFP-GagPol, was co-purified in comparable amounts to endogenous Gag by this mCherry-Atg26-TRAP (Figure 4.16C lanes 7, 8, 9 and 10). Expression of GFP-tagged Gag also inhibited endogenous virus activity: In the presence of GFP-Gag, there was no endogenous Gag in the input or bound fraction detectable (Figure 4.16C lanes 1,2,3 and 7,8,9; D). Immunoblot analysis with Gag antibody also detected weak bands at about 76 kDa (molecular weight of endogenous Gag) in the presence of GFP-Gag (Figure 4.16C lanes 7 and 9). However, these signals were most likely degradation products of GFP-Gag, because this band was also detectable in the absence of the L-A virus (*Δl-a/atg1Δ*)(Figure 4.16.C lane 8). In agreement with the GFP-Atg26-TRAP (Figure 4.16A and B), absence of the endogenous L-A virus did not influence interaction between mCherry-Atg26 and GFP-tagged Gag (Figure 4.16C, compare lanes 7 and 8).

Examinations of the bound fractions by CBB staining of SDS-PAGE and EtBr staining of agarose gels were consistent with the immunoblot analysis (Figure 4.16D): the presence of GFP-tagged Gag versions interfered with co-isolation of detectable amounts of L-A dsRNA.

To further test whether GFP- or mCherry-tagged Gag have similar properties as endogenous Gag, a GFP-TRAP was performed using GFP-Gag as bait (Fig 4.17A and B). For this experiment, extracts from *ATG26-HA* cells (chromosomally HA-tagged) ectopically expressing GFP-Gag or GFP alone together with mCherry-Gag or mCherry were incubated with GFP-TRAP beads.

## Results

Co-isolation of chromosomally expressed Atg26-HA further confirmed an interaction between Gag and Atg26 (Fig 4.17A). Moreover, the bait GFP-Gag was able to bind mCherry-Gag, suggesting that both tagged versions of Gag are able to form homo-oligomers comparable to endogenous Gag. The GFP moiety is theoretically orientated to the inside of a GFP-Gag virus particle and thus not accessible for GFP-TRAP beads. Thereby, this experiment indirectly showed that formation of whole virus particles using tagged Gag was doubtful. However, it is possible that GFP-Gag virus particles were formed in the cell but destabilized during the CoIP. In this case, the virus particles would open and allow interaction with GFP-TRAP beads.

For microscopic analyses of these constructs, *ATG26-HA* cells ectopically expressing GFP-Gag and mCherry-Gag were used (Figure 4.17C). In many cells, the signals of both constructs were highly mobile dots. Therefore, these investigations were problematic. The switch between the GFP- and the mCherry channel and the exposure times (0.3 sec) made it impossible to detect potential colocalization of the two signals (Figure 4.17C, cell 1). However, there were also cells with less mobile or fixed dots. In these cells, a clear colocalisation of GFP-Gag and mCherry-Gag was detectable (Figure 4.17C, cell 2), suggesting self-assembly of tagged Gag.

In time-lapse microscopy with 0.44 sec episodes, the mobility of tagged Gag was validated by using GFP-Gag(Pol) and a C-terminally tagged version of Gag. Most signals were mobile during the time periods (Figure 4.17D and E, left). Only a few dots had a relatively constant localisation, illustrated on the right site as white blocks created by the Fiji plugin "Integral Blocks PMCC" (Figure 4.17D and E, right). By comparing both fusion proteins, it seemed that Gag-GFP forms larger dots than GFP-Gag(Pol). Furthermore, in this microscopic analyses, the size or signal intensity of the dots seemed to negatively correlate with the mobility.

The results of this chapter indicated that the tested tagged versions of Gag have similar properties as endogenous Gag regarding the expression level, the stability, the affinity to Atg26 and the ability to self-assemble. However, it was also shown that tagged Gag and/or its transcripts inhibited the endogenous L-A virus.

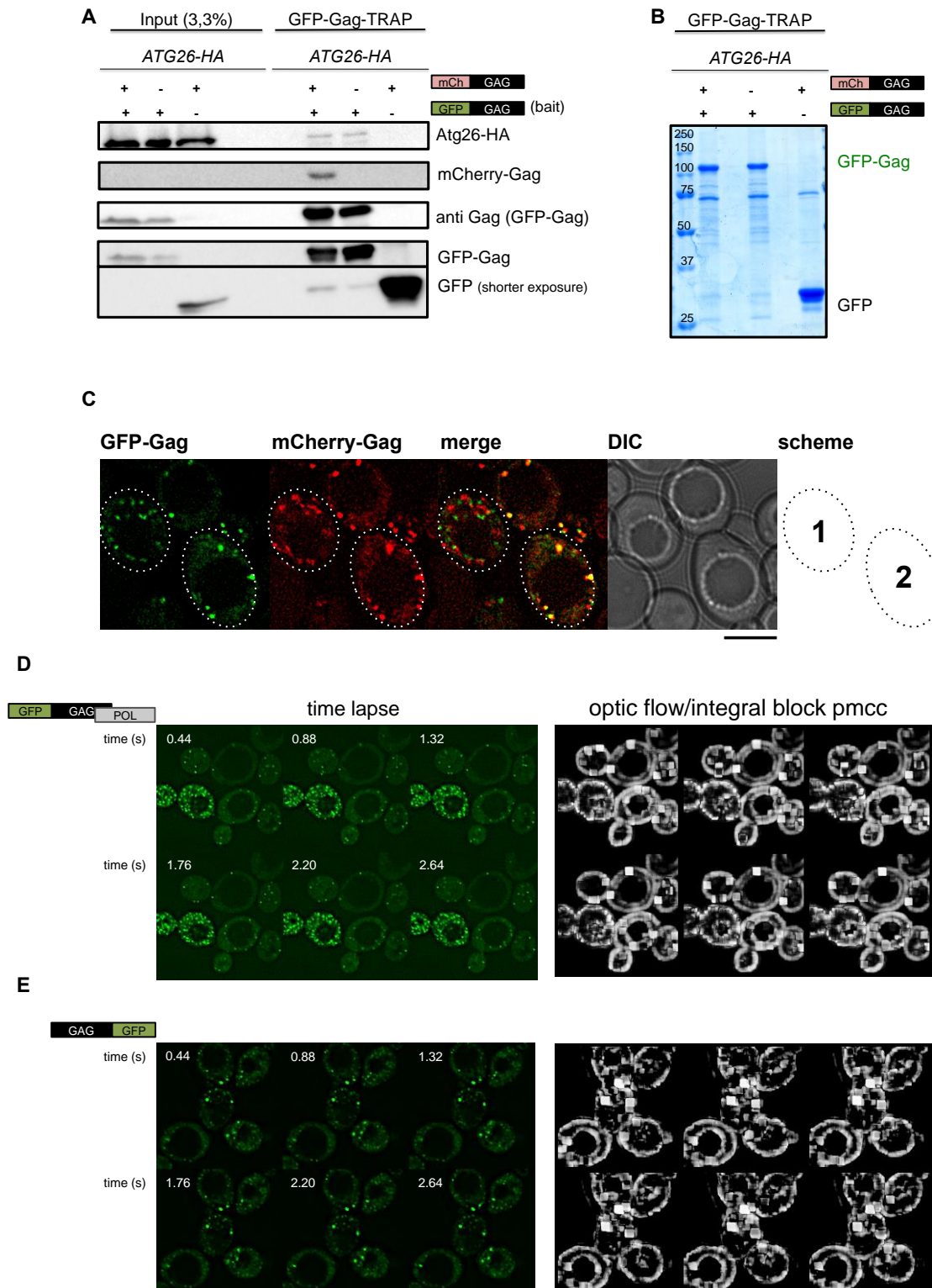


**Figure 4.17 GFP-Gag binds Atg26-HA and mCherry-Gag**

(A and B) GFP-Gag-TRAP. GFP-TRAP beads were incubated with lysates from *ATG26-HA* cells expressing GFP-Gag or GFP alone together with mCherry-Gag or mCherry alone. Co-isolated proteins were monitored by (A) immunoblotting and (B) CBB staining of SDS-PAGE.

(C) *ATG26-HA* strains ectopically expressing GFP-Gag and mCherry-Gag were analysed by fluorescence microscopy. Cell 1 was chosen as an example for highly mobile GFP-Gag and mCherry-Gag dots, whereas cell 2 demonstrates fixed dots that colocalize. Scale bar: 5  $\mu$ m.

(D and E) Time-lapse microscopy of cells expressing GFP-GagPol or Gag-GFP (left). GFP dots with constant localisation were illustrated by using the Fiji plugin "optic flow/integral block pmcc" (right). White blocks show GFP dots with constant localisation in the chosen z-axis. All other GFP signals were mobile.

### 4.10 Autophagy of GFP-tagged Gag depends on Atg26

Results of this thesis showed that Atg26 is transported to the vacuole by autophagy and that it localizes at the PAS, both in an Atg8-dependent manner (chapter 4.4 to 4.6). In further studies, L-A Gag was identified as an interaction partner of Atg26 (chapter 4.7 and 4.8). Altogether, these observations raised the question if Atg26 might be involved in autophagic degradation of virus particles, a heretofore unknown mechanism in yeast. One possibility to monitor autophagy is the vacuolar degradation assay that measures vacuolar processing of GFP-tagged marker proteins (Figure 4.9A). To analyse whether virophagy exists in yeast and whether Atg26 is involved in this process, GFP-tagged versions of L-A Gag were analysed by the vacuolar degradation assay. For experimental exclusion that Atg26 is involved in unselective, bulk autophagy, Pgk1-GFP was used as marker for this pathway (Welter et al., 2010).

*Wild type* or *atg26Δ* cells expressing Pgk1-GFP or GFP-tagged versions of Gag, were grown to  $OD_{600} \sim 3$  and then shifted to starvation medium (SD-N). At the time points 0, 2, 4 and 6 hours,  $\sim 3 OD_{600}$  were taken for alkaline lysis. For this study, three different constructs with pUG36 as backbone were analysed: (1) GFP-Gag (Figure 4.18B and C), (2) Gag-GFP (Figure 4.18D and E) and (3) GFP-GagPol (Figure 4.18F and G). In these experiments, the expression levels of the Gag constructs were varied by regulating the *MET25* promoter with methionine (high expression: 0.0 mM methionine; low expression: 0.8 mM methionine). Immunoblots were quantified by calculating the ratio of free GFP and GFP-tagged Gag (or Pgk1) ( $signal_{free\ GFP} / signal_{GFP-tagged\ Gag}$ ) (Figure 4.18, right). As the signals in wt cells were most stable after 4 h of starvation, these values were set to 100%.

As similar shown in previous studies (Cao and Klionsky, 2007), autophagy of Pgk1-GFP did not differ in wt and *atg26Δ* cells, indicating no involvement of Atg26 in unselective macroautophagy (Figure 4.18A).

# Results

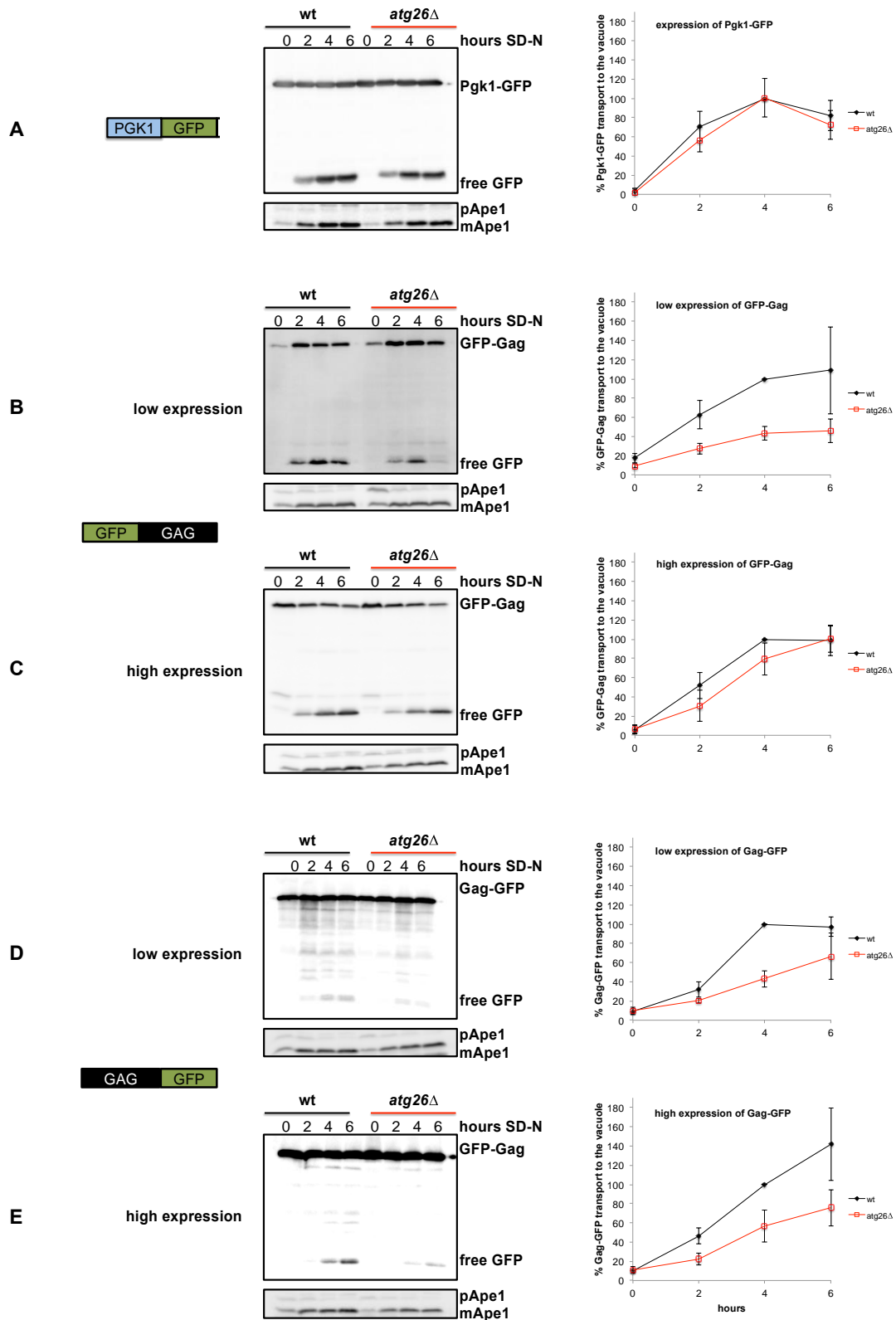
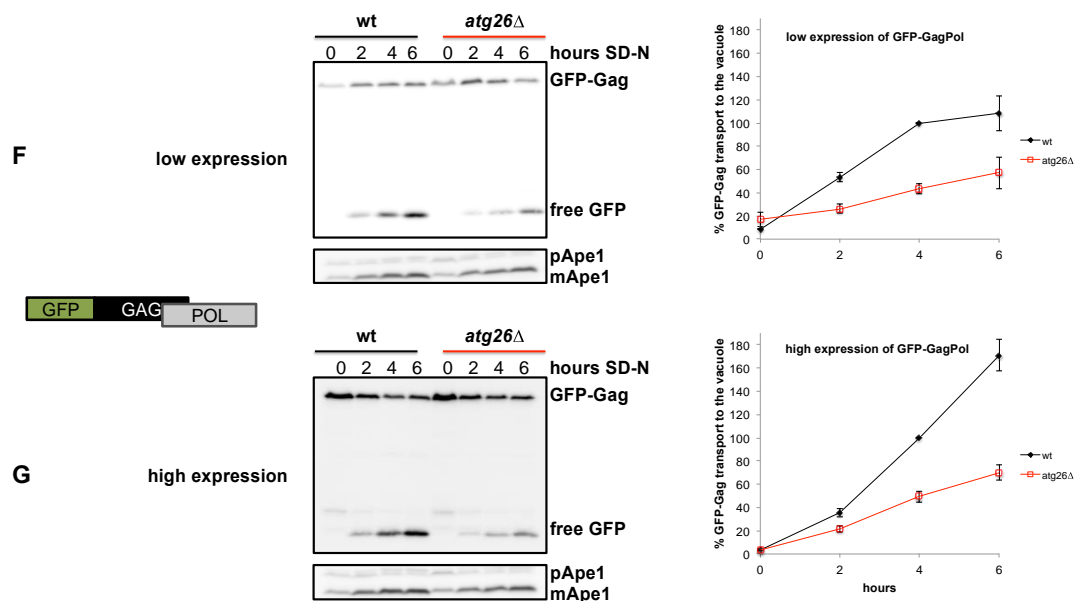


Figure 4.18 GFP-tagged Gag is transported to the vacuole upon autophagy induction





**Figure 4.18 (continued)**

Vacuolar degradation assay. Wild type or *atg26Δ* cells expressing GFP-tagged Gag under control of the *MET25* promoter were grown in CM medium with 0.8 mM (low expression) or without methionine (high expression) to an  $OD_{600} \sim 3$ , then shifted to SD-N. Samples were taken at the indicated time points. Samples were analysed by immunoblots and quantified by calculating the ratio of free GFP and cytosolic GFP-tagged Gag (or Pgk1). Error bars indicate  $\pm$ SEM.

- (A) Autophagy of Pgk1-GFP (endogenous promoter)
- (B) Autophagy of GFP-Gag (GFP-Gag construct) under low expression level
- (C) Autophagy of GFP-Gag (GFP-Gag construct) under high expression level
- (D) Autophagy of Gag-GFP under low expression level
- (E) Autophagy of Gag-GFP under high expression level
- (F) Autophagy of GFP-Gag (GFP-GagPol construct) under low expression level
- (G) Autophagy of GFP-Gag (GFP-GagPol construct) under high expression level

Dissecting the GFP-Gag construct under both expression conditions, autophagy of GFP-Gag showed a maximum after 4 to 6 hours of starvation in wt cells (Figure 4.18B and C). In *atg26Δ* cells, autophagy of low expressed GFP-Gag was clearly reduced. These cells showed only 40–50 % autophagic activity (Figure 4.18B). Autophagy of overexpressed GFP-Gag was only slightly reduced in *atg26Δ* cells (Figure 4.18C).

Gag-GFP showed comparable behaviour as GFP-Gag: a maximum of free GFP after 4–6 hours and relatively unstable measurements after 6 hours of starvation. Deletion of *ATG26* caused a 50% reduction of Gag-GFP autophagy (Figure 4.18.D and E). Remarkably, the ratio of free GFP to Gag-GFP during starvation was much smaller compared to the other constructs. Thus, it seemed that C-terminally tagged Gag is more stable or autophagy-resistant than the N-terminally GFP-tagged Gag versions.

## Results

In wt cells, low expression of the GFP-GagPol construct resulted in a peak of autophagy after 4 to 6 hours (Figure 4.18F), whereas a high expression level of this construct caused a clear maximum after 6 hours of starvation (Figure 4.18G). Deletion of *ATG26* negatively affected autophagy of GFP-Gag under low and high expression level as indicated by a 50–60% reduction of autophagic activity. As already mentioned in chapter 4.9, the GFP-Gag-Pol triple fusion protein was not detectable by immunoblotting. However, it seemed to influence the behaviour of GFP-Gag and its autophagic degradation.

In summary, the results of this chapter demonstrated Atg26-dependent autophagic degradation of GFP-tagged Gag upon starvation. For the first time, these data presented an autophagic phenotype of Atg26 in *S. cerevisiae*. Since autophagy of the highly expressed GFP-GagPol construct was constantly detectable over the longest period, this construct was used for further studies.

### 4.11 Genetic dissection of GFP-Gag autophagy

Analysis of the GFP-GagPol construct demonstrated that its product GFP-Gag was degraded in the vacuole under starvation and that deletion of *ATG26* obviously repressed this process (chapter 4.10).

The genetic analysis of autophagic GFP-Gag degradation was extended to discover further genes that might be involved in this process. Therefore, deletion strains of interest transformed with pUG36-GFP-GagPol were grown to  $OD_{600} \sim 3$  in CM medium without methionine to induce high expression of GFP-Gag (and, hypothetically, GFP-Gag-Pol). Then, cells were shifted to SD-N medium and analysed by the vacuolar degradation assay, as already described in chapter 4.10.

The selective autophagy adaptor Atg11 was one interesting candidate to clarify if GFP-Gag might be processed by selective autophagy. *atg11Δ* cells showed no free GFP suggesting a selective autophagic mechanism for GFP-Gag degradation (Figure 4.19A and D).

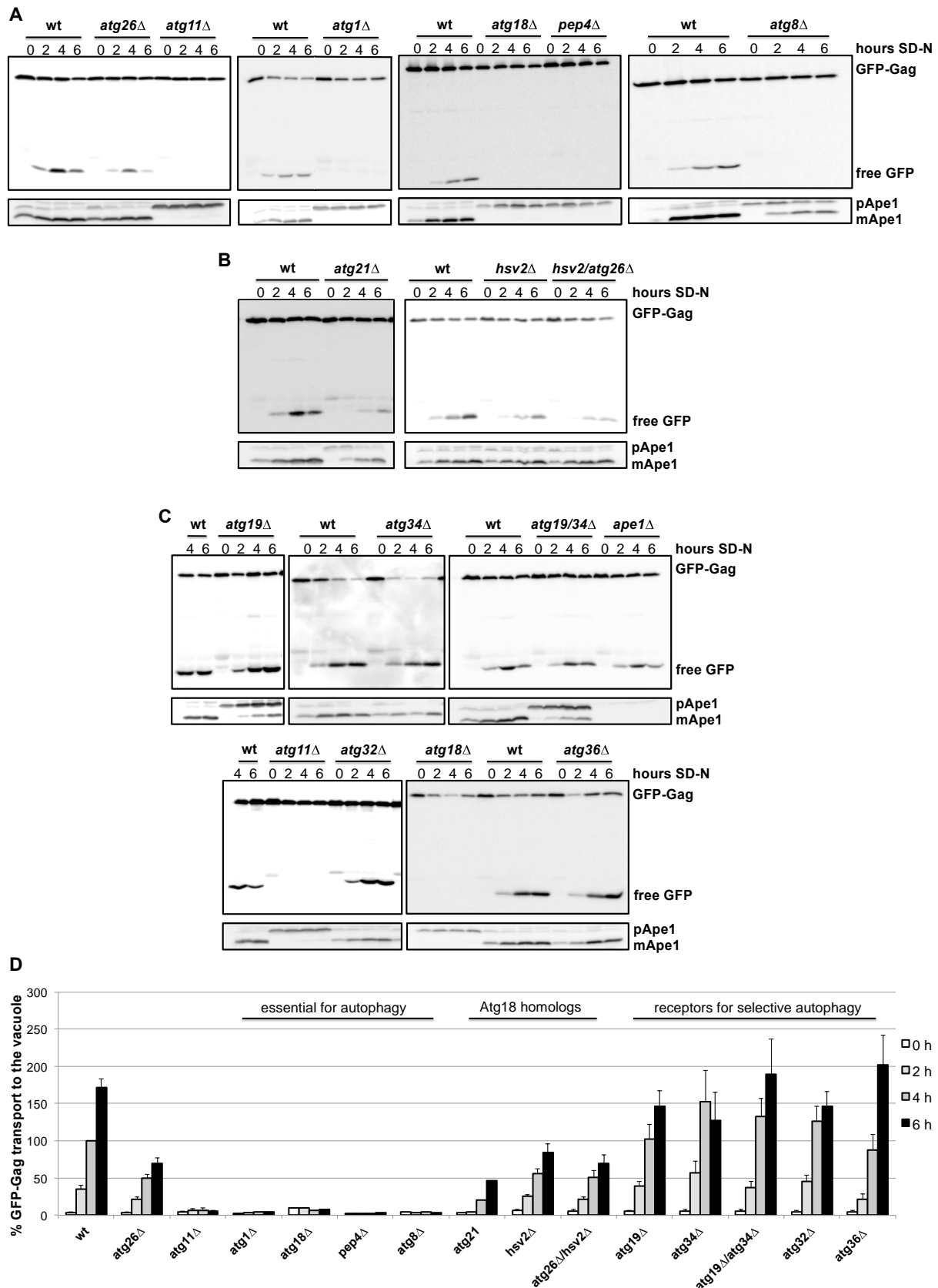


**Figure 4.19 Genetic dissection of GFP-Gag autophagy**

(A–C) Vacuolar degradation assay. Different strains expressing GFP-GagPol under control of the *MET25* promoter were grown in CM medium without methionine (high expression) to an  $OD_{600} \sim 3$ , and then shifted to SD-N. Samples were taken at the indicated time points and analysed by immunoblotting.

(D) Quantification of GFP-Gag autophagy. Immunoblots were quantified by calculating the ratio of free GFP and cytosolic GFP-tagged Gag. Error bars indicate  $\pm$ SEM.

## Results

To find out whether GFP-Gag is delivered to the vacuole by canonical autophagy, some autophagy-related proteins of the core machinery were tested: The serine/threonine kinase Atg1, the PROPPIN Atg18 and the ubiquitin-like protein Atg8 were in focus. Furthermore, the vacuolar protease Pep4 necessary for degradation of autophagic bodies in the vacuole was investigated. The strains *atg1Δ*, *atg18Δ*, *atg8Δ* and *pep4Δ* showed no vacuolar processing of GFP-Gag, indicating a transport of GFP-Gag to the vacuole by canonical autophagy (Figure 4.19A and D).

In further investigations, the Atg18 homologs Atg21 and Hsv2 of the PROPPIN family were analysed (Figure 4.19B and D). Atg21 is required for the Cvt pathway, PMN and efficient starvation induced autophagy, whereas Hsv2 is only necessary for efficient PMN (Barth et al., 2002; Krick et al., 2008a; Welter et al., 2010). Deletion of *ATG21* caused a more than 70% reduction of GFP-Gag autophagy. In *hsv2Δ* cells, autophagic degradation of GFP-Gag was about 40% decreased. Additional deletion of *ATG26* in this strain (*hsv2Δ/atg26Δ*) resulted in 50-60% reduction, comparable to the single deletion of *ATG26*.

The involvement of the Atg26, Atg11, Atg21 and Hsv2 in autophagy of GFP-tagged Gag(Pol) suggests that this mechanism is not starvation-induced bulk, unselective autophagy, but rather a selective autophagic pathway (Figure 4.19A, B and D). In yeast, selective autophagy receptors have in common that they physically link their cargos to the selective adapter Atg11 and Atg8. Deletion of such autophagic receptors leads to drastic decreased autophagic transport to the vacuole of respective cargos or complete interruption of selective autophagy (Farré et al., 2013; Motley et al., 2012; Okamoto et al., 2009; Shintani et al., 2002; Suzuki et al., 2010). These receptors (Cvt pathway: Atg19 and Atg34; mitophagy: Atg32; pexophagy: Atg36) were analysed to test whether they influence autophagic degradation of GFP-Gag. Investigations of *atg19Δ*, *atg34Δ*, *atg19/34Δ*, *atg32Δ* or *atg36Δ* cells have shown that these selective receptors are not required for autophagic degradation of GFP-Gag (Figure 4.19C and D).

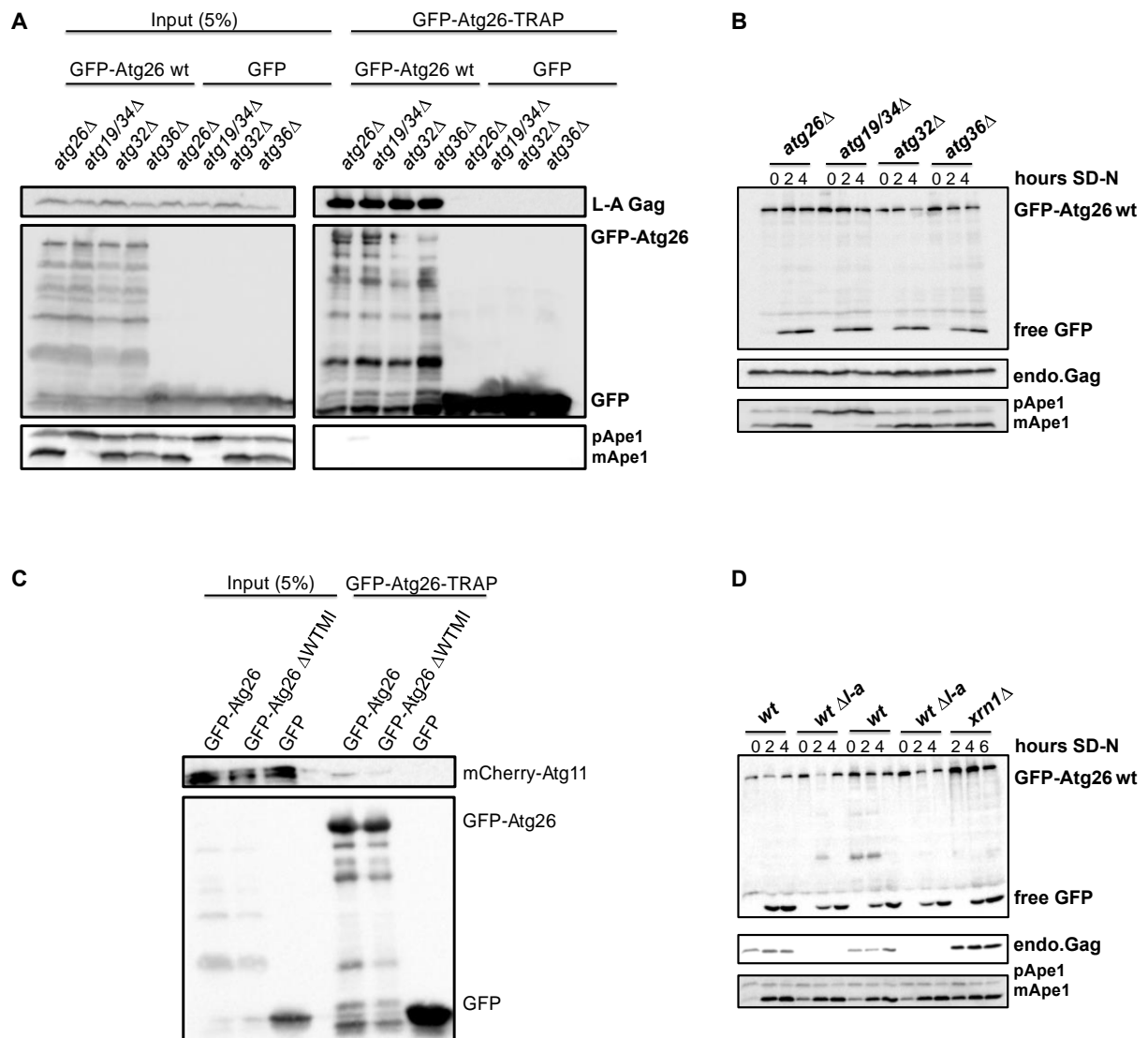


#### Figure 4.20 Known receptors for selective autophagy are not involved in the Atg26-Gag interaction and autophagy of GFP-Atg26

(A) GFP-Atg26-TRAP. Extracts from *atg26Δ*, *atg19Δ/atg34Δ*, *atg32Δ* or *atg36Δ* cells expressing GFP-Atg26 or GFP alone were incubated with GFP-TRAP beads. Input and bound fractions were analysed by immunoblotting.

(B) Vacuolar degradation assay. Growing *atg26Δ*, *atg19Δ/atg34Δ*, *atg32Δ* or *atg36Δ* cells expressing GFP-Atg26 wt were shifted to SD-N. Samples were taken at the indicated time points and analysed by immunoblotting.

(C) GFP-Atg26-TRAP. Extracts from *atg26Δ* cells expressing GFP-Atg26, GFP-Atg26 ΔWTMI or GFP alone together with mCherry-Atg11 were used for GFP-TRAP. Input and bound fractions were analysed by immunoblot analysis.

(D) Vacuolar degradation assay. Growing wt cells, infected or non-infected ( $\Delta l-a$ ) by the L-A virus, and *xrn1Δ* cells expressing GFP-Atg26 wt were shifted to SD-N. Samples were taken at the indicated time points and analysed by immunoblotting.

To further exclude that these selective receptors have a role in (GFP-)Gag degradation or somehow influence the physical Atg26/Gag interaction, an established GFP-TRAP with the respective deletion strains was performed using GFP-Atg26 as bait (Figure 4.20A). As negative control, GFP alone was expressed in the different deletion strains. These

## Results

interaction studies clearly demonstrate that the selective receptors did not effect the Atg26-Gag interaction. By using the vacuolar degradation assay to analyse GFP-Atg26 degradation in these strains, it was additionally shown that these selective receptors have no influence on autophagic processing of GFP-Atg26 (Figure 4.20B).

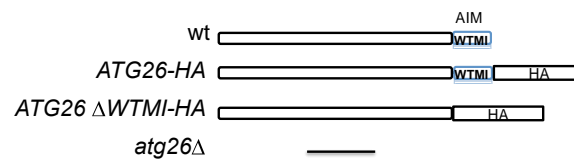
In a further GFP-Atg26-TRAP experiment, it was tested whether Atg26 interacts with the selective adapter Atg11. For this, protein extracts from cells expressing GFP-Atg26, GFP-Atg26  $\Delta$ WTMI or GFP in combination with mCherry-Atg11 were incubated with GFP-TRAP beads (Figure 4.20C). By this method, a weak Atg26-Atg11 interaction was detectable. Furthermore, it seemed that the AIM of Atg26 influences the interaction.

By performing the vacuolar degradation assay with wt cells infected or non-infected ( $\Delta$ *l-a*) by the L-A virus and *xrn1* $\Delta$  cells expressing GFP-Atg26 wt, it was tested whether the L-A virus influences autophagic degradation of GFP-Atg26 (Figure 4.20D). Immunoblot analysis showed that absence (wt  $\Delta$ *l-a*) or excess (*xrn1* $\Delta$ ) of the L-A virus did not or hardly correlate with autophagic degradation of GFP-Atg26 (Figure 4.20D).

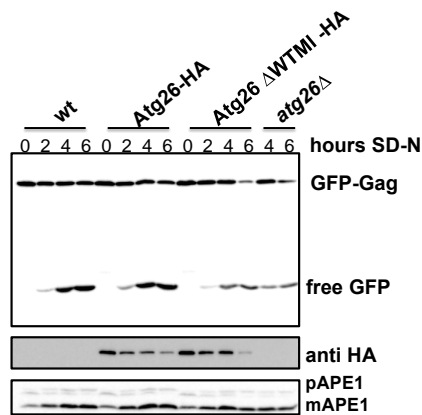
In chapter 4.6, it was experimentally validated that Atg26 is AIM-dependently transported the vacuole during starvation; data of chapter 4.10 and this chapter revealed a role of Atg26 in autophagy of GFP-Gag (chapter 4.9, 4.10). These observations raised the question whether the very C-terminal AIM of Atg26 is also relevant for GFP-Gag transport to the vacuole. Two chromosomally HA-tagged *ATG26* strains, including *ATG26-HA* and *ATG26*  $\Delta$ WTMI-*HA*, were generated (Figure 4.21A) and analysed by performing the vacuolar degradation assay with the GFP-GagPol construct (as described above) to answer this question (Figure 4.21B and C).

Performing the vacuolar degradation assay, a *wild type* level of GFP-Gag degradation was detectable in *ATG26-HA* strains, indicating that the C-terminal HA tag has no influence on the structure or function of Atg26. Only the measurement after 6 hours showed a 12 % decrease in GFP-Gag degradation (Figure 4.21B and C). An about 30% reduction of GFP-Gag autophagy was measurable for *ATG26*  $\Delta$ WTMI-*HA* cells suggesting that the very C-terminal AIM of Atg26 and thus its interaction with Atg8 enhances the efficiency of GFP-Gag autophagy (Figure 4.21B and C). Furthermore, these observations and the fact that Atg26 and Gag interact with each other (chapter 4.7 and 4.8) gave first hints that these two proteins are co-transported to the vacuole by autophagy.

A



B



C

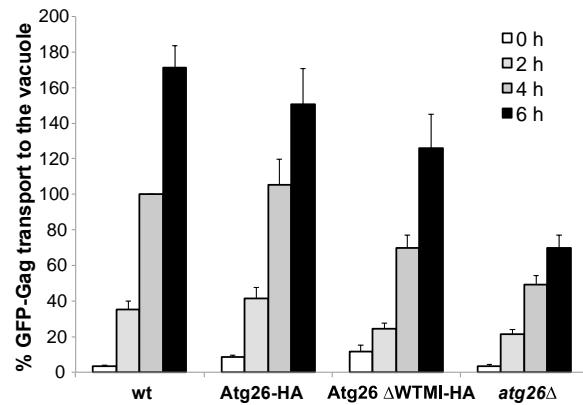


**Figure 4.21 The C-terminal AIM of Atg26 is necessary for efficient autophagy of GFP-Gag(Pol)**

(A) Scheme of the analysed strains: wt, *ATG26-HA*, *ATG26  $\Delta$ WTMI-HA* and *atg26 $\Delta$*

(B) Vacuolar degradation assay. Wild type, *ATG26-HA*, *ATG26  $\Delta$ WTMI-HA* or *atg26 $\Delta$*  cells expressing GFP-GagPol under control of the *MET25* promoter were grown in CM medium without methionine (high expression) to an  $OD_{600} \sim 3$ , then shifted to SD-N. Samples were taken at the indicated time points and analysed by immunoblotting.

(C) Quantification of autophagy of GFP-Gag. Immunoblots were quantified by calculating the ratio of free GFP and cytosolic GFP-tagged Gag ( $n \geq 8$ ). Error bars indicate  $\pm$ SEM.

### 5 Discussion

Autophagy is an evolutionary conserved degradative pathway for the removal and recycling of cytosolic components and organelles to maintain the cellular homeostasis. This intracellular process is characterized by the formation of a double-membrane-layered vesicle, called autophagosome. In yeast, autophagy is initiated at the PAS with the formation of a double-membrane structure, the phagophore, which elongates to engulf cytoplasmic components. Autophagosome formation is completed by closure of the phagophore. Finally, the outer membrane of the autophagosome fuses with the vacuole leading to degradation of the inner membrane together with the cargo (Feng et al., 2013; Reggiori and Klionsky, 2013).

Initially, autophagy was defined as a non-selective, bulk degradation pathway in response to starvation. However, the knowledge about autophagic regulators enormously increased in the last decade. Now, there exists clear evidence that removal of dysfunctional organelles, clearance of protein aggregates, and elimination of intracellular pathogens, are highly selective autophagic processes that involve cargo recognition by the autophagic machinery (Kraft et al., 2010; Liu et al., 2014; Okamoto, 2014). In yeast, selective pathways were shown to mediate turnover of damaged mitochondria and removal of surplus peroxisomes (Kanki and Klionsky, 2010; Motley et al., 2012; Okamoto, 2014; Okamoto et al., 2009). Furthermore, it was shown that the ER, ribosomes, lipid droplets and non-essential parts of the nucleus are selective cargos of autophagy (Bernales et al., 2006a; Kraft et al., 2008; Krick et al., 2008b; van Zutphen et al., 2014). The Cvt pathway is a biosynthetic process that selectively targets resident hydrolases to the vacuole. However, this process is also categorized as selective autophagy, because it requires the autophagic machinery and is mechanistically equivalent to the other selective pathways (Lynch-Day and Klionsky, 2010; Reggiori and Klionsky, 2013). Recently, it was demonstrated that components of the Cvt pathway are also involved in selective autophagy of Ty1 retrotransposon VLPs to down-regulate transposition that causes chromosomal mutation (Suzuki et al., 2011).

In this study, it was discovered that also the major coat protein Gag of the *S. cerevisiae* virus L-A might be degraded by selective autophagy, indicated by the involvement of Atg11 and the two PROPPINs Atg21 and Hsv2, which are typical regulators of selective autophagy. Furthermore, it was shown that Atg26, whose function was unclear so far, interacts with L-A Gag and is a further mediator of L-A Gag autophagy.



### 5.1 Searching for new Atg8 interaction partners

Atg8 is a key component for autophagosome biogenesis and mediates cargo recognition during selective autophagy. These two central roles make Atg8 to an ideal bait for screens and proteomic approaches to find new proteins that are involved in autophagy or related processes. For example, the mammalian autophagy receptors NBR1, Nix and optineurin were identified as ATG8 (LC3/GABARAP) binders by using *ScAtg8*, LC3B and GABARAPL2 as baits for yeast two-hybrid screens (Kirkin et al., 2009b; Novak et al., 2010; Wild et al., 2011). TBC-domain containing Rab GAPs, which function as regulatory factors in autophagy, were also found to interact with mATG8 orthologs by yeast two-hybrid screens (Popovic et al., 2012). MS analyses investigating the 6 human ATG8 homologs as baits for CoIPs identified a further huge number of ATG8 interaction partners (Behrends et al., 2010). A further method to find new ATG8 binders was phage display by screening a randomized peptide library with GABARAP as affinity ligand. Calreticulin was predicted as a GABARAP binder by this approach and validated in further experiments (Mohrlüder et al., 2007). In a recent study based on a microscopic screen analysing the effect of siRNA knockdown on autophagy-related location of GFP-LC3B, TRIM5 $\alpha$  was identified as an Atg8 binder and shown in further experiments to act as selective receptor for degradation of viral capsids (Mandell et al., 2014). However, the screening methods only predicted putative Atg8 binders, but did not further characterize the interaction site. In consequence, further experiments were required to test whether the interaction occurs AIM-dependently or differently.

In this study, GFP-tagged Atg8 wt and two AIM-binding site mutants, including a W-site (L50A) and a L-site mutation (Y49A), were used as affinity ligands in a GFP-TRAP and following MS analysis (Figure 4.1, 4.2, 4.3 and 4.5). In parallel, the relevance of the N-terminal FK-motif was analysed using GFP-Atg8 F5GK6G as bait for GFP-TRAP experiments and following proteomic analysis. GFP-Atg8 S3AT4A as bait, containing substitutions of non-conserved amino acids in the N-terminal region, was used as a further control (Figure 4.1, 4.2, 4.3 and 4.5). The following quantitative MS analysis of the different Atg8 baits was established to get information about the specificity and, thus, the confidence of putative Atg8 interactors. Furthermore, this proteomic approach should reflect whether putative binding partners interact via an AIM or differently.

The known Atg8 binders Atg19, Ape1 and Fas1/2 were used as marker proteins to test the quality of the established GFP-Atg8-TRAP by immunoblotting (Figure 4.1B and C).

## Discussion

Atg19, Ape1, Fas1 and Fas2 were identified with high peptide count (Figure 4.3A and B) and showed the expected binding pattern (Figure 4.5B). These results supported the quality of the MS approach of this study. However, Atg21 was not detected by MS, although it was already identified as a putative Atg8 binder in previous studies (Juris et al., unpublished) and was clearly detectable by immunoblot analysis in previous GFP-Atg8-TRAP experiments (Figure 4.1B and C). Therefore, it seems possible that Atg21 was incompatible with the preparation of the samples for MS analysis. Further proven interaction partners of Atg8 that have not been identified by MS of this study were the mitophagy receptor Atg32 and the Cdc48 adapter Shp1, which were shown in previous reports to directly interact with Atg8 (Krick et al., 2010; Okamoto et al., 2009). Regarding that Atg32 and Shp1 were not analysed by immunoblotting in previous GFP-TRAP experiments, it cannot be excluded that the chosen buffer conditions were not optimal to capture these proteins.

However, the quality of the MS analysis was further supported by identification of the known Atg8 binders Atg3 and Atg34 with the expected AIM-dependent interaction pattern (Suzuki et al., 2010; Yamaguchi et al., 2010). Atg4 and Atg7, which are direct interactors of Atg8 and necessary for its conjugation to PE (Nakatogawa, 2013), were also specifically detected by MS analysis.

Furthermore, 17 of 25 newly identified Atg8 interactors were experimentally validated (Figure 4.4). In following binding studies, the COPI proteins and especially Atg26 showed the same binding pattern predicted by this MS analysis (Figure 4.5).

Taken together, the approach of this study allowed rapid validation of the numerous proteins identified by MS.

### 5.2 Newly identified Atg8 interaction partner

90 of about 430 proteins identified by MS were predicted as putatively specific Atg8 interactors (Figure 4.3). The web resource STRING was used to categorize the putative interactors by their cellular function (Figure 4.4) (Szklarczyk et al., 2010). Major functional groups are autophagy, COPI and COPII vesicles, protein folding (chaperones) and rRNA processing. However, many proteins could not be grouped, since they are not involved in similar cellular processes or have no obvious functional similarities (Figure 4.4E).

The majority of identified Atgs (Atg3, Atg4, Atg7, Atg19 and Atg34) were shown in

## Discussion

previous reports to directly interact with Atg8 (Wild et al., 2013), as discussed above. Therefore, the functional link between Atg8 and **autophagy** was used as internal controls of the CoIPs (GFP-Atg8-TRAP) and MS analysis.

In MS analysis and further binding studies, the whole **COPI coatomer complex** was identified to form a complex with Atg8. All components of the COPI complex interact in a W-site- and FK-motif-dependent manner. Therefore, it can be speculated that Atg8 binds only a single component of the whole complex directly by the W-site and the FK-motif and thereby co-isolates also the remaining subunits of the COPI complex (Figure 4.5C and D). However, based on the analysis of this study, it is not possible to estimate which of the component(s) might be the direct Atg8 binder(s). Interestingly, the interaction of Atg8 and the COPI complex depends on the W-site and FK-motif, similar to the binding pattern of the PROPPIN Atg21 that directly interaction with Atg8 via its  $\beta$ -propeller (compare Figure 4.1B, C and 4.5C, D)(Juris et al., unpublished). Structural analyses of previous studies showed that the COPI components Cop1 and Sec27 have a  $\beta$ -propeller domain (Jackson, 2014). Therefore, it can be speculated that these two proteins might be directly involved in Atg8 binding also via their  $\beta$ -propeller domains.

The COPI complex is necessary for retrograde transport of vesicles within the Golgi stack or from the cis-Golgi to the ER (Jackson, 2014). Less is known about a direct interrelationship of COPI vesicles and Atg8 or autophagy. For yeast, vander Vaart et al. (2010) tested the involvement of the COPI components Ret2 and Ret3 in autophagic GFP-Atg8 processing by using thermosensitive strains. However, no effect on macroautophagy was measured comparing permissive and restrictive temperature (der Vaart et al., 2010). For mammalian cells, it was demonstrated that siRNA depletion of COPI causes defects in early endosome function and thereby blocks autophagic flux (Razi et al., 2009; Tooze and Razi, 2009). In yeast, a subcomplex of COPI (COPIb) was shown to participate in endosomal sorting to the vacuole, but an involvement in autophagy was not tested (Gabriely et al., 2007). In a proteomic approach, Graef et al. (2013) revealed a physical interaction between Atg8 and COPI proteins, but without further analysis of this interaction (Graef et al., 2013).

**COPII** vesicles mediate the ER-Golgi transport and are initiated and formed by the major coatomer components Sar1, the Sec23/Sec24 subcomplex and the Sec13/Sec31 subcomplex (Jensen and Schekman, 2010). Especially recent studies showed that COPII vesicles are membrane sources for expansion of the phagophore in yeast and mammals

## Discussion

(Ge et al., 2013; Graef et al., 2013; Schroder et al., 2008; Suzuki et al., 2013; Tan et al., 2013). In the MS analyses of this study, Sec23, the GAP of Sar1 GTPase, and Sfb3, a further subcomponent of Sec23/Sec24 complex, were identified as putative AIM-dependent Atg8 binders (Figure 4.3A). Unfortunately, experimental validation of a putative Sec23/Atg8 interaction was not possible, since the chromosomal GFP-tagged Sec23, used for binding studies, seemed to be not functional, indicated by highly decreased growth rate (not shown). In agreement, the Sec23-GFP was generally not detectable by immunoblotting (not shown). Nonetheless, previous studies based on MS analysis also gave a hint that Atg8 might directly interact with Sec23 (Graef et al., 2013). Furthermore, Tan et al. (2013) revealed that Sec23 recruits COPII vesicles as membrane sources to the PAS via an direct interaction with the TRAPPIII complex. Therefore, Sec23 seems to be directly involved in autophagy (Tan et al., 2013). In this study, a weak interaction between Atg8 and Sfb3 was detectable via pull down experiments (Figure 4.4D). Since Sfb3 and Sec23 are physically linked, it is possible that these two proteins were co-isolated as a complex via GFP-Atg8.

The **chaperones** Ssa1, Ssa2 and Hsp42 were identified as further putative Atg8 interactors. In the context of autophagy, Ssa1 and Ssa2 were shown to interact with prApe1. This interaction is not necessary for self-assembly of prApe1, but rather for efficiency of the Cvt pathway (Satyanarayana et al., 2000; Silles et al., 2000). A further chaperone identified in this study was Hsp42. During protein folding stress, this chaperone locates at peripheral protein aggregates and is necessary for formation of these compartments. But, an involvement of autophagic proteins in formation or clearance of these sites is yet unknown (Specht et al., 2011).

MS analyses also identified a large group of **rRNA processing** proteins. In this group, the majority of proteins interact L-site- and FK-motif-dependently with Atg8. Therefore, similar to the COPI proteins, it can be hypothesized that Atg8 directly binds only single components of large complexes involved in rRNA processing. None of these rRNA proteins were shown in previous studies to be involved in autophagy. But, it can be speculated that some of these ribosome-associated proteins might have a function in ribophagy. However, ubiquitin protease Ubp3 and its cofactor Bre5, which are involved in ribophagy (Kraft and Peter, 2008; Kraft et al., 2009), were not identified by MS analysis of this study. A functional involvement of Atg8 in rRNA processing seems very unlikely, but needs further analysis.

All these putative Atg8 interaction partner would need further functional investigation to determine a relevance for autophagy or an involvement of Atg8 in respective cellular mechanisms.

### 5.3 Atg26 is an AIM-containing protein

Atg26 is involved in mirco-and macropexophagy in *P. pastoris*, whereas its function in *S. cerevisiae* was unknown so far. In previous studies, it has been excluded that Atg26 is involved in unselective macroautophagy, the Cvt pathway, pexophagy, mitophagy and PMN (Cao and Klionsky, 2007; Krick et al., 2008b; Okamoto et al., 2009).

In the MS analysis of this study, Atg26 was identified as an Atg8 interaction partner. Furthermore, MS analysis and following interaction studies demonstrated that both AIM-binding sites of Atg8 are necessary for this interaction, suggesting that Atg26 might contain an AIM or is linked to Atg8 via an AIM-containing protein (Figure 4.3A, Figure 4.5E and F). Validation by the split-ubiquitin assay gave a first hint for a direct interaction of Atg8 and Atg26 (Figure 4.6). Direct pull down assays for a further validation could not be established in this study, because it was not possible to recombinantly express the full-length 135-kDa-protein.

Alternatively, based on the hint that Atg26 might be an AIM-containing protein, a search for putative AIMs in the protein sequence of Atg26 was started. Previous reports indicated that aromatic residues on position 0 and hydrophobic residues on position +3 are prerequisites for AIMs. Secondary characteristics are the accumulation of acidic residues and avoidance of basic residues in the surrounding sequences (Alemu et al., 2012; Birgisdottir et al., 2013; Noda et al., 2010). On the basis of these common simplified features, putative AIMs were predicted and motif conservation was analysed by sequence alignment. By this method, a sequence in the very C-terminal region (Atg26 1191-1198) was predicted as the most likely AIM (Figure 4.7).

Sequence conservation was also considered in previous studies for prediction and validation of AIMs. For example, the AIM of Nix, a mammalian selective receptor for mitophagy, was predicted by sequence alignment of already known AIMs with various Nix orthologs. By this method, a single AIM with a high similarity to the AIM of Atg19 was found and validated by further experiments (Novak et al., 2010). Bioinformatics were also used for calculating the AIM in Atg1/ULK1 (Kraft et al., 2012). In this case, the AIM sequence was shown to be highly conserved from yeast to human and

## Discussion

experimentally validated in three independent studies (Alemu et al., 2012; Kraft et al., 2012; Nakatogawa et al., 2012b). By sequence alignment of Atg19 and the human cargo receptor p62, Sawa-Makarska et al. (2014) found sequence homology of C-terminal regions surrounding the Atg11 binding site in Atg19 and the p62 AIM. Thereby, the cryptic AIMS of Atg19 were identified (Sawa-Makarska et al., 2014). Motif conservation was also tested to search for AIMS and Atg11-binding sites in the pexophagy receptors Atg36 and *PpAtg30*, and the mitophagy receptor Atg32 (Farré et al., 2013; Kondo-Okamoto et al., 2012). These receptor proteins were shown to have a common modules of these two motifs, where the respective AIM is in close proximity and upstream of the Atg11-binding site (Farré et al., 2013).

Kalvari et al (2014) developed the web resource iLir for prediction of AIMS (Kalvari et al., 2014). The algorithm of the software predicts putative AIMS (called xLIRs) based on the sequences of all known AIMS. iLIR was publicly available soon after the C-terminal AIM of Atg26 was experimentally validated in this study. Therefore, this prediction tool was not used for searching putative AIMS in Atg26. However, iLIR further validated the C-terminal AIM in Atg26, because this sequence motif was the only predicted xLIR in Atg26.

In this study, the predicted C-terminal AIM of Atg26 was validated by five different interaction studies, including a GFP-Atg26-TRAP, a GST-Atg8 PD, two variants of a GFP-Atg8-TRAP and a split ubiquitin assay (Figure 4.8B to F). In addition, the requirement for the W-site and the L-site in Atg8 for the interaction with Atg26 further confirm that the Atg8/Atg26 interaction is directly mediated by the AIM of Atg26 (chapter 4.2 and 4.3).

Recently, Atg19 was shown to have further motifs, so called cryptic AIMS, that mediate interaction with Atg8, in addition to the canonical AIM (Sawa-Makarska et al., 2014). Based on the experiments of this study, it is not possible to exclude that Atg26 might have further regions that bind Atg8. A weak interaction between Atg8 and Atg26 lacking the C-terminal AIM was still detectable by a GST-Atg8 pull down assay (Figure 4.8C). Furthermore, binding studies via the split-ubiquitin assay gave a hint that there might be still a weak interaction also when the AIM is deleted: Cells expressing Cub-Atg26 1-1194 and Nub-Atg8 still were able to grow on FOA plates, which indicates interaction (Figure 4.8F). However, putative additional Atg8 binding sites or cryptic AIMS would have an extremely lower affinity to Atg8 than the C-terminal AIM, since all other binding

## Discussion

studies detected no interaction when this sequence was deleted (Figure 4.8B,D and F).

It was shown for all published AIM-containing proteins that deletion or mutation of their AIMS lead to autophagic phenotypes. In this study, the physiological role of the AIM in Atg26 was demonstrated by showing its requirement for targeting Atg26 to the PAS, since deletion of the AIM caused drastic reduction in PAS localisation (see Figure 4.10). In contrast, recent studies revealed that the autophagic core protein Atg1 is recruited to the PAS independently of its AIM. Furthermore, the Atg1 kinase activity and the physical interaction with Atg13 were not influenced when the AIM was mutated. Thereby, interaction with Atg8 is not necessary for early autophagic function of Atg1 (Kraft et al., 2012; Nakatogawa et al., 2012b). Similar, the Cvt receptors Atg19 and Atg34 are Atg8-independently recruited to the PAS (Shintani et al., 2002; Suzuki et al., 2010).

In this study, it was demonstrated that Atg26 is AIM-dependently transported to the vacuole by autophagy, shown by a decreased autophagic processing of GFP-Atg26 lacking the AIM (Figure 4.9C and E). These observations suggested that Atg8 recruits Atg26 to the forming phagophore during autophagy, as it was similarly shown in previous studies for selective receptors or Atg1 (Kraft et al., 2012; Nakatogawa et al., 2012b; Shintani and Klionsky, 2004; Suzuki et al., 2010). Previous reports suggested that the majority of AIM-containing proteins become involved in selective autophagy via their AIMS. Regarding the selective receptors, Atg19 and Atg34 recruitment to the phagophore by Atg8 is necessary to transport the Cvt cargos to the vacuole (Noda et al., 2010; Sawa-Makarska et al., 2014; Suzuki et al., 2010). Similar, mitophagy or pexophagy is reduced if the AIM in Atg32 or Atg36 is mutated (Farré et al., 2013; Kondo-Okamoto et al., 2012; Okamoto et al., 2009). The autophagic core protein Atg1 is also associated with the phagophore by its AIM (Kraft et al., 2012; Nakatogawa et al., 2012b). However, the function of Atg1 in this context is still conflicting, since it is not clear whether mutation of the AIM only influences the Cvt pathway or also unselective, bulk macroautophagy (Kraft et al., 2012; Nakatogawa et al., 2012b). It has been proposed that the AIM-dependent recruitment of Atg1 to the phagophore might facilitate autophagosome formation. Alternatively, autophagic degradation of Atg1 might be a way for down-regulation of the activated Atg1 complex (Kraft et al., 2012). The AIM in Atg3 might be necessary to liberate Atg8 from its interaction with Atg19 to allow PE conjugation of Atg8 during the Cvt pathway (Yamaguchi et al., 2010). The non-canonical AIM of Atg12 seems to be the only AIM that is not specifically involved in selective autophagy, since it

## Discussion

mediates association of the Atg12-Atg5/Atg16 complex with the convex outer membrane of the phagophore during autophagosome biogenesis (Kaufmann et al., 2014). However, the functional analyses of the AIM in Atg26 compared with those of other AIMS suggested that Atg26 might act in selective autophagy. In line with this, it was also demonstrated that Atg26 is involved in autophagy of the (GFP-tagged) major coat protein Gag of the L-A virus and that this mechanism depends on the AIM of Atg26 (Figure 4.18B–G; 4.21). The proposed function of Atg26 in this autophagic mechanism will be discussed later (chapter 5.7.3).

In this study, it was shown that overexpression of GFP-Atg26 leads to reduction of Ape1 maturation, while overexpression of GFP-Atg26 with mutated or deleted AIM has only slight effects on Ape1 maturation, indicating an AIM-dependent inhibition of the Cvt pathway (Figure 4.9D and F). It can be proposed that non-physiological high amounts of GFP-Atg26 counteract with other AIM-containing proteins. Therefore, overexpression of GFP-Atg26 wt might compete with the Cvt receptor Atg19 for Atg8 binding and thereby inhibits the Cvt pathway. It can be also speculated that excess of Atg26 interferes with the interactions of Atg8 and Atg3 or Atg1, which both were shown to be AIM-dependently involved in the Cvt pathway (Kraft et al., 2012; Yamaguchi et al., 2010). Kaufmann et al. (2014) demonstrated by *in vitro* experiments that the AIM-containing mitophagy receptor Atg32 competes with the interaction between Atg8 and the non-canonical AIM of Atg12 and thereby causes disassembly of the Atg12-Atg5/Atg16 membrane scaffold (Kaufmann et al., 2014). Therefore, overexpression of GFP-Atg26 might also reduce the Atg8/Atg12 interaction and thereby inhibit autophagosome or Cvt vesicle biogenesis. In this study, the GFP-Atg26 overexpression effect was analysed only for the Cvt pathway. It would be interesting to test in further experiments whether other autophagic pathways are influenced by overexpression of GFP-Atg26.

Sequence alignment of Atg26 orthologs clearly indicate sequence conservation of the very C-terminal AIM (Figure 4.7D) (Asakura et al., 2009; Warnecke et al., 1999). In *Pichia pastoris*, *PpAtg26* is necessary for extension of the PAS into the MIPA, a cup-shaped, Atg8-positive membrane related to the isolation membrane (Yamashita et al., 2006). Oku et al. (2003) reported for *PpAtg26* that deletion of the C-terminal region 766-1211, including the catalytic domain for synthesis of sterol glycosides and the predicted C-terminal AIM, has no effect on PAS or MIPA localisation (Oku et al., 2003). In



## Discussion

another study, it was shown that the phosphoinositide binding domain of Atg26, comprising the PH and the GRAM domain, mediates PAS and MIPA localisation due to the interaction with PI4P (Yamashita et al., 2006). Therefore, in contrast to *ScAtg26*, it can be speculated that the predicted C-terminal AIM in *PpAg26* might not be necessary for recruitment to Atg8-positive membranes. However, this hypothesis has to be further investigated in this model organism.

*CoAtg26* of the plant pathogenic fungus *Colletotrichum orbiculare* (*C. langenaria*) also contains a conserved C-terminal AIM (Figure 4.7D). Asakura et al. (2009) published that *CoAtg26* is involved in pexophagy in this model organism. Furthermore, it was demonstrated that pexophagy correlates with the pathogenicity of this fungus. Therefore, Atg26 has also a function in host invasion (Asakura et al., 2009; Yoshimoto et al., 2010). It was shown that production of sterol glycosides by the catalytic domain is necessary for these two functions. However, this phenotype was demonstrated by deletion of the C-terminal region (864-1475), including the catalytic domain and the predicted C-terminal AIM. Consequently, it cannot be excluded that the detected phenotype is also caused by the AIM deletion in *CoAtg26*. However, first, the predicted C-terminal AIM has to be validated in binding studies for this organism. In following investigation, it would be interesting to analyse whether the predicted AIM is involved in pexophagy and the pathogenicity.

### 5.4 Identification of L-A Gag as an Atg26 interaction partner

The virus L-A is a dsRNA totivirus that is frequently found in laboratory strains of *S. cerevisiae*. As shown for other totiviruses, the way of infection is cytoplasmatic transmission from mother to daughter cell or during mating. L-A has a 4.6 kb genome that contains two overlapping genes, *GAG* and *POL*. The first gene encodes for the major coat protein Gag and, with a frequency of 1% to 2%, a -1 ribosomal frameshift event occurs to produce the Gag-Pol fusion protein. Pol is a RNA-dependent RNA polymerase necessary for replication of the virus (Dinman et al., 1991; Icho and Wickner, 1989; Wickner et al., 2013).

In this study, the major coat protein Gag of the L-A virus was identified as an Atg26 interaction partner by MS analysis (chapter 4.7). The high amount of L-A Gag and viral dsRNA in the bound fraction of the GFP-Atg26-TRAP gave clear hints that Atg26 might interact with multimers of Gag or even complete virus-like particles (Figure 4.11A and

## Discussion

B). These findings also showed for the first time that our laboratory strain WCG4a is infected by the virus. The viral dsRNA, co-purified by the GFP-Atg26-TRAP, was reverse-transcribed in cDNA, cloned and sequenced to get further evidence that Gag identified by MS is from the L-A virus and not from other *S. cerevisiae* totiviruses such as L-BC or L-A-lus (Figure 4.11D).

Sequence analysis of this study showed only a few differences to published L-A sequences (Icho and Wickner, 1989): 6 missense mutations in the GAG region cause conserved substitutions of amino acids in the protein sequence (Gag: Ile328Val, Lys383Arg, Gly542Ser and Asn633Ser; Pol: Lys720Arg, Val754Ala). The amino acid substitution Gly542Ser is located near the functional important trench-like active site, where the cap-snatching mechanism occurs (Figure 5.1) (Fujimura and Esteban, 2011; Tang et al., 2005). The residues Tyr150, Asp152, Tyr452, Tyr538 were shown to be essential for attachment of the host RNA to His154 (Fujimura and Esteban, 2011; Tang et al., 2005). However, nothing is known about an involvement of Gly542 in this process. Therefore, it is very likely that the Gly542Ser substitution causes no functional differences to the cap-snatching mechanism described for L-A Gag in previous studies (Fujimura and Esteban, 2011).

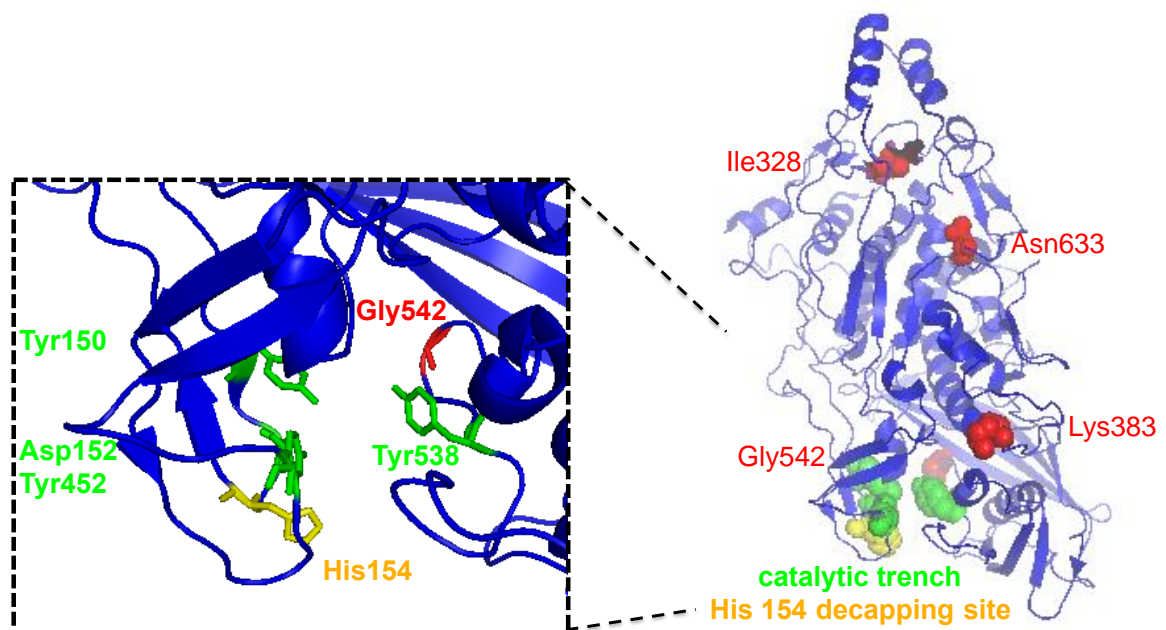


**Figure 5.1 Cartoon representation of L-A Gag (modified from (Tang et al., 2005))**

Amino acids that are substituted in L-A Gag (WCG4a) identified in this study are marked in red.

## Discussion

The amino acid substitutions in the RdRP (Pol) of L-A WCG4a (Lys720Arg, Val754Ala) are located in the region that mediates interaction with the single-stranded (+) transcript for encapsidation. Nevertheless, also in this case, it seems very unlikely that these two conserved mutations lead to a different mechanism of encapsidation shown for (Gag-)Pol in previous studies (Fujimura and Esteban, 2000; Ribas et al., 1994). Furthermore, sequence alignment of L-A Gag with further closely related Gag proteins of *S. cerevisiae* totiviruses (L-BC and L-A-lus) indicate that the identified virus of our laboratory strain WCG4a has a nearly identical sequence to the published L-A Gag and not to other *S. cerevisiae* totiviruses (Figure S1). Therefore, the *S. cerevisiae* totivirus identified in this study can be taxonomically classified as L-A virus.

In addition to the missense mutation, 15 silent mutations were observed by cDNA sequencing. Regarding that the respective virus RNA contains the -1 ribosomal frameshift site, the packaging signal for ssRNA/Pol interaction and the replication site (Figure 2.10) (Icho and Wickner, 1989; Wickner et al., 2013), it was checked whether the mutations are in this critical regions. However, none of these silent mutations are located in the -1 ribosomal frameshift site or in the packaging signal for ssRNA/Pol. The replication site, which is in the extreme 3'-terminal region, was not sequenced in this study. Taken together, despite some sequence differences, the L-A variant identified in WCG4a should have the same properties as L-A analysed in previous studies. Therefore, further basic features of L-A from WCG4a identified in this study were not analysed.

*S. cerevisiae* strains carrying the L-A virus are often also infected by smaller about 2 kb dsRNAs called M satellites or killer viruses, including M1, M2 and M28 (Schmitt and Breinig, 2006; Wickner et al., 2013). Replication of M satellites depends on the presence of the L-A virus in the same cell, since M satellites uses L-A Gag and Gag-Pol for their own separate encapsidation and replication cycle (Fujimura et al., 1990). Therefore, L-A is also called helper virus. M satellites encode the killer toxins (K1, K2 or K28) that are post-translationally processed and secreted from infected cells (killer cells). The killer toxins K1 and K2 are pore-forming proteins that disrupt membrane function of non-infected, sensitive cells and thereby kills them, whereas K28 enters the cell by endocytosis and retrograde transport to block DNA synthesis in the nucleus in non-infected, sensitive cells (Schmitt and Reiter, 2008). M-satellite-infected cells are resistant to respective killer toxins and, therefore, have a selective advantage over non-

infected cells (Rodríguez-Cousiño et al., 2013; Schmitt and Breinig, 2006; Schmitt and Reiter, 2008).

In this study, a further about 2 kb fragment was co-isolated from WCG4a cell lysates using GFP-Atg26-TRAP experiments (Figure 4.11B) or GST-Atg26 (187-569) pull downs (Figure 4.14.1C). Since the dsRNA genomes of killer viruses have a size of about 2 kb, it can be speculated that WCG4a is also infected by a killer virus. However, it is also possible that ssRNA of the L-A virus was co-isolated, since L-A (+) transcripts run faster in agarose gels (Esteban et al., 2008). Gel-purification of the co-isolated 2 kb fragments and following RNase A treatment would be a option in further studies to distinguish dsRNA and ssRNA, since dsRNA is RNase A resistant (Edskes et al., 1998). As a further control, treatment with RNase III, which specifically degrades dsRNA (Castón et al., 1997), could be tested. Performing killer toxin assays that detect the killer phenotype of killer-virus-infected strains would be a further method to clarify whether WCG4a is a killer strain.

Using cell lysate from the strain BY4741 for GFP-Atg26-TRAP experiments, co-isolation of L-A dsRNA was detectable, but not a 2 kb fragment (Figure 4.12B). This observation would be in agreement with previous reports, which showed that this laboratory strain is infected by L-A, but not by killer viruses (Rodríguez-Cousiño et al., 2013).

### **5.5 The PH domain (187-337) and an undefined region (338-569) mediate Gag binding of Atg26**

Investigation of this study showed that the PH domain (187-337) and an undefined region (338-569) of Atg26 mediate the interaction with L-A Gag. It was demonstrated that both domains bind Gag independently of each other and combination of both regions (187-569) led to a additive affinity to L-A Gag (summarized in Figure 4.13F). However, it was not possible to get clear evidence for a direct interaction, since the results of the split-ubiquitin assay were inconsistent and the interaction shown by a direct pull down assay was weak (Figure 4.15). It is possible that the chosen protein tags, the puffer conditions or the conditions for recombinant protein expression are not optimal for validation of the Gag-Atg26 interaction via direct pull down assay. Therefore, these parameters have to be tested in further studies.

PH domains are well known for their ability to specifically interact with phosphoinositides for membrane targeting (Lemmon, 2008). However, Yu et al. (2004)

## Discussion

demonstrated by analyses of 33 yeast PH domains that only one third of these domains has this property (Yu et al., 2004). The PH domain of Atg26 was categorized as a unspecific phosphoinositide binder, since it had very weak affinities to phosphoinositides and this domain alone was not capable of membrane targeting (Yu et al., 2004).

Two independent phosphoinositide-binding motifs are known for PH domains that both are in the  $\beta 1/\beta 2$  loop between the first two  $\beta$ -strands of the overall 7-stranded  $\beta$ -sandwich structure. The first binding site contains the motif  $KX_n(K/R)XR$ , whereas the second binding site shares a  $(K/R)X(Y/W)$  motif (Anand et al., 2012). However, sequence analyses revealed that the PH domain of *S. cerevisiae* Atg26 and orthologs contain none of these two phosphoinositide-binding motifs (Figure 5.2) (Lemmon, 2004). Consequently, it can be speculated that the PH domain of Atg26 is not capable of membrane targeting. Nonetheless, this issue has to be tested in further studies by analysing membrane association.

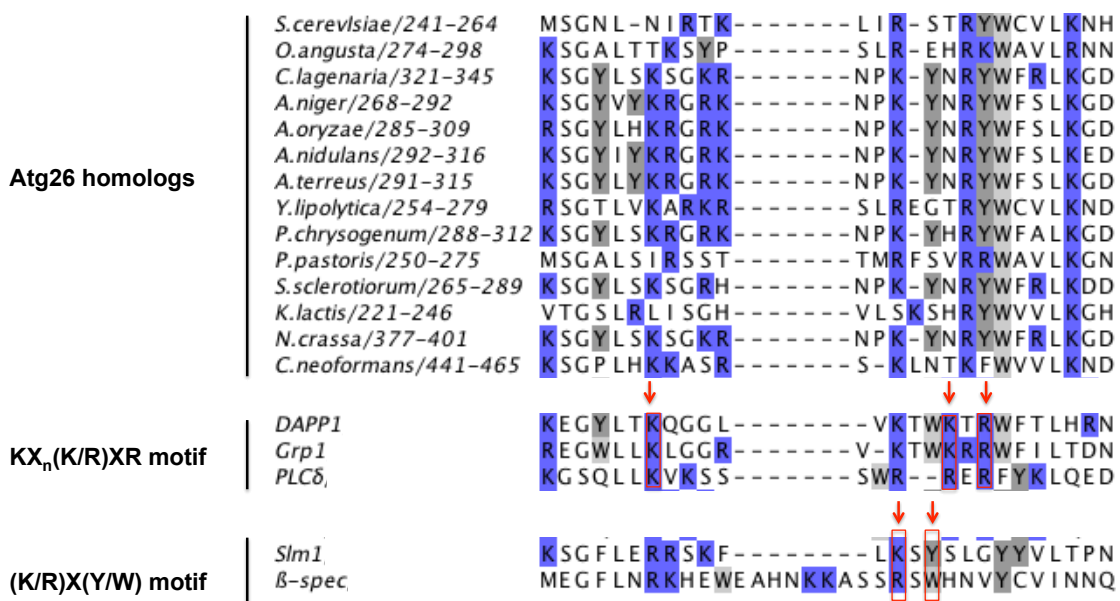


**Figure 5.2** Sequence alignments of Atg26 homologs with regions of known phosphoinositide-binding motifs in PH domains (K/R=blue; Y/W=grey; arrowheads show sequence motif)

Based on the experiments of this study, it can be hypothesised that Atg26 (187-569) interacts with Gag independently of any membrane association, since all GFP-Atg26-TRAPs were performed with the soluble phase of Triton-100-treated cell lysates (chapter 4.7 and 4.8).

In previous reports, the ability of membrane targeting was tested for the PH domain of

*PpAtg26* in *Pichia pastoris* (Oku et al., 2003; Yamashita et al., 2006). It was shown by membrane association experiments that *PpAtg26* sedimented in the detergent (Triton-100)-resistant fraction (100.000 g pellet, P100). In addition, it was demonstrated that this detergent-insolubility depends on its PH domain and not on the other domains (Oku et al., 2003). This observations led the authors to the conclusion that the PH domain mediates interaction with detergent-insoluble lipid rafts (Oku et al., 2003; Yamashita et al., 2006). However, it is possible that also the PH domain of *PpAtg26* mediates interaction with high-molecular weight complexes that reside in the detergent-resistant P100 fraction. There is no knowledge available about viruses in *P. pastoris*. Therefore, it would be highly speculative that the PH domain of *PpAtg26* might be involved in VLP binding also in this model organism. In this study, no subcellular fractionation analyses for *ScAtg26* and L-A Gag were performed. Nonetheless, previous studies detected the L-A VLPs in the P100 fraction (Fujimura and Esteban, 2000; Fujimura et al., 1992a). Therefore, it can be speculated that also *ScAtg26* co-fractionates PH-domain-dependently with L-A VLPs.

In this study, the region 187-337 in *ScAtg26* was chosen for analysis of the PH domain in interaction studies. However, it has to be considered that SMART predicts a truncated GRAM domain for the first 40-50 amino acids of this region (187 to about 235) ([smart.embl-heidelberg.de](http://smart.embl-heidelberg.de)). It is unclear whether this short fragment is necessary for the Atg26-Gag interaction or capable of membrane binding. Therefore, it would be interesting to analyse in further binding studies whether the PH domain without this short N-terminal region still interacts with Gag.

### 5.6 Identification of virus-related Atg26 interaction partners

The PH domain (187-337) and an undefined region of Atg26 (338-569) were shown to mediate the interaction with L-A Gag (Figure 4.13 and 4.14). In a pull down approach, recombinantly expressed GST-Atg26 187-569 was used as bait to identify further components that associate with the Atg26/Gag complex. Co-purification of high amounts of L-A virus-like particles by GST-Atg26 187-569 was shown by immunoblotting and EtBr staining of agarose gels and further validated that Atg26 (187-569) interacts with the L-A virus (Figure 4.14.1). Many additional bands were detectable by CBB staining of the bound fraction using GST-Atg26 (187-569) as bait. Only distinct bands with a higher molecular weight than GST-Atg26 were chosen for MS analysis to avoid detection of

## Discussion

degradation products of the bait (Figure 4.14.2).

Interestingly, the 5' exonuclease **Xrn1/Kem1**, specific for uncapped RNA, was identified by MS analysis as putative component of the Atg26/Gag complex. Previous reports have shown that deletion of *XRN1* leads to increase of the L-A virus level, whereas overexpression can be used to eliminate the virus (Esteban et al., 2008). It was proposed that the viral cap-snatching mechanism, which transfers the cap from host RNA to the viral RNA, is not completely efficient and, thus, uncapped viral (+) transcripts become rapidly degraded by Xrn1 (Kenna et al., 1993; Masison et al., 1995; Wickner et al., 2013). Based on the MS analysis of this study, it can be hypothesised that Xrn1 directly associates with L-A VLPs to down-regulate uncapped viral (+) transcript before the viral cap-snatching mechanism occurs. A L-A virus-independent interaction between Xrn1 and Atg26 seems unlikely. However, further binding studies are necessary to validate Xrn1 as an interaction partner and to analyse how Xrn1 is associated with the Atg26/Gag complex.

A further interesting candidate identified by MS analysis was the **eIF2 $\alpha$  kinase Gcn2** that regulates translation and induces autophagy in response to amino acid starvation (Carroll et al., 2014). Amino acid depletion causes accumulation of uncharged transfer RNAs that activate the Gcn2 kinase activity by interaction. Activated Gcn2 regulates the downstream cascade of the general control of nutrients (GCN) pathway (Abeliovich, 2014; Dever et al., 1992). In this pathway, activated Gcn2 phosphorylates eukaryotic initiation factor 2 $\alpha$  (eIF2 $\alpha$ ) that leads to translation of the transcription factor Gcn4. This transcription factor activates genes required for amino acid biosynthesis and autophagy (Ecker et al., 2010). Interestingly, it was demonstrated for mammalian cells that GCN2 also becomes activated by virus infection and, thereby, is an important factor in antiviral stress response (Berlanga et al., 2006; del Pino et al., 2012). Furthermore, it was shown by *in vitro* studies that viral RNA increases the GCN2 kinase activity, suggesting that GCN2 senses RNA viruses to induce host defence (Berlanga et al., 2006; del Pino et al., 2012; He et al., 2014). Regarding the MS analysis in this study, it can be speculated that Gcn2 might also be involved in antiviral response in yeast cells. However, preliminary binding studies are necessary to validate Gcn2 as a putative component of the Atg26/Gag complex.

### 5.7 Atg26 is involved in selective autophagy of L-A Gag

Recently, Suzuki et al (2011) published that the VLPs of the retrotransposon Ty1 are degraded by selective autophagy to down-regulate transposition. In this pathway, the Cvt receptor Atg19 binds Ty1 VLPs and recruits them to the Ape1 complex for autophagic degradation (Suzuki et al., 2011).

#### 5.7.1 GFP-tagged Gag as a tool to measure autophagy of the L-A virus

##### 5.7.1.1 Analysis of GFP- and mCherry-tagged Gag in binding studies

In this study, it was shown that Atg26 interacts with VLPs of the L-A virus (chapter 4.7 and 4.8). In addition, Atg26 was shown to bind Atg8 via its canonical C-terminal AIM and that this sequence is functionally involved in PAS localisation of Atg26 and its autophagic transport to the vacuole (chapter 4.4-4.6). This link between the L-A virus and autophagy raised the question whether L-A VLPs are also degraded by autophagy, such as Ty1 VLPs, and how Atg26 might be involved in this process. Therefore, a method had to be established to further characterize the Atg26/Gag interaction and to measure autophagy of the L-A virus. In this study, *GAG* and *GAGPOL* cDNA was generated and cloned in GFP and mCherry vectors.

Binding studies using GFP- and RFP-TRAP revealed that tagged Gag or GagPol still interact with Atg26, similar to endogenous L-A Gag (Figure 4.16). However, no endogenous Gag or dsRNA was detectable when tagged Gag was expressed in the cell. This observation is in line with previous studies, demonstrating that even expression of untagged virus cDNA is capable of endogenous virus exclusion (Valle et al., 1993). However, the reason for this interference of the endogenous virus propagation remained unclear.

Structure analyses revealed that the N- and the C-terminal domains are exposed inside the viral coat (Naitow et al., 2002; Tang et al., 2005). Therefore, it can be speculated that the GFP- or mCherry tagged Gag constructs used in the present study cause sterical hindrance during encapsidation of endogenous viral (+) transcripts and thereby block the replication cycle. It was initially hypothesized that expression of the GFP-GagPol construct, which expresses GFP-Gag and GFP-GagPol, overcomes the block of the endogenous virus, since the Pol fusion part should also be able to bind and incorporate the (+) transcript. However, expression of this construct also blocks the propagation of the endogenous virus (Figure 4.16C and D).



## Discussion

Previous studies showed that the N-terminus of Gag is acetylated by the N-acetyltransferase complex, including Mak3, Mak10 and Mak31 encoded by the host genome. Mak3 recognises the four N-terminal amino acids of Gag and catalyses acetylation of the start methionine. It was shown that deletion of *MAK3* avoids Gag assembly and that unpackaged Gag is highly unstable (Tercero and Wickner, 1992; Tercero et al., 1993). In the present study, complex formation of mCherry-Gag and GFP-Gag was analysed in GFP-TRAP experiments to test self-assembly of tagged Gag. Although both fusion proteins should not be able to become acetylated by Mak3, however, using GFP-Gag as a bait, it was possible to co-isolate mCherry-Gag (Figure 4.17A). Thus, it can be concluded that N-terminal tagged Gag is able to self-assemble and is stable. But, it remains unclear whether these constructs form complete (120-meric) VLPs.

C-terminally GFP-tagged Gag that ought to become acetylated was not analysed by binding studies, but also blocks propagation of the endogenous virus (not shown). However, previous studies demonstrated that a C-terminally GFP-tagged Gag forms stable VLPs in yeast (Powilleit et al., 2007). Nonetheless, further binding studies are required to test whether the Gag-GFP construct used here is able to self-assemble in the cell. Using the Gag-GFP construct as bait for co-isolation of mCherry-Gag in GFP-TRAP experiments would be a method to analyse this issue. Furthermore, comparing all tagged versions of Gag used in the present study with endogenous Gag in gel filtration experiments would be helpful to get clear evidence that these constructs are able to form complete VLPs.

### 5.7.1.2 Fluorescence microscopic analysis of GFP and mCherry-tagged Gag

It was shown by IEM of immunogold-labelled Gag that VLPs are located in the cytosol and that the L-A replication cycle also occurs there (Dihanich et al., 1989; Wickner et al., 2013). Less is known about the detailed cytosolic localisation of L-A, since there are no detailed fluorescence microscopy analyses or more recent IEM studies of L-A VLPs available. However, Nolan et al. (2006) generated a GFP-tagged Gag-Pol construct, where GFP was inserted into an external loop of Gag. Since L-A VLPs diffuse through fusion pores during mating and have a defined size of about 40 nm, the authors used the Gag-Pol-GFP constructs to analyse the expansion of fusion pores (Nolan et al., 2006). Fluorescence microscopy showed a diffuse cytosolic signal and dot-like structures,

## Discussion

where about half of the dots were mobile (Nolan et al., 2006). However, the cytosolic localisation of this construct and the ability to form complete VLPs was not further characterized (Nolan et al., 2006). In the present study, fluorescence microscopic analyses also revealed that expression of the GFP-Gag(Pol) and mCherry-Gag constructs leads to formation of highly mobile and fixed cytosolic dots in the cell (Figure 4.17 C and D). Unfortunately, the required exposure time in combination with the needed switch between the channels was too long for detection of colocalisation of mobile GFP-Gag and mCherry dots. Formaldehyde-fixation of respective cells would be a possibility to determine the exact colocalisation rate of mCherry-Gag and GFP-Gag in further studies. However, less mobile or fixed dots showed a clear colocalisation of GFP-Gag and mCherry-Gag (Figure 4.17C). Dot formation of GFP-tagged Gag(Pol) and colocalisation with mCherry-Gag might be a further hint that the analysed tagged Gag constructs are able to self-assemble. As mentioned before, it remains unclear and has to be investigated in further experiments whether the N-terminally tagged Gag constructs form complete VLPs. Based on the microscopic analyses in this study, it is also possible to exclude that mCherry- and GFP-Gag aggregate as misfolded proteins in deposition sites, since the majority of the dots were highly mobile (Figure 4.17C and D).

Fluorescence microscopy of cells expressing the C-terminally GFP-tagged Gag construct showed larger dots that were often less mobile (Figure 4.17E). Previous reports showed that VLPs of the Ty1 retroelement form cluster in distinct cytosolic foci that might be necessary for VLP assembly (Checkley et al., 2013; Checkley et al., 2010). Therefore, it can be speculated that Gag-GFP is capable of self-assembly and might form enlarged VLP clusters at distinct loci. However, it can also be hypothesised that L-A Gag-GFP accumulates into deposition sites for misfolded proteins. In further investigations, using fluorescence marker for subcellular compartments would be an option to determine the localisation of these enlarged dots formed by Gag-GFP.

Taken together, the GFP-tagged L-A Gag versions analysed in this study bind Atg26 and are able to self-assemble, shown by binding studies and fluorescence microscopy. But, it seems that these constructs are not able to incorporate viral (+) transcripts during encapsidation and might thereby block proliferation of the endogenous L-A virus. Nonetheless, these data indicate that the GFP-tagged Gag constructs have similar features as endogenous Gag.

### 5.7.1.3 Detection of autophagic processing of GFP-tagged Gag(Pol)

Using the vacuolar degradation assay, the GFP-tagged constructs were tested as putative tools to measure autophagic processing of L-A Gag during nitrogen starvation. Under different expression levels, all tested constructs showed that GFP-tagged Gag is transported to the vacuole by autophagy leading to its processing and accumulation of free GFP (Figure 4.18). However, as discussed above (chapter 5.7.1.1 and 5.7.1.2), it is not clear whether complete VLPs, formed by GFP-tagged Gag, are degraded by this mechanism.

Furthermore, it was shown that Atg26, whose function was unknown so far, is involved in autophagic degradation of GFP-tagged Gag, indicated by a 50% reduction of GFP-Gag processing in *atg26Δ* cells. This observation gave a hint that GFP-tagged Gag is degraded by a selective mechanism.

### 5.7.2 Selective autophagy of L-A Gag

Proteins of the autophagic core machinery are necessary for unselective, bulk autophagy and selective autophagy. Recognition of specific cargos and its recruitment to the phagophore are additional features of selective autophagic pathways. Therefore, further proteins are necessary. For example, the Cvt pathway needs the selective receptor Atg19, the selective adaptor Atg11, the PROPPIN Atg21 and further components in addition to the autophagic core machinery (Lynch-Day and Klionsky, 2010; Nair et al., 2010; Shintani et al., 2002; Yorimitsu and Klionsky, 2005). Mitophagy and pexophagy are further receptor-mediated selective pathways that also need the adapter Atg11, the specific receptors, Atg32 or Atg36 (*PpAtg30*), and further components (Kanki et al., 2009; Motley et al., 2012; Okamoto et al., 2009). For ribophagy, it is unknown whether a selective receptor is involved (Kraft and Peter, 2008; Kraft et al., 2008). However, this process is defined as a selective pathway, since ribosomes are faster degraded by autophagy than other cytosolic components. Furthermore, the ubiquitin ligase Rsp5 and the ubiquitin protease Ubp3/Bre5, which are not required for bulk autophagy, were shown to be involved in this process (Kraft and Peter, 2008; Kraft et al., 2008). The two kinds of ER-phagy, induced by ER-stress or starvation, are further selective pathways. The involvement of Atg11, Atg19, Atg20 and the actin cytoskeleton indicates that ER-phagy is an selective pathway (Bernales et al., 2006a; Cebollero et al., 2012b; Hamasaki et al., 2005; Lipatova et al., 2013; Mazon et al., 2007). Microautophagic pathways in

## Discussion

yeast, such as PMN and lipophagy in *S. cerevisiae*, or micropexophagy in *Pichia pastoris*, also involve the autophagic core proteins. Furthermore, these pathways require the vacuolar membrane protein Vac8 and further regulators that are not involved in bulk macroautophagy (Krick et al., 2008b; Oku et al., 2006; van Zutphen et al., 2014).

In the present study, it was shown that the autophagic core proteins Atg1, Atg8 and Atg18 are involved in degradation of GFP-Gag(Pol) (Figure 4.19A), indicating an canonical autophagic mechanism. The requirement of proteinase A (Pep4) indicates that degradation of GFP-Gag(Pol) occurs in the vacuole, further supporting that this process is mediated by canonical autophagy. The involvement of the proteins Atg26, Atg11, Atg21 and Hsv2, which are not essential for unselective autophagy (Cheong et al., 2008; Kim et al., 2001; Krick et al., 2008a; Meiling-Wesse et al., 2004; Stromhaug et al., 2004), indicate a selective autophagic mechanism (Figure 4.19A, B and D). Furthermore, it was experimentally excluded in this study that known receptor-mediated selective pathways are involved in degradation of GFP-Gag(Pol) by showing that the Cvt receptors, Atg19 and Atg34 (Shintani et al., 2002; Suzuki et al., 2010), the mitophagy receptor Atg32 (Kanki et al., 2009; Okamoto et al., 2009) and the pexophagy receptor Atg36 (Motley et al., 2012) do not mediate this process (Figure 4.19C and D). Suzuki et al. (2010) revealed that Atg19 also mediates autophagy of VLPs of the Ty1 retroelement during starvation (Suzuki et al., 2011). Regarding that the L-A virus has similar features as Ty1 retroelements, it was initially proposed that Atg19 might also mediate degradation of L-A Gag. However, in this study, it was clearly shown that L-A Gag is degraded by a different autophagic mechanism than Ty1 Gag.

Based on the genetic dissection in this study, it cannot be excluded that GFP-Gag is degraded by microautophagy (Figure 4.19). The PROPPINs Atg21 and Hsv2 were shown to be involved in the microautophagic pathway PMN. Deletion of *ATG21* caused a severe reduction of PMN and deletion of *HSV2* caused a milder phenotype (Krick et al., 2008a). Both proteins are involved in autophagy of GFP-Gag to the same extent (Figure 4.19B). In *P. pastoris*, *PpAtg26* mediates MIPA formation during micropexophagy (Oku et al., 2003; Yamashita et al., 2007). Therefore, *ScAtg26* might have also a microautophagy-related function in *S. cerevisiae*. However, so far, no MIPA-like structure was observed in *S. cerevisiae*. Moreover, fluorescence microscopy of GFP-Atg26 showed no comparable structure (Figure 4.10). Nonetheless, further analyses are necessary to get clear evidence whether macro- or microautophagy mediates degradation of GFP-Gag.

## Discussion

Regarding that Vac8 is a proposed adaptor for microautophagy, it would be an option to test whether Vac8 also mediates autophagic processing of GFP-Gag(Pol). Furthermore, IEM would be a possibility to morphologically distinguish macroautophagy and microautophagy of (immunogold-labelled) L-A VLPs.

Interestingly, previous studies showed that the occurrence of killer viruses (the L-A virus in combination with M satellites) in *S. cerevisiae* and other yeast species might be linked to the lack of RNA interference (RNAi) mechanisms in these species (Drinnenberg et al., 2011). During evolution, *S. cerevisiae* had lost the RNA interference (RNAi) pathway (Nicolás et al., 2013). The RNAi pathway involves the ribonuclease III Dicer that digests dsRNA into small interfering (si)RNAs. Argonaute, a further endonuclease of RNAi, recognises the small RNA and carries it to the specific transcript to cleave it. RNAi is involved in post-transcriptional repression of endogenous genes and heterochromatin formation. Furthermore, it is a defence mechanism against transposable elements and viruses (Billmyre et al., 2013; Nicolás et al., 2013). The RNAi pathway is highly conserved among eukaryotes with the exception of *S. cerevisiae* and other budding yeast species known to have dsRNA killer viruses. Loss of RNAi in *S. cerevisiae* is explainable by the incompatibility of RNAi and dsRNA viruses, including helper viruses and killer viruses. Therefore, the selective advantage caused by the killer phenotype seemed to be evolutionary more important than RNAi as defence mechanism against invasive nucleic acids (Drinnenberg et al., 2011; Drinnenberg et al., 2009). However, loss of RNAi must be compensated by alternative mechanisms to regulate retrotransposons and viruses. Recently, Suzuki et al. (2011) showed that transposition of the Ty1 retroelement during starvation is regulated by a selective, Atg19-dependent autophagic mechanism (Suzuki et al., 2011). In the present study, it was demonstrated for the first time that L-A Gag is degraded by autophagy under nutrient depletion. This would be a further regulatory mechanism against the virus, in addition to the antiviral activity of Xrn1 and other proteins. This autophagic mechanism might not have the function to eliminate the L-A virus, since this would also remove the beneficial killer system, but rather could be used to generate further amino acid resources by degradation of these large 120-meric L-A VLPs under starvation.

### 5.7.3 Proposed function of Atg26

In the present study, an involvement of Atg26 in autophagy was confirmed by showing five features typical for autophagic proteins: First, Atg26 interacts with Atg8 via an AIM (chapter 4.4), equivalent to selective receptors and the core proteins Atg1, Atg3 and Atg12 (Farré et al., 2013; Kaufmann et al., 2014; Kraft et al., 2012; Nakatogawa et al., 2012b; Noda et al., 2008; Pfaffenwimmer et al., 2014; Suzuki et al., 2010; Yamaguchi et al., 2010). Second, Atg26 locates at the PAS (chapter 4.6), where most of the Atgs at least transiently locate (Feng et al., 2013; Suzuki et al., 2007). Third, Atg26 is AIM-dependently transported to the vacuole by autophagy (chapter 4.5), as shown for most of the selective receptors and Atg1 (Kraft et al., 2012; Shintani et al., 2002; Suzuki et al., 2010). Fourth, overexpression of Atg26 leads to a decrease in Ape1 maturation in an AIM-dependent manner. This suggests an inhibitory effect on the Cvt pathway by competing with other Atg8 binders (chapter 4.5). Fifth, Atg26 is involved in selective autophagy of GFP-tagged L-A Gag (chapter 4.10 and 4.10).

In further experiments of this study, it was demonstrated that Atg26 interacts with L-A Gag via its PH domain and a further region (chapter 4.7 and 4.8). Furthermore, binding studies showed that known selective receptors are not involved in the Atg26/Gag interaction (Figure 4.20A). The fact that Atg26 is involved in selective autophagy of Gag and, in addition, physically linked to this cargo leads to the hypotheses that Atg26 might act as a selective receptor in this autophagic process. Regarding all known selective receptors in yeast, Atg26 and the Cvt receptors Atg19 and Atg34 seem to have the most features in common, since these receptor proteins are physically linked to a cytosolic cargo. Furthermore, all cargos, including prApe1, Ams1, Ty1 Gag (cargos of Atg19 and/or Atg34) and L-A Gag (interactor of Atg26) self-assemble to homo-multimeric complexes (Brookman et al., 1995; Hutchins and Klionsky, 2001; Kim et al., 1997; Tang et al., 2005; Watanabe et al., 2009). However, it is still unclear whether Atg26 directly interacts with L-A Gag or further components are involved. It can also be speculated that post-translational modifications regulate this interaction. For example, previous reports showed that ubiquitylation and deubiquitylation may play a role in ribophagy (Cebollero et al., 2012b; Kraft et al., 2008). In fact, especially in mammalian cells, ubiquitylation of cargos is often necessary for their recognition by the selective receptors (Stolz et al., 2014). Interestingly, it was shown for xenophagy in mammals that ubiquitylated *Salmonella enterica*, as bacterial cargo, is recognized by the selective receptors p62,

## Discussion

optineurin and NDP52 (Stolz et al., 2014; Thurston et al., 2009; Wild et al., 2011), whereas virus capsids (HIV-1, Sindbis Virus) might be ubiquitin-independently recognized by TRIM5 $\alpha$  and p62 (Mandell et al., 2014; Orvedahl et al., 2010; Sumpter and Levine, 2011). However, it remains unclear whether ubiquitylation plays a role for complex formation of Atg26 and L-A. Therefore, further experiments are necessary to answer whether ubiquitylation or other post-translational modifications are involved in complex formation of Atg26 and L-A Gag, and its relevance for autophagy of L-A Gag.

Interestingly, MS analysis of this study (Figure 4.14.2) showed that the serine/threonine kinase Gcn2 was co-isolated using GST-Atg26 (187-569) as a bait in a pull down assay. It can be speculated that the kinase activity of Gcn2 regulates the Atg26-Gag interaction or autophagic degradation of the virus. However, as mentioned before, Gcn2 has to be validated preliminary as an Atg26 or L-A Gag interactor in further binding studies.

The two regions in Atg26, including the PH domain (187-337) and an undefined region (338-569), were shown to bind L-A Gag independent of each other. Therefore, it can also be speculated that Atg26 is able to link L-A VLPs leading to clustering before its autophagic transport to the vacuole. Comparing wt and *atg26 $\Delta$*  cells expressing GFP-tagged Gag by fluorescence microscopy would be an option to analyse whether the presence of Atg26 leads to clustering of GFP-tagged Gag (VLPs) in the cell. Gel filtration experiments, comparing endogenous L-A Gag of wt and *atg26 $\Delta$*  cells, would be a further method to test whether Atg26 is capable of linking L-A VLPs, leading to a molecular weight shift.

Atg26 further shares with the selective receptors Atg19 and Atg34 that they all have a canonical AIM at the C-terminal region (chapter 4.4) (Noda et al., 2008; Suzuki et al., 2010), whereas the AIMs in the organellophagy receptors Atg32, Atg36 and *PpAtg30* are at other positions (Farré et al., 2013; Okamoto et al., 2009). However, the presence of an AIM in Atg26 does not confirm its function as an selective receptor, since there are many example in yeast (Atg1, Atg3 and Atg12) and especially in mammals that AIM-containing proteins often have other functions (Birgisdottir et al., 2013; Kraft et al., 2012; Yamaguchi et al., 2010). But, the experiments of the present study also suggest that Atg26 might be involved in recruitment of L-A Gag to the phagophore, since deletion of the C-terminal AIM in Atg26 decreases autophagy of GFP-Gag(Pol) (Figure 4.21). This would be in agreement with the function of AIMs in other selective receptors, since deletion or mutation of their AIMs also causes a reduction of the respective selective

## Discussion

autophagic pathways (Farré et al., 2013; Kondo-Okamoto et al., 2012; Noda et al., 2008; Suzuki et al., 2010).

In this study, it was shown that Atg26 interacts with the adaptor for selective autophagy Atg11 (Figure 4.20C), further supporting a putative receptor function of Atg26, since all known receptors are Atg11 binders (Farré et al., 2013; Okamoto et al., 2009; Shintani et al., 2002; Suzuki et al., 2010). However, it remains unclear whether the detected Atg26/Atg11 interaction is direct, which is also a common feature of all known selective receptors. Therefore, further binding studies, such as direct pull down assays, are necessary to get clear evidence for a direct interaction. It could also be speculated that Atg26 has similar Atg11-binding sequences as known selective receptors (Farré et al., 2013; Kondo-Okamoto et al., 2012; Pfaffenwimmer et al., 2014). As shown for the AIM in Atg26 in this study (chapter 4.4), by using bioinformatics, it might be possible to predict a putative sequence motif. Further binding studies then are necessary to map and validate this sequence.

Experiments in this study demonstrated that, also in the absence of L-A Gag, GFP-Atg26 locates at the PAS (not shown) and is transported to the vacuole by autophagy (Figure 4.20D). Therefore, it is possible that the autophagic function of Atg26 does not only depend on the interaction with the L-A virus or its presents in general. In previous reports, the selective receptor Atg34 was shown to be delivered to the vacuole also in the absence of its cargo Ams1 (Suzuki et al., 2010). In this context, the authors speculated that Atg34 might be a receptor for further unknown cargos (Suzuki et al., 2010). Therefore, based on the speculation that Atg26 might have a receptor function, it can be further proposed that there might exist further so far unknown cargos that are recruited to the phagophore (or other Atg8-positive membranes) by Atg26. Regarding that Atg26 is a large protein and thereby might have many binding partner, it could be possible that Atg26 link further proteins/cargos to the autophagic machinery. Further detailed MS analysis using Atg26 as bait for pull down assays or CoIPs would be an option to identify further interactors.

Considering that deletion of *ATG26* does not cause complete block of L-A Gag autophagy, there might exist further proteins that recruit L-A Gag to the phagophore. Since autophagy of Gag was induced by starvation in this study, it might be also possible that a portion of GFP-Gag becomes randomly degraded by unselective, bulk autophagy. It can be further hypothesized that the kind of autophagy for L-A Gag degradation depends on



## Discussion

the (self-)assembly state of (GFP-)Gag (monomeric, oligomeric, or complete VLPs). In this context, it would be interesting to analyse whether GFP-Gag mutants that are unable to self-assemble become degraded by unselective, bulk autophagy or by Atg26-dependent selective autophagy.

In this study, an AIM was mapped at the C-terminus of Atg26 and the region 187-569, including a PH domain and an undefined region, was determined to mediate interaction with L-A Gag (chapter 4.4 and 4.8). However, the function of the catalytic domain of Atg26 (UDPGT) remains an open question. It would be very interesting to determine whether production of sterol glycosides plays a role in autophagy of Gag. Therefore, a glycosyltransferase-dead mutant of Atg26 has to be generated and analysed in further studies.

Furthermore, it remains unclear whether the PH and/or the GRAM domain mediate phosphoinositide-dependent membrane association and how putative membrane association may be involved in autophagy of L-A Gag. Subcellular fractionation or microscopic analyses of truncated versions of Atg26 could be used to investigate these issues.

## 5.8 Conclusion

In this study, it was shown that Atg26 interacts with the autophagic core protein Atg8 and the major coat protein Gag of the L-A virus. Moreover, Atg26 is Atg8-dependently recruited to the phagophore and involved in L-A Gag processing by autophagy.

It can be proposed that Atg26 has the function to recruit L-A Gag or complete L-A VLPs to the phagophore for their selective autophagic degradation.

## 6 Appendix

L-A/1-680	1	MLRFVTKNSQDKSSDLFSICSD---RGT FVAHNRVRTDFKFD---NLVFNRYVG-----VSQKFT
L-A/1-680	1	MLRFVTKNSQDKSSDLFSICSD---RGT FVAHNRVRTDFKFD---NLVFNRYVG-----VSQKFT
L-A-lus/1-680	1	MLRFVTKNSQDKSSDLFSICSD---KGT FVAHNRVRTDFKFD---NLVFNRYVG-----VSQKFT
LB-C/1-697	1	-----MSSLNSLLPEYFKPKTNLNI NSSRVQYGFNARIDMQYEDDSTGRKGRPNAFMSNTVA
L-A/1-680	55	LVGNPTVCFNEGSSYLEGIAKKYLTLDGGLAIDNVLNELRSTCGIPGNAVASHAYNITSWRWYDNHVALL
L-A/1-680	55	LVGNPTVCFNEGSSYLEGIAKKYLTLDGGLAIDNVLNELRSTCGIPGNAVASHAYNITSWRWYDNHVALL
L-A-lus/1-680	55	LVGNPKVCFNEGSSYLEGIAKKYLTLDGGLAIDNVLNELRSTCGIPGNAVASHAYNITSWRWYDNHVALL
LB-C/1-697	60	FIGNYEGIIVDDIPILDGLRADIFDTHGDLDMGLVEDALSKSTMIRRNVPYTYAY-ASELLYKRNLTSLF
L-A/1-680	125	MNMLRAYHLQVLTEQGQYSAGDIPMYHDGHVKI--KL--PVTIDDTAGPTQFAWPSDRSDSYPDWAQFS
L-A/1-680	125	MNMLRAYHLQVLTEQGQYSAGDIPMYHDGHVKI--KL--PVTIDDTAGPTQFAWPSDRSDSYPDWAQFS
L-A-lus/1-680	125	MNMLRAYHLQVLEQGQYSAGSYPMYHDGHVKI--KLDTPISDDE--APDSFKWPSDRTTDTYPDWAQFS
LB-C/1-697	129	YNMLRLYYIKKWGSI-KYEKDAI-FYDNGHACLNRQLFKSRDA-----SLESLSLPE-AEIA
L-A/1-680	191	ESFPSIDVPYLDVRLTVTEVNFVLMMSKWHRRTN-----LAIDYEAPQLADKFA
L-A/1-680	191	ESFPSIDVPYLDVRLTVTEVNFVLMMSKWHRRTN-----LAIDYEAPQLADKFA
L-A-lus/1-680	191	ESFPSIDVPYLDVRLTVTEVNFVLMMSKWHRRTN-----LAIDYEAPALADKFA
LB-C/1-697	186	MLDPGLEFPEEDVPAI L-----WHGRVSSRATCILGQACSEFAPLAPFSLAHYSPQLTRKLF
L-A/1-680	242	YRHALTVDQADEWIEGDRIDDQFRPPSSKVMLSALRKYNHNRLYNQFYTAQQLAQIMMKVPVPCAEGY
L-A/1-680	242	YRHALTVDQADEWIEGDRIDDQFRPPSSKVMLSALRKYNHNRLYNQFYTAQQLAQIMMKVPVPCAEGY
L-A-lus/1-680	242	YRHALTVDQADEWIEGDRIDDQFRPPSSKVMMSALRKYNHNRLYNQFYTAQQLAQIMMKVPVPCAEGY
LB-C/1-697	243	VNAPAGIEPS---SGRYTHEDVK-----DAITILV SANQAYTDFEAYLMLAQLT LVSVPRTAEAS
L-A/1-680	312	AWLMHDALVNI PKFGSVRGRYPFLLSGDAALIQATA---LEDWSAIM---AKPELVFTYAMQVSVALNT
L-A/1-680	312	AWLMHDALVNI PKFGSVRGRYPFLLSGDAALIQATA---LEDWSAIM---AKPELVFTYAMQVSVALNT
L-A-lus/1-680	312	AWLMHDALVNI PKFGSVRGRYPFLLAGDAALIQATA---LEDWSAIM---AKPELIFTYAMQVAVALNT
LB-C/1-697	301	AWFINAGMVNMP T LSCANGYYP-----ALTNVNPYHRLDTWKDTLNHWVAYPDMLFYH----SVAMIE
L-A/1-680	375	GLYLRRVVKRTGFGTTIDDSYEDGAFLQPETFVQ-----AALACCTGQDAPLNGMSDYYVVTYP
L-A/1-680	375	GLYLRRVVKRTGFGTTIDDSYEDGAFLQPETFVQ-----AALACCTGQDAPLNGMSDYYVVTYP
L-A-lus/1-680	375	GLYLRRVVKRTGFGTTVDDSYEDGAFLQPETFVQ-----AAIACCTGQDAPLNGMSDYYVVTYP
LB-C/1-697	360	SCYV---ELGNVARVSDAINKYTFTLSVQGRPVMNRGIIVDLTLVAMRTGREISLPYPVSCGLTRT
L-A/1-680	432	DLLDFDAVTQVPI TVIE---PAGYNI VDDHLL---VVVGVPVACSPYMI FPVAAF--DTANPYCGNF--VI
L-A/1-680	432	DLLDFDAVTQVPI TVIE---PAGYNI VDDHLL---VVVGVPVACSPYMI FPVAAF--DTANPYCGNF--VI
L-A-lus/1-680	432	DLLDFDTITRVPVTVLE---PEGYNIQDGAL---EVTGVPVACSPYMI FPVAAF--DEANPYSGSF--VI
LB-C/1-697	426	DALLQGTETHVPPVVVKDIDMPQYNAIDKDVIEGQETVIKVKQLPAMYPIYTYGINTTEFYSDHFEDQV
L-A/1-680	492	KAANKYLKRG-AVYDKLEAW-KLAWALRVAGYDTHFKVYGDTHGLTKFYADNSDT---WTHI-----PEF
L-A/1-680	492	KAANKYLKRG-AVYDKLEAW-KLAWALRVAGYDTHFKVYGDTHGLTKFYADNSDT---WTHI-----PEF
L-A-lus/1-680	492	KPALKYLKRG-ALYAKLEAW-KLAWAMRIAGYDTEFKACGNTHGLSKFYADNSDS---WTHI-----PEF
LB-C/1-697	496	QVEMAPIDNCKAVFNDARKFSKFM SIMRMMNDVTATDLVTGRKVS N-WADNSGRFLYTDVKYEGQTAPE
L-A/1-680	552	VTDDGVMEV---FVTAIER-----RARHFVLELPRLNSPAFFRSVEVSTTIYDTHVQAGAHA
L-A/1-680	552	VTDDGVMEV---FVTAIER-----RARHFVLELPRLNSPAFFRSVEVSTTIYDTHVQAGAHA
L-A-lus/1-680	552	VSDEEVTEV---YVTNIER-----RARHFVLELPRLNSPAFFKPEVSTAIYDTHVQAGTFS
LB-C/1-697	565	LVDMDTVKARDHCWVSI VDPNGTMNLSYKMTNFRAMAFSR---NKPLYMTGGSVRTIATGNRYDA----
L-A/1-680	605	VYHASRI-----NLD-----YVKPVSTGIQVINAGELKSYWGSVRRTOQGLGVVGLTMP
L-A/1-680	605	VYHASRI-----NLD-----YVKPVSTGIQVINAGELKSYWGSVRRTOQGLGVVGLTMP
L-A-lus/1-680	605	VYHASRI-----NLD-----YVKPVSAIQVINAGELRNWGSVRRTOQGLGVVGLTMP
LB-C/1-697	627	---AERLRAMDETLRLKPKFKITEKLDFRVAAYAI PSLSG---SNMPSLHH-----QEQLQISEVDAE
L-A/1-680	654	AVMPTGEP TAGAAHEELIEQADNVLVE
L-A/1-680	654	AVMPTGEP TAGAAHEELIEQADNVLVE
L-A-lus/1-680	654	AVMPTGERTAGTAHEDLIEQTENVLVE
LB-C/1-697	683	PINPIGE-----DELPPDIE-----

**Figure S1** Sequence alignments of L-A Gag (WCG4a) identified in this study (red, bottom) with published sequences of L-A, L-A-lus and L-BC.

Amino acids that are substituted in L-A Gag (WCG4a) identified in this study are marked in red. Conserved amino acids are shown in blue.

## 7 Bibliography

- Abeliovich, H.** (2014). Regulation of autophagy by amino acid availability in *S. cerevisiae* and mammalian cells. *Amino Acids*.
- Abeliovich, H., Dunn, W., Kim, J. and Klionsky, D.** (2000). Dissection of autophagosome biogenesis into distinct nucleation and expansion steps. *J Cell Biol* **151**, 1025–34.
- Alemu, E. A., Lamark, T., Torgersen, K. M., Birgisdottir, A. B., Larsen, K. B., et al.** (2012). ATG8 family proteins act as scaffolds for assembly of the ULK complex: sequence requirements for LC3-interacting region (LIR) motifs. *Journal of Biological Chemistry* **287**, 39275–39290.
- Amar, N., Lustig, G., Ichimura, Y., Ohsumi, Y. and Elazar, Z.** (2006). Two newly identified sites in the ubiquitin-like protein Atg8 are essential for autophagy. *EMBO Rep* **7**, 635–642.
- Anand, K., Anand, K., Maeda, K., Maeda, K., Gavin, A.-C. and Gavin, A.-C.** (2012). Structural analyses of the Slm1-PH domain demonstrate ligand binding in the non-canonical site. *PLoS ONE* **7**, e36526.
- Ano, Y., Hattori, T., Kato, N. and Sakai, Y.** (2005). Intracellular ATP correlates with mode of pexophagy in *Pichia pastoris*. *Biosci Biotechnol Biochem* **69**, 1527–1533.
- Aoki, Y., Kanki, T., Hirota, Y., Kurihara, Y., Saigusa, T., Uchiumi, T. and Kang, D.** (2011). Phosphorylation of Serine 114 on Atg32 mediates mitophagy. *Mol Biol Cell* **22**, 3206–3217.
- Araki, Y., Ku, W.-C., Akioka, M., May, A. I., Hayashi, Y., et al.** (2013). Atg38 is required for autophagy-specific phosphatidylinositol 3-kinase complex integrity. *J Cell Biol* **203**, 299–313.
- Asakura, M., Ninomiya, S., Sugimoto, M., Oku, M., Yamashita, S. I., Okuno, T., Sakai, Y. and Takano, Y.** (2009). Atg26-Mediated Pexophagy Is Required for Host Invasion by the Plant Pathogenic Fungus *Colletotrichum orbiculare*. *Plant Cell* **21**, 1291–1304.
- Ashford, T. and Porter, K.** (1962). Cytoplasmic components in hepatic cell lysosomes. *J Cell Biol* **12**, 198–202.
- Baba, M., Osumi, M., Scott, S. V., Klionsky, D. J. and Ohsumi, Y.** (1997). Two distinct pathways for targeting proteins from the cytoplasm to the vacuole/lysosome. *J Cell Biol* **139**, 1687–1695.
- Backues, S. K., Orban, D. P., Bernard, A., Singh, K., Cao, Y. and Klionsky, D. J.** (2014). Atg23 and Atg27 act at the early stages of Atg9 trafficking in *S. cerevisiae*. *Traffic* n/a–n/a.
- Barth, H., Meiling-Wesse, K., Epple, U. and Thumm, M.** (2001). Autophagy and the cytoplasm to vacuole targeting pathway both require Aut10p. *FEBS Lett* **508**, 23–28.

## Bibliography

- Barth, H., Meiling-Wesse, K., Epple, U. and Thumm, M.** (2002). Mai1p is essential for maturation of proaminopeptidase I but not for autophagy. *FEBS Lett* **512**, 173–179.
- Beauregard, A., Beauregard, A., Curcio, M. J., Curcio, M. J., Belfort, M. and Belfort, M.** (2008). The take and give between retrotransposable elements and their hosts. *Annu Rev Genet* **42**, 587–617.
- Behrends, C., Sowa, M. E., Gygi, S. P. and Harper, J. W.** (2010). Network organization of the human autophagy system. *Nature* **466**, 68–76.
- Benard, L., Carroll, K., Valle, R. C. and Wickner, R. B.** (1998). Ski6p is a homolog of RNA-processing enzymes that affects translation of non-poly(A) mRNAs and 60S ribosomal subunit biogenesis. *Mol Cell Biol* **18**, 2688–2696.
- Benard, L., Carroll, K., Valle, R. C., Masison, D. C. and Wickner, R. B.** (1999). The ski7 antiviral protein is an EF1-alpha homolog that blocks expression of non-Poly(A) mRNA in *Saccharomyces cerevisiae*. *J Virol* **73**, 2893–2900.
- Berlanga, J. J., Ventoso, I., Harding, H. P., Deng, J., Ron, D., Sonenberg, N., Carrasco, L. and de Haro, C.** (2006). Antiviral effect of the mammalian translation initiation factor 2alpha kinase GCN2 against RNA viruses. *EMBO J* **25**, 1730–1740.
- Bernales, S., McDonald, K. and Walter, P.** (2006a). Autophagy counterbalances endoplasmic reticulum expansion during the unfolded protein response. *PLoS Biol* **4**, e423.
- Bernales, S., Papa, F. and Walter, P.** (2006b). Intracellular signaling by the unfolded protein response. *Annu Rev Cell Dev Biol* **22**, 487–508.
- Billmyre, R. B., Calo, S., Feretzaki, M., Wang, X. and Heitman, J.** (2013). RNAi function, diversity, and loss in the fungal kingdom. *Chromosome Res* **21**, 561–572.
- Birgisdottir, Á. B., Lamark, T. and Johansen, T.** (2013). The LIR motif - crucial for selective autophagy. *J Cell Sci* **126**, 3237–3247.
- Blanc, A., Goyer, C. and Sonenberg, N.** (1992). The coat protein of the yeast double-stranded RNA virus L-A attaches covalently to the cap structure of eukaryotic mRNA. *Mol Cell Biol* **12**, 3390–3398.
- Bockler, S. and Westermann, B.** (2014). Mitochondrial ER contacts are crucial for mitophagy in yeast. *Developmental Cell* **28**, 450–458.
- Brookman, J. L., Stott, A. J., Cheeseman, P. J., Adamson, C. S., Holmes, D., Cole, J. and Burns, N. R.** (1995). Analysis of TYA protein regions necessary for formation of the Ty1 virus-like particle structure. *Virology* **212**, 69–76.
- Budovskaya, Y., Stephan, J., Reggiori, F., Klionsky, D. and Herman, P.** (2004). The Ras/cAMP-dependent protein kinase signaling pathway regulates an early step of the autophagy process in *Saccharomyces cerevisiae*. *J Biol Chem* **279**, 20663–20671.
- Cao, Y. and Klionsky, D. J.** (2007). Atg26 is not involved in autophagy-related pathways

## Bibliography

- in *Saccharomyces cerevisiae*. *Autophagy* **3**, 17–20.
- Carroll, B., Korolchuk, V. I. and Sarkar, S.** (2014). Amino acids and autophagy: cross-talk and co-operation to control cellular homeostasis. *Amino Acids*.
- Castón, J. R., Trus, B. L., Booy, F. P., Wickner, R. B., Wall, J. S., et al.** (1997). Structure of L-A virus: a specialized compartment for the transcription and replication of double-stranded RNA. *J Cell Biol* **138**, 975–985.
- Cebollero, E., der Vaart, van, A., Zhao, M., Rieter, E., Klionsky, D. J., Helms, J. B. and Reggiori, F.** (2012a). Phosphatidylinositol-3-phosphate clearance plays a key role in autophagosome completion. *Curr Biol* **22**, 1545–1553.
- Cebollero, E., Reggiori, F. and Kraft, C.** (2012b). Reticulophagy and ribophagy: regulated degradation of protein production factories. *International Journal of Cell Biology* **2012**, 182834.
- Chan, E. Y. W., Longatti, A., McKnight, N. C. and Tooze, S. A.** (2009). Kinase-inactivated ULK proteins inhibit autophagy via their conserved C-terminal domains using an Atg13-independent mechanism. *Mol Cell Biol* **29**, 157–171.
- Chaturvedi, P., Misra, P. and Tuli, R.** (2011). Sterol Glycosyltransferases—The Enzymes That Modify Sterols. *Appl Biochem Biotechnol* **165**, 47–68.
- Checkley, M. A., Mitchell, J. A., Eizenstat, L. D., Lockett, S. J. and Garfinkel, D. J.** (2013). Ty1 gag enhances the stability and nuclear export of Ty1 mRNA. *Traffic* **14**, 57–69.
- Checkley, M. A., Nagashima, K., Lockett, S. J., Nyswaner, K. M. and Garfinkel, D. J.** (2010). P-body components are required for Ty1 retrotransposition during assembly of retrotransposition-competent virus-like particles. *Mol Cell Biol* **30**, 382–398.
- Cheong, H., Nair, U., Geng, J. and Klionsky, D. J.** (2008). The Atg1 kinase complex is involved in the regulation of protein recruitment to initiate sequestering vesicle formation for nonspecific autophagy in *Saccharomyces cerevisiae*. *Mol Biol Cell* **19**, 668–681.
- Chew, L. H., Setiaputra, D., Klionsky, D. J. and Yip, C. K.** (2013). Structural characterization of the *Saccharomyces cerevisiae* autophagy regulatory complex Atg17-Atg31-Atg29. *Autophagy* **9**.
- Cuervo, A. M. and Wong, E.** (2014). Chaperone-mediated autophagy: roles in disease and aging. *Cell Res* **24**, 92–104.
- Darsow, T., Rieder, S. and Emr, S.** (1997). A multispecificity syntaxin homologue, Vam3p, essential for autophagic and biosynthetic protein transport to the vacuole. *J Cell Biol* **138**, 517–529.
- del Pino, J., Jiménez, J. L., Ventoso, I., Castelló, A., Muñoz-Fernández, M. Á., de Haro, C. and Berlanga, J. J.** (2012). GCN2 has inhibitory effect on human immunodeficiency virus-1 protein synthesis and is cleaved upon viral infection. *PLoS*

## Bibliography

*ONE* 7, e47272.

**Deosaran, E., Larsen, K. B., Hua, R., Sargent, G., Wang, Y., Kim, S., Lamark, T., Jauregui, M., Law, K., Lippincott-Schwartz, J., et al.** (2013). NBR1 acts as an autophagy receptor for peroxisomes. *J Cell Sci* **126**, 939–952.

**der Vaart, van, A., Griffith, J. and Reggiori, F.** (2010). Exit from the Golgi is required for the expansion of the autophagosomal phagophore in yeast *Saccharomyces cerevisiae*. *Mol Biol Cell* **21**, 2270–2284.

**Deter, R. L., Baudhuin, P. and De Duve, C.** (1967). Participation of lysosomes in cellular autophagy induced in rat liver by glucagon. *J Cell Biol* **35**, C11–6.

**Dever, T. E., Feng, L., Wek, R. C., Cigan, A. M., Donahue, T. F. and Hinnebusch, A. G.** (1992). Phosphorylation of initiation factor 2 alpha by protein kinase GCN2 mediates gene-specific translational control of GCN4 in yeast. *Cell* **68**, 585–596.

**Dice, J.** (1990). Peptide sequences that target cytosolic proteins for lysosomal proteolysis. *Trends Biochem Sci* **15**, 305–309.

**Dihanich, M., van Tuinen, E., Lambris, J. D. and Marshallsay, B.** (1989). Accumulation of viruslike particles in a yeast mutant lacking a mitochondrial pore protein. *Mol Cell Biol* **9**, 1100–1108.

**Dinman, J. D., Icho, T. and Wickner, R. B.** (1991). A -1 ribosomal frameshift in a double-stranded RNA virus of yeast forms a gag-pol fusion protein. *Proc Natl Acad Sci USA* **88**, 174–178.

**Dooley, H. C., Tamura, N., Razi, M., Oku, M., Polson, H. E. J., Sakai, Y., Girardin, S. E., Wilson, M. I. and Tooze, S. A.** (2014). WIPI2 Links LC3 Conjugation with PI3P, Autophagosome Formation, and Pathogen Clearance by Recruiting Atg12-5-16L1. *Mol Cell* 1–15.

**Dove, S. K., Dong, K., Kobayashi, T., Williams, F. K. and Michell, R. H.** (2009). Phosphatidylinositol 3,5-bisphosphate and Fab1p/PIKfyve underPPIn endo-lysosome function. *Biochem J* **419**, 1.

**Drinnenberg, I. A., Fink, G. R. and Bartel, D. P.** (2011). Compatibility with killer explains the rise of RNAi-deficient fungi. *Science* **333**, 1592.

**Drinnenberg, I. A., Weinberg, D. E., Xie, K. T., Mower, J. P., Wolfe, K. H., Fink, G. R. and Bartel, D. P.** (2009). RNAi in budding yeast. *Science* **326**, 544–550.

**Dunn, W.** (1990a). Studies on the mechanisms of autophagy: maturation of the autophagic vacuole. *J Cell Biol* **110**, 1935–1945.

**Dunn, W.** (1990b). Studies on the mechanisms of autophagy: formation of the autophagic vacuole. *J Cell Biol* **110**, 1923–1933.

**Ecker, N., Mor, A., Journo, D. and Abeliovich, H.** (2010). Induction of autophagic flux by amino acid deprivation is distinct from nitrogen starvation-induced

## Bibliography

macroautophagy. *Autophagy* **6**.

**Edskes, H. K., Ohtake, Y. and Wickner, R. B.** (1998). Mak21p of *Saccharomyces cerevisiae*, a Homolog of Human CAATT-binding Protein, Is Essential for 60 S Ribosomal Subunit Biogenesis. *Journal of Biological Chemistry* **273**, 28912–28920.

**Epple, U., Eskelinen, E. and Thumm, M.** (2003). Intravacuolar membrane lysis in *Saccharomyces cerevisiae*. Does vacuolar targeting of Cvt17/Aut5p affect its function? *J Biol Chem* **278**, 7810–7821.

**Epple, U., Suriapranata, I., Eskelinen, E. and Thumm, M.** (2001). Aut5/Cvt17p, a Putative Lipase Essential for Disintegration of Autophagic Bodies inside the Vacuole. *J Bacteriol* **183**, 5942–5955.

**Esteban, R., Vega, L. and Fujimura, T.** (2008). 20S RNA narnavirus defies the antiviral activity of SKI1/XRN1 in *Saccharomyces cerevisiae*. *J Biol Chem* **283**, 25812–25820.

**Farré, J.-C., Burkenroad, A., Burnett, S. F. and Subramani, S.** (2013). Phosphorylation of mitophagy and pexophagy receptors coordinates their interaction with Atg8 and Atg11. *EMBO Rep*.

**Farré, J.-C., Krick, R., Subramani, S. and Thumm, M.** (2009). Turnover of organelles by autophagy in yeast. *Curr Opin Cell Biol* **21**, 522–530.

**Farré, J.-C., Manjithaya, R., Mathewson, R. D. and Subramani, S.** (2008). PpAtg30 tags peroxisomes for turnover by selective autophagy. *Dev Cell* **14**, 365–376.

**Farré, J.-C., Vidal, J. and Subramani, S.** (2007). A cytoplasm to vacuole targeting pathway in *P. pastoris*. *Autophagy* **3**, 230–234.

**Feng, Y., He, D., Yao, Z. and Klionsky, D. J.** (2013). The machinery of macroautophagy. *Cell Res* **24**, 24–41.

**Fujimura, T. and Esteban, R.** (2000). Recognition of RNA encapsidation signal by the yeast L-A double-stranded RNA virus. *J Biol Chem* **275**, 37118–37126.

**Fujimura, T. and Esteban, R.** (2013). Cap snatching in yeast L-BC double-stranded RNA totivirus. *Journal of Biological Chemistry* **288**, 23716–23724.

**Fujimura, T. and Esteban, R.** (2011). Cap-snatching mechanism in yeast L-A double-stranded RNA virus. *Proc Natl Acad Sci U S A* **108**, 17667–17671.

**Fujimura, T. and Wickner, R. B.** (1988). Replicase of L-A virus-like particles of *Saccharomyces cerevisiae*. In vitro conversion of exogenous L-A and M1 single-stranded RNAs to double-stranded form. *J Biol Chem* **263**, 454–460.

**Fujimura, T., Esteban, R., Esteban, L. M. and Wickner, R. B.** (1990). Portable encapsidation signal of the L-A double-stranded RNA virus of *S. cerevisiae*. *Cell* **62**, 819–828.

**Fujimura, T. and Wickner, R. B.** (1992a). Interaction of two cis sites with the RNA replicase of the yeast L-A virus. *J Biol Chem* **267**, 2708–2713.

## Bibliography

- Fujimura, T., Ribas, J. C., Makhov, A. M. and Wickner, R. B.** (1992b). Pol of gag-pol fusion protein required for encapsidation of viral RNA of yeast L-A virus. *Nature* **359**, 746–749.
- Fujioka, Y., Noda, N. N., Nakatogawa, H., Ohsumi, Y. and Inagaki, F.** (2010). Dimeric coiled-coil structure of *Saccharomyces cerevisiae* Atg16 and its functional significance in autophagy. *Journal of Biological Chemistry* **285**, 1508–1515.
- Fujioka, Y., Suzuki, S. W., Yamamoto, H., Kondo-Kakuta, C., Kimura, Y., Hirano, H., Akada, R., Inagaki, F., Ohsumi, Y. and Noda, N. N.** (2014). nsmb.2822(1). *Nat Struct Mol Biol* **21**, 513–521.
- Gabriely, G., Kama, R. and Gerst, J. E.** (2007). Involvement of specific COPI subunits in protein sorting from the late endosome to the vacuole in yeast. *Mol Cell Biol* **27**, 526–540.
- Gavin, A., Bosche, M., Krause, R., Grandi, P., Marzioch, M., Bauer, A., Schultz, J., Rick, J., Michon, A., Cruciat, C., et al.** (2002). Functional organization of the yeast proteome by systematic analysis of protein complexes. *Nature* **415**, 141–147.
- Ge, L., Baskaran, S., Schekman, R. and Hurley, J. H.** (2014). The protein-vesicle network of autophagy. *Curr Opin Cell Biol* **29C**, 18–24.
- Ge, L., Melville, D., Zhang, M. and Schekman, R.** (2013). The ER-Golgi intermediate compartment is a key membrane source for the LC3 lipidation step of autophagosome biogenesis. *Elife* **2**, e00947.
- Geng, J., Nair, U., Yasumura-Yorimitsu, K. and Klionsky, D. J.** (2010). Post-Golgi Sec proteins are required for autophagy in *Saccharomyces cerevisiae*. *Mol Biol Cell* **21**, 2257–2269.
- Goffeau, A., Barrell, B., Bussey, H., Davis, R., Dujon, B., Feldmann, H., Galibert, F., Hoheisel, J., Jacq, C., Johnston, M., et al.** (1996). Life with 6000 genes. *Science* **274**, 546.
- Graef, M., Friedman, J. R., Graham, C., Babu, M. and Nunnari, J.** (2013). ER exit sites are physical and functional core autophagosome biogenesis components. *Mol Biol Cell*.
- Hamasaki, M., Furuta, N., Matsuda, A., Nezu, A., Yamamoto, A., et al.** (2013). Autophagosomes form at ER-mitochondria contact sites. *Nature* **495**, 389–393.
- Hamasaki, M., Noda, T., Baba, M. and Ohsumi, Y.** (2005). Starvation triggers the delivery of the endoplasmic reticulum to the vacuole via autophagy in yeast. *Traffic* **6**, 56–65.
- Hanada, T., Noda, N. N., Satomi, Y., Ichimura, Y., Fujioka, Y., Takao, T., Inagaki, F. and Ohsumi, Y.** (2007). The Atg12-Atg5 conjugate has a novel E3-like activity for protein lipidation in autophagy. *J Biol Chem* **282**, 37298–37302.
- Harding, T., Morano, K., Scott, S. and Klionsky, D.** (1995). Isolation and characterization of yeast mutants in the cytoplasm to vacuole protein targeting



## Bibliography

- pathway. *J Cell Biol* **131**, 591–602.
- Hartwell, L. H.** (2004). Yeast and cancer. *Biosci. Rep.* **24**, 523–544.
- He, H., Singh, I., Wek, S. A., Dey, S., Baird, T. D., Wek, R. C. and Georgiadis, M. M.** (2014). Crystal Structures of GCN2 Protein Kinase C-terminal Domains Suggest Regulatory Differences in Yeast and Mammals. *Journal of Biological Chemistry* **289**, 15023–15034.
- Ho, K.-H., Chang, H.-E. and Huang, W.-P.** (2009). Mutation at the cargo-receptor binding site of Atg8 also affects its general autophagy regulation function. *Autophagy* **5**, 461–471.
- Hong, S. B., Kim, B.-W., Lee, K.-E., Kim, S. W., Jeon, H., et al.** (2011). Insights into noncanonical E1 enzyme activation from the structure of autophagic E1 Atg7 with Atg8. *Nat Struct Mol Biol* **18**, 1323–1330.
- Hong, S. B., Kim, B. W., Kim, J. H. and Song, H. K.** (2012). mh5068. *Acta Cryst (2012). D68*, 1409–1417 [doi:10.1107/S0907444912034166] 1–9.
- Hosokawa, N., Hara, T., Kaizuka, T., Kishi, C., Takamura, A., Miura, Y., Iemura, S., Natsume, T., Takehana, K., Yamada, N., et al.** (2009). Nutrient-dependent mTORC1 Association with the ULK1-Atg13-FIP200 Complex Required for Autophagy. *Mol Biol Cell*.
- Huang, W. P., Scott, S. V., Kim, J. and Klionsky, D. J.** (2000). The itinerary of a vesicle component, Aut7p/Cvt5p, terminates in the yeast vacuole via the autophagy/Cvt pathways. *J Biol Chem* **275**, 5845–5851.
- Huber, A., Bodenmiller, B., Uotila, A., Stahl, M., Wanka, S., Gerrits, B., Aebersold, R. and Loewith, R.** (2009). Characterization of the rapamycin-sensitive phosphoproteome reveals that Sch9 is a central coordinator of protein synthesis. *Genes Dev* **23**, 1929–1943.
- Huh, W., Falvo, J., Gerke, L., Carroll, A., Howson, R., Weissman, J. and O'Shea, E.** (2003). Global analysis of protein localization in budding yeast. *Nature* **425**, 686–691.
- Hurley, J. H. and Schulman, B. A.** (2014). Atomistic autophagy: the structures of cellular self-digestion. *Cell* **157**, 300–311.
- Hutchins, M. and Klionsky, D.** (2001). Vacuolar localization of oligomeric alpha-mannosidase requires the cytoplasm to vacuole targeting and autophagy pathway components in *Saccharomyces cerevisiae*. *J Biol Chem* **276**, 20491–20498.
- Hutchins, M., Veenhuis, M. and Klionsky, D.** (1999). Peroxisome degradation in *Saccharomyces cerevisiae* is dependent on machinery of macroautophagy and the Cvt pathway. *J Cell Sci* **112**, 4079–4087.
- Ichimura, Y., Kirisako, T., Takao, T., Satomi, Y., Shimonishi, Y., Ishihara, N., Mizushima, N., Tanida, I., Kominami, E., Ohsumi, M., et al.** (2000). A ubiquitin-like

## Bibliography

system mediates protein lipidation. *Nature* **408**, 488–492.

- Ichimura, Y., Kumanomidou, T., Sou, Y.-S., Mizushima, T., Ezaki, J., Ueno, T., Kominami, E., Yamane, T., Tanaka, K. and Komatsu, M.** (2008). Structural basis for sorting mechanism of p62 in selective autophagy. *J Biol Chem* **283**, 22847–22857.
- Icho, T. and Wickner, R. B.** (1989). The double-stranded RNA genome of yeast virus L-A encodes its own putative RNA polymerase by fusing two open reading frames. *J Biol Chem* **264**, 6716–6723.
- Ishihara, N., Hamasaki, M., Yokota, S., Suzuki, K., Kamada, Y., Kihara, A., Yoshimori, T., Noda, T. and Ohsumi, Y.** (2001). Autophagosome requires specific early Sec proteins for its formation and NSF/SNARE for vacuolar fusion. *Mol Biol Cell* **12**, 3690–3702.
- Jackson, L. P.** (2014). Structure and mechanism of COPI vesicle biogenesis. *Curr Opin Cell Biol* **29**, 67–73.
- Janke, C., Magiera, M., Rathfelder, N., Taxis, C., Reber, S., Maekawa, H., Moreno-Borchart, A., Doenges, G., Schwob, E., Schiebel, E., et al.** (2004). A versatile toolbox for PCR-based tagging of yeast genes: new fluorescent proteins, more markers and promoter substitution cassettes. *Yeast* **21**, 947–962.
- Jao, C. C., Ragusa, M. J., Stanley, R. E. and Hurley, J. H.** (2013). A HORMA domain in Atg13 mediates PI 3-kinase recruitment in autophagy. *Proc Natl Acad Sci U S A* **110**, 5486–5491.
- Jensen, D. and Schekman, R.** (2010). COPII-mediated vesicle formation at a glance. *J Cell Sci* **124**, 1–4.
- Kabeya, Y., Kamada, Y., Baba, M., Takikawa, H., Sasaki, M. and Ohsumi, Y.** (2005). Atg17 functions in cooperation with Atg1 and Atg13 in yeast autophagy. *Mol Biol Cell* **16**, 2544–2553.
- Kabeya, Y., Noda, N. N., Fujioka, Y., Suzuki, K., Inagaki, F. and Ohsumi, Y.** (2009). Characterization of the Atg17-Atg29-Atg31 complex specifically required for starvation-induced autophagy in *Saccharomyces cerevisiae*. *Biochem Biophys Res Commun* **389**, 612–615.
- Kakuta, S., Yamamoto, H., Negishi, L., Kondo-Kakuta, C., Hayashi, N. and Ohsumi, Y.** (2012). Atg9 Vesicles Recruit Vesicle-tethering Proteins Trs85 and Ypt1 to the Autophagosome Formation Site. *Journal of Biological Chemistry* **287**, 44261–44269.
- Kalvari, I., Tsompanis, S., Mulakkal, N. C., Osgood, R., Johansen, T., Nezis, I. P. and Promponas, V. J.** (2014). iLIR: A web resource for prediction of Atg8-family interacting proteins. *Autophagy* **10**, 913–925.
- Kamada, Y., Funakoshi, T., Shintani, T., Nagano, K., Ohsumi, M. and Ohsumi, Y.** (2000). Tor-mediated induction of autophagy via an Apg1 protein kinase complex. *J Cell Biol* **150**, 1507–1513.
- Kanki, T. and Klionsky, D. J.** (2010). The molecular mechanism of mitochondria

## Bibliography

- autophagy in yeast. *Mol Microbiol* **75**, 795–800.
- Kanki, T., Kurihara, Y., Jin, X., Goda, T., Ono, Y., Aihara, M., Hirota, Y., Saigusa, T., Aoki, Y., Uchiumi, T., et al.** (2013). Casein kinase 2 is essential for mitophagy. *EMBO Rep* **14**, 788–794.
- Kanki, T., Wang, K., Cao, Y., Baba, M. and Klionsky, D. J.** (2009). Atg32 is a mitochondrial protein that confers selectivity during mitophagy. *Dev Cell* **17**, 98–109.
- Kaufmann, A. and Wollert, T.** (2014). Scaffolding the expansion of autophagosomes. *Autophagy* **10**, 1343–1345.
- Kaufmann, A., Beier, V., Franquelim, H. G. and Wollert, T.** (2014). Molecular mechanism of autophagic membrane-scaffold assembly and disassembly. *Cell* **156**, 469–481.
- Kenna, M., Stevens, A., McCammon, M. and Douglas, M. G.** (1993). An essential yeast gene with homology to the exonuclease-encoding XRN1/KEM1 gene also encodes a protein with exoribonuclease activity. *Mol Cell Biol* **13**, 341–350.
- Kihara, A., Noda, T., Ishihara, N. and Ohsumi, Y.** (2001). Two Distinct Vps34 Phosphatidylinositol 3-Kinase Complexes Function in Autophagy and Carboxypeptidase Y Sorting in *Saccharomyces cerevisiae*. *J Cell Biol* **152**, 519–530.
- Kim, J., Kamada, Y., Stromhaug, P., Guan, J., Hefner-Gravink, A., Baba, M., Scott, S., Ohsumi, Y., Dunn, W. and Klionsky, D.** (2001). Cvt9/Gsa9 functions in sequestering selective cytosolic cargo destined for the vacuole. *J Cell Biol* **153**, 381–96.
- Kim, J., Scott, S., Oda, M. and Klionsky, D.** (1997). Transport of a large oligomeric protein by the cytoplasm to vacuole protein targeting pathway. *J Cell Biol* **137**, 609–618.
- Kirisako, T., Ichimura, Y., Okada, H., Kabeya, Y., Mizushima, N., Yoshimori, T., Ohsumi, M., Takao, T., Noda, T. and Ohsumi, Y.** (2000). The reversible modification regulates the membrane-binding state of Apg8/Aut7 essential for autophagy and the cytoplasm to vacuole targeting pathway. *J Cell Biol* **151**, 263–276.
- Kirkin, V., Lamark, T., Johansen, T. and Dikic, I.** (2009a). NBR1 cooperates with p62 in selective autophagy of ubiquitinated targets. *Autophagy* **5**, 732–733.
- Kirkin, V., Lamark, T., Sou, Y.-S., Bjørkøy, G., Nunn, J. L., Bruun, J.-A., Shvets, E., McEwan, D. G., Clausen, T. H., Wild, P., et al.** (2009b). A role for NBR1 in autophagosomal degradation of ubiquitinated substrates. *Mol Cell* **33**, 505–516.
- Klionsky, D. J. and Schulman, B. A.** (2014). Dynamic regulation of macroautophagy by distinctive ubiquitin-like proteins. *Nat Struct Mol Biol* **21**, 336–345.
- Klionsky, D. J., Cuervo, A. M. and Seglen, P. O.** (2007). Methods for monitoring autophagy from yeast to human. *Autophagy* **3**, 181–206.

## Bibliography

- Klionsky, D., Cueva, R. and Yaver, D.** (1992). Aminopeptidase I of *Saccharomyces cerevisiae* is localized to the vacuole independent of the secretory pathway. *J Cell Biol* **119**, 287–299.
- Knop, M., Siegers, K., Pereira, G., Zachariae, W., Winsor, B., Nasmyth, K. and Schiebel, E.** (1999). Epitope tagging of yeast genes using a PCR-based strategy: more tags and improved practical routines. *Yeast* **15**, 963–972.
- Komatsu, M., Tanida, I., Ueno, T., Ohsumi, M., Ohsumi, Y. and Kominami, E.** (2001). The C-terminal region of an Apg7p/Cvt2p is required for homodimerization and is essential for its E1 activity and E1-E2 complex formation. *J Biol Chem* **276**, 9846–54.
- Kondo-Okamoto, N., Noda, N. N., Suzuki, S. W., Nakatogawa, H., Takahashi, I., Matsunami, M., Hashimoto, A., Inagaki, F., Ohsumi, Y. and Okamoto, K.** (2012). Autophagy-related protein 32 acts as autophagic degron and directly initiates mitophagy. *Journal of Biological Chemistry* **287**, 10631–10638.
- Kraft, C. and Peter, M.** (2008). Is the Rsp5 ubiquitin ligase involved in the regulation of ribophagy? *Autophagy* **4**, 838–840.
- Kraft, C., Deplazes, A., Sohrmann, M. and Peter, M.** (2008). Mature ribosomes are selectively degraded upon starvation by an autophagy pathway requiring the Ubp3p/Bre5p ubiquitin protease. *Nat Cell Biol* **10**, 602–610.
- Kraft, C., Kijanska, M., Kalie, E., Siergiejuk, E., Lee, S. S., Semplicio, G., Stoffel, I., Brezovich, A., Verma, M., Hansmann, I., et al.** (2012). Binding of the Atg1/ULK1 kinase to the ubiquitin-like protein Atg8 regulates autophagy. *EMBO J* **31**, 3691–3703.
- Kraft, C., Peter, M. and Hofmann, K.** (2010). Selective autophagy: ubiquitin-mediated recognition and beyond. *Nat Cell Biol* **12**, 836–841.
- Kraft, C., Reggiori, F. and Peter, M.** (2009). Selective types of autophagy in yeast. *BBA - Molecular Cell Research* **1793**, 1404–1412.
- Krick, R., Bremer, S., Welter, E., Eskelinen, E.-L. and Thumm, M.** (2011). Cheating on ubiquitin with Atg8. *Autophagy* **7**, 250–251.
- Krick, R., Bremer, S., Welter, E., Schlotterhose, P., Muehe, Y., Eskelinen, E.-L. and Thumm, M.** (2010). Cdc48/p97 and Shp1/p47 regulate autophagosome biogenesis in concert with ubiquitin-like Atg8. *J Cell Biol* **190**, 965–973.
- Krick, R., Busse, R. A., Scacioc, A., Stephan, M., Janshoff, A., Thumm, M. and Kühnel, K.** (2012). Structural and functional characterization of the two phosphoinositide binding sites of PROPPINS, a  $\beta$ -propeller protein family. *Proc Natl Acad Sci U S A* **109**, E2042–9.
- Krick, R., Henke, S., Tolstrup, J. and Thumm, M.** (2008a). Dissecting the localization and function of Atg18, Atg21 and Ygr223c. *Autophagy* **4**, 896–905.
- Krick, R., Muehe, Y., Prick, T., Bremer, S., Schlotterhose, P., Eskelinen, E.-L., Millen, J., Goldfarb, D. S. and Thumm, M.** (2008b). Piecemeal microautophagy of the

## Bibliography

- nucleus requires the core macroautophagy genes. *Mol Biol Cell* **19**, 4492–4505.
- Krick, R., Tolstrup, J., Appelles, A., Henke, S. and Thumm, M.** (2006). The relevance of the phosphatidylinositolphosphat-binding motif FRRGT of Atg18 and Atg21 for the Cvt pathway and autophagy. *FEBS Lett* **580**, 4632–4638.
- Kuma, A., Mizushima, N., Ishihara, N. and Ohsumi, Y.** (2002). Formation of the approximately 350-kDa Apg12-Apg5-Apg16 multimeric complex, mediated by Apg16 oligomerization, is essential for autophagy in yeast. *J Biol Chem* **277**, 18619–18625.
- Lang, T., Reiche, S., Straub, M., Bredschneider, M. and Thumm, M.** (2000). Autophagy and the cvt pathway both depend on AUT9. *J Bacteriol* **182**, 2125–2133.
- Lämmli, U.** (1970). Cleavage of structural proteins during the assembly of the head of Bacteriophage T4. *Nature* **227**, 680–685.
- Lemmon, M. A.** (2004). Pleckstrin homology domains: not just for phosphoinositides. *Biochem Soc Trans* **32**, 707–711.
- Lemmon, M. A.** (2008). Membrane recognition by phospholipid-binding domains. *Nat Rev Mol Cell Biol* **9**, 99–111.
- Li, W.-W., Li, J. and Bao, J.-K.** (2012). Microautophagy: lesser-known self-eating. *Cell Mol Life Sci* **69**, 1125–1136.
- Lipatova, Z., Belogortseva, N., Zhang, X. Q., Kim, J., Taussig, D. and Segev, N.** (2012). Regulation of selective autophagy onset by a Ypt/Rab GTPase module. *Proc Natl Acad Sci U S A* **109**, 6981–6986.
- Lipatova, Z., Shah, A. H., Kim, J. J., Mulholland, J. W. and Segev, N.** (2013). Regulation of ER-phagy by a Ypt/Rab GTPase module. *Mol Biol Cell*.
- Liu, L., Sakakibara, K., Chen, Q. and Okamoto, K.** (2014). Receptor-mediated mitophagy in yeast and mammalian systems. *Cell Res* **24**, 787–795.
- Loewith, R. and Hall, M. N.** (2011). Target of rapamycin (TOR) in nutrient signaling and growth control. *Genetics* **189**, 1177–1201.
- Longtine, M., McKenzie, A., Demarini, D., Shah, N., Wach, A., Brachat, A., Philippsen, P. and Pringle, J.** (1998). Additional modules for versatile and economical PCR-based gene deletion and modification in *Saccharomyces cerevisiae*. *Yeast* **14**, 953–961.
- Luque, D., González, J. M., Garriga, D., Ghabrial, S. A., Havens, W. M., Trus, B., Verdaguier, N., Carrascosa, J. L. and Castón, J. R.** (2010). The T=1 capsid protein of *Penicillium chrysogenum* virus is formed by a repeated helix-rich core indicative of gene duplication. *J Virol* **84**, 7256–7266.
- Lynch-Day, M. A. and Klionsky, D. J.** (2010). The Cvt pathway as a model for selective autophagy. *FEBS Letters* **584**, 1359–1366.

## Bibliography

- Lynch-Day, M. A., Bhandari, D., Menon, S., Huang, J., Cai, H., Bartholomew, C. R., Brumell, J. H., Ferro-Novick, S. and Klionsky, D. J.** (2010). Trs85 directs a Ypt1 GEF, TRAPP3, to the phagophore to promote autophagy. *Proc Natl Acad Sci U S A* **107**, 7811–7816.
- Ma, C., Agrawal, G. and Subramani, S.** (2011). Peroxisome assembly: matrix and membrane protein biogenesis. *J Cell Biol* **193**, 7–16.
- Mager, W. H. and Winderickx, J.** (2005). Yeast as a model for medical and medicinal research. *Trends Pharmacol. Sci.* **26**, 265–273.
- Mandell, M. A., Jain, A., Arko-Mensah, J., Chauhan, S., Kimura, T., Dinkins, C., Silvestri, G., Münch, J., Kirchhoff, F., Simonsen, A., et al.** (2014). TRIM proteins regulate autophagy and can target autophagic substrates by direct recognition. *Dev Cell* **30**, 394–409.
- Manjithaya, R., Nazarko, T. Y., Farré, J.-C. and Subramani, S.** (2010). Molecular mechanism and physiological role of pexophagy. *FEBS Lett* **584**, 1367–1373.
- Mao, K., Chew, L. H., Inoue-Aono, Y., Cheong, H., Nair, U., Popelka, H., Yip, C. K. and Klionsky, D. J.** (2013a). Atg29 phosphorylation regulates coordination of the Atg17-Atg31-Atg29 complex with the Atg11 scaffold during autophagy initiation. *Proc Natl Acad Sci U S A* **110**, E2875–84.
- Mao, K., Wang, K., Liu, X. and Klionsky, D. J.** (2013b). The Scaffold Protein Atg11 Recruits Fission Machinery to Drive Selective Mitochondria Degradation by Autophagy. *Developmental Cell* **26**, 9–18.
- Mao, K., Wang, K., Zhao, M., Xu, T. and Klionsky, D. J.** (2011). Two MAPK-signaling pathways are required for mitophagy in *Saccharomyces cerevisiae*. *J Cell Biol* **193**, 755–767.
- Mari, M., Griffith, J., Rieter, E., Krishnappa, L., Klionsky, D. J. and Reggiori, F.** (2010). An Atg9-containing compartment that functions in the early steps of autophagosome biogenesis. *J Cell Biol* **190**, 1005–1022.
- Masison, D. C., Blanc, A., Ribas, J. C., Carroll, K., Sonenberg, N. and Wickner, R. B.** (1995). Decoying the cap- mRNA degradation system by a double-stranded RNA virus and poly(A)- mRNA surveillance by a yeast antiviral system. *Mol Cell Biol* **15**, 2763–2771.
- Matsushita, M., Suzuki, N. N., Obara, K., Fujioka, Y., Ohsumi, Y. and Inagaki, F.** (2007). Structure of Atg5-Atg16, a complex essential for autophagy. *J Biol Chem* **282**, 6763–6772.
- Matsuura, A., Tsukada, M., Wada, Y. and Ohsumi, Y.** (1997). Apg1p, a novel protein kinase required for the autophagic process in *Saccharomyces cerevisiae*. *Gene* **192**, 245–250.
- Mazon, M., Eraso, P. and Portillo, F.** (2007). Efficient degradation of misfolded mutant Pma1 by endoplasmic reticulum-associated degradation requires Atg19 and the

## Bibliography

Cvt/autophagy pathway. *Mol Microbiol* **63**, 1069–1077.

**Meiling-Wesse, K., Barth, H., Voss, C., Barmark, G., Muren, E., Ronne, H. and Thumm, M.** (2002). Yeast Mon1p/Aut12p functions in vacuolar fusion of autophagosomes and cvt-vesicles. *FEBS Lett* **530**, 174–180.

**Meiling-Wesse, K., Barth, H., Voss, C., Eskelinen, E., Epple, U. and Thumm, M.** (2004). Atg21 is required for effective recruitment of Atg8 to the preautophagosomal structure during the Cvt pathway. *J Biol Chem* **279**, 37741–37750.

**Meiling-Wesse, K., Epple, U., Krick, R., Barth, H., Appelles, A., Voss, C., Eskelinen, E. and Thumm, M.** (2005). Trs85 (Gsg1), a Component of the TRAPP Complexes, Is Required for the Organization of the Preautophagosomal Structure during Selective Autophagy via the Cvt Pathway. *J Biol Chem* **280**, 33669–33678.

**Michell, R. H., Heath, V. L., Lemmon, M. A. and Dove, S. K.** (2006). Phosphatidylinositol 3,5-bisphosphate: metabolism and cellular functions. *Trends Biochem Sci* **31**, 52–63.

**Miller-Fleming, L., Giorgini, F. and Outeiro, T. F.** (2008). Yeast as a model for studying human neurodegenerative disorders. *Biotechnol. J.* **3**, 325–338.

**Mizushima, N., Noda, T. and Ohsumi, Y.** (1999). Apg16p is required for the function of the Apg12p-Apg5p conjugate in the yeast autophagy pathway. *EMBO J* **18**, 3888–3896.

**Mizushima, N., Noda, T., Yoshimori, T., Tanaka, Y., Ishii, T., George, M. D., Klionsky, D. J., Ohsumi, M. and Ohsumi, Y.** (1998a). A protein conjugation system essential for autophagy. *Nature* **395**, 395–398.

**Mizushima, N., Sugita, H., Yoshimori, T. and Ohsumi, Y.** (1998b). A new protein conjugation system in human. The counterpart of the yeast Apg12p conjugation system essential for autophagy. *J Biol Chem* **273**, 33889–33892.

**Mohrlüder, J., Stangler, T., Hoffmann, Y., Wiesehan, K., Mataruga, A. and Willbold, D.** (2007). Identification of calreticulin as a ligand of GABARAP by phage display screening of a peptide library. *FEBS J* **274**, 5543–5555.

**Mortimore, G. E. and Pösö, A. R.** (1987). Intracellular protein catabolism and its control during nutrient deprivation and supply. *Annu. Rev. Nutr.* **7**, 539–564.

**Motley, A. M., Nuttall, J. M. and Hetteima, E. H.** (2012). 2852.full. *EMBO J* **31**, 2852–2868.

**Mukaiyama, H., Baba, M., Osumi, M., Aoyagi, S., Kato, N., Ohsumi, Y. and Sakai, Y.** (2004). Modification of a ubiquitin-like protein Paz2 conducted micropexophagy through formation of a novel membrane structure. *Mol Biol Cell* **15**, 58–70.

**Mukaiyama, H., Oku, M., Baba, M., Samizo, T., Hammond, A., Glick, B., Kato, N. and Sakai, Y.** (2002). Paz2 and 13 other PAZ gene products regulate vacuolar engulfment of peroxisomes during micropexophagy. *Genes Cells* **7**, 75–90.

## Bibliography

- Müller, J. and Johnsson, N.** (2008). Split-ubiquitin and the split-protein sensors: chessman for the endgame. *ChemBioChem* **9**, 2029–2038.
- Nair, U., Cao, Y., Xie, Z. and Klionsky, D. J.** (2010). Roles of the lipid-binding motifs of Atg18 and Atg21 in the cytoplasm to vacuole targeting pathway and autophagy. *Journal of Biological Chemistry* **285**, 11476–11488.
- Nair, U., Jotwani, A., Geng, J., Gammoh, N., Richerson, D., Yen, W.-L., Griffith, J., Nag, S., Wang, K., Moss, T., et al.** (2011). SNARE Proteins Are Required for Macroautophagy. *Cell* **146**, 290–302.
- Nair, U., Yen, W.-L., Mari, M., Cao, Y., Xie, Z., Baba, M., Reggiori, F. and Klionsky, D. J.** (2012). A role for Atg8-PE deconjugation in autophagosome biogenesis. *Autophagy* **8**, 780–793.
- Naitow, H., Tang, J., Canady, M., Wickner, R. B. and Johnson, J. E.** (2002). L-A virus at 3.4 Å resolution reveals particle architecture and mRNA decapping mechanism. *Nat Struct Biol* **9**, 725–728.
- Nakatogawa, H.** (2013). Two ubiquitin-like conjugation systems that mediate membrane formation during autophagy. *Essays Biochem.* **55**, 39–50.
- Nakatogawa, H., Ichimura, Y. and Ohsumi, Y.** (2007). Atg8, a ubiquitin-like protein required for autophagosome formation, mediates membrane tethering and hemifusion. *Cell* **130**, 165–178.
- Nakatogawa, H., Ishii, J., Asai, E. and Ohsumi, Y.** (2012a). Atg4 recycles inappropriately lipidated Atg8 to promote autophagosome biogenesis. *Autophagy* **8**, 177–186.
- Nakatogawa, H., Ohbayashi, S., Sakoh-Nakatogawa, M., Kakuta, S., Suzuki, S. W., Kirisako, H., Kondo-Kakuta, C., Noda, N. N., Yamamoto, H. and Ohsumi, Y.** (2012b). The autophagy-related protein kinase Atg1 interacts with the ubiquitin-like protein Atg8 via the Atg8 family interacting motif to facilitate autophagosome formation. *Journal of Biological Chemistry* **287**, 28503–28507.
- Nakatogawa, H., Suzuki, K., Kamada, Y. and Ohsumi, Y.** (2009). Dynamics and diversity in autophagy mechanisms: lessons from yeast. *Nat Rev Mol Cell Biol* **10**, 458–467.
- Nazarko, T. Y., Farré, J.-C. and Subramani, S.** (2009). Peroxisome size provides insights into the function of autophagy-related proteins. *Mol Biol Cell* **20**, 3828–3839.
- Nazarko, T. Y., Farré, J.-C., Polupanov, A. S., Sibirny, A. A. and Subramani, S.** (2007a). Autophagy-related pathways and specific role of sterol glucoside in yeasts. *Autophagy* **3**, 263–265.
- Nazarko, T. Y., Polupanov, A. S., Manjithaya, R. R., Subramani, S. and Sibirny, A. A.** (2007b). The requirement of sterol glucoside for pexophagy in yeast is dependent on the species and nature of peroxisome inducers. *Mol Biol Cell* **18**, 106–118.



## Bibliography

- Neiman, A. M.** (2005). Ascospore formation in the yeast *Saccharomyces cerevisiae*. *Microbiol Mol Biol Rev* **69**, 565–584.
- Nicolás, F. E., Torres-Martínez, S. and Ruiz-Vázquez, R. M.** (2013). Loss and Retention of RNA Interference in Fungi and Parasites. *PLoS Pathog* **9**, e1003089.
- Noda, N. N., Kumeta, H., Nakatogawa, H., Satoo, K., Adachi, W., Ishii, J., Fujioka, Y., Ohsumi, Y. and Inagaki, F.** (2008). Structural basis of target recognition by Atg8/LC3 during selective autophagy. *Genes Cells* **13**, 1211–1218.
- Noda, N. N., Ohsumi, Y. and Inagaki, F.** (2010). Atg8-family interacting motif crucial for selective autophagy. *FEBS Letters* **584**, 1379–1385.
- Noda, N. N., Satoo, K., Fujioka, Y., Kumeta, H., Ogura, K., Nakatogawa, H., Ohsumi, Y. and Inagaki, F.** (2011). Structural Basis of Atg8 Activation by a Homodimeric E1, Atg7. *Mol Cell* **44**, 462–475.
- Noda, T. and Ohsumi, Y.** (1998). Tor, a phosphatidylinositol kinase homologue, controls autophagy in yeast. *J Biol Chem* **273**, 3963–3966.
- Noda, T., Kim, J., Huang, W. P., Baba, M., Tokunaga, C., Ohsumi, Y. and Klionsky, D. J.** (2000). Apg9p/Cvt7p is an integral membrane protein required for transport vesicle formation in the Cvt and autophagy pathways. *J Cell Biol* **148**, 465–480.
- Nolan, S., Cowan, A. E., Koppel, D. E., Jin, H. and Grote, E.** (2006). FUS1 regulates the opening and expansion of fusion pores between mating yeast. *Mol Biol Cell* **17**, 2439–2450.
- Novak, I., Kirkin, V., McEwan, D. G., Zhang, J., Wild, P., Rozenknop, A., Rogov, V., Löhr, F., Popovic, D., Occhipinti, A., et al.** (2010). Nix is a selective autophagy receptor for mitochondrial clearance. *EMBO Rep* **11**, 45–51.
- Obara, K., Sekito, T. and Ohsumi, Y.** (2006). Assortment of phosphatidylinositol 3-kinase complexes--Atg14p directs association of complex I to the pre-autophagosomal structure in *Saccharomyces cerevisiae*. *Mol Biol Cell* **17**, 1527–1539.
- Obara, K., Sekito, T., Niimi, K. and Ohsumi, Y.** (2008). The Atg18-Atg2 complex is recruited to autophagic membranes via phosphatidylinositol 3-phosphate and exerts an essential function. *J Biol Chem* **283**, 23972–23980.
- Ohashi, Y. and Munro, S.** (2010). Membrane delivery to the yeast autophagosome from the Golgi-endosomal system. *Mol Biol Cell* **21**, 3998–4008.
- Ohtake, Y. and Wickner, R. B.** (1995). Yeast virus propagation depends critically on free 60S ribosomal subunit concentration. *Mol Cell Biol* **15**, 2772–2781.
- Okamoto, K.** (2014). Organellophagy: Eliminating cellular building blocks via selective autophagy. *J Cell Biol* **205**, 435–445.
- Okamoto, K., Kondo-Okamoto, N. and Ohsumi, Y.** (2009). Mitochondria-anchored receptor Atg32 mediates degradation of mitochondria via selective autophagy. *Dev*

## Bibliography

*Cell* **17**, 87–97.

- Oku, M., Nishimura, T., Hattori, T., Ano, Y., Yamashita, S. and Sakai, Y.** (2006). Role of Vac8 in formation of the vacuolar sequestering membrane during micropexophagy. *Autophagy* **2**, 272–279.
- Oku, M., Warnecke, D., Noda, T., Müller, F., Heinz, E., Mukaiyama, H., Kato, N. and Sakai, Y.** (2003). Peroxisome degradation requires catalytically active sterol glucosyltransferase with a GRAM domain. *EMBO J* **22**, 3231–3241.
- Orvedahl, A., MacPherson, S., Sumpter, R., Tallóczy, Z., Zou, Z. and Levine, B.** (2010). Autophagy protects against Sindbis virus infection of the central nervous system. *Cell Host Microbe* **7**, 115–127.
- Pan, X. and Goldfarb, D. S.** (1998). YEB3/VAC8 encodes a myristylated armadillo protein of the *Saccharomyces cerevisiae* vacuolar membrane that functions in vacuole fusion and inheritance. *J Cell Sci* **111 ( Pt 15)**, 2137–2147.
- Pan, X., Roberts, P., Chen, Y., Kvam, E., Shulga, N., Huang, K., Lemmon, S. and Goldfarb, D.** (2000). Nucleus-vacuole junctions in *Saccharomyces cerevisiae* are formed through the direct interaction of Vac8p with Nvj1p. *Mol Biol Cell* **11**, 2445–2457.
- Pankiv, S. and Johansen, T.** (2010). FYCO1: linking autophagosomes to microtubule plus end-directing molecular motors. *Autophagy* **6**, 550–552.
- Pankiv, S., Alemu, E. A., Brech, A., Bruun, J.-A., Lamark, T., Øvervatn, A., Bjørkøy, G. and Johansen, T.** (2010). FYCO1 is a Rab7 effector that binds to LC3 and PI3P to mediate microtubule plus end-directed vesicle transport. *J Cell Biol* **188**, 253–269.
- Pankiv, S., Clausen, T. H., Lamark, T., Brech, A., Bruun, J.-A., Outzen, H., Øvervatn, A., Bjørkøy, G. and Johansen, T.** (2007). p62/SQSTM1 binds directly to Atg8/LC3 to facilitate degradation of ubiquitinated protein aggregates by autophagy. *J Biol Chem* **282**, 24131–24145.
- Papinski, D., Schuschnig, M., Reiter, W., Wilhelm, L., Barnes, C. A., Majolica, A., Hansmann, I., Pfaffenwimmer, T., Kijanska, M., Stoffel, I., et al.** (2014). Early Steps in Autophagy Depend on Direct Phosphorylation of Atg9 by the Atg1 Kinase. *Mol Cell*.
- Pfaffenwimmer, T., Reiter, W., Brach, T., Nogellova, V., Papinski, D., Schuschnig, M., Abert, C., Ammerer, G., Martens, S. and Kraft, C.** (2014). Hrr25 kinase promotes selective autophagy by phosphorylating the cargo receptor Atg19. *EMBO Rep*.
- Pink, M., Verma, N., Rettenmeier, A. W. and Schmitz-Spanke, S.** (2010). CBB staining protocol with higher sensitivity and mass spectrometric compatibility. *Electrophoresis* **31**, 593–598.
- Popovic, D., Akutsu, M., Novak, I., Harper, J. W., Behrends, C. and Dikic, I.** (2012). Rab GTPase-Activating Proteins in Autophagy: Regulation of Endocytic and Autophagy Pathways by Direct Binding to Human ATG8 Modifiers. *Mol Cell Biol* **32**,

## Bibliography

1733–1744.

- Powilleit, F., Breinig, T. and Schmitt, M. J.** (2007). Exploiting the Yeast L-A Viral Capsid for the In Vivo Assembly of Chimeric VLPs as Platform in Vaccine Development and Foreign Protein Expression. *PLoS ONE* **2**, e415 EP –.
- Ragusa, M. J., Stanley, R. E. and Hurley, J. H.** (2012). Architecture of the Atg17 Complex as a Scaffold for Autophagosome Biogenesis. *Cell* **151**, 1501–1512.
- Razi, M., Chan, E. Y. W. and Tooze, S. A.** (2009). Early endosomes and endosomal coatomer are required for autophagy. *J Cell Biol* **185**, 305–321.
- Reggiori, F. and Klionsky, D. J.** (2013). Autophagic processes in yeast: mechanism, machinery and regulation. *Genetics* **194**, 341–361.
- Reggiori, F., Tucker, K., Stromhaug, P. and Klionsky, D.** (2004). The Atg1-Atg13 complex regulates Atg9 and Atg23 retrieval transport from the pre-autophagosomal structure. *Dev Cell* **6**, 79–90.
- Ribas, J. C., Fujimura, T. and Wickner, R. B.** (1994). A cryptic RNA-binding domain in the Pol region of the L-A double-stranded RNA virus Gag-Pol fusion protein. *J Virol* **68**, 6014–6020.
- Rieder, S. and Emr, S.** (1997). A novel RING finger protein complex essential for a late step in protein transport to the yeast vacuole. *Mol Biol Cell* **8**, 2307–2327.
- Rieter, E., Rieter, E., Vinke, F., Vinke, F., Bakula, D., Bakula, D., Cebollero, E., Cebollero, E., Ungermann, C., Ungermann, C., et al.** (2013). Atg18 function in autophagy is regulated by specific sites within its  $\beta$ -propeller. *J Cell Sci* **126**, 593–604.
- Roberts, P., Moshitch-Moshkovitz, S., Kvam, E., O'Toole, E., Winey, M. and Goldfarb, D.** (2003). Piecemeal microautophagy of nucleus in *Saccharomyces cerevisiae*. *Mol Biol Cell* **14**, 129–141.
- Rodríguez-Cousiño, N., Gómez, P. and Esteban, R.** (2013). L-A-lus, a new variant of the L-A totivirus found in wine yeasts with Klus killer toxin-encoding Mlus double-stranded RNA: possible role of killer toxin-encoding satellite rnas in the evolution of their helper viruses. *Appl Environ Microbiol* **79**, 4661–4674.
- Romanov, J., Walczak, M., Ibiricu, I., Schüchner, S., Ogris, E., Kraft, C. and Martens, S.** (2012). Mechanism and functions of membrane binding by the Atg5-Atg12/Atg16 complex during autophagosome formation. *EMBO J* **31**, 4304–4317.
- Sakoh-Nakatogawa, M., Matoba, K., Asai, E., Kirisako, H., Ishii, J., et al.** (2013). Atg12-Atg5 conjugate enhances E2 activity of Atg3 by rearranging its catalytic site. *Nat Struct Mol Biol* **20**, 433–439.
- Satoo, K., Noda, N. N., Kumeta, H., Fujioka, Y., Mizushima, N., Ohsumi, Y. and Inagaki, F.** (2009). The structure of Atg4B-LC3 complex reveals the mechanism of LC3 processing and delipidation during autophagy. *EMBO J* **28**, 1341–1350.

## Bibliography

- Satyanarayana, C., Schroder-Kohne, S., Craig, E., Schu, P. and Horst, M.** (2000). Cytosolic Hsp70s are involved in the transport of aminopeptidase 1 from the cytoplasm into the vacuole. *FEBS Lett* **470**, 232–238.
- Sawa-Makarska, J., Abert, C., Romanov, J., Zens, B., Ibiricu, I. and Martens, S.** (2014). Cargo binding to Atg19 unmasks additional Atg8 binding sites to mediate membrane–cargo apposition during selective autophagy. *Nat Cell Biol* **16**, 425–433.
- Schmidhals, K., Helma, J., Zolghadr, K., Rothbauer, U. and Leonhardt, H.** (2010). Novel antibody derivatives for proteome and high-content analysis. *Anal Bioanal Chem* **397**, 3203–3208.
- Schmitt, M. J. and Breinig, F.** (2006). Yeast viral killer toxins: lethality and self-protection. *Nat Rev Microbiol* **4**, 212–221.
- Schmitt, M. J. and Reiter, J.** (2008). Viral induced yeast apoptosis. *Biochimica et Biophysica Acta (BBA) - Molecular Cell Research* **1783**, 1413–1417.
- Schneider, J. L. and Cuervo, A. M.** (2014). Autophagy and human disease: emerging themes. *Curr. Opin. Genet. Dev.* **26C**, 16–23.
- Schroder, L. A., Ortiz, M. V. and Dunn, W. A.** (2008). The membrane dynamics of pexophagy are influenced by Sar1p in *Pichia pastoris*. *Mol Biol Cell* **19**, 4888–4899.
- Schu, P., Takegawa, K., Fry, M., Stack, J., Waterfield, M. and Emr, S.** (1993). Phosphatidylinositol 3-kinase encoded by yeast VPS34 gene essential for protein sorting. *Science* **260**, 88–91.
- Schwarten, M., Stoldt, M., Mohrlüder, J. and Willbold, D.** (2010). Solution structure of Atg8 reveals conformational polymorphism of the N-terminal domain. *Biochem Biophys Res Commun* **395**, 426–431.
- Scott, S., Guan, J., Hutchins, M., Kim, J. and Klionsky, D.** (2001). Cvt19 is a receptor for the cytoplasm-to-vacuole targeting pathway. *Mol Cell* **7**, 1131–1141.
- Scott, S., Nice, D., Nau, J., Weisman, L., Kamada, Y., Keizer-Gunnink, I., Funakoshi, T., Veenhuis, M., Ohsumi, Y. and Klionsky, D.** (2000). Apg13p and Vac8p are part of a complex of phosphoproteins that are required for cytoplasm to vacuole targeting. *J Biol Chem* **275**, 25840–25849.
- Seglen, P., Gordon, P., Holen, I. and Hoyvik, H.** (1991). Hepatocytic autophagy. *Biomed Biochim Acta* **50**, 373–381.
- Sekito, T., Kawamata, T., Ichikawa, R., Suzuki, K. and Ohsumi, Y.** (2009). Atg17 recruits Atg9 to organize the pre-autophagosomal structure. *Genes Cells* **14**, 525–538.
- Shintani, T. and Klionsky, D.** (2004). Cargo proteins facilitate the formation of transport vesicles in the cytoplasm to vacuole targeting pathway. *J Biol Chem* **279**, 29889–29894.
- Shintani, T., Huang, W., Stromhaug, P. and Klionsky, D.** (2002). Mechanism of cargo

## Bibliography

- selection in the cytoplasm to vacuole targeting pathway. *Dev Cell* **3**, 825–837.
- Shintani, T., Mizushima, N., Ogawa, Y., Matsuura, A., Noda, T. and Ohsumi, Y.** (1999). Apg10p, a novel protein-conjugating enzyme essential for autophagy in yeast. *EMBO J* **18**, 5234–5241.
- Silles, E., Mazon, M., Gevaert, K., Goethals, M., Vandekerckhove, J., Leber, R. and Sandoval, I.** (2000). Targeting of aminopeptidase I to the yeast vacuole is mediated by Ssa1p, a cytosolic member of the 70-kDa stress protein family. *J Biol Chem* **275**, 34054–34059.
- Specht, S., Miller, S. B. M., Mogk, A. and Bukau, B.** (2011). Hsp42 is required for sequestration of protein aggregates into deposition sites in *Saccharomyces cerevisiae*. *J Cell Biol* **195**, 617–629.
- Stanley, R. E., Ragusa, M. J. and Hurley, J. H.** (2014). The beginning of the end: how scaffolds nucleate autophagosome biogenesis. *Trends Cell Biol* **24**, 73–81.
- Stasyk, O. V., Nazarko, T. Y., Stasyk, O. G., Krasovska, O. S., Warnecke, D., Nicaud, J.-M., Cregg, J. M. and Sibirny, A. A.** (2003). Sterol glucosyltransferases have different functional roles in *Pichia pastoris* and *Yarrowia lipolytica*. *Cell Biol Int* **27**, 947–952.
- Stephan, J. S., Yeh, Y.-Y., Ramachandran, V., Deminoff, S. J. and Herman, P. K.** (2009). The Tor and PKA signaling pathways independently target the Atg1/Atg13 protein kinase complex to control autophagy. *Proc Natl Acad Sci USA* **106**, 17049–17054.
- Stolz, A., Stolz, A., Ernst, A., Ernst, A., Dikic, I. and Dikic, I.** (2014). Cargo recognition and trafficking in selective autophagy. *Nat Cell Biol* **16**, 495–501.
- Straub, M., Bredschneider, M. and Thumm, M.** (1997). AUT3, a serine/threonine kinase gene, is essential for autophagocytosis in *Saccharomyces cerevisiae*. *J Bacteriol* **179**, 3875–3883.
- Stromhaug, P., Reggiori, F., Guan, J., Wang, C. and Klionsky, D.** (2004). Atg21 is a phosphoinositide binding protein required for efficient lipidation and localization of Atg8 during uptake of aminopeptidase I by selective autophagy. *Mol Biol Cell* **15**, 3553–3566.
- Sumpter, R. and Levine, B.** (2011). Selective autophagy and viruses. *Autophagy* **7**.
- Suzuki, K., Kirisako, T., Kamada, Y., Mizushima, N., Noda, T. and Ohsumi, Y.** (2001). The pre-autophagosomal structure organized by concerted functions of APG genes is essential for autophagosome formation. *EMBO J* **20**, 5971–5981.
- Suzuki, K., Kondo, C., Morimoto, M. and Ohsumi, Y.** (2010). Selective transport of alpha-mannosidase by autophagic pathways: identification of a novel receptor, Atg34p. *Journal of Biological Chemistry* **285**, 30019–30025.
- Suzuki, K., Kubota, Y., Sekito, T. and Ohsumi, Y.** (2007). Hierarchy of Atg proteins in pre-autophagosomal structure organization. *Genes Cells* **12**, 209–218.
- Suzuki, K., Morimoto, M., Kondo, C. and Ohsumi, Y.** (2011). Selective Autophagy

## Bibliography

- Regulates Insertional Mutagenesis by the Ty1 Retrotransposon in *Saccharomyces cerevisiae*. *Developmental Cell* **21**, 358–365.
- Suzuki, K., Akioka, M., Kondo-Kakuta, C., Yamamoto, H. and Ohsumi, Y.** (2013). Fine mapping of autophagy-related proteins during autophagosome formation in *Saccharomyces cerevisiae*. *J Cell Sci*.
- Szklarczyk, D., Franceschini, A., Kuhn, M., Simonovic, M., Roth, A., Minguéz, P., Doerks, T., Stark, M., Muller, J., Bork, P., et al.** (2010). The STRING database in 2011: functional interaction networks of proteins, globally integrated and scored. *Nucleic Acids Res* **39**, D561–D568.
- Taherbhoy, A. M., Tait, S. W., Kaiser, S. E., Williams, A. H., Deng, A., et al.** (2011). Atg8 transfer from Atg7 to Atg3: a distinctive E1-E2 architecture and mechanism in the autophagy pathway. *Mol Cell* **44**, 451–461.
- Takehige, K., Baba, M., Tsuboi, S., Noda, T. and Ohsumi, Y.** (1992). Autophagy in yeast demonstrated with proteinase-deficient mutants and conditions for its induction. *J Cell Biol* **119**, 301–311.
- Tallóczy, Z., Jiang, W., Virgin, H. W., Leib, D. A., Scheuner, D., Kaufman, R. J., Eskelinen, E.-L. and Levine, B.** (2002). Regulation of starvation- and virus-induced autophagy by the eIF2 $\alpha$  kinase signaling pathway. *Proc Natl Acad Sci USA* **99**, 190–195.
- Tan, D., Cai, Y., Wang, J., Zhang, J., Menon, S., et al.** (2013). The EM structure of the TRAPPIII complex leads to the identification of a requirement for COPII vesicles on the macroautophagy pathway. *Proc Natl Acad Sci USA* **110**, 19432–19437.
- Tanaka, C., Tan, L. J., Mochida, K., Kirisako, H., Koizumi, M., Asai, E., Sakoh-Nakatogawa, M., Ohsumi, Y. and Nakatogawa, H.** (2014). Hrr25 triggers selective autophagy-related pathways by phosphorylating receptor proteins. *J Cell Biol* **207**, 91–105.
- Tang, J., Naitow, H., Gardner, N. A., Kolesar, A., Tang, L., et al.** (2005). The structural basis of recognition and removal of cellular mRNA 7-methyl G “caps” by a viral capsid protein: a unique viral response to host defense. *J. Mol. Recognit.* **18**, 158–168.
- Taylor, R., Chen, P.-H., Chou, C.-C., Patel, J. and Jin, S. V.** (2012). KCS1 deletion in *Saccharomyces cerevisiae* leads to a defect in translocation of autophagic proteins and reduces autophagosome formation. *Autophagy* **8**, 19–18.
- Tercero, J. C. and Wickner, R. B.** (1992). MAK3 encodes an N-acetyltransferase whose modification of the L-A gag NH<sub>2</sub> terminus is necessary for virus particle assembly. *J Biol Chem* **267**, 20277–20281.
- Tercero, J. C., Dinman, J. D. and Wickner, R. B.** (1993). Yeast MAK3 N-acetyltransferase recognizes the N-terminal four amino acids of the major coat protein (gag) of the L-A double-stranded RNA virus. *J Bacteriol* **175**, 3192–3194.
- Teter, S., Eggerton, K., Scott, S., Kim, J., Fischer, A. and Klionsky, D.** (2001).

## Bibliography

- Degradation of lipid vesicles in the yeast vacuole requires function of Cvt17, a putative lipase. *J Biol Chem* **276**, 2083–2087.
- Thumm, M., Egner, R., Koch, B., Schlumpberger, M., Straub, M., Veenhuis, M. and Wolf, D. H.** (1994). Isolation of autophagocytosis mutants of *Saccharomyces cerevisiae*. *FEBS Lett* **349**, 275–280.
- Thurston, T. L. M., Ryzhakov, G., Bloor, S., Muhlinen, von, N. and Randow, F.** (2009). The TBK1 adaptor and autophagy receptor NDP52 restricts the proliferation of ubiquitin-coated bacteria. *Nat Immunol* **10**, 1215–1221.
- Tooze, S. A. and Razi, M.** (2009). The essential role of early endosomes in autophagy is revealed by loss of COPI function. *Autophagy* **5**, 874–875.
- Tsukada, M. and Ohsumi, Y.** (1993). Isolation and characterization of autophagy-defective mutants of *Saccharomyces cerevisiae*. *FEBS Lett* **333**, 169–174.
- Tucker, K., Reggiori, F., Dunn, W. and Klionsky, D.** (2003). Atg23 is essential for the cytoplasm to vacuole targeting pathway and efficient autophagy but not pexophagy. *J Biol Chem* **278**, 48445–48452.
- Tuttle, D. L. and Dunn, W. A.** (1995). Divergent modes of autophagy in the methylotrophic yeast *Pichia pastoris*. *J Cell Sci* **108 (Pt 1)**, 25–35.
- Uetz, P., Giot, L., Cagney, G., Mansfield, T., Judson, R., Knight, J., Lockshon, D., Narayan, V., Srinivasan, M., Pochart, P., et al.** (2000). A comprehensive analysis of protein-protein interactions in *Saccharomyces cerevisiae*. *Nature* **403**, 623–627.
- Umekawa, M. and Klionsky, D. J.** (2012). Ksp1 Kinase Regulates Autophagy via the Target of Rapamycin Complex 1 (TORC1) Pathway. *Journal of Biological Chemistry* **287**, 16300–16310.
- Valle, R. P. and Wickner, R. B.** (1993). Elimination of L-A double-stranded RNA virus of *Saccharomyces cerevisiae* by expression of gag and gag-pol from an L-A cDNA clone. *J Virol* **67**, 2764–2771.
- van Zutphen, T., Todde, V., de Boer, R., Kreim, M., Hofbauer, H. F., Wolinski, H., Veenhuis, M., der Klei, van, I. J. and Kohlwein, S. D.** (2014). Lipid droplet autophagy in the yeast *Saccharomyces cerevisiae*. *Mol Biol Cell* **25**, 290–301.
- Walther, T. C. and Farese, R. V., Jr** (2012). Lipid Droplets and Cellular Lipid Metabolism. *Annu Rev Biochem* **81**, 687–714.
- Wang, C., Stromhaug, P., Shima, J. and Klionsky, D.** (2002). The Ccz1-Mon1 protein complex is required for the late step of multiple vacuole delivery pathways. *J Biol Chem* **277**, 47917–44727.
- Wang, J., Tan, D., Cai, Y., Reinisch, K. M., Walz, T. and Ferro-Novick, S.** (2014). A requirement for ER-derived COPII vesicles in phagophore initiation. *Autophagy* **10**, 708–709.
- Wang, J., Menon, S., Yamasaki, A., Chou, H.-T., Walz, T., et al.** (2013a). Ypt1 recruits

## Bibliography

- the Atg1 kinase to the preautophagosomal structure. *Proc Natl Acad Sci U S A* **110**, 9800–9805.
- Wang, K., Jin, M., Liu, X. and Klionsky, D. J.** (2013b). Proteolytic processing of Atg32 by the mitochondrial i-AAA protease Yme1 regulates mitophagy. *Autophagy* **9**, 1828–1836.
- Wang, K., Yang, Z., Liu, X., Mao, K., Nair, U., et al.** (2012). Phosphatidylinositol 4-kinases are required for autophagic membrane trafficking. *Journal of Biological Chemistry* **287**, 37964–37972.
- Wang, X., Li, X. and Li, Y.** (2007). A modified Coomassie Brilliant Blue staining method at nanogram sensitivity compatible with proteomic analysis. *Biotechnol Lett* **29**, 1599–1603.
- Wang, Z., Wilson, W., Fujino, M. and Roach, P.** (2001). Antagonistic controls of autophagy and glycogen accumulation by Snf1p, the yeast homolog of AMP-activated protein kinase, and the cyclin-dependent kinase Pho85p. *Mol Cell Biol* **21**, 5742–5752.
- Warnecke, D., Erdmann, R., Fahl, A., Hube, B., Muller, F., Zank, T., Zähringer, U. and Heinz, E.** (1999). Cloning and functional expression of UGT genes encoding sterol glucosyltransferases from *Saccharomyces cerevisiae*, *Candida albicans*, *Pichia pastoris*, and *Dictyostelium discoideum*. *J Biol Chem* **274**, 13048–13059.
- Watanabe, Y., Noda, N. N., Honbou, K., Suzuki, K., Sakai, Y., Ohsumi, Y. and Inagaki, F.** (2009). Crystallization of *Saccharomyces cerevisiae* alpha-mannosidase, a cargo protein of the Cvt pathway. *Acta Crystallogr Sect F Struct Biol Cryst Commun* **65**, 571–573.
- Watanabe, Y., Noda, N. N., Kumeta, H., Suzuki, K., Ohsumi, Y. and Inagaki, F.** (2010). Selective transport of alpha-mannosidase by autophagic pathways: structural basis for cargo recognition by Atg19 and Atg34. *Journal of Biological Chemistry* **285**, 30026–30033.
- Weidberg, H., Shvets, E., Shpilka, T., Shimron, F., Shinder, V. and Elazar, Z.** (2010). LC3 and GATE-16/GABARAP subfamilies are both essential yet act differently in autophagosome biogenesis. *EMBO J* **29**, 1792–1802.
- Welter, E., Thumm, M. and Krick, R.** (2010). Quantification of nonselective bulk autophagy in *S. cerevisiae* using Pgk1-GFP. *Autophagy* **6**, 794–797.
- Welter, E., Montino, M., Reinhold, R., Schlotterhose, R., Krick, R., Dudek, J., Rehling, P. and Thumm, M.** (2013). Uth1 is a mitochondrial inner membrane protein dispensable for post-log phase and rapamycin-induced mitophagy. *FEBS J.*
- Wickner, R. B.** (1992). Double-stranded and single-stranded RNA viruses of *Saccharomyces cerevisiae*. *Annu. Rev. Microbiol.* **46**, 347–375.
- Wickner, R. B., Fujimura, T. and Esteban, R.** (2013). Viruses and prions of *Saccharomyces cerevisiae*. *Adv. Virus Res.* **86**, 1–36.



## Bibliography

- Wild, P., Farhan, H., McEwan, D. G., Wagner, S., Rogov, V. V., Brady, N. R., Richter, B., Korac, J., Waidmann, O., Choudhary, C., et al.** (2011). Phosphorylation of the autophagy receptor optineurin restricts Salmonella growth. *Science* **333**, 228–233.
- Wild, P., McEwan, D. G. and Dikic, I.** (2013). The LC3 interactome at a glance. *J Cell Sci* **127**, 3–9.
- Wilson, W. A. and Roach, P. J.** (2002). Nutrient-regulated protein kinases in budding yeast. *Cell* **111**, 155–158.
- Yamaguchi, M., Noda, N. N., Nakatogawa, H., Kumeta, H., Ohsumi, Y. and Inagaki, F.** (2010). Autophagy-related protein 8 (Atg8) family interacting motif in Atg3 mediates the Atg3-Atg8 interaction and is crucial for the cytoplasm-to-vacuole targeting pathway. *Journal of Biological Chemistry* **285**, 29599–29607.
- Yamaguchi, M., Noda, N. N., Yamamoto, H., Shima, T., Kumeta, H., Kobashigawa, Y., Akada, R., Ohsumi, Y. and Inagaki, F.** (2012). Structural Insights into Atg10-Mediated Formation of the Autophagy-Essential Atg12-Atg5 Conjugate. *Structure* **20**, 1244–1254.
- Yamamoto, H., Kakuta, S., Watanabe, T. M., Kitamura, A., Sekito, T., Kondo-Kakuta, C., Ichikawa, R., Kinjo, M. and Ohsumi, Y.** (2012a). Atg9 vesicles are an important membrane source during early steps of autophagosome formation. *J Cell Biol* **198**, 219–233.
- Yamashita, S., Oku, M., Wasada, Y., Ano, Y. and Sakai, Y.** (2006). PI4P-signaling pathway for the synthesis of a nascent membrane structure in selective autophagy. *J Cell Biol* **173**, 709–717.
- Yamashita, S.-I., Oku, M. and Sakai, Y.** (2007). Functions of PI4P and sterol glucoside are necessary for the synthesis of a nascent membrane structure during pexophagy. *Autophagy* **3**, 35–37.
- Yang, Z., Huang, J., Geng, J., Nair, U. and Klionsky, D. J.** (2006). Atg22 recycles amino acids to link the degradative and recycling functions of autophagy. *Mol Biol Cell* **17**, 5094–5104.
- Yeh, Y.-Y., Shah, K. H. and Herman, P. K.** (2011). An Atg13 protein-mediated self-association of the Atg1 protein kinase is important for the induction of autophagy. *Journal of Biological Chemistry* **286**, 28931–28939.
- Yen, W.-L., Legakis, J. E., Nair, U. and Klionsky, D. J.** (2007). Atg27 is required for autophagy-dependent cycling of Atg9. *Mol Biol Cell* **18**, 581–593.
- Yen, W.-L., Shintani, T., Nair, U., Cao, Y., Richardson, B. C., Li, Z., Hughson, F. M., Baba, M. and Klionsky, D. J.** (2010). The conserved oligomeric Golgi complex is involved in double-membrane vesicle formation during autophagy. *J Cell Biol* **188**, 101–114.
- Yorimitsu, T. and Klionsky, D.** (2005). Atg11 links cargo to the vesicle-forming machinery in the cytoplasm to vacuole targeting pathway. *Mol Biol Cell* **16**, 1593–

1605.

- Yorimitsu, T., Nair, U., Yang, Z. and Klionsky, D. J.** (2006). Endoplasmic reticulum stress triggers autophagy. *J Biol Chem* **281**, 30299–30304.
- Yorimitsu, T., Zaman, S., Broach, J. R. and Klionsky, D. J.** (2007). Protein kinase A and Sch9 cooperatively regulate induction of autophagy in *Saccharomyces cerevisiae*. *Mol Biol Cell* **18**, 4180–4189.
- Yoshimoto, K., Takano, Y. and Sakai, Y.** (2010). Autophagy in plants and phytopathogens. *FEBS Letters* **584**, 1350–1358.
- Young, A. R. J., Chan, E. Y. W., Hu, X. W., Köchl, R., Crawshaw, S. G., High, S., Hailey, D. W., Lippincott-Schwartz, J. and Tooze, S. A.** (2006). Starvation and ULK1-dependent cycling of mammalian Atg9 between the TGN and endosomes. *J Cell Sci* **119**, 3888–3900.
- Yu, J., Mendrola, J., Audhya, A., Singh, S., Keleti, D., DeWald, D., Murray, D., Emr, S. and Lemmon, M.** (2004). Genome-wide analysis of membrane targeting by *S. cerevisiae* pleckstrin homology domains. *Mol Cell* **13**, 677–688.
- Yu, Z.-Q., Ni, T., Hong, B., Wang, H.-Y., Jiang, F.-J., Zou, S., Chen, Y., Zheng, X.-L., Klionsky, D. J., Liang, Y., et al.** (2012). Dual roles of Atg8-PE deconjugation by Atg4 in autophagy. *Autophagy* **8**, 883–892.
- Yuga, M., Gomi, K., Klionsky, D. J. and Shintani, T.** (2011). Aspartyl Aminopeptidase Is Imported from the Cytoplasm to the Vacuole by Selective Autophagy in *Saccharomyces cerevisiae*. *Journal of Biological Chemistry* **286**, 13704–13713.

### 8 Acknowledgement

Im hohen Maße möchte ich mich bei Herrn Prof. Michael Thumm bedanken für die Bereitstellung des Themas meiner Doktorarbeit. Des Weiteren bedanke ich mich für die hilfreichen Diskussionen and Ratschläge bezüglich meiner wissenschaftlichen Arbeit.

Frau Prof. Stefanie Pöggeler danke ich für die Übernahme des Zweitgutachtens.

Den Mitgliedern meines Thesis Committees Herrn Prof. Michael Thumm, Frau Prof. Stefanie Pöggeler und Frau Dr. Karin Kühnel möchte ich danken für die Unterstützung meiner Arbeit durch Diskussionen und Anregungen.

Besonderer Dank gilt Rosi, die mir während meiner Doktorandenzeit mit Ratschlägen zur Seite stand, besonders während des Zusammenschreibens meiner Arbeit.

Ich danke Petra, Marco, Lisa M. und meinen ehemaligen Kolleginnen Lisa J. und Evelyn für die freundschaftliche gemeinsame Zeit im Labor und außerhalb.

Außerdem möchte ich mich bedanken bei Yvonne Pasing (Leibniz-Institut für Analytische Wissenschaften, ISAS eV, D-44227 Dortmund, Germany), Olaf Bernhard und Dr. Bernhard Schmidt (Institute of Cellular Biochemistry, University of Göttingen) für die MS Analysen, die für erheblichen Progress meiner Arbeit gesorgt haben.

Ich danke meiner Familie und meinen Freunden für die Unterstützung und alles Weitere.

## 9 Curriculum vitae

Name: Peter Rube

Born 7. 8.1984 in Korbach (Hessen), Germany

01/2011 - present **Dissertation at the Georg-August-University of Göttingen**  
Institute of Cellular Biochemistry (Universitätsmedizin,  
Göttingen) Prof. Dr. Michael Thumm

10/2005 – 09/2010 **Studies in Biology at the University of Kassel (Diploma)**

**Major subjects:** Biochemistry, Cell biology and Genetics

**Diploma thesis:** University of Kassel, Department of  
Biochemistry, Prof. Dr. F.W. Herberg

**Title:** "Charakterisierung künstlicher Bindeproteine gegen MAP-  
Kinasen in lebenden Zellen"

**Diploma Grade:** "sehr gut"

1995 - 2004 **Gymnasium:** Alte Landesschule, Korbach

## Publications

**Parizek, P., Kummer, L., Rube, P., Prinz, A., Herberg, F. W. and Plückthun, A. (2012).** Ankyrin Repeat Proteins (Darpins) as Novel Isoform-Specific Intracellular Inhibitors of c-Jun N-Terminal Kinases. *ACS Chem Biol* **7**, 1356-66

**Kummer, L., Parizek, P., Rube, P., Millgramm, B., Prinz, A., Mittl, P. R. E., Kaufholz, M., Zimmermann, B., Herberg, F. W. and Plückthun, A. (2012).** Phosphorylation-specific ERK kinase binders from designed ankyrin repeat protein libraries. *Proc Natl Acad Sci U S A* **109**, E2248-57